

UNIVERSIDAD



DE EXTREMADURA

Departamento de Ingeniería Química y Química Física

Tesis Doctoral

---

**Eliminación de contaminantes emergentes  
del agua mediante ozonación solar  
fotocatalítica**

---

Diego Hernán Quiñones Murillo

Conformidad de los directores de Tesis:

---

Dr. Fernando J. Beltrán Novillo

---

Dr. Pedro M. Álvarez Peña

2014





---

**Eliminación de contaminantes emergentes del  
agua mediante ozonación solar fotocatalítica**

**Degradation of emerging contaminants in  
water by solar photocatalytic ozonation**

---

Memoria de Tesis presentada a la Universidad de  
Extremadura para aspirar al grado de

**Doctor con Mención Internacional**

Presentada por:

Diego Hernán Quiñones Murillo

Badajoz, España

2014



Este trabajo ha sido posible gracias al soporte económico del Ministerio de Economía y Competitividad (MINECO) a través de los proyectos CTQ2009-13459-C05-05 y CTQ2012-35789-C02-01, el Fondo Europeo para el Desarrollo Regional y la concesión de una beca FPI del MINECO.



# Agradecimientos

## (Acknowledgements)

En forma de agradecimiento quiero dedicar este trabajo, que es fruto de mi esfuerzo y dedicación, a todas aquellas personas que durante este largo camino han estado a mi lado, brindándome su apoyo y estima incondicional. Aquellos mismos que día a día han celebrado mis triunfos y, en mis fracasos, se han convertido en pilares fundamentales para no desfallecer y perseverar.

A Dios, por darme la vida, por poner en mi camino a personas maravillosas y por todas las bendiciones y regalos que me concede día tras día.

A mi madre María, el pilar más importante de mi vida, quien siempre me ha ofrecido un inmenso cariño y quien a través de sus sabios consejos me ha enseñado a enfrentar los retos de la vida. A mi padre Milciades, a mis hermanos: Hernando, Héctor, Mary, Nora, Jairo y Luz Dary, y a mis sobrinos: Valentina, Laura, Karol, Iván, Esteban, Jackeline, Edier y Jorge, porque a pesar de la distancia, siempre me he sentido acompañado y respaldado por ellos.

Al Dr. Fernando Beltrán, por creer en mí y permitirme hacer parte de su grupo de trabajo. Espero haber retribuido en alguna manera toda la confianza depositada en mí y el apoyo recibido durante todo este tiempo. Al Dr. Pedro Álvarez, por su disposición, su valiosa guía y asesoramiento durante el desarrollo de esta Tesis. A la Dra. Ana Rey, por sus importantes aportes y participación activa en gran parte de este trabajo.

My heartfelt thanks also go to Dr. Gianluca Li Puma for giving me the opportunity to do a research stay at his group in Loughborough (U.K.). To my lab and office fellows there: *Arkadaşım* Aydın, Chiara, Marco and Jorgelina. It was really wonderful to share so many lunches, beers, trips and nice talks with you guys. Likewise, I want to extend special thanks to the Chemical Engineering and Human Resources Departments at the Loughborough University for their kind help during my stay there.

A mis amigos incondicionales en Colombia: Ana, Vanessa, Rodrigo, Viviana, Pilar y Mónica. A quienes se han convertido en mi familia en España: Natalia, el Dr. Óscar, Mayela, Rui, Mara, César, Javier, Luz, Patricia, Jorge, Heidi y Víctor. Muchas gracias por ser parte de mi vida, por transmitirme toda su buena energía y por compartir conmigo todos aquellos momentos de tristezas y alegrías.

Al Departamento de Ingeniería Química y Química Física de la Universidad de Extremadura por acogerme durante estos cuatro años de Tesis. A mis compañeros de trabajo en el grupo de investigación: Almudena, Ángel, Ruth, Gracia, Nico, Azahara, Fanny, Rafael, Mercedes, Teresa, Juan Carlos, Miriam, Guadalupe, Ana Mary e Isidro; y a los demás compañeros del Departamento: Gloria, Patricia, Elena, Paco, Nuria, Fernando y María Jesús. Un agradecimiento especial al Sr. Sagasti por su buen humor, amistad, paciencia y toda la colaboración que me brindó durante este tiempo. A los profesores: Olga, Eva, Juan F., Javier R., Benito, Javier B., Joaquín, Francisco, Teresa y Juan L. A Felipe, por ayudarme diligentemente a resolver todos mis asuntos legales. Cada uno de ellos aportó un granito de arena para el desarrollo de este trabajo y gracias al esfuerzo de todos hoy logramos un triunfo más.

Al Departamento de Química Orgánica en la Universidad de Córdoba. A mis queridos amigos: Lucrecia y Antonio. A mis excompañeros de Máster: Manolo, Elena, Vicente, Alina, Fran, Dolores, Marisa, Yimo y Kaquisco; y a los Dres. Marinas, padre e hijo. Guardo recuerdos muy especiales de mi paso por Córdoba, donde viví uno de los años más increíbles de mi vida y conocí a personas que dejaron una huella muy importante en mí.

A mis tres Almas Máter: Universidad de Antioquia, Universidad de Córdoba y Universidad de Extremadura. Al Ministerio de Economía y Competitividad por la concesión de una beca predoctoral FPI. A la Fundación Carolina por otorgarme una ayuda para realizar un Máster.

A los que no haya mencionado explícitamente en estas líneas pero que, de una u otra manera, me han ayudado para que esta Tesis sea una realidad.

¡A todos, infinitas gracias!





# Contents

<b>Summary .....</b>	<b>7</b>
<b>List of acronyms, abbreviations and symbols .....</b>	<b>17</b>
<b>Chapter I: Introduction and objectives .....</b>	<b>21</b>
1.1. Global water situation .....	23
1.1.1. European Union legal framework.....	24
1.1.2. Emerging contaminants .....	27
1.1.3. Priority and emerging contaminants in Spain.....	29
1.2. Advanced oxidation processes .....	30
1.2.1. Photocatalysis .....	32
A. Heterogeneous photocatalysis .....	32
B. Homogeneous photocatalysis .....	34
C. Solar systems .....	35
1.2.2. Ozonation treatments .....	37
A. Photolytic ozonation.....	38
B. Catalytic ozonation.....	39
C. Photocatalytic ozonation.....	40
1.3. Model compounds used in this investigation .....	41
1.3.1. Acetaminophen .....	41
1.3.2. Antipyrine .....	41
1.3.3. Bisphenol A .....	42
1.3.4. Caffeine.....	43
1.3.5. Diuron.....	43
1.3.6. 4-chloro-2-methylphenoxyacetic acid (MCPA) .....	44
1.3.7. Metoprolol .....	44
1.3.8. o-phenylphenol .....	45
1.3.9. Terbutylazine .....	45
1.3.10. Testosterone.....	46
1.4. Objectives.....	46
1.5. Organization of the Thesis .....	48
1.6. References.....	49

<b>Chapter II: Methodology</b> .....	<b>59</b>
2.1. Chemicals .....	61
2.2. Experimental set-ups .....	63
2.2.1. Laboratory-scale set-ups .....	63
A. Catalyst preparation .....	63
B. Solar simulator for photoactivity tests .....	66
2.2.2. Pilot-scale solar plant .....	67
2.3. Analytical methods .....	68
2.3.1. Concentration of pollutants in water .....	68
2.3.2. Identification of degradation intermediates .....	69
2.3.3. Total organic and inorganic carbon (TOC, IC) .....	70
2.3.4. Dissolved ozone concentration .....	70
2.3.5. Gas-phase ozone concentration .....	71
2.3.6. Total dissolved iron concentration .....	72
2.3.7. Iron (II) concentration .....	72
2.3.8. Hydrogen peroxide concentration .....	73
2.3.9. Dissolved boron concentration .....	74
2.3.10. Biological oxygen demand .....	75
2.3.11. Chemical oxygen demand .....	75
2.3.12. Acute toxicity .....	76
2.3.13. Turbidity .....	76
2.3.14. Conductivity .....	77
2.3.15. Phenolic nature intermediates .....	77
2.3.16. Ions (phosphate, nitrate, sulfate and chloride) concentration .....	78
2.3.17. pH and temperature .....	78
2.4. Catalyst characterization .....	78
2.4.1. X-ray diffraction (XRD) .....	78
2.4.2. X-ray photoelectron spectroscopy (XPS) .....	79
2.4.3. Nitrogen adsorption-desorption isotherms .....	80
2.4.4. Inductively coupled plasma .....	82
2.4.5. SQUID Magnetometry .....	82
2.4.6. Diffuse reflectance UV-Vis spectroscopy (DR-UV-Vis) .....	83
2.4.7. Fourier transform infrared spectroscopy (FTIR) .....	84
2.4.8. Scanning electron microscopy-Energy dispersive X-ray analysis (SEM-EDX) .....	84
2.5. References .....	84
 <b>Chapter III: Application of solar photocatalytic ozonation for the degradation of emerging contaminants in water in a pilot plant</b> .....	 <b>89</b>
3.1. Abstract .....	91

3.2. Introduction.....	92
3.3. Materials and methods .....	94
3.3.1 Chemicals .....	94
3.3.2. Experimental set-up .....	95
3.3.3. Experimental procedure.....	95
3.3.4. Analytical methods .....	96
3.4. Results and discussion .....	97
3.4.1. Preliminary experiments .....	97
3.4.2. Target compounds depletion and total organic carbon removal .....	97
A. ECs adsorption onto TiO <sub>2</sub> .....	100
B. Photolysis .....	100
C. Photocatalytic oxidation .....	100
D. Ozonation and photolytic ozonation.....	102
E. Photocatalytic ozonation.....	104
F. TiO <sub>2</sub> systems .....	104
3.4.3. Synergistic effect assessment.....	105
3.4.4. Ozone consumption .....	107
3.4.5. Effect of inorganic species.....	109
3.4.6. Kinetic aspects of AOP systems investigated.....	110
A. AOP systems at pH 3.....	110
B. AOP systems at pH 7.....	115
3.5. Conclusions.....	118
3.6. Supplementary information.....	118
3.7. Acknowledgements.....	124
3.8. References.....	124

**Chapter IV: Removal of emerging contaminants from municipal WWTP secondary effluents by solar photocatalytic ozonation. A pilot-scale study. .... 131**

4.1. Abstract .....	133
4.2. Introduction.....	134
4.3. Materials and methods .....	135
4.3.1. Secondary effluent samples .....	135
4.3.2. Experimental set-up and procedure.....	136
4.3.3. Analytical methods .....	138
4.4. Results and discussion .....	139
4.4.1. ECs depletion and TOC removal .....	139
4.4.2. Hydroxyl radical exposure.....	145
4.4.3. Phenolic intermediates.....	147
4.4.4. Biodegradability measurements.....	148
4.4.5. Toxicity tests.....	148

4.4.6. Influence of the H <sub>2</sub> O <sub>2</sub> /Fe(III) ratio .....	150
4.4.7. Simplified comparison of operating costs .....	150
4.5. Conclusions .....	152
4.6. Acknowledgements .....	152
4.7. References .....	152

**Chapter V: Simulated solar–light assisted photocatalytic ozonation of metoprolol over titania-coated magnetic activated carbon..... 155**

5.1. Abstract .....	157
5.2. Introduction .....	158
5.3. Experimental section .....	160
5.3.1. Preparation of catalyst .....	160
5.3.2. Catalyst characterization .....	160
5.3.3. Photocatalytic experiments .....	161
5.4. Results and discussion .....	162
5.4.1. Characterization of TiO <sub>2</sub> magnetic activated carbon .....	162
5.4.2. Photocatalytic activity .....	167
A. Photodegradation of MTP .....	167
B. Influence of initial MTP concentration .....	171
C. Catalyst stability and reusability .....	173
5.5. Conclusions .....	174
5.6. Acknowledgements .....	175
5.7. References .....	175

**Chapter VI: Enhanced activity and reusability of TiO<sub>2</sub> loaded magnetic activated carbon for solar photocatalytic ozonation ..... 181**

6.1. Abstract .....	183
6.2. Introduction .....	184
6.3. Experimental section .....	185
6.3.1. Catalyst preparation .....	185
6.3.2. Characterization of the catalysts .....	186
6.3.3. Photocatalytic activity measurements .....	187
6.4. Results and discussion .....	189
6.4.1. Characterization of the fresh catalysts .....	189
6.4.2. Catalytic activity .....	195
A. Effect of radiation wavelength .....	198
B. Simplified mechanistic approach .....	202
C. Catalyst reusability .....	205
6.5. Conclusions .....	208
6.6. Supplementary information .....	208
6.6.1. Analytical determination of MTP intermediates .....	208

6.6.2. MTP intermediates identification .....	209
6.6.3. MTP intermediates evolution during different treatments .....	211
6.7. Acknowledgements .....	212
6.8. References .....	212
<b>Chapter VII: Boron doped TiO<sub>2</sub> catalysts for photocatalytic ozonation of aqueous mixtures of common herbicides and pesticides: Diuron, o-phenylphenol, MCPA and terbuthylazine .....</b>	<b>217</b>
7.1. Abstract .....	219
7.2. Introduction .....	220
7.3. Experimental section .....	221
7.3.1. Catalysts preparation .....	221
7.3.2. Characterization of the catalysts .....	221
7.3.3. Photocatalytic activity measurements .....	222
7.4. Results and discussion .....	223
7.4.1. Catalysts characterization .....	223
7.4.2. Photocatalytic activity .....	229
7.4.3. Catalyst stability .....	236
7.5. Conclusions .....	238
7.6. Supplementary information .....	238
7.7. Acknowledgements .....	242
7.8. References .....	243
<b>Chapter VIII: Conclusions .....</b>	<b>247</b>
8.1. General conclusions .....	249
8.2. Conclusiones generales .....	253
<b>Annex .....</b>	<b>257</b>
A.1. Journal publications .....	259
A.2. Peer reviewed conference papers .....	259



# Summary

The research in this Thesis has been mainly performed at the research group *Trataguas*, from the *Departamento de Ingeniería Química y Química Física* of the *Universidad de Extremadura*. It is a part of an extensive research program on the elimination of emerging contaminants in water through the application of advanced oxidation processes (AOPs), being developed by the *Trataguas* group and financed by several funds. Particularly, this research has been supported by the *Ministerio de Economía y Competitividad* (Spain) through the projects CTQ2009-13459-C05-05 and CTQ2012-35789-C02-01, titled “*Integración de procesos de fotocatalisis solar en la depuración biológica de aguas residuales para la eliminación de contaminantes emergentes*” and “*Preparación de catalizadores y su aplicación en la eliminación de contaminantes refractarios de aguas residuales mediante ozonación fotocatalítica*”, respectively. It has been also granted by *European Regional Development Fund* (EFRD). A part of this research was carried out at the research group of *Environmental Nanocatalysis & Photoreaction Engineering* of the *Department of Chemical Engineering* at *Loughborough University* (United Kingdom) thanks to a research visit supported by the *Ministerio de Economía y Competitividad* (Grant reference: EEBB-I-13-06251).

The significance of this Thesis lies in bringing up effective alternatives to combat the plight of the presence of priority and emerging contaminants (ECs) in water. Many of these substances have been found to be recalcitrant to biological and physicochemical processes conventionally applied in wastewater treatment plants and, as a result, there is a widespread occurrence of them in water bodies with the consequent potential risk to all living species. This has arisen great interest in the scientific community to develop new treatment technologies to deal with this kind of contaminants in order to improve the quality of the treated wastewater prior to be safely discharged into public water bodies or even to make possible its reuse.

Priority pollutants are chemicals which present a significant risk to or via the aquatic environment. The European Union, through the Directive on Environmental Quality Standards (Directive 2008/105/EC), designated 33 substances or groups of substances as priority or priority hazardous substances

including metals and their compounds, pesticides and polyaromatic hydrocarbons among others. As a review of the priority substances provisions has to be done at least every four years, in 2012 fifteen new substances were proposed as priority pollutants, including some pharmaceutical compounds such as 17  $\alpha$ -ethinyloestradiol or diclofenac. On the other hand, ECs or contaminants of emerging concern are chemicals that recently have been shown to occur widely in water resources and identified as being a potential environmental or public health risk, and yet adequate data do not exist to determine their risk. They are to be included in the list of priority pollutants if their risks are confirmed.

The ECs category includes personal care products, pharmaceuticals, drugs, surfactants, industrial additives, pesticides, and household products, etc. Particularly, pharmaceutical products, some industrial additives and pesticides have recently focused special attention of the research community. Pharmaceuticals, due to their high worldwide demand, are continually discharged into the environment through domestic, hospital and industrial drains, whereas industrial and agricultural residues can contaminate large quantities of water, as these sectors consume most of the fresh water available for human activities (19% and 70% respectively according to the Food and Agriculture Organization of the United Nations, 2010).

In recent decades, a number of advanced oxidation processes (AOPs) have been researched and developed as alternatives to conventional treatments (e.g., biological and physicochemical methods) for the removal of priority and emerging pollutants. All AOPs are characterized by their capability of exploiting the high reactivity of free radicals, mainly hydroxyl radical ( $\cdot\text{OH}$ ), which are suitable for achieving high removal and mineralization of pollutants. Among the most studied AOPs, Fenton and photo-Fenton like processes,  $\text{TiO}_2$  photocatalytic oxidation or ozone-based processes such as  $\text{O}_3/\text{H}_2\text{O}_2$  or  $\text{O}_3/\text{UV}$  systems can be highlighted.

As one of the limitations for the application of photochemical AOPs at industrial scale is their high operativity costs, the use of sunlight as a natural source of radiation is proposed, thus avoiding costs associated with acquisition, maintenance, replacement and power consumption of UV lamps.

In this Thesis, the degradation of several compounds, which have been selected as model representatives of various types of priority and emerging contaminants, has been studied. Particularly, the model compounds used in this research are acetaminophen (analgesic and anti-inflammatory), antipyrine (analgesic and antipyretic), metoprolol ( $\beta$ -blocker), caffeine (stimulant), testosterone (steroid hormone), bisphenol A (industrial plasticizer), diuron (herbicide), MCPA (herbicide), o-phenylphenol (bacteriostat and fungicide) and terbuthylazine



(herbicide). These compounds have been subjected to some AOPs, including photo-assisted Fenton-like, ozonation and photocatalytic oxidation processes, as well as several combinations of them. Natural and simulated solar light have been used throughout the research as radiation source. Of special interest in this work are some solar photocatalytic ozonation processes, which make simultaneous use of ozone, solar radiation and catalysts.

This Thesis was designed to cover three main parts:

- Firstly, the research was focused on the application of some solar photocatalytic (based on the use of iron as catalyst) and ozonation processes for the degradation of a mixture of acetaminophen, antipyrine, bisphenol A, caffeine, metoprolol and testosterone in water. The degradation experiments were conducted in a pilot plant that makes use of sunlight as energy source. The efficacy of each system in terms of mineralization was evaluated. Also, the synergistic effects by simultaneous application of ozonation and photocatalysis were assessed in terms of mineralization, ozone consumption and reaction rates. Additionally, titanium dioxide (TiO<sub>2</sub> P25) was used as a reference catalytic material in photocatalytic processes for comparative purposes due to its extended application in this field.

The above-mentioned treatment systems were also tested for the removal of ECs in real wastewater samples collected from the secondary effluent of a municipal wastewater treatment plant of Badajoz (Spain). In this case, an estimation of the ECs depletion time as function of the reactor size and the intensity of radiation is proposed, the effect of the initial H<sub>2</sub>O<sub>2</sub>/Fe(III) mass ratio was evaluated and the toxicity of the treated samples was assessed using a *Daphnia Magna* bioassay. Finally, an economic evaluation of operativity costs at pilot scale was performed.

It was found that solar photolysis and photocatalytic oxidation using Fe(III) did not lead to an important compound degradation, while TiO<sub>2</sub> photocatalysis, photo-Fenton, as well as single, photolytic and photocatalytic ozonations were able to remove the target compounds and reduce the organic carbon content to some extent. The combination of photocatalytic oxidation, assisted by TiO<sub>2</sub>, or, the Fenton reagent, and ozonation resulted to be the most efficient system for the mineralization of the contaminants, leading to 80-93% TOC removal. Results also demonstrate that in the ozone-based treatments the compounds mineralization occurs in the slow kinetic regime. As a result, the indirect oxidation pathway via hydroxyl radical is an important contribution to the overall degradation process.

A reduction in the efficiency of these processes was observed when the ECs were present in wastewater treatment plant secondary effluents. In this case, it was observed that iron-based systems at pH 3 were more effective than TiO<sub>2</sub> mediated processes at pH 7. Toxicity of the samples to *D. Magna* increased at the beginning of the oxidation treatment and was reduced at larger TOC removal degrees. In the cases of photolytic ozonation, photo-Fenton and photocatalytic ozonation (assisted by TiO<sub>2</sub>, Fe(III) and Fe(III)/H<sub>2</sub>O<sub>2</sub>) toxicity was reduced below the initial value. Some solar photocatalytic ozonation processes, such as Fe(III)/O<sub>3</sub>/light/pH 3 and Fe(III)/H<sub>2</sub>O<sub>2</sub>/O<sub>3</sub>/light/pH 3 can be cheaper than the solar photo-Fenton system to mineralize the treated samples.

- The second part of this work deals with the preparation, characterization and use of magnetic catalysts consisting of TiO<sub>2</sub> nanoparticles supported on activated carbon. The catalysts were synthesized using a commercial activated carbon as support. This was first magnetized by thermal reduction of ferric nitrate previously impregnated on the activated carbon. Then, anatase TiO<sub>2</sub> particles were supported onto the activated magnetic carbon by a sol-gel method. The catalyst photoactivity was evaluated in a laboratory-scale system performing photocatalytic experiments under simulated solar radiation. For these experiments, metoprolol was selected as target EC to be degraded.

Titanium dioxide and magnetic iron oxide contents in the catalyst were identified as key variables to obtain a photo-efficient and easily recoverable catalyst. In this sense, a catalyst optimization study was carried out.

Radiation wavelength seemed to play an important role in photolytic and photocatalytic ozonation, so the effect of different wavelengths on the process performance was investigated. Further experiments were carried out to evaluate the catalyst stability and reusability throughout successive photocatalytic ozonation runs.

Catalysts led to complete removal of metoprolol and mineralization degrees up to 85% in solar photocatalytic ozonation experiments at laboratory scale. The target compound, metoprolol, was mainly removed through direct ozone reactions, independently of the catalyst composition. However, mineralization rate depended on the anatase content of the catalyst. Stability and reusability of the catalysts were demonstrated to be rather good throughout a series of consecutive photocatalytic ozonation runs with no important alteration of the catalysts properties.

- The third part of the Thesis is focused on the synthesis, characterization and application of TiO<sub>2</sub> powder catalysts with improved properties. To this purpose, boron was used as dopant. In this investigation diuron, o-phenylphenol acid, 2-methyl-4-chlorophenoxy and terbuthylazine, which are pesticides of widespread

use, were chosen as model compounds. Photoactivity of catalysts was assessed by photocatalytic oxidation and photocatalytic ozonation experiments carried out in a laboratory-scale solar simulator.

B-doped TiO<sub>2</sub> catalysts (having between 0.5-0.8 wt% of interstitial boron) were more active than bare TiO<sub>2</sub> in the treatment of the target compounds. Stability of the catalyst was also tested. It was found that the mineralization level was maintained at about 75% after three consecutive runs of photocatalytic ozonation.

## **Keywords**

---

Activated carbon, Advanced Oxidation Processes, emerging contaminants, pharmaceuticals, magnetic photocatalyst, pesticides, photo-Fenton, solar photocatalytic ozonation, synthesis of catalysts, titania, water remediation.

# Resumen

La Tesis Doctoral que se presenta en esta memoria ha sido desarrollada en el grupo de investigación *Trataguas*, perteneciente al *Departamento de Ingeniería Química y Química Física* de la *Universidad de Extremadura*. Este trabajo se enmarca dentro de una serie de investigaciones acerca de la aplicación de Procesos Avanzados de Oxidación para la eliminación de contaminantes emergentes en aguas que se han venido desarrollando en el grupo *Trataguas* durante los últimos años. Esta investigación ha sido financiada principalmente por el *Ministerio de Economía y Competitividad* (España) a través de los proyectos del Programa Nacional de Investigación CTQ2009-13459-C05-05, titulado “*Integración de procesos de fotocatalisis solar en la depuración biológica de aguas residuales para la eliminación de contaminantes emergentes*” y CTQ2012-35789-C02-01, titulado “*Preparación de catalizadores y su aplicación en la eliminación de contaminantes refractarios de aguas residuales mediante ozonación fotocatalítica*”. Adicionalmente se ha recibido financiación del *Fondo Europeo de Desarrollo Regional* (FEDER). Asimismo, una parte del trabajo se ha desarrollado en el grupo de investigación *Environmental Nanocatalysis & Photoreaction Engineering* del *Chemical Engineering Department* de la *Loughborough University* (Reino Unido) gracias a una estancia breve de investigación financiada por el *Ministerio de Economía y Competitividad* de España (Referencia de la ayuda: EEBB-I-13-06251).

La relevancia del estudio desarrollado en esta Tesis radica en el planteamiento de alternativas que resulten eficaces para solucionar la problemática que representa la presencia de contaminantes prioritarios y emergentes en el agua. Este tipo de contaminantes son, generalmente, persistentes ante los procesos biológicos y físico-químicos que convencionalmente se emplean en las estaciones depuradoras de aguas residuales, por lo que su presencia en aguas naturales es frecuente con el potencial riesgo para el ecosistema acuático. Su continua detección en cuerpos de agua ha despertado en la comunidad científica un interés por desarrollar nuevas tecnologías de purificación que logren su depuración con el fin de mejorar la calidad de las aguas residuales antes de ser vertidas a cauces públicos o que se permita su reutilización.

Los contaminantes prioritarios del agua son sustancias químicas que representan un riesgo significativo para el medio acuático o a través del mismo. La Unión Europea a través de la Directiva 2008/105/CE, relativa a las normas de calidad ambiental, establece una lista de 33 sustancias químicas o grupos de sustancias peligrosas prioritarias que incluye metales, pesticidas, hidrocarburos poliaromáticos, entre otros. En 2012, tras una revisión de las disposiciones relacionadas con las sustancias prioritarias, se han propuesto 15 sustancias nuevas como contaminantes prioritarios, entre ellos algunos compuestos farmacéuticos como el 17  $\alpha$ -etinilestradiol o diclofenaco. Por otro lado, los contaminantes emergentes (ECs) los cuales son sustancias químicas que recientemente se han detectado en cuerpos de agua y que son potencialmente peligrosos para la salud pública y ambiental, también serían incluidos en la lista de contaminantes prioritarios de comprobarse sus efectos adversos. Dentro del grupo de ECs se incluyen productos de higiene personal, fármacos, drogas, surfactantes, aditivos industriales, pesticidas, productos de uso doméstico, entre otros.

Los fármacos, algunos aditivos industriales y los pesticidas han concentrado especial atención en la comunidad científica. En el caso de los fármacos debido a que por su elevada demanda a nivel mundial son descargados al medio ambiente en forma continua a través de los vertederos domésticos, hospitalarios e industriales. Por su parte los productos de uso industrial y agrícola contaminan grandes cantidades de agua ya que éstos sectores consumen la mayor parte del agua dulce disponible para las actividades humanas (19 y 70% respectivamente, según la *Food and Agriculture Organization* de las Naciones Unidas, 2010).

En las últimas décadas, se han investigado e implementado procesos avanzados de oxidación (PAOs) como alternativa a los métodos convencionales, biológicos y fisicoquímicos para la eliminación de contaminantes prioritarios y emergentes. Estos procesos se basan en la generación de radicales libres, especialmente el radical hidroxilo ( $\cdot\text{OH}$ ), que son especies transitorias de vida media muy corta y con alto poder oxidante, de modo que resultan muy eficaces en la eliminación y mineralización de un gran número de contaminantes.

Dado que una de las limitaciones para el empleo de PAOs a escala industrial son sus altos costes de operación, el uso de la luz solar como fuente de radiación se perfila como una alternativa eficaz puesto que se evitan costes de operación debidos a la adquisición, mantenimiento, reemplazo y consumo de energía por parte de lámparas UV.

En esta Tesis Doctoral se ha estudiado la eliminación de varios compuestos orgánicos que han sido seleccionados como modelo y que son representativos de

varios tipos de contaminantes prioritarios y emergentes, que con frecuencia se detectan en cuerpos de agua. Concretamente, los compuestos que se han utilizado en esta investigación son acetaminofeno (analgésico y antiinflamatorio), antipirina (analgésico y antipirético), metoprolol ( $\beta$ -bloqueante), cafeína (estimulante), testosterona (hormona esteroide), bisfenol A (aditivo plastificante de uso industrial), diurón (herbicida), MCPA (herbicida), o-fenilfenol (bactericida y fungicida) y terbutilazina (herbicida). Para su eliminación se han empleado algunos PAOs incluyendo procesos foto-Fenton, de oxidación fotocatalítica y de ozonación, así como algunas combinaciones de los anteriores. Como fuente de radiación se ha utilizado luz solar, natural y simulada. El proceso más relevante de esta investigación por su carácter más novedoso es la ozonación solar fotocatalítica, consistente en el uso simultáneo de ozono, radiación solar y algún catalizador.

La investigación se ha planificado para desarrollar tres bloques o áreas principales de trabajo:

- El primero se ha centrado principalmente en el estudio de sistemas homogéneos de ozonación fotocatalítica basados en el empleo de Fe(III), Fe(III)/H<sub>2</sub>O<sub>2</sub> (un tipo de reactivo Fenton) para la degradación de una mezcla de acetaminofeno, antipirina, bisfenol A, cafeína, metoprolol y testosterona en agua ultrapura. Los ensayos se realizaron en una planta piloto que aprovecha la luz solar como fuente de energía. Se evaluó la eficacia de cada sistema en la mineralización de los contaminantes. Asimismo se cuantificó el efecto sinérgico obtenido mediante la aplicación simultánea de ozonación y fotocátalisis en términos de mineralización, consumo de ozono y velocidades de reacción. Adicionalmente, se empleó el dióxido de titanio, TiO<sub>2</sub> P25, como catalizador de referencia, dada su alta aplicación en este tipo de procesos.

Los sistemas de tratamiento citados en el párrafo anterior también se aplicaron para el tratamiento de muestras de agua residual real recolectadas del efluente secundario de una estación depuradora de aguas residuales de Badajoz (España). En este caso, además, se realizó una estimación del tiempo de vida media de los compuestos en función del tamaño del reactor y de la intensidad de radiación UVA. Se evaluó el efecto de la relación másica inicial de H<sub>2</sub>O<sub>2</sub>/Fe(III) en el proceso de ozonación fotocatalítica, así como la toxicidad de las muestras tratadas empleando *Daphnia Magna* como indicador. Finalmente, se efectuó una evaluación económica de los costes de operación requeridos a escala piloto para eliminar y mineralizar los contaminantes

Mediante fotólisis solar y oxidación fotocatalítica usando Fe(III) no se consiguió una degradación significativa de los compuestos ni mineralización de la mezcla en agua ultrapura. La aplicación de procesos de fotocátalisis con TiO<sub>2</sub>, foto-Fenton y de ozonación sencilla, fotolítica y fotocatalítica permitieron

la eliminación completa de los contaminantes y grados de conversión de carbono orgánico total entre 7 y 93% en agua ultrapura. La combinación de la oxidación fotocatalítica, usando tanto  $\text{TiO}_2$  como el reactivo Fenton, y ozonación condujo a porcentajes de mineralización del 80 y 93%, respectivamente. En los sistemas basados en ozono, la mineralización de los compuestos se produce en régimen cinético lento, por tanto la oxidación indirecta con los radicales hidroxilo es una contribución importante en el proceso.

Se observó una reducción en la eficiencia de estos procesos cuando los contaminantes estaban presentes en muestras de efluentes secundarios de una planta de tratamiento de aguas residuales. En este caso, los sistemas basados en hierro a pH 3 fueron más eficaces que los procesos que emplean  $\text{TiO}_2$  a pH 7. La toxicidad de la muestras de reacción aumentó durante los primeros minutos pero disminuyó cuando se alcanzaron mayores grados de mineralización. Para los ensayos de ozonación fotocatalítica, foto-Fenton y ozonación fotocatalítica (con  $\text{TiO}_2$ ,  $\text{Fe(III)}$  y  $\text{Fe(III)/H}_2\text{O}_2$ ) la toxicidad al final del proceso fue inferior al valor inicial. Los sistemas de ozonación fotocatalítica basados en hierro a pH 3 como el  $\text{Fe(III)/O}_3/\text{luz}$  y el  $\text{Fe(III)/H}_2\text{O}_2/\text{O}_3/\text{luz}$  resultaron ser más baratos que el proceso foto-Fenton a escala piloto.

- En el segundo bloque se sintetizaron, caracterizaron y utilizaron catalizadores magnéticos de  $\text{TiO}_2$  soportado sobre carbón activo. Los catalizadores se sintetizaron empleando un carbón activo comercial como soporte, el cual se magnetizó mediante reducción térmica de nitrato férrico previamente impregnado sobre el carbón. Posteriormente, se soportaron partículas de  $\text{TiO}_2$  en fase anatasa siguiendo un método sol-gel. La fotoactividad de estos catalizadores se evaluó en un sistema a escala de laboratorio mediante reacciones de ozonación fotocatalítica con luz solar simulada. El compuesto modelo empleado fue metoprolol.

Se optimizó el contenido de dióxido de titanio y óxido magnético de hierro en el catalizador con el fin de obtener propiedades fotocatalíticas y magnéticas mejoradas en los catalizadores. Adicionalmente, se evaluó el efecto del catalizador con radiación de diferentes longitudes de onda. Finalmente, se estudió su estabilidad y reutilización mediante su empleo en ensayos sucesivos de ozonación fotocatalítica.

El uso de estos catalizadores en procesos de ozonación fotocatalítica a escala de laboratorio empleando luz solar artificial permitió la completa eliminación de metoprolol y porcentajes de mineralización hasta de 85%. Se observó que los catalizadores son estables y pueden recuperarse magnéticamente para ser

reutilizados, ya que no se presentó una variación importante de las propiedades de los mismos luego de 50 horas de uso.

- El tercer bloque se enfocó hacia la síntesis, caracterización y aplicación de catalizadores en polvo de  $\text{TiO}_2$  con propiedades mejoradas, para lo cual se empleó boro como agente dopante. En este bloque se usaron como compuestos modelo algunos pesticidas de uso difundido, tales son diurón, o-fenilfenol, ácido 2-metil-4-clorofenoxiacético y terbutilazina. La fotoactividad de los catalizadores se evaluó mediante ensayos de fotocátalisis y ozonación fotocatalítica a escala de laboratorio en un simulador solar.

Los catalizadores de  $\text{TiO}_2$  dopados con B (con un contenido final de boro intersticial entre 0,5 y 0,8 % en peso) fueron más activos que el  $\text{TiO}_2$  no dopado en el tratamiento de los compuestos seleccionados, mediante fotocátalisis y ozonación fotocatalítica solar. Luego de 3 ciclos consecutivos de uso en reacciones de ozonación fotocatalítica, los catalizadores conservan su estabilidad y se pueden alcanzar porcentajes de mineralización de hasta 75%.

### **Palabras clave**

---

Carbón activo, contaminantes emergentes, dióxido de titanio, fármacos, fotocatalizador magnético, foto-Fenton, ozonación fotocatalítica solar, pesticidas, procesos avanzados de oxidación, síntesis de catalizadores, tratamiento de aguas.



# List of acronyms, abbreviations and symbols

$\cdot\text{OH}$	Hydroxyl radical
a.u.	Arbitrary units
AC	Activated carbon
ACE	Acetaminophen
$A_{i\text{nm}}$	Absorbance at $i$ nm
ANT	Antipyrine
AOPs	Advanced Oxidation Processes
BIS	Bisphenol A
B-TiO <sub>2</sub>	Boron doped titania catalyst
CAF	Caffeine
$C_i$	Concentration of compound $i$ in liquid phase
$C_{i,0}$	Initial concentration of $i$ in liquid phase
$C_{i,g}$	Concentration of compound $i$ in gas phase
CPC	Compound parabolic collector
$d_A$	Anatase crystallite size
$D_i$	Diffusivity of $i$ in the liquid phase
DIU	Diuron
$d_M$	Magnetite or maghemite crystallite size
$d_p$	Particle size (grain size)
$e^-_{CB}$	Electron promoted to semiconductor conduction band
ECs	Emerging compounds
EDX	Energy Dispersive X-ray
$E_g$	Band gap energy
FeC	Magnetic activated carbon
$h^+_{VB}$	Hole generated in semiconductor valence band
Ha	Hatta number
HPLC	High-performance liquid chromatography
$h\nu$	Radiation
ICP-MS	Inductively Coupled Plasma Mass Spectrometry

ICP-OES	Inductively Coupled Plasma Optical Spectroscopy
K	Equilibrium constant
k	Reaction rate constant
$k_{app}$	Pseudo-first order apparent rate constant
$k_i$	Rate constant of the reaction referred to compound <i>i</i>
$k_L$	Individual liquid side mass transfer coefficient
$k_{O_3-i}$	Rate constant for direct reaction between <i>i</i> and ozone
$k_{OH-i}$	Rate constant for reaction between <i>i</i> and hydroxyl radical
K <sub>ow</sub>	Octanol-water partition coefficient
$k_{UV}$	Photolytic degradation rate constant
LC <sub>50</sub>	Lethal concentration with 50% mortality
MCPA	2-methyl-4-chlorophenoxyacetic acid
$M_s$	Saturation magnetization
MTP	Metoprolol
MWWTP	Municipal wastewater treatment plant
$N_{O_3}$	Ozone absorption rate
OPP	o-phenylphenol
P/P <sub>0</sub>	Relative pressure
P25	Titanium dioxide P25
PAOs	Procesos Avanzados de Oxidación
pCBA	p-chlorobenzoic acid
pKa	Negative logarithm of the dissociation constant
$Q_g$	Gas flow rate
$r_{O_3}$	Ozone reaction rate
$S_{BET}$	BET surface
SEM	Scanning Electron Microscopy
$S_{EXT}$	External surface
SHE	Standard hydrogen electrode
SI	Synergy index
SQUID	Superconducting Quantum Interference Device
T	Temperature
TBA	Terbutylazine
TiFeC	Titania-coated magnetic activated carbon
TOC	Total organic carbon
TST	Testosterone
UV	Ultraviolet light
V	Volume
v/v	Volume ratio
$V_i$	Volume of <i>i</i>
$V_{MICRO}$	Micropore volumen
wt%	Weight percent

WW	Wastewater
WWTP	Wastewater treatment plant
XPS	X-ray Photoelectron Spectroscopy
XRD	X-ray Diffraction
$z_G$	Ratio between the ozone consumed and TOC
$\varepsilon_i$	Molar adsorptivity at $i$ nm
$\eta$	Ozone consumption rate per mg TOC removed





## Chapter I

This chapter provides background information about the environmental problem concerning the presence of emerging contaminants in water. Also, some theory concepts about the advanced oxidation processes used in this research to deal with this kind of pollutants is given. The purpose of the study and research objectives are also presented. Finally, a description of the organization of the present Thesis is given.

### Contents

- 1.1.** Global water situation
- 1.2.** Advanced oxidation processes
- 1.3.** Model compounds used in this investigation
- 1.4.** Objectives
- 1.5.** Organization of the thesis
- 1.6.** References



## **1.1. Global water situation**

---

Water is a natural resource indispensable for the balance of the planet Earth. Besides being used as a commodity and being the primary input for agricultural and industrial production, it also fulfills an essential role as a prerequisite for all human, animal and plant life [1]. Two thirds of the planet surface is covered by water, however, despite this physical abundance, water is a limited resource and the planet is facing an increasing water shortage problem. Only 2.5% of the water in the planet is freshwater and just 0.4% of it is available and suitable for human consumption. Moreover, the worldwide population is growing rapidly, which increases dramatically the water demand and makes even more evident the negative impacts due to an excessive and irrational use of this resource [2,3].

Over the course of the twentieth century, the global population tripled while water use increased around six-fold [2]. Along with the growth in water demand over time, an increase in wastewater production has been observed. It is estimated that every day around two million tons of sewage and other effluents are globally drained into the natural water systems. Those waste streams, which mostly come from domestic, industrial and agricultural sectors, are the main sources of water pollution since they contain a devastating large number of pollutants such as pathogens, organic compounds, synthetic chemicals, nutrients and heavy metals. All of these substances affect water quality making this resource unfit for any purpose and jeopardizing the health and well-being of creatures that use those waters [4].

According to the World Health Organization, globally, every year over 1 billion people do not have access to safe drinking water and 1.7 million die because of diseases related to the pollution of water [5]. Given the accelerated population growth and the insufficient management strategies applied to deal with water issues, it is estimated that, by year 2025, around 1 billion people will be living in areas with moderate or severe water shortages. Even more, this figure could be doubled by 2050 [6]. Likewise, it is expected that in the next 50 years some ecosystems that depend on water for survival will be destroyed to supply water for human activities [7].

### 1.1.1. European Union legal framework

All the problems previously mentioned highlight the need for regulations that control the use of water in order to have a better and more efficient availability of this important resource. The European Union (EU) water framework directive 2000/60/CE, partially modified by directive 2008/105/CE, is a response to this need. This directive states that water must be protected and defended, and suggests the implementation of measures to reverse any significant and sustained upward trend in the concentration of any pollutant resulting from the impact of human activity in order to progressively reduce pollution. Several substances or groups of substances of priority concern due to their persistence, toxicity, accumulation and widespread use and detection in waters, including metals, pesticides, phthalates, polycyclic aromatic hydrocarbons, and endocrine disruptors have been identified as priority or hazardous substances. Many of them are either regulated, and must be removed to reach safe concentration values in order to preserve the quality and the ecological status of water [8,9], or have been identified as possible priority substances or hazardous substances and are under revision [10].

Particularly, annex II of directive 2008/105/CE [11] presents a list of 33 substances (or groups of substances) which has been classified as priority and priority hazardous substances (as shown in Table 1.1) and have to be monitored and controlled in EU surface waters. This list includes metals, pesticides and polyaromatic hydrocarbons among others.

**Table 1.1.** List of priority substances in the field of EU water policy (Directive 2008/105/CE)

Number	CAS number <sup>(1)</sup>	EU number <sup>(2)</sup>	Name of priority substance <sup>(3)</sup>	Priority hazardous substance
1	15972-60-8	240-110-8	Alachlor	
2	120-12-7	204-371-1	Anthracene	X
3	1912-24-9	217-617-8	Atrazine	
4	71-43-2	200-753-7	Benzene	
5	not applicable	not applicable	Brominated diphenylether <sup>(4)</sup>	X <sup>(5)</sup>
	32534-81-9	not applicable	Pentabromodiphenylether	
6	7440-43-9	231-152-8	Cadmium and its compounds	X
7	85535-84-8	287-476-5	Chloroalkanes, C <sub>10-13</sub> <sup>(4)</sup>	X
8	470-90-6	207-432-0	Chlorfenvinphos	



**Table 1.1. (continued)** List of priority substances in the field of EU water policy (Directive 2008/105/CE)

Number	CAS number <sup>(1)</sup>	EU number <sup>(2)</sup>	Name of priority substance <sup>(3)</sup>	Priority hazardous substance
9	2921-88-2	220-864-4	Chlorpyrifos (Chlorpyrifos-ethyl)	
10	107-06-2	203-458-1	1,2-dichloroethane	
11	75-09-2	200-838-9	Dichloromethane	
12	117-81-7	204-211-0	Di(2-ethylhexyl)phthalate (DEHP)	
13	330-54-1	206-354-4	Diuron	
14	115-29-7	204-079-4	Endosulfan	X
15	206-44-0	205-912-4	Fluoranthene <sup>(6)</sup>	
16	118-74-1	204-273-9	Hexachlorobenzene	X
17	87-68-3	201-765-5	Hexachlorobutadiene	X
18	608-73-1	210-158-9	Hexachlorocyclohexane	X
19	34123-59-6	251-835-4	Isoproturon	
20	7439-92-1	231-100-4	Lead and its compounds	
21	7439-97-6	231-106-7	Mercury and its compounds	X
22	91-20-3	202-049-5	Naphthalene	
23	7440-02-0	231-111-14	Nickel and its compounds	
24	25154-52-3	246-672-0	Nonylphenol	X
	104-40-5	203-199-4	(4-nonylphenol)	X
25	1806-26-4	217-302-5	Octylphenol	
	140-66-9	not applicable	(4-(1,1',3,3'-tetramethylbutyl)-phenol)	
26	608-93-5	210-172-5	Pentachlorobenzene	X
27	87-86-5	231-152-8	Pentachlorophenol	
28	not applicable	not applicable	Polyaromatic hydrocarbons	X
	50-32-8	200-028-5	(Benzo(a)pyrene)	X
	205-99-2	205-911-9	(Benzo(b)fluoranthene)	X
	191-24-2	205-883-8	(Benzo(g,h,i)perylene)	X
	207-08-9	205-916-6	(Benzo(k)fluoranthene)	X
	193-39-5	205-893-2	(Indeno(1,2,3-cd)pyrene)	X

**Table 1.1. (continued)** List of priority substances in the field of EU water policy (Directive 2008/105/CE)

Number	CAS number <sup>(1)</sup>	EU number <sup>(2)</sup>	Name of priority substance <sup>(3)</sup>	Priority hazardous substance
29	122-34-9	204-535-2	Simazine	
30	not applicable	not applicable	Tributyltin compounds	X
	36643-28-4	not applicable	(Tributyltin-cation)	X
31	12002-48-1	234-413-4	Trichlorobenzenes	
32	67-66-3	200-663-8	Trichloromethane (chloroform)	
33	1582-09-8	216-428-8	Trifluralin	

<sup>(1)</sup> CAS: Chemical Abstracts Service.

<sup>(2)</sup> EU number: European inventory of existing commercial substances (Einecs) or European list of notified chemical substances (Elincs).

<sup>(3)</sup> Where groups of substances have been selected, typical individual representatives are listed as indicative parameters (in brackets and without number). For these groups of substances, the indicative parameter must be defined through the analytical method.

<sup>(4)</sup> These groups of substances normally include a considerable number of individual compounds.

<sup>(5)</sup> Only pentabromobiphenylether (CAS-number 32534-81-9).

<sup>(6)</sup> Fluoranthene is on the list as an indicator of other, more dangerous polyaromatic hydrocarbons.

In annex III of directive 2008/105/CE a list of substances were identified as being subject to review for possible identification as priority substances or priority hazardous substances. Such substances are aminomethylphosphonic acid, bentazon, bisphenol a, dicofol, EDTA, free cyanide, glyphosate, mecoprop (MCPP), musk xylene, perfluorooctane sulphonic acid (PFOS), quinoxifen (5,7-dichloro-4-(p-fluorophenoxy)quinoline), dioxins and polychlorinated biphenyls (PCBs).

Then, in 2012, in an effort towards improving the quality of surface waters, 15 new substances including industrial chemicals as well as substances used in biocides, pharmaceuticals and plant protection products, were proposed as priority pollutants [12]. The proposed priority substances are:

- Plant protection products: acetonifol, bifentox, cypermethrin, dicofol, heptachlor and quinoxifen.
- Substances used in biocidal products: cybutryne, dichlorvos and terbutryn.
- Industrial chemicals: PFOS and hexabromocyclododecane (HBCDD).
- Combustion by-products: dioxin and dioxin-like PCBs.
- Pharmaceutical substances: 17  $\alpha$ -ethinylestradiol (EE2), 17  $\beta$ -estradiol (E2) and diclofenac.

Pharmaceuticals were proposed for the first time in order to address the potential harmful effects of their presence in the aquatic environment as they can affect fish health, reducing successful reproduction, for example, and harming other living organisms.

### 1.1.2. Emerging contaminants

During the last decades, the development of advanced analytical techniques has allowed the detection of new groups of compounds in natural water bodies and wastewater treatment plant effluents. This has revealed the fact that many of the substances discharged in water streams, or their metabolites, are refractory to the conventional processes applied during the treatment of wastewaters. Many of these substances, which are known as emerging contaminants (ECs), are identified as being a potential environmental or public health risk, though adequate data do not exist to determine definitely their risk. In general, they are characterized by their continuous release into the water cycle, since they are consumed at large scale worldwide, and by their high stability and solubility in water. Consequently, they need special management strategies to be safely removed from water.

Figure 1.1 shows a scheme indicating the main sources of ECs incorporation into the environment and the pathways to reach groundwater and surface waters. ECs could be directly incorporated into water streams from leaking storage tanks and sewers, discharge of WWTP effluents, landfill leachates and movement of pollutants through soil to surface and groundwater. Additionally, treated effluents from industrial plants and sewage works can be discharged into surface water. Also, surface and ground water can interact through the hydrologic cycle [13].

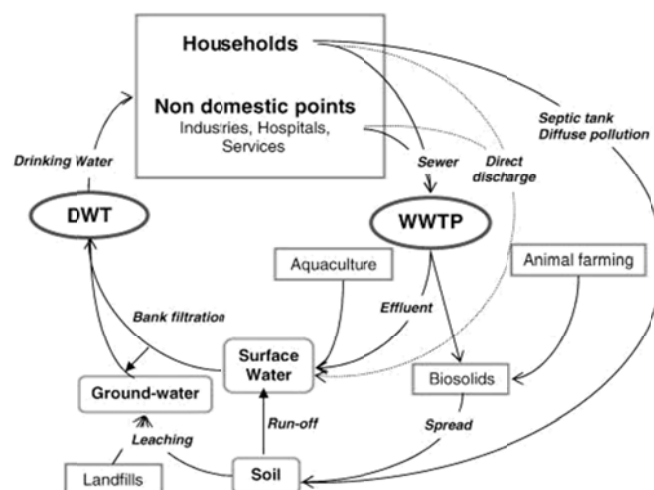


**Figure 1.1.** Emerging compounds in the environment (Adapted from [14])

Of all ECs, agricultural, industrial and household products deserve especial attention. Agriculture accounts for 70% of total withdrawals of freshwater consumed in the world [15] and a large amount of agricultural nutrients and pesticides reach surface and groundwater mainly by direct run-off, leaching, careless disposal of containers and equipment washing [16]. Regarding industrial and domestic sectors, due to the large worldwide consumption of products, an increasing release of chemical additives, reagents and household products as pharmaceuticals and personal care products to the environment through industrial, hospital and domestic drains has been observed in the last decades [7, 17]. Table 1.2. shows a list of selected ECs.

According to that mentioned above, one would expect that ECs are candidates for future regulation depending on the research results about their effects and consequences on the environment and considering their occurrence in water ecosystems.

**Table 1.2.** Classes of ECs [14,18]

Compound class	Examples
Pharmaceuticals	
<i>Veterinary and human antibiotics</i>	Trimethoprim, erythromycin, lincomycin, sulfamethoxazole
<i>Analgesics and anti-inflammatory drugs</i>	Codeine, ibuprofen, acetaminophen, acetylsalicylic acid, diclofenac, fenoprofen
<i>Psychiatric drugs</i>	Diazepam
<i>Lipid regulators</i>	Bezafibrate, clofibrac acid, fenofibrac acid
<i><math>\beta</math>-blockers</i>	Metoprolol, propranolol, timolol
<i>X-ray contrast media</i>	Iopromide, iopamidol, diatrizoate
Steroids and hormones (contraceptives)	Estradiol, estrone, estriol, diethylstilbestrol, testosterone
Personal care products	
<i>Fragrances</i>	Nitro, polycyclic and macrocyclic musks
<i>Sun-screen agents</i>	Benzophenone, methylbenzylidene camphor
<i>Insect repellents</i>	N,N-diethyltoluamide
Antiseptics	Triclosan, chlorophene

**Table 1.2. (continued)** Classes of ECs

Compound class	Examples
Surfactants and surfactant metabolites	Alkylphenol ethoxylates, alkylphenols (nonylphenol and octylphenol), alkylphenol carboxylates
Flame retardants	Polybrominated diphenyl ethers (PBDEs), tetrabromo bisphenol A, tris(2-chloroethyl)phosphate
Industrial additives and agents	Chelating agents (EDTA), aromatic sulfonates
Gasoline additives	Dialkyl ethers, methyl-t-butyl ether (MTBE)
Disinfection by-products	Iodo-THMs, bromoacids, bromoacetonitriles, bromoaldehydes, cyanoformaldehyde, bromate, NDMA
Pesticides	Mecoprop (MCP), 2-methyl-4-chlorophenoxyacetic acid (MCPA), 2,4-dichlorophenoxyacetic acid (2,4-D), dichlorprop (2,4-DP), 2,4,5-trichlorophenoxyacetic acid (2,4,5-T), 4-(2,4-dichlorophenoxy)butyric acid (2,4-DB)

### 1.1.3. Priority and emerging contaminants in Spain

In Spain, it is in progress the Plan nacional de calidad de las aguas: Saneamiento y depuración (PNCA, 2007-2015), which is aimed to implement more efficient sanitation and wastewater treatment systems [19]. Despite that, the processes applied in most of the WWTPs are secondary treatments unable to eliminate xenobiotic compounds. In fact, several investigations on the occurrence of ECs in surface and ground waters of some areas of Spain have pointed out the presence of ECs at significant concentration levels. The most detected priority and emerging contaminants are pesticides, pharmaceutical active compounds and some personal care products [20–25].

These investigations state that the most ubiquitously detected compounds are the pesticides atrazine (and its transformation product desethylatrazine), simazine, terbutylazine, terbutryn, isoproturon, diuron, and alachlor; the pharmaceuticals acetaminophen, diclofenac, codeine, naproxen, ibuprofen, ofloxacin, ciprofloxacin, erythromycin, hydrochlorothiazide, atenolol, ranitidine, ketoprofen, naproxen, carbamazepine, sulfamethoxazole, sulfapyridine, sulfaquinoxaline, furosemide, caffeine, nicotine, atenolol; the musks galaxolide and tonalide; the UV filters

benzophenone-3, 2-ethylhexyl-p-methoxy cinnamate and octocrylene; and the antiseptics triclosan and chlorophene.

Therefore, the application of tertiary treatments is recommended to reduce the impact on natural waters due to the discharge of WWTP effluents and allow the reuse of the latter for different purposes.

## 1.2. Advanced oxidation processes

As regulatory environmental requirements are becoming more stringent because of increasing ecological risks associated with environmental pollution, various treatment technologies are being studied and developed as alternatives to efficiently degrade persistent contaminants. Advanced oxidation processes (AOPs) are methods that can fulfil these requirements. These processes involve the generation of powerful and relatively non-selective transient oxidizing species, primarily the hydroxyl radical ( $\cdot\text{OH}$ ), which have a high oxidation potentials as shown in Table 1.3. [26,27]. The hydroxyl radical is effective to destroy organic chemicals since it is a reactive electrophile which reacts rapidly and non-selectively with almost all electron-rich organic compounds.

**Table 1.3.** Redox potentials of some oxidizing agents [28]

Oxidizing agent	Electrochemical oxidation potential (V, 25°C)
Fluorine (F)	2.87
Hydroxyl radical ( $\cdot\text{OH}$ )	2.86
Oxygen atom (O)	2.42
Ozone molecule ( $\text{O}_3$ )	2.07
Hydrogen peroxide ( $\text{H}_2\text{O}_2$ )	1.78
Chlorine (Cl)	1.36
Chlorine dioxide ( $\text{ClO}_2$ )	1.27
Permanganate ( $\text{MnO}_4$ )	1.24
Oxygen molecule ( $\text{O}_2$ )	1.23

The AOPs can be classified, according to the use of radiation, into photochemical and non-photochemical processes. The radiation may arise from a natural source

(solar light) or from an artificial source (UV-visible radiation lamps). Figure 1.2. shows some AOPs according to this classification.

According to Figure 1.2. most of the AOPs are processes carried out at near ambient temperature and pressure. In general, they involve the combination of oxidizing agents, such as  $\text{H}_2\text{O}_2$  or  $\text{O}_3$ , catalysts, and/or radiation (e.g. ultraviolet, visible) to generate hydroxyl radicals in sufficient concentration to effectively achieve water purification [29].

Advantages of AOPs, compared to other processes, for removing organic chemicals are that they do not transfer the contaminants to a separate phase and usually do not produce a waste stream. They require less energy consumption than other processes as incineration. Some AOPs might be capable of completely mineralize the organic contaminants of effluents allowing the reuse of water. Although complete mineralization is not usually practical as high doses of reagents and/or radiation are required, it can be beneficial the transformation of refractory pollutants into products treatable by cheaper methods such as biological oxidation. Techniques as reverse osmosis and filtration transfer the contaminants to a concentrate phase, which must be disposed of, and adsorption with activated carbon transfers the contaminants to the surface of a solid, which may need to be disposed of once it reaches exhaustion [30,31].

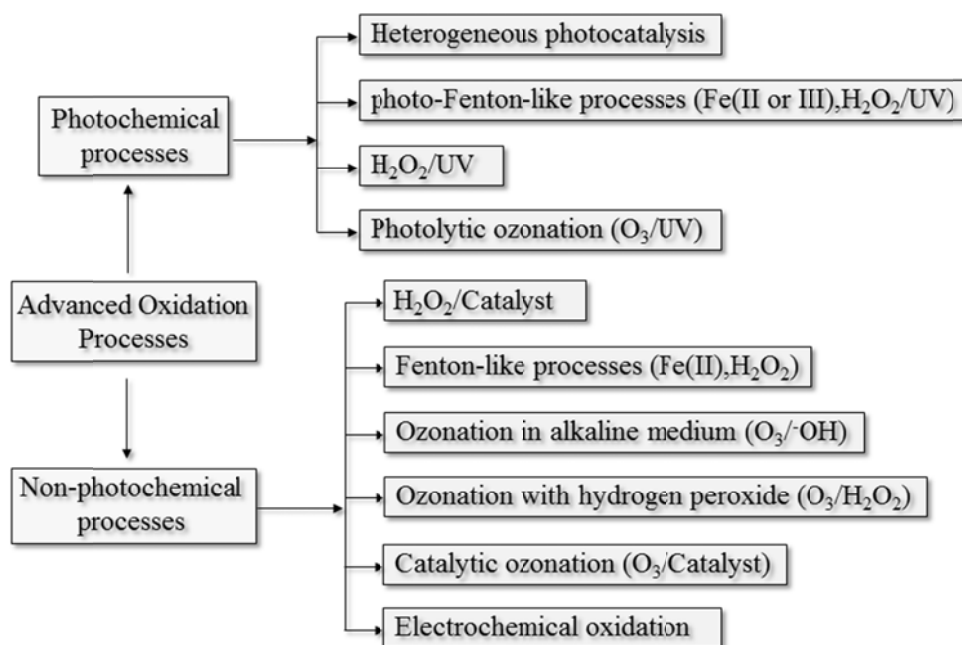


Figure 1.2. Classification of AOPs [28,31]

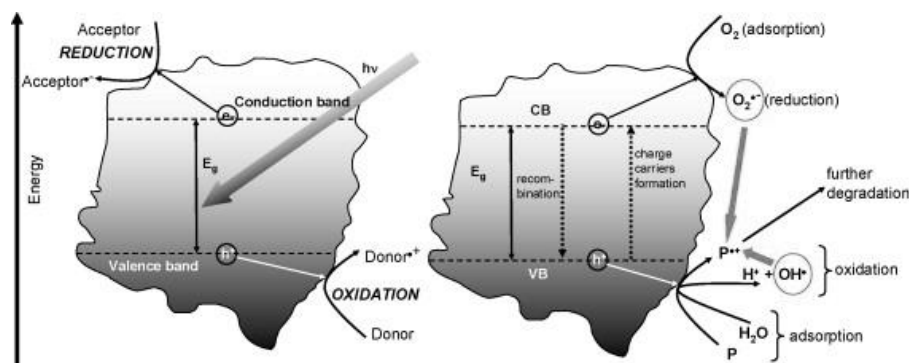
In this work, solar heterogeneous photocatalysis using  $\text{TiO}_2$ , photo-Fenton like processes, catalytic ozonation, photolytic ozonation and photocatalytic ozonation have been studied as AOPs for water treatment processes.

### 1.2.1. Photocatalysis

#### A. Heterogeneous photocatalysis

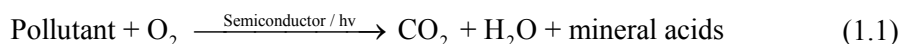
In a heterogeneous photocatalytic processes, the chemical reactions are induced by the photo-excitation of a solid semiconductor as a result of the absorption of electromagnetic radiation possessing enough energy to excite valence band electrons, promoting them to conduction band and generating valence band holes [32].

Photo-oxidation takes place when the target molecule has an oxidation potential less positive than that of the semiconductor valence band. Similarly, photo-reduction occurs when the reduction potential of the molecule is less negative than that of the conduction band, as illustrated in Figure 1.3.



**Figure 1.3.** Schematic representation of the formation of the electron-hole pairs in a semiconductor particle (Taken from [33]).

Degradation and mineralization of organic compounds using heterogeneous photocatalysis can be described, as a whole, as follows [33]:



The rate and efficiency of a photocatalytic reaction depend on factors that govern the kinetics of photocatalysis such as initial concentration of reactant, radiation



flux, mass of catalyst, pH, temperature, and type and concentration of oxidizing species. Table 1.4. briefly summarizes the effect produced by each of these parameters.

**Table 1.4.** Parameters affecting heterogeneous photocatalytic processes and their effects [33]

Parameter	Principal effect
Reactants concentrations	The initial rate of disappearance of the pollutant usually is fitted to a Langmuir–Hinshelwood kinetic. Accordingly, the reaction rate is proportional to the fraction of the surface covered by the substrate, the reaction rate constant, the concentration of species and the reactant adsorption constant. The reaction can be more complex when there are intermediates or other compounds which can compete with the target reactant for adsorption sites.
Mass of catalyst	The reaction rate generally increases with the catalyst concentration until a limiting value, which depends on the working conditions. When catalyst concentration is very high, a photon scavenging effect is obtained since turbidity of the suspension impedes penetration of light in the reactor.
pH	pH may affect the surface properties of the catalyst and the chemical form of the compound to be degraded. Accordingly, pH may have effects on the degradation rate and the setting characteristics.
Temperature	Photocatalytic oxidation is usually performed at room temperature, being the optimum range comprised between 20° and 80°C. However, at very low temperatures (<0°C) the apparent activation energy increases and the desorption of the final product becomes the rate limiting step. On the other hand, when temperature increases above 80°C and approaching to the boiling point of water, the exothermic adsorption of reactants becomes disfavoured and tends to become the rate limiting step.
Radiant flux	The rate of reaction is usually proportional to the radiant flux. This confirms the photo-induced nature of the activation of the catalytic process.
Oxygen concentration	Oxygen may be involved in the formation oxidizing species (superoxide, hydrogen peroxide, hydroxyl radicals) and prevent reduction reactions. Increasing the oxygen concentration in aqueous solution is reported to slightly increase the reaction rate.

Among the known semiconductor photo-catalysts (ZnO, WO<sub>3</sub>, CdS, ZnS, SrTiO<sub>3</sub>, SnO<sub>2</sub>), TiO<sub>2</sub> in its anatase phase, has deserved particular interest due to its high oxidizing power, chemical stability and low cost [34]. Titanium dioxide (anatase) has an energy band gap ( $E_g$ ) of 3.2 eV and can be activated by UV illumination with a wavelength up to 387.5 nm [32]. This catalyst offers a great number of possibilities of application. Nanocrystalline TiO<sub>2</sub> immobilized on supporting materials such as glass, sand, or zeolite can improve the separation efficiency. The incorporation of magnetic components into TiO<sub>2</sub> nanoparticle-based catalysts may, therefore, enhance the separation and recovery of nanosized TiO<sub>2</sub> [34].

Aeroxide® TiO<sub>2</sub> P25 is a commercial titania catalyst that has been established as a standard catalyst because of its relatively high level of activity in many photocatalytic reaction systems [35]. It contains anatase and rutile phases in a mass ratio of about 3:1, with a very low content of amorphous particles (around 1%) [36]. It has a non-porous surface area with a BET surface of  $55 \pm 15 \text{ m}^2 \text{ g}^{-1}$  and crystallite sizes of about 30 nm associated aggregates of about 0.1  $\mu\text{m}$  diameter of [37].

Since, at the ground level, the solar radiation spectrum starts at 300 nm, only 4–5% of the solar energy could be utilized in TiO<sub>2</sub> photocatalytic applications. Compositional doping of TiO<sub>2</sub> has been the approach generally taken to widen the optical response of TiO<sub>2</sub> to visible light wavelengths by narrowing the semiconductor band gap [38]. Some other effects reached by doping titania are: i) the formation of new phases dispersed into the semiconductor which trap the photo-generated charge carriers and inhibits the recombination of generated electron-hole pairs [39,40]; ii) the increasing in the surface area of the catalyst. These effects can lead to an enhanced catalytic performance compared to that of the pristine semiconductor [41,42].

## B. Homogeneous photocatalysis

A typical application of homogeneous photocatalysis is the decomposition of H<sub>2</sub>O<sub>2</sub> catalyzed by ferrous iron (Fe(II)) or ferric iron (Fe(III)) under acidic conditions via a free radical chain reaction which produces  $\cdot\text{OH}$ . Such processes are known as Fenton or Fenton-like systems [26].

The rate of removal of organic pollutants and the extent of mineralization that are reached using the Fe(II)/H<sub>2</sub>O<sub>2</sub> and Fe(III)/H<sub>2</sub>O<sub>2</sub> reagents can be considerably improved by the application of near-UV radiation and visible light. This process is called the photo-Fenton [26]. The enhancement is due to the photo-reduction of

Fe(III) to Fe(II) and the photolysis of  $\text{H}_2\text{O}_2$ , which leads to a higher production of hydroxyl radicals, as shown in Figure 1.4.

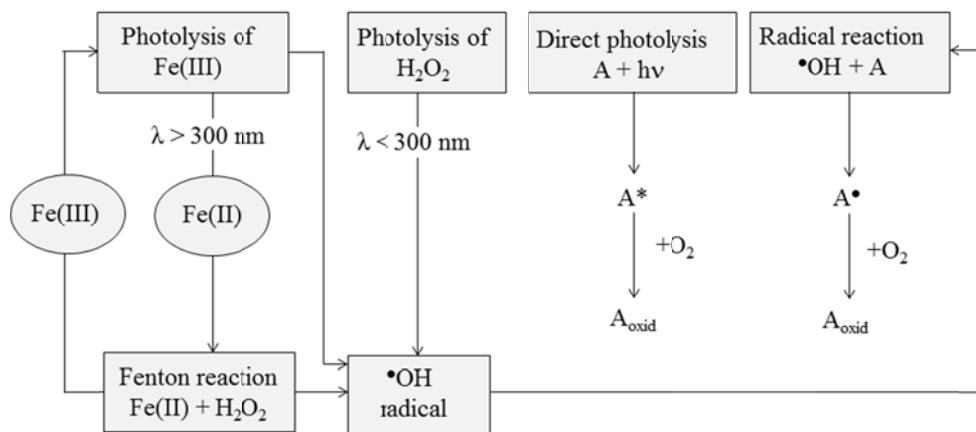


**Figure 1.4.** Scheme of chemical reactions in the photo-Fenton reaction (A is the target contaminant, while  $\text{A}^\bullet$  and  $\text{A}^*$  are reaction intermediates). (Taken from [43])

A limitation of Fenton and photo-Fenton processes is the narrow range of pH this processes can be applied. Thus pH must be kept below 3 to avoid the formation and subsequent precipitation of iron oxyhydroxides species. Another drawback is the need to recover iron ions from solution after the treatment. To overcome these drawbacks, the immobilization of ion species on a solid matrix would enable its use the application of the treatment process at higher pH and the easy recovery of the catalyst [44].

### C. Solar systems

The use of solar radiation as energy source in photocatalytic processes can be economically advantageous as the use of artificial UV lamps might be reduced. However, one of the disadvantages of solar photocatalytic processes is that wavelengths below 290 nm cannot be exploited since radiation under 290 nm is not expected to reach the Earth's surface as it is mostly retained by gases in the atmosphere [45].

As only nearly 4–6% of the total solar spectrum corresponds to UV region, which is usually the most exploitable fraction for photocatalytic processes, it is necessary to develop water detoxification processes that can use both direct and diffuse UV radiation reaching the Earth's surface. To this end, solar reactors with especial designs have been developed to make an efficient use of incident photons. These reactors must fulfill some characteristics as: i) they must be made of transparent materials to allow the photons to reach the water treated, ii) piping and valve

system must resist the pressure of water which normally ranges between 2–7 bar, iii) reactor reflecting surfaces to effectively concentrate the radiation must be made of low-cost, low-density, high-reflectivity materials, being usually aluminum the best choice, and iv) the reactor geometry must favor the complete absorption of incident photons in the system. Usually thermal isolation is not required as usually photocatalytic treatments are carried out at ambient conditions,

Non-concentrating solar collectors are the type of technology most used in solar photocatalytic applications. These collectors are designed for working temperatures lower than 150°C and can make use of both direct and diffuse radiation. Compound parabolic collectors (CPC), which consist of static collectors with a reflection surface following an involute around a cylindrical reactor tube, are widely used in solar photochemical applications and they have been found to provide the best optics for low concentration systems. Due to the reflector design, almost all the UV radiation reaching the CPC aperture area is used for the photocatalytic process in the reactor [46] as shown in Figure 1.4, which is a representation of the effect of solar radiation reflection in a CPC glass with 0° and 35° as incident angles.

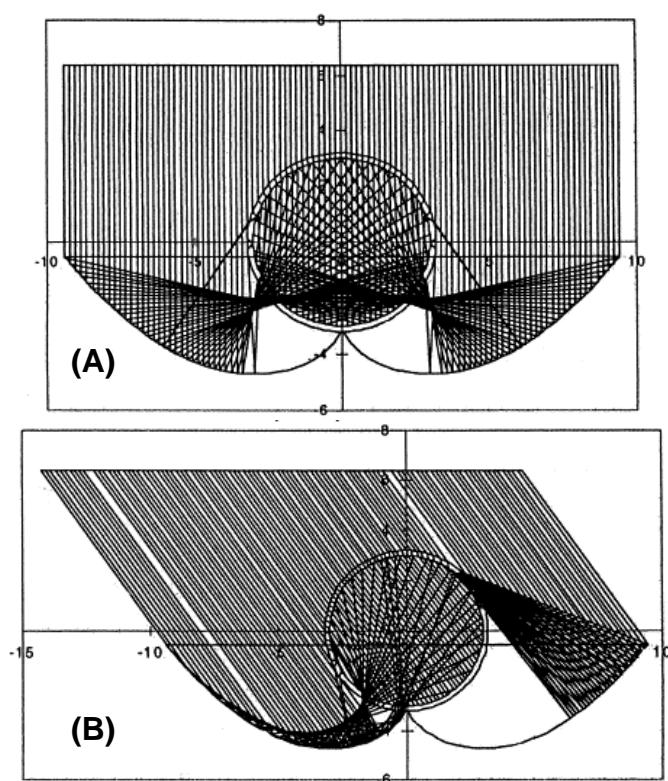


**Figure 1.4.** Representation of an 1-sun concentration factor CPC design and the effect of solar radiation reflection on glass surface for 0° (A) and 35° (B) incident angles (Adapted from [46])

The CPC schematized in Figure 1.4. has a concentration factor (i.e. how much the light reaching the reactor can be concentrated and used [47]) of 1 sun. For heterogeneous processes, it is important to avoid any possible deposition of the catalyst. Thus, the Reynolds number ( $Re$ ) must always be above 4000 to ensure a turbulent flow [46].

A great number of publications on the application of solar photocatalytic processes for the degradation of organic contaminants at laboratory scale [48–51], describe the use of solar simulators, which are provided with mercury or xenon lamps and filters. These small-scale systems allow the prediction of the effect of different parameters of the system as well the feasibility, treatment time appropriate system size as a previous stage for pilot or full-scale research and development.

### 1.2.2. Ozonation treatments

Ozone applications in the treatment of water and wastewater can be as disinfectant or biocide, oxidant to remove organic pollutants and pre or post treatment agent to aid in other unit operations as coagulation, flocculation, sedimentation, biological oxidation and carbon adsorption [52]. This molecule is highly unstable and, therefore, has to be produced on site prior to its use. It reacts selectively with certain organic compounds (e.g., aromatics, alkenes and alkynes). Such reactivity is attributed to its electronic configuration, which makes it an extremely reactive compound. Table 1.5. shows some physicochemical properties of ozone:

**Table 1.5.** Physicochemical properties of ozone [52]

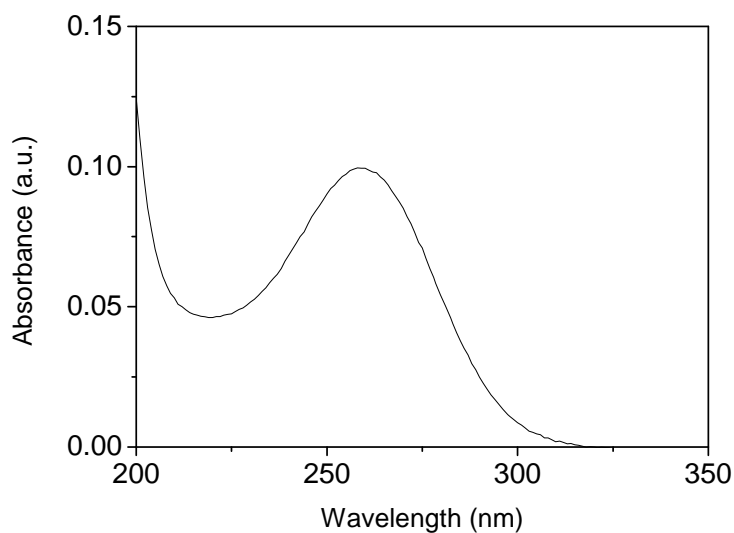
Property	Value
Melting point	-251°C
Boiling point	-112°C
Critical pressure	54.62 atm
Critical temperature	-12.1°C
Specific gravity (-183°C)	1.71 g cm <sup>-3</sup>
Heat of vaporization (-112°C)	2980 cal mol <sup>-1</sup>
Heat of formation (1 atm, 25°C)	33880 cal mol <sup>-1</sup>
Free energy of formation (1 atm, 25°C)	38860 cal mol <sup>-1</sup>

However, as ozone has a selective nature, it has a limited capacity to achieve the complete mineralization of organic matter because of the typical formation and accumulation of intermediates recalcitrant to ozone attack, such as short-chain carboxylic acids or alcohols.

Ozone can also react indirectly with pollutants through secondary oxidants, primarily the hydroxyl radical, generated by aqueous decomposition of ozone. Such decomposition can be accelerated at high pH and by the presence of UV radiation, hydrogen peroxide or catalysts [53].

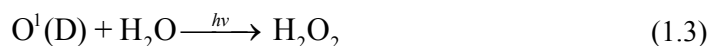
### A. Photolytic ozonation

Figure 1.5. shows the absorption spectrum of aqueous ozone in the UV range [53]. It can be observed a broad band centered at about 254 nm, with a maximum absorption coefficient of  $3314 \text{ L mol}^{-1} \text{ cm}^{-1}$  [54,55]. Thus, in the presence of UV radiation ozone undergoes photolysis that results in the production of hydrogen peroxide. Then, hydrogen peroxide, in turns, can undergo direct photolysis and/or react with ozone itself. Both reactions result in the formation of hydroxyl radicals, thus enhancing the oxidizing power of the system.



**Figure 1.5.** Ozone spectrum in the UV region

There is general agreement on the reactions involved in the  $\text{O}_3/\text{UV}$  oxidation process [56]:



Under these conditions the system has the chemical behaviour of both  $\text{O}_3/\text{H}_2\text{O}_2$  and  $\text{H}_2\text{O}_2/\text{UV}$  systems.

In systems using visible light also ozone photo-dissociation can take place as the ozone molecule can weakly absorb radiation in the visible light region (Chappuis band: 375–603 nm, and Wulf system > 700 nm [57]) leading to photo-dissociation into O (3P) and  $\text{O}_2$  [58].

### B. Catalytic ozonation

Catalyst either dispersed in the aqueous phase or as solids, the latter suspended or in a fixed bed, can be used to improve ozone decomposition leading to a series of reactions that enhance organic compounds depletion.

Black carbon as well as activated carbon have been shown to promote ozone transformation through surface reactions that propagate in the aqueous phase, thus accelerating the ozone transformation into secondary oxidants [59]. Another example of heterogeneous catalytic ozonation is the use of a semiconductor as  $\text{TiO}_2$ . In this case, ozone can be decomposed on Lewis sites of the  $\text{TiO}_2$  surface [60].

Regarding homogeneous catalytic ozonation, ozone decomposition can be carried out by metal ions present in aqueous solution. As an example, Saudela and Brillas reported a catalytic ozonation mechanism in the presence of Fe(II) ions through the formation of an iron complex which is subsequently oxidized by ozone to lead to the formation of hydroxyl radicals [61]. Typical homogeneous catalysts for aqueous ozone reactions are transition metals such as Fe(II), Mn(II), Ni(II) and Ag(I) [62].

The reaction of ozone with hydrogen peroxide can also promote the formation of hydroxyl radicals.  $\text{H}_2\text{O}_2$  reacts slowly with ozone but its conjugate base,  $\text{HO}_2^-$ , is very reactive towards ozone. Therefore, at neutral or alkaline conditions the rate of ozone decomposition in aqueous solution containing hydrogen peroxide is favoured [53].

### C. Photocatalytic ozonation

As a novel AOP, the simultaneous combination of ozone and a photocatalyst in the presence of UV radiation, the so-called photocatalytic ozonation, has attracted high interest recently [63].

In addition to the classical decomposition of aqueous ozone and its photo-dissociation, in photocatalytic ozonation systems assisted by titania (or any other photoactive semiconductor), ozone can generate hydroxyl radicals through the formation of the ozonide radical in the adsorption layer of a catalyst. This radical rapidly reacts with the  $H^+$  in solution to give  $HO_3^{\bullet}$  and subsequently produces the hydroxyl radical [62].

In the photo-Fenton system, both direct and indirect reactions of ozone can take place by decomposition with  $Fe^{2+}$  species and reaction with hydrogen peroxide present in the medium.

Figure 1.6. depicts a scheme which shows the main pathways involved in photocatalytic ozonation systems.

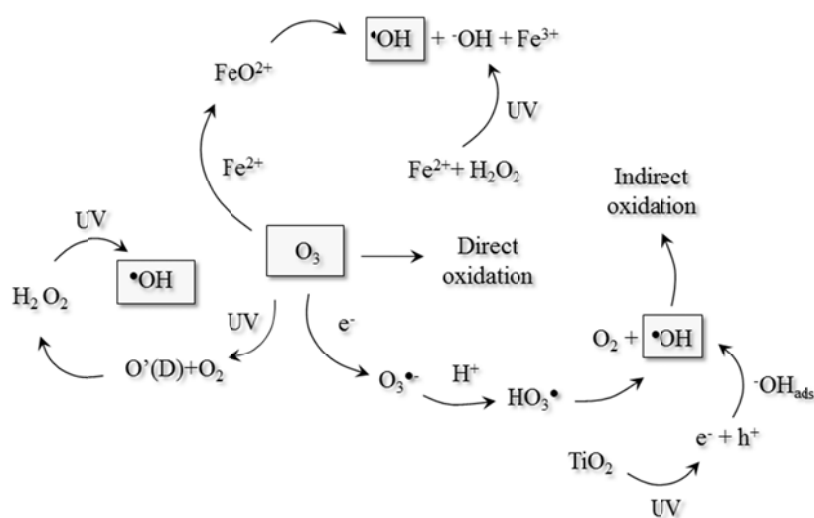


**Figure 1.5.** Pathways of the photocatalytic ozonation assisted by photo-Fenton and heterogeneous photocatalysis

The mechanisms of photocatalytic ozonation through  $O_3/Fe(III)/H_2O_2/UV$  and  $O_3/TiO_2/UV$  are discussed more extensively in Section 3.4. (Results and discussion) of Chapter III.



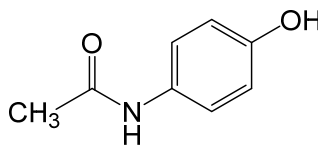
### 1.3. Model compounds used in this investigation

In this research, different emerging and priority pollutants have been selected as model compounds to study their removal in water by different treatments. These compounds, which are representatives of various types of priority and emerging contaminants, are acetaminophen, antipyrine, metoprolol, caffeine, testosterone, bisphenol A, diuron, MCPA, o-phenylphenol and terbuthylazine. These compounds have been subjected to some solar AOPs, including photo-assisted Fenton-like, ozonation and photocatalytic oxidation processes, as well as several combinations of them. Some of their physicochemical properties are summarized next.

#### 1.3.1. Acetaminophen

Acetaminophen (ACE), also known as paracetamol or tylenol, is one of the most sold over-the-counter analgesic, anti-inflammatory and antipyretic medication. It is found in over 100 products either alone or in combination with other medications. Liver toxicity is probably one of the commonest outcomes from acute ACE overdose [64,65]. It is often detected in sewage treatment plant effluents, surface water and drinking water [66]. ACE has been found to cause multiple endocrine disturbances in the human adult testis, particularly in the interstitial compartment [67]. Table 1.6. shows some of its main physicochemical properties.

**Table 1.6.** Physicochemical properties of acetaminophen [68]

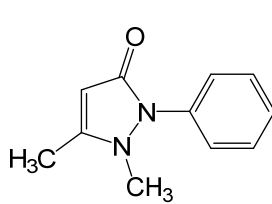
Molecular formula	C <sub>8</sub> H <sub>9</sub> NO <sub>2</sub>	Chemical structure: 
Molar mass	151.16 g mol <sup>-1</sup>	
Melting point	170°C	
Water solubility	14 mg mL <sup>-1</sup> at 25°C	
Log Kow	0.46	
Toxicity	LC <sub>50</sub> (48 h, <i>D. Magna</i> ): 20.1 mg L <sup>-1</sup>	

#### 1.3.2. Antipyrine

Antipyrine (ANT), also known as phenazone, is an analgesic and antipyretic largely consumed in many countries (e.g., ~0.35 g consumed/year-person in Germany). ANT represents one of the most commonly identified pharmaceuticals in the environment with a high environmental persistence. Long-term exposure to

ANT can cause organ damages due to its toxicity toward mucosa and lungs. Its removal within conventional wastewater treatment facilities is reported to be very poor [69,70]. Table 1.7. shows some physicochemical properties of antipyrine.

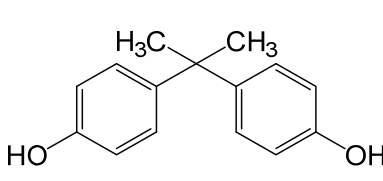
**Table 1.7.** Physicochemical properties of antipyrine [70,71]

Molecular formula	$C_{11}H_{12}N_2O$	Chemical structure:
Molar mass	$188.23 \text{ g mol}^{-1}$	
Melting point	$114^\circ\text{C}$	
Water solubility	$51.9 \text{ mg mL}^{-1}$ at $25^\circ\text{C}$	
Log Kow	0.38	
Toxicity	$LC_{50}$ (96 h, <i>Fresh water fish</i> ): $500 \text{ mg L}^{-1}$	

### 1.3.3. Bisphenol A

Bisphenol A (BIS) is a high production-volume chemical used as plasticizer in the manufacturing of polycarbonate plastics as well as epoxy resins. The effects of BIS at the tissue level include alterations in the histo-architecture of the mammary gland, prostate, testis, ovaries, adipose tissue, and brain. It has been detected in rivers, municipal sewage treatment plants effluents, tap water and bottled water [72,73]. Exposure to this endocrine disruptor in humans is mainly through food although other nonfood exposures such as residential water supply have been also suggested [72]. BIS is rapidly metabolized by the body but not by the fetal compartment where it can accumulate [74]. Table 1.8. shows some physicochemical properties of bisphenol A.

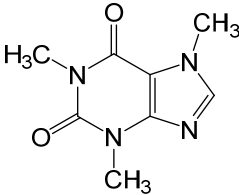
**Table 1.8.** Physicochemical properties of bisphenol A [75–78]

Molecular formula	$C_{15}H_{16}O_2$	Chemical structure:
Molar mass	$228.29 \text{ g mol}^{-1}$	
Melting point	$156^\circ\text{C}$	
Water solubility	$0.2 \text{ mg mL}^{-1}$ at $25^\circ\text{C}$	
Log Kow	3.2	
Toxicity	$LC_{50}$ (48 h, <i>D. Magna</i> ): $12.8 \text{ mg L}^{-1}$	

### 1.3.4. Caffeine

Caffeine (CAF) is probably the most widely used psychoactive drug [79]. The occurrence of CAF has been documented in marine and estuarine systems, natural waterways, surface water and WWTP effluents reflecting the fact that this compound is not completely removed in many sewage treatment plants [80]. CAF may cause subtle effects acting as a pseudo-persistent pollutant due to its continuous release in the environment [81]. CAF-exposure during pregnancy has been found to induce fetal skeletal growth retardation in rats [82,83].

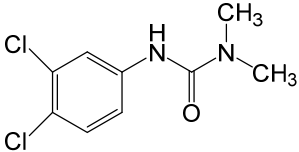
**Table 1.9.** Physicochemical properties of caffeine [71,84]

Molecular formula	$C_8H_{10}N_4O_2$	Chemical structure:
Molar mass	$194.19 \text{ g mol}^{-1}$	
Melting point	$237^\circ\text{C}$	
Water solubility	$16 \text{ mg mL}^{-1}$ at $25^\circ\text{C}$	
Log Kow	0.07	
Toxicity	$LC_{50}$ (24 h, <i>D. Magna</i> ): $683.7 \text{ mg L}^{-1}$	

### 1.3.5. Diuron

Diuron (DIU) is an herbicide derived from urea that is considered to be a priority hazardous substance by the EU [85], as a consequence, its use will be progressively suppressed within 20 years of delivery [86]. Due to its high persistence (one month to one year), DIU can be found in many environments such as soil, sediments and water. Toxic effects of DIU have been reported on freshwater invertebrates (e.g. *Lumbriculus variegatus*, *Hyalella azteca* and *Physa gyrina*) affecting their growth and survival [87].

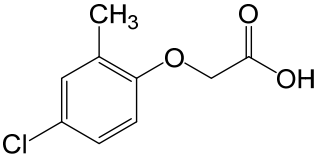
**Table 1.10.** Physicochemical properties of diuron [86,88,89]

Molecular formula	$C_9H_{10}Cl_2N_2O$	Chemical structure:
Molar mass	$233.09 \text{ g mol}^{-1}$	
Melting point	$159^\circ\text{C}$	
Water solubility	$0.042 \text{ mg mL}^{-1}$ at $20^\circ\text{C}$	
Log Kow	2.6	
Toxicity	$LC_{50}$ (48 h, <i>D. Magna</i> ): $1.4 \text{ mg L}^{-1}$	

### 1.3.6. 4-chloro-2-methoxyphenylacetic acid (MCPA)

MCPA is a selective broadleaf weed-control herbicide and one of the pesticides most frequently found in drinking water [90]. It has been reported to have endocrine-disrupting activity in invertebrates [91]. Some of its physicochemical properties are summarized in Table 1.11.

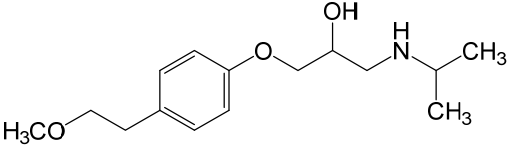
**Table 1.11.** Physicochemical properties of MCPA

Molecular formula	C <sub>9</sub> H <sub>9</sub> ClO <sub>3</sub>	Chemical structure: 
Molar mass	200.60 g mol <sup>-1</sup>	
Melting point	121°C	
Water solubility	293 mg mL <sup>-1</sup> at 20°C	
Log Kow	1.42	
Toxicity	LC <sub>50</sub> (96h, <i>Rainbow trout</i> ): 232 mg L <sup>-1</sup>	

### 1.3.7. Metoprolol

Metoprolol (MTP) is a cardioselective β<sub>1</sub>-adrenergic blocking agent used for acute myocardial infarction [92]. MTP and atenolol together account for more than 80% of total β-blockers consumption in Europe. Particularly, during the last years, MTP usage increased by a factor of 4 [93]. This β-blocker, frequently detected in water bodies [94,95], affects the reproduction and growth of some species (e.g. rainbow trout) [96].

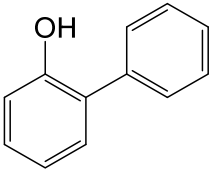
**Table 1.12.** Physicochemical properties of metoprolol [97]

Molecular formula	C <sub>15</sub> H <sub>25</sub> NO <sub>3</sub>	Chemical structure: 
Molar mass	267g mol <sup>-1</sup>	
Melting point	120°C	
Water solubility	169 mg mL <sup>-1</sup> at 25°C	
Log Kow	1.88	
Toxicity	LC <sub>50</sub> (48 h, <i>D. Magna</i> ): 76.2 mg L <sup>-1</sup>	

### 1.3.8. o-phenylphenol

Production of o-phenylphenol (OPP) and use in rubber chemicals, food packaging, as an intermediate for dyes, and as a food preservative may result in its release to the environment through various waste streams; its use as a pesticide and household disinfectant and for sapstain control in freshly cut lumber is expected to result in its direct release to the environment [98]. OPP is one of the substances being under revision by EU since it was identified as a potential endocrine disruptor. Then its use as a preservative is being subjected to evaluation [99].

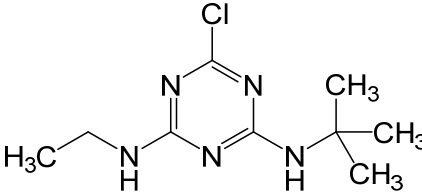
**Table 1.13.** Physicochemical properties of o-phenylphenol

Molecular formula	C <sub>12</sub> H <sub>10</sub> O	Chemical structure: 
Molar mass	170.21 g mol <sup>-1</sup>	
Melting point	60°C	
Water solubility	0.2 mg mL <sup>-1</sup> at 25°C	
Log Kow	3.09	
Toxicity	LC <sub>50</sub> (72 h, <i>D. Magna</i> ): 0.71 mg L <sup>-1</sup>	

### 1.3.9. Terbutylazine

Terbutylazine (TBA) is a selective herbicide, widely used within the EU; however its frequent detection in surface and ground water, together with its intrinsic toxicological properties, may pose a risk for both human and environmental health [100].

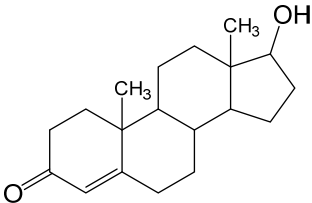
**Table 1.14.** Physicochemical properties of terbutylazine

Molecular formula	C <sub>9</sub> H <sub>16</sub> ClN <sub>5</sub>	Chemical structure: 
Molar mass	229.71 g mol <sup>-1</sup>	
Melting point	179°C	
Water solubility	0.0085 mg mL <sup>-1</sup> at 25°C	
Log Kow	3.40	
Toxicity	LC <sub>50</sub> (48 h, <i>D. Magna</i> ): 21.2 mg L <sup>-1</sup>	

### 1.3.10. Testosterone

Testosterone (TST) is a representative androgenic hormone that can occur artificially or naturally. Agricultural application of manure is an important source of TST and other steroid hormones that are reported to have a strong sorption in the soil, from which they are thought to be transported to ground and surface waters [101]. Some of its main physicochemical properties are shown in Table 1.15.

**Table 1.15.** Physicochemical properties of testosterone [102,103]

Molecular formula	$C_{19}H_{28}O_2$	Chemical structure: 
Molar mass	$288.42 \text{ g mol}^{-1}$	
Melting point	$155^\circ\text{C}$	
Water solubility	$0.025 \text{ mg mL}^{-1}$ at $25^\circ\text{C}$	
Log Kow	3.22	
Toxicity	$LC_{50}$ (96h, <i>Neomysis integer</i> ): $5.6 \text{ mg L}^{-1}$	

## 1.4. Objectives

Given the global concern owing to the presence of emerging contaminants in aquatic ecosystems, the present study aims to contribute with new results and discussions leading to the development of more efficient strategies for the depletion of such contaminants in water. To this end, various AOPs were applied to treat some contaminants frequently detected in water, which have been selected as model compounds, namely acetaminophen, antipyrine, bisphenol A, caffeine, diuron, metoprolol, MCPA, o-phenylphenol, terbuthylazine and testosterone. This purpose is intended to be achieved by conducting the following specific research objectives:

**OBJECTIVE 1: Application of AOPs at pilot scale in a CPC reactor using solar radiation for the degradation of a mixture of emerging compounds in ultrapure water and municipal wastewater:**

Specific objectives of this piece of research are to:

- 1.1 Conduct pilot experiments to degrade mixtures of emerging compounds by the application of homogeneous photocatalytic systems based on Fe(III) and Fe(III)/H<sub>2</sub>O<sub>2</sub> in the presence of solar radiation.
- 1.2 Evaluate the application of ozonation and solar photolytic ozonation.
- 1.3 Evaluate the effect of the joint application of homogeneous photocatalysis based on Fe(III) and ozonation.
- 1.4 Study the application of heterogeneous photocatalytic systems based on the use of Aeroxide® TiO<sub>2</sub> P25 as catalyst.
- 1.5 Evaluate the effect of the joint application of heterogeneous photocatalysis based on TiO<sub>2</sub> and ozonation.
- 1.6 Determine the kinetic regime of ECs mineralization (i.e., TOC removal).
- 1.7 Validate the results obtained in ultrapure water through the application of the oxidation systems to treat real wastewater samples containing a mixture of selected emerging contaminants.

**OBJECTIVE 2: Improvement of heterogeneous photocatalytic processes based on TiO<sub>2</sub> by the application of photocatalysts with improved adsorption and separation properties.**

Specific objectives of this piece of research are to:

- 2.1 Prepare photo-active magnetic catalysts based on titania particles on activated carbon.
- 2.2 Characterize the synthesized catalysts and evaluate their applicability for the degradation of emerging compounds in ultrapure water at laboratory scale using simulated solar light in processes of photocatalysis and photocatalytic ozonation.
- 2.3 Optimize the load of iron and titania on the catalysts.
- 2.4 Evaluate the effect of the wavelength of the radiation applied on the photocatalysts performance.
- 2.5 Evaluate the stability and reusability of the photocatalysts through successive photocatalytic ozonation runs.

**OBJECTIVE 3: Preparation of TiO<sub>2</sub> catalysts doped with B to improve the performance of the catalyst:**

Specific objectives of this piece of research are to:

- 3.1 Prepare photoactive enhanced titania powder catalysts by doping TiO<sub>2</sub> with boron and optimize the boron load in the catalysts.
- 3.2 Characterize the synthesized catalysts and evaluate their application for the degradation of emerging compounds in ultrapure water at laboratory scale using simulated solar light.
- 3.3 Evaluate the stability and reusability of the photocatalyst through successive photocatalytic ozonation runs.

**1.5. Organization of the Thesis**

---

Results of this Thesis are presented as a collection of research articles, which either have already been published or submitted for publication to scientific international journals. In addition, **Chapter I** and **Chapter II** are presented as an introduction to the topic of the Thesis and as a detailed description of the experimental methods, respectively.

**Chapter I** provides the background information about the research problem: the presence of emerging contaminants in water and the use of advanced oxidation processes to deal with this kind of pollutants. The general and specific objectives of the Thesis are also presented.

In **Chapter II** a description of the experimental procedures and analytical methods followed throughout the research is presented.

Results of the studies conducted to achieve **Objective 1** are presented in **Chapter III** and **Chapter IV**. **Chapter III** describes the application of ozonation, photocatalytic oxidation processes based on conventional catalysts (TiO<sub>2</sub> and Fenton like) and the joint application of both in the treatment of a mixture of six emerging contaminants at pilot-scale using solar radiation as energy source in ultrapure water. The target contaminants are acetaminophen, antipyrine, bisphenol A, caffeine, metoprolol and testosterone. **Chapter IV** reports on the use of the above-mentioned treatment systems for the degradation of emerging contaminants in a secondary effluent from a municipal wastewater treatment plant in the depletion of such contaminants in a matrix of urban wastewater.



**Objective 2** is addressed in **Chapter V** and **Chapter VI**. **Chapter V** focuses on the synthesis and characterization of a titania supported on magnetic activated carbon composite photocatalyst, which was satisfactorily used for the degradation of metoprolol in water by ozonation, photocatalysis and photocatalytic ozonation processes carried out at laboratory scale using artificial solar radiation. Then, some attempts to enhance the magnetic separability and photoactivity of activated carbon–titania photocatalysts were carried out as described in **Chapter VI**. The catalyst reusability and activity under different radiation wavelengths were also evaluated as reported in this chapter.

**Chapter VII** describes the preparation of a boron-doped titania catalyst according to the **Objective 3**. This catalyst was characterized and used for the depletion of a mixture of pesticides chosen as target contaminants, namely diuron, o-phenylphenol, MCPA and terbuthylazine.

Main conclusions of the research are summarized in **Chapter VIII**. Finally a list of the journal publications and conference papers resulting from the whole work is presented in an **Annex** chapter.

## 1.6. References

---

- [1] S.L. Postel, *Entering an era of water scarcity: the challenges ahead*, Ecol. Appl. 10 (2000) 941–948.
- [2] T.L. Anderson, B. Scarborough, L.R. Watson, *Water crises, water rights, and water markets*, in: *Encyclopedia of energy, natural resource, and environmental economics: resources*, Elsevier Science, 2013.
- [3] K. Kümmerer, *The presence of pharmaceuticals in the environment due to human use – present knowledge and future challenges*, J. Environ. Manage. 90 (2009) 2354–2366.
- [4] E. Corcoran, C. Nellesmann, E. Baker, R. Bos, D. Osborn, H. Savelli, *Sick Water? The central role of wastewater management in sustainable development. A rapid response assessment*, United Nations Environment Programme, UN-HABITAT, GRID-Arendal, Norway, 2010.
- [5] World Health Organization (WHO), *The world health report 2002: Reducing Risks, Promoting Healthy Life*, Sadag, Geneva, 2002.

- [6] J.C. Glen, T.J. Gordon, *The Millennium Project: Challenges we face at the millennium, technological forecasting and social change* 66, Elsevier Inc, New York, 2001.
- [7] W.A. Jury, H.J. Vaux, *The emerging global water crisis: Managing scarcity and conflict between water users*, in: *Advances in Agronomy*, Elsevier Inc., 2007.
- [8] *Directive of the European Parliament and of the council 2000/60/EC, Establishing a framework for community action in the field of water policy. Official Journal C513, 23/10/2000.*
- [9] T. Deblonde, C.C. Leguille, P. Hartemann, *Emerging pollutants in wastewater: A review of the literature*, *Int. J. Hyg. Environ. Health.* 214 (2011) 442–448.
- [10] M.J. Martínez-Bueno, M.J. Gomez, S. Herrera, M.D. Hernando, A. Agüera, A.R. Fernández-Alba, *Occurrence and persistence of organic emerging contaminants and priority pollutants in five sewage treatment plants of Spain: Two years pilot survey monitoring*, *Environ. Pollut.* 164 (2012) 267–273.
- [11] *Directive of the European Parliament and of the council 2008/105/EC, On environmental quality standards in the field of water policy, amending and subsequently repealing Council Directives 82/176/EEC, 83/513/EEC, 84/156/EEC, 84/491/EEC, 86/280/EEC and amending Directive 2000/60/EC of the European Parliament and of the Council.*
- [12] European Commission, *Environment and Water: proposal to reduce water pollution risks - IP/12/88 31/01/2012.*
- [13] J.L. Arumí, D. Rivera, E. Muñoz, M. Billib, *Interactions between groundwater and surface water in the Bio Bio region of Chile*, *Obras y Proyectos* 12 (2012) 4–13.
- [14] M. Petrović, S. González, D. Barceló, *Analysis and removal of emerging contaminants in wastewater and drinking water*, *TrAC-Trends Anal. Chem.* 10 (2003) 685–696.
- [15] A. Calzadilla, K. Rehdanz, R.S.J. Tol, *The economic impact of more sustainable water use in agriculture: A computable general equilibrium analysis*, *J. Hydrol.* 384 (2010) 292–305.
- [16] I.K. Konstantinou, D.G. Hela, T.A. Albanis, *The status of pesticide pollution in surface waters (rivers and lakes) of Greece. Part I. Review on occurrence and levels*, *Environ. Pollut.* 141 (2003) 555–570.

- [17] M. Stuart, D. Lapworth, E. Crane, A. Hart, *Review of risk from potential emerging contaminants in UK groundwaters*, *Sci. Total Environ.* 446 (2012) 1–21.
- [18] D. Barceló. *Emerging pollutants in water analysis*, *TrAC-Trend Anal. Chem.* 22 (2003) 14–16.
- [19] Ministerio de Medio Ambiente del Gobierno de España, *Plan Nacional de Calidad de las Aguas: Saneamiento y Aprovechamiento, 2007–2015*.
- [20] A. Jurado, E. Vázquez-Suñé, J. Carrera, M. López de Alda, E. Pujades, D. Barceló, *Emerging organic contaminants in groundwater in Spain: A review of sources, recent occurrence and fate in a European context*, *Sci. Total Environ.* 440 (2012) 82–94.
- [21] G. Teijon, L. Candela, K. Tamoh, A. Molina-Díaz, A.R. Fernández-Alba *Occurrence of emerging contaminants, priority substances (2008/105/CE) and heavy metals in treated wastewater and groundwater at Depurbaix facility (Barcelona, Spain)*, *Sci. Total Environ.* 408 (2010) 3584–3595.
- [22] F. Bono-Blay, A. Guart, B. de la Fuente, Pedemonte, M.P. Pastor, A. Borrell, S. Lacorte, *Survey of phthalates, alkylphenols, bisphenol A and herbicides in Spanish source waters intended for bottling*, *Environ. Sci. Pollut. Res.* 19 (2012) 3339–3349.
- [23] M.J. Martínez, M.J. Gomez, S. Herrera, M.D. Hernando, A. Agüera, A.R. Fernández-Alba, *Occurrence and persistence of organic emerging contaminants and priority pollutants in five sewage treatment plants of Spain: Two years pilot survey monitoring*, *Environ. Pollut.* 164 (2012) 267–273.
- [24] J. Robles-Molina, B. Gilbert-López, J.F. García-Reyes, A. Molina-Díaz, *Monitoring of selected priority and emerging contaminants in the Guadalquivir River and other related surface waters in the province of Jaén, South East Spain*, *Sci. Total Environ.* 479–480 (2014) 247–257.
- [25] Y. Cabeza, L. Candela, D. Ronen, G. Teijon, *Monitoring the occurrence of emerging contaminants in treated wastewater and groundwater between 2008 and 2010. The Baix Llobregat (Barcelona, Spain)*, *J. Hazard. Mat.* 239–240 (2012) 32–39.
- [26] U.S. Environmental Protection Agency, *Handbook on advanced photochemical oxidation processes*, Office of Research and Development, Washington DC, 1998.
- [27] R. Munter, *Advanced oxidation processes – current status and prospects*, *Proc. Estonian Acad. Sci. Chem.* 50 (2001) 59–80.

- [28] O. Legrini, E. Oliveros y A.M. Braun, *Photochemical processes for water treatment*, Chem. Rev. 93 (1993) 671–698.
- [29] W.H. Glaze, J.W. Kang, D.H. Chapin, *The chemistry of water treatment processes involving ozone, hydrogen peroxide and UV-radiation*, Ozone-Sci. Eng. 9 (1987) 335–352.
- [30] K.J. Howe, D.W. Hand, J.C. Crittenden, R.R. Trussell, G. Tchobanoglous, *MWH's Water Treatment: Principles and Design*, John Wiley, New Jersey, 2012.
- [31] X. Domènech, W.F. Jardim, M.I. Litter, *Procesos avanzados de oxidación para la eliminación de contaminantes*, in: *Eliminación de contaminantes por fotocatalisis heterogénea*, Texto colectivo elaborado por la Red CYTED VIII-G, 2004.
- [32] B. Ohtani, *Preparing articles on photocatalysis—beyond the illusions, misconceptions, and speculation*, Chem. Lett. 37 (2008) 217–229.
- [33] S. Malato, P. Fernández-Ibáñez, M.I. Maldonado, J. Blanco, W. Gernjak, *Decontamination and disinfection of water by solar photocatalysis: Recent overview and trends*, Cat. Today 147 (2009) 1–59.
- [34] Y. Ruzmanova, M. Stoller, A. Chianese, *Photocatalytic treatment of olive mill wastewater by magnetic core titanium dioxide nanoparticles*, Chem. Eng. Trans. 32 (2013) 2269–2274.
- [35] B. Ohtani, O.O. Prieto-Mahaney, D. Li, R. Abe, *What is Degussa (Evonik) P25? Crystalline composition analysis, reconstruction from isolated pure particles and photocatalytic activity test*, J. Photochem. Photobiol. A Chem. 216 (2010) 179–182.
- [36] T. Ohno, K. Sarukawa, K. Tokieda, M. Matsumura, *Morphology of a TiO<sub>2</sub> photocatalyst (Degussa, P-25) consisting of anatase and rutile crystalline phases*, J. Catal. 203 (2001) 82–86.
- [37] E. Grabowska, H. Remita, A. Zaleska, *Photocatalytic activity of TiO<sub>2</sub> loaded with metal clusters*, Physicochem. Probl. Miner. Process. 45(2010) 29–38.
- [38] C.A. Gimes, G.K. Mor, *TiO<sub>2</sub> nanotube arrays: Synthesis, properties, and applications*, Springer Science Bussines Media, LLC, 2009.
- [39] P. Dharmarajan, A. Sabastiyan, M. Yosuva Suvaikin, S. Titus, C. Muthukumar, *Photocatalytic degradation of reactive dyes in effluents employing copper doped titanium dioxide nanocrystals and direct sunlight*, Chem. Sci. Trans. 2 (2013) 1450–1458.

- [40] A. Zalezka, *Doped-TiO<sub>2</sub>: A review*, Recent Patents on Engineering 2 (2008) 57-64.
- [41] W. Zhou, Z. Lin Wan, *Three-dimensional nanoarchitectures: designing next-generation devices*, Springer, 2011.
- [42] L.L. Long, A.Y. Zhang, J. Yang, X. Zhang, H.Q. Yu, *A green approach for preparing doped TiO<sub>2</sub> single crystals*, ACS Appl. Mater. Interfaces 6 (2014) 16712-16720.
- [43] S.M. Kim, S.U. Geissen, A. Vogelpohl, *Landfill Leachate Treatment by a photoassisted Fenton Reaction*, Wat. Sci. Tech. 35 (1997) 239-248.
- [44] D. Mantzavinos, D. Kassinos, *Removal of residual pharmaceuticals from aqueous systems by advanced oxidation processes*, Environ. Int. 35 (2009) 402-417.
- [45] J.L. Lean, *Short term, direct indices of solar variability*, Space Sci. Rev. 94 (2000) 39-51.
- [46] D. Robert, S. Malato, *Solar photocatalysis: a clean process for water detoxification*, Sci. Total Environ. 291 (2002) 85-97.
- [47] R. Hastings, M. Wall, *Sustainable solar housing: Exemplary buildings and technologies*, Quicksilver Drive, Sterling USA, 2012.
- [48] V. Romero, F. Méndez-Arriaga, P. Marco, J. Giménez, S. Esplugas, *Comparing the photocatalytic oxidation of metoprolol in a solarbox and a solar pilot plant reactor*, Chem. Eng. J. 254 (2014) 17-29.
- [49] I. Michael, E. Hapeshi, C. Michael, D. Fatta-Kassinos, *Solar Fenton and solar TiO<sub>2</sub> catalytic treatment of ofloxacin in secondary treated effluents: Evaluation of operational and kinetic parameters*, Water Res. 44 (2010) 5450-5462.
- [50] B. Bayarri, J. Giménez, M.I. Maldonado, S. Malato, S. Esplugas, *2,4-Dichlorophenol degradation by means of heterogeneous photocatalysis. Comparison between laboratory and pilot plant performance*, Chem. Eng. J. 232 (2013) 405-417.
- [51] L. Prieto-Rodríguez, S. Miralles-Cuevas, I. Oller, P. Fernández-Ibáñez, A. Agüera, J. Blanco, S. Malato, *Optimization of mild solar TiO<sub>2</sub> photocatalysis as a tertiary treatment for municipal wastewater treatment plant effluents*, Appl. Catal. B-Environ. 128 (2012) 119-125.
- [52] F.J. Beltrán, *Ozone reaction kinetics for water and wastewater systems*, Lewis Publishers, CRC Press. Boca Raton, Florida USA, 2003.

- [53] S.J. Masten, S.H.R. Davies, *The use of ozonation to degrade organic contaminants in wastewaters*, Environ. Sci. Technol. 28 (1994) 180A–185A.
- [54] C. von Sonntag, U. von Gunten, *Chemistry of ozone in water and wastewater treatment. From basic principles to applications*, IWA Publishing, Glasgow, 2012.
- [55] L. Forni, D. Bahnemann, E.J. Hart, *Mechanism of the hydroxide ion initiated decomposition of ozone in aqueous solution*, J. Phys. Chem. 86 (1982) 255–259.
- [56] R. Andreozzi, V. Caprio, A. Insola, R. Marotta, *Advanced oxidation processes (AOP) for water purification and recovery*, Catal. Today 53 (1999) 51–59.
- [57] J. Brion, A. Chakir, J. Charbonnier, D. Daumont, C. Parisse, J. Malicet, *Absorption spectra measurements for the ozone molecule in the 350–830 nm region*, J. Atmos. Chem. 30 (1998) 291–299.
- [58] M. Früchtl, C. Janssen, T. Röckmann, *Isotope effects in photo dissociation of ozone with visible light*, Geophys. Res. Abstr. 16 (2014) EGU2014-7214.
- [59] H. Valdés, C.A. Zaror, *Heterogeneous and homogeneous catalytic ozonation of benzothiazole promoted by activated carbon: Kinetic approach*, Chemosphere 65 (2006) 1131–1136.
- [60] J. Nawrocki, B. Kasprzyk-Hordern, *The efficiency and mechanisms of catalytic ozonation*, Appl. Catal. B-Environ. 99 (2010) 27–42.
- [61] R. Sauleda, E. Brillas, *Mineralization of aniline and 4-chlorophenol acidic solution by ozonation catalyzed with  $Fe^{2+}$  and UVA light*, Appl. Catal. B-Environ. 29 (2001) 135–145.
- [62] A.Ö. Yıldırım, Ş. Gül, O. Eren, E. Kuşvuran, *A comparative study of ozonation, homogeneous catalytic ozonation, and photocatalytic ozonation for C.I. reactive red 194 azo dye degradation*, Clean – Soil, Air, Water, 39 (2011) 795–805.
- [63] T.E. Agustina, H.M. Ang, V.K. Vareek, *A review of synergistic effect of photocatalysis and ozonation on wastewater treatment*, J. Photochem. Photobiol. C Photochem. Rev. 6 (2005) 264–273.
- [64] K. Shankar, H.M. Mehendale, Acetaminophen, Encyclopedia of Toxicology (Third Edition), Elsevier, 2014.
- [65] D.K. Baheti, *World clinics: anesthesia, critical care, and pain - pain management*, in *Labor and Delivery*, Jaypee Brothers Medical Publishers, 2014.

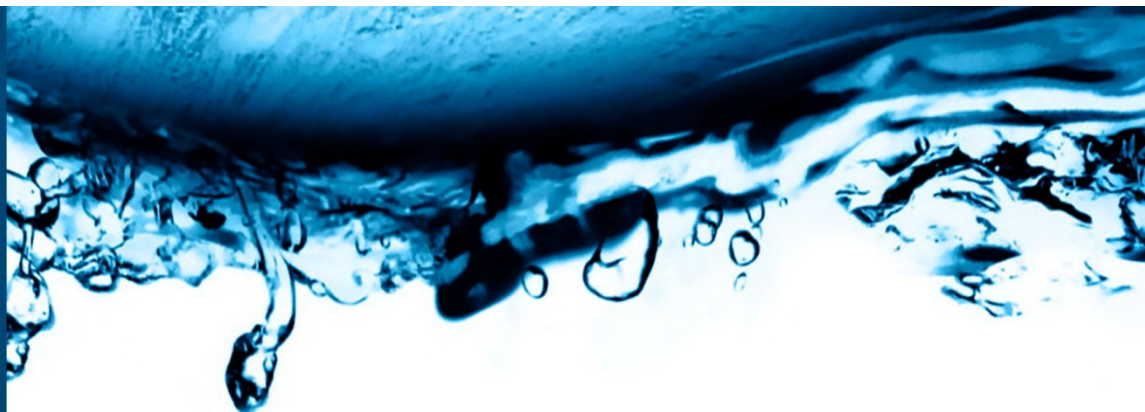
- [66] M.D.G. de Luna, M.L. Veciana, C.C. Su, M.C. Lu, *Acetaminophen degradation by electro-Fenton and photoelectro-Fenton using a double cathode electrochemical cell*, J. Hazard. Mater. 217–218 (2012) 200–207.
- [67] O. Albert, C. Desdoits-Lethimonier, L. Lesné, A. Legrand, F. Guillé, K. Bensalah, N. Dejucq-Rainsford, B. Jégou, *Paracetamol, aspirin and indomethacin display endocrine disrupting properties in the adult human testis in vitro*, Hum. Reprod. 28 (2013) 1890–1898.
- [68] G.H. Han, H.G. Hur, S.D. Kim, *Ecotoxicological risk of pharmaceuticals from wastewater treatment plants in Korea: occurrence and toxicity to Daphnia magna*, Environ. Toxicol. Chem. 25 (2006) 265–271.
- [69] C. Tan, N. Gao, Y. Deng, W. Rong, S. Zhou, N. Lu, *Degradation of antipyrine by UV, UV/H<sub>2</sub>O<sub>2</sub> and UV/PS*, J. Hazard. Mater. 260 (2013) 1008–1016.
- [70] C. Tan, N. Gao, Y. Deng, L. Li, J. Deng, S. Zhou, *Kinetic oxidation of antipyrine in heat-activated persulfate*, Desalin. Water Treat., (2013) 1–9, DOI: 10.1080/19443994.2013.848414.
- [71] J. Sangster, *LOGKOW Databank, A Databank of Evaluated Octanol-Water partition coefficients*, Sangster Res. Lab., Montreal Canada, 1994.
- [72] V.A. Santhi, N. Sakai, E.D. Ahmad, A.M. Mustafa, *Occurrence of bisphenol A in surface water, drinking water and plasma from Malaysia with exposure assessment from consumption of drinking water*, Sci. Total Environ. 427–428 (2012) 332–338.
- [73] J.A. Rogers, L. Metz, V.W. Yong, *Review: endocrine disrupting chemicals and immune responses: A focus on bisphenol-A and its potential mechanisms*, Mol Immunol. 53 (2013) 421–430.
- [74] P. Allard, *Bisphenol A (Chapter 27)*, in: *Biomarkers in toxicology*, Elsevier Inc., 2014.
- [75] J. Michałowicz, *Bisphenol A – Sources, toxicity and biotransformation*, Environ. Toxicol. Pharmacol. 37 (2014) 738–758.
- [76] Y.J. Kim, U. Platt, M.B. Gu, H. Iwahashi, *Atmospheric and biological environmental monitoring*, Springer-Verlag Berlin H.
- [77] H.C. Alexander, D.C. Dill, L.W. Smith, P.D. Guiney, P. Dorn, *Bisphenol A: acute aquatic toxicity*, Environ. Toxicol. Chem. 7 (1988) 19–26.
- [78] M. Hirano, H. Ishibashi, N. Matsumura, Y. Nagao, N. Watanabe, A. Watanabe, N. Onikura, K. Kishhi, K. Arizono, *Acute toxicity responses of two*

- crustaceans, *Americamysis bahia* and *Daphnia magna*, to endocrine disrupters, *J. Health Sci.* 20 (2004) 97-100.
- [79] R.M. Gilbert, *Caffeine consumption*, *Prog. Clin. Biol. Res.* 58 (1984) 185-213.
- [80] Z.R. Rey, E.F. Granek, S. Sylvester, *Occurrence and concentration of caffeine in Oregon coastal waters*, *Mar. Pollut. Bull.* 64 (2012) 1417-1424.
- [81] A. Zarrelli, M. DellaGreca, M.R. Iesce, M. Lavorgna, F. Temussi, L. Schiavone, E. Criscuolo, A. Parrella, L. Previtiera, M. Isidori, *Ecotoxicological evaluation of caffeine and its derivatives from a simulated chlorination step*, *Sci. Total Environ.* 470–471 (2014) 453–458.
- [82] Y. Tan, J. Liu, Y. Deng, H. Cao, D. Xu, F. Cu, Y. Lei, J. Magdalou, M. Wu, L. Chen, H. Wang, *Caffeine-induced fetal rat over-exposure to maternal glucocorticoid and histone methylation of liver IGF-1 might cause skeletal growth retardation*, *Toxicol. Lett.* 214 (2012) 279-287.
- [83] L. Guilhermino, T. Diamantino, M.C. Silva, A.M.V.M. Soares, *Acute toxicity test with *Daphnia magna*: An alternative to mammals in the prescreening of chemical toxicity?*, *Ecotoxicol. Environ. Saf.* 46 (2000) 357-362.
- [84] D.M. Whitacre, *Reviews of environmental contamination and toxicology*, Springer-Verlag Berlin H., 2010.
- [85] S. Balakrishnan, K. Takeda, H. Sakugawa, *Occurrence of Diuron and Irgarol in seawater, sediments and plankton of Seto Inland Sea, Japan*, *Geochemical Journal*, 46 (2012) 169–177.
- [86] S. Giacomazzi, N. Cochet, *Environmental impact of diuron transformation: a review*, *Chemosphere* 56 (2004) 1021-1032.
- [87] J.C. López-Doval, M. Poquet, I. Muñoz, *Sublethal effects of the herbicide diuron on the freshwater snail *Physella acuta**, *Limnetica* 33 (2014) 205-216.
- [88] E.M. Hartgers, G.H. Aalderink, P.J. Van den Brink, R. Gylstra, J. Wilfred, F. Wiegman, T.C.M. Brock, *Ecotoxicological threshold levels of a mixture of herbicides (atrazine, diuron and metolachlor) in freshwater microcosms*, *Aquat. Ecol.* 32 (1998) 135-152.
- [89] R. Krieger, *Handbook of pesticide toxicology, Two-volume set: Principles and agents*, Academic Press, 2001.
- [90] A Topalov, B Abramović, D Molnár-Gábor, J Csanádi, O Arcson, *Photocatalytic oxidation of the herbicide (4-chloro-2-methylphenoxy)acetic acid (MCPA) over TiO<sub>2</sub>*, *J. Photochem. Photobiol. A Chem.* 140 (2001) 249-253.



- [91] UK Environment Agency, *R&D Technical Report E67 – Endocrine function in aquatic invertebrates and evidence for disruption by environmental pollutants*, Bristol.
- [92] M. Cleuvers, *Initial risk assessment for three beta-blockers found in the aquatic environment*, *Chemosphere* 59 (2005) 199-205.
- [93] V. Romero, P. Marco, J. Giménez, S. Esplugas, *Adsorption and photocatalytic decomposition of the  $\beta$ -blocker metoprolol in aqueous titanium dioxide suspensions: Kinetics, intermediates, and degradation pathways*, *Int. J. Photoenergy* 2013 (2013), DOI: 10.1155/2013/138918.
- [94] S.W. Nam, B.I. Jo, Y. Yoon, K.D. Zoh, *Occurrence and removal of selected micropollutants in a water treatment plant*, *Chemosphere* 95 (2014) 156-165.
- [95] J.A. Plant, N. Voulvoulis, K.V. Ragnarsdottir, *Pollutants, human health and the environment: A risk based approach*, Wiley-Blackwell, 2011.
- [96] A. Massarsky, V.L. Trudeau, T.W. Moon,  *$\beta$ -blockers as endocrine disruptors: the potential effects of human  $\beta$ -blockers on aquatic organisms*, *J. Exp. Zool. A Ecol. Genet. Physiol.* 315 (2011) 251-265.
- [97] A. Villegas-Navarro, E. Rosas-L, J.L. Reyes, *The heart of *Daphnia magna*: effects of four cardioactive drugs*, *Comp. Biochem. Physiol. C Pharmacol.* 136 (2003) 127–134.
- [98] PubChem, Open Chemistry Database, National Center for Biotechnology Information, U.S.
- [99] Scientific committee on consumer safety (SCCS), *Request for a scientific opinion for the use as preservative of o-Phenylphenol, Sodium ophenylphenate, Potassium o-phenylphenate, MEA o-Phenylphenate CAS n. 90-43-7, 132-27-4, 13707-65-8, 84145-04-0 -Submission I.*
- [100] P. Grenni, M.S. Rodríguez-Cruz, E. Herrero-Hernández, J.M. Marín-Benito, M.J. Sánchez-Martín, A.B. Caracciolo, *Effects of wood amendments on the degradation of terbutylazine and on soil microbial community activity in a clay loam soil*, *Water Air and Soil Pollution* 223 (2012) 5401-5412.
- [101] D.W. Kolpin, E.T. Furlong, M.T. Meyer, E.M. Thurman, S.D. Zaugg, L.B. Barber, H.T. Buxton, *Pharmaceuticals, hormones, and other organic wastewater contaminants in U.S. streams, 1999–2000: A national reconnaissance*, *Environ. Sci. Technol.* 36 (2002) 1202-1211.
- [102] I.R. Barbosa, A.J.A. Nogueira, A.M.V.M. Soares, *Acute and chronic effects of testosterone and 4-hydroxyandrostenedione to the crustacean *Daphnia magna**, *Ecotoxicol. Environmen. Saf.* 71 (2008) 757-764.

- [103] T. Verslycke, S. Poelmans, K. de Wasch, H.F. de Brabander, C.R. Janssen, *Testosterone and energy metabolism in the estuarine mysid Neomysis Integer (crustacea: mysidacea) following exposure to endocrine disruptors*, Environ. Toxicol. Chem. 23 (2004) 1289–1296.



## Chapter II

This chapter describes the chemicals and materials used throughout the research. Additionally, a description of the analytical methods and procedures, experimental set-ups, and characterization techniques used is provided.

### Contents

- 2.1. Chemicals
- 2.2. Experimental set-ups
- 2.3. Analytical methods
- 2.4. Catalyst characterization
- 2.5. References



## 2.1. Chemicals

Compounds, commercial reagents and gases used throughout this research, as well as their CAS code, purity and manufacturer, are indicated in Table 2.1.

**Table 2.1.** List of chemicals and materials

Reagent	Chemical Formula	CAS	Purity	Manufacturer
<i>Pollutants</i>				
o-phenylphenol	C <sub>12</sub> H <sub>10</sub> O	90-43-7	99%	S.A.
Acetaminophen	C <sub>8</sub> H <sub>9</sub> NO <sub>2</sub>	103-90-2	99%	S.A.
Antipyrine	C <sub>11</sub> H <sub>12</sub> N <sub>2</sub> O	60-80-0	99%	S.A.
Bisphenol A	C <sub>15</sub> H <sub>16</sub> O <sub>2</sub>	80-05-7	>99%	S.A.
Caffeine	C <sub>8</sub> H <sub>10</sub> N <sub>4</sub> O <sub>2</sub>	58-08-2	99%	S.A.
Diuron	C <sub>9</sub> H <sub>10</sub> Cl <sub>2</sub> N <sub>2</sub> O	330-54-1	≥98%	S.A.
MCPA	C <sub>9</sub> H <sub>9</sub> ClO <sub>3</sub>	94-74-6	≥95%	S.A.
Metoprolol tartrate	C <sub>34</sub> H <sub>56</sub> N <sub>2</sub> O <sub>12</sub>	56392-17-7	>99%	S.A.
Terbutylazine	C <sub>9</sub> H <sub>16</sub> ClN <sub>5</sub>	5915-41-3	98.8%	S.A.
Testosterone	C <sub>19</sub> H <sub>28</sub> O <sub>2</sub>	58-22-0	≥99%	S.A.
<i>Materials for synthesis of catalysts</i>				
Activated carbon, 12-20 mesh		7440-44-0		S.A.
<i>Reagents for analysis and reactants</i>				
1,10-phenanthroline monohydrate	C <sub>12</sub> H <sub>8</sub> N <sub>2</sub> ·H <sub>2</sub> O	5144-89-8	99%	S.A.
Acetic acid	C <sub>2</sub> H <sub>4</sub> O <sub>2</sub>	64-19-7	100%	M.K.
Acetonitrile	C <sub>2</sub> H <sub>3</sub> N	75-05-8	99.99%	F.C.
Ammonia solution	NH <sub>4</sub> OH	7664-41-7	35%	F.C.
Ammonium acetate	C <sub>2</sub> H <sub>7</sub> O <sub>2</sub> N	631-61-8	≥98%	S.A.
Ammonium fluoride	NH <sub>4</sub> F	12125-01-8	>98%	S.A.
Azomethine-H monosodium salt	C <sub>17</sub> H <sub>12</sub> NNaO <sub>8</sub> S <sub>2</sub> ·xH <sub>2</sub> O	206752-32-1	~95%	S.A.
Calcium chloride dihydrate solution	CaCl <sub>2</sub> ·2H <sub>2</sub> O	10035-04-8	294 mg L <sup>-1</sup>	M.B.
Boric acid	H <sub>3</sub> BO <sub>3</sub>	10043-35-3	≥99.5%	F.C.
Catalase from bovine liver		9001-05-2	3390 units mg <sup>-1</sup> solid	S.A.
Cobalt(II) chloride 6-hydrate	CoCl <sub>2</sub> ·6H <sub>2</sub> O	7791-13-1	>99%	P.R.

**Table 2.1. (continued) List of chemicals and materials**

Reagent	Chemical Formula	CAS	Purity	Manufacturer
<i>Reagents for analysis and reactants</i>				
Ephippia of Daphnia Magna				M.B.
Ethanol	C <sub>2</sub> H <sub>6</sub> O	64-17-5	99.5%	P.R.
Ethylene glycol	C <sub>2</sub> H <sub>6</sub> O <sub>2</sub>	107-21-1	99.8%	S.A.
Ethylenediamine tetraacetic acid	C <sub>10</sub> H <sub>16</sub> N <sub>2</sub> O <sub>8</sub>	60-00-4	99.995%	S.A.
Folin & Ciocalteu's phenol reagent			2 mol L <sup>-1</sup>	S.A.
Hydrochloric acid	HCl	7647-01-0	37%	F.C.
Hydrogen peroxide	H <sub>2</sub> O <sub>2</sub>	7722-84-1	30% w/v	M.K.
Indigo carmine	C <sub>16</sub> H <sub>8</sub> N <sub>2</sub> Na <sub>2</sub> O <sub>8</sub> S <sub>2</sub>	860-22-0	≥98%	S.A.
Iron(III) nitrate 9-hydrate	FeN <sub>3</sub> O <sub>9</sub> ·9H <sub>2</sub> O	7782-61-8	98%	P.R.
Iron(III) perchlorate hydrate	Cl <sub>3</sub> FeO <sub>12</sub> ·xH <sub>2</sub> O	15201-61-3		S.A.
Isopropanol	C <sub>3</sub> H <sub>8</sub> O	67-63-0	≥99%	S.A.
L-ascorbic acid	C <sub>6</sub> H <sub>8</sub> O <sub>6</sub>	50-81-7	99%	S.A.
LCK 414				L.G.
Magnesium sulfate heptahydrate solution	MgSO <sub>4</sub> ·7H <sub>2</sub> O	10034-99-8	123.25 mg L <sup>-1</sup>	M.B.
Nitric acid	HNO <sub>3</sub>	7697-37-2	65%	P.R.
Orthophosphoric acid	H <sub>3</sub> PO <sub>4</sub>	7664-38-2	85.4%	F.C.
Oxalic acid dihydrate	C <sub>2</sub> H <sub>2</sub> O <sub>4</sub> ·2H <sub>2</sub> O	607-006-00-8	≥99.5%	S.A.
p-chlorobenzoic acid	C <sub>7</sub> H <sub>5</sub> ClO <sub>2</sub>	74-11-3	>98%	M.K.
Potassium chloride solution	KCl	7447-40-7	5.75 mg L <sup>-1</sup>	M.B.
Potassium phosphate dibasic	K <sub>2</sub> HPO <sub>4</sub>	7758-11-4	≥98%	S.A.
Potassium phosphate monobasic	KH <sub>2</sub> PO <sub>4</sub>	7778-77-0	≥98%	S.A.
Sodium bicarbonate	NaHCO <sub>3</sub>	144-55-8	99.7%	P.R.
Sodium bicarbonate solution	NaHCO <sub>3</sub>	144-55-8	67.75 mg L <sup>-1</sup>	M.B.
Sodium carbonate	Na <sub>2</sub> CO <sub>3</sub>	497-19-8	≥98%	S.A.
Sodium hexametaphosphate	(NaPO <sub>3</sub> ) <sub>n</sub>	68915-31-1	65-70%	P.R.
Sodium hydroxide	NaOH	1310-73-2	97%	P.R.
Sodium thiosulfate 5-hydrate	Na <sub>2</sub> S <sub>2</sub> O <sub>8</sub> H <sub>10</sub>	10102-17-7	>99%	P.R.
Spectroquant ® iron test				M.K.

**Table 2.1. (continued)** List of chemicals and materials

Reagent	Chemical Formula	CAS	Purity	Manufacturer
<i>Reagents for analysis and reactants</i>				
Spirulina powder		724424-92-4		M.B.
Thioglycolic acid	C <sub>2</sub> H <sub>4</sub> O <sub>2</sub> S	68-11-1	≥98%	S.A.
Titanium(IV) butoxide	C <sub>16</sub> H <sub>36</sub> O <sub>4</sub> Ti	5593-70-4	97%	S.A.
Titanium dioxide, Aeroxide P25	TiO <sub>2</sub>	13463-67-7		E.D.
Titanium(IV) oxysulfate-sulfuric acid solution	O <sub>5</sub> STi·xH <sub>2</sub> SO <sub>4</sub>	123334-00-9	27-31%, H <sub>2</sub> SO <sub>4</sub> basis	S.A.
Ultrapure water	H <sub>2</sub> O			M.Q.
<i>Compressed gasses</i>				
Helium	He	7440-59-7	>99.999%	A.L.
Nitrogen	N <sub>2</sub>	7727-37-9	>99.999%	A.L.
Oxygen	O <sub>2</sub>	7782-44-7	>99.95%	A.L.
Synthetic air			21% O <sub>2</sub> , 79% N <sub>2</sub> (± 0.5%)	A.L.

A.L.: Abelló Linde, E.D.: Evonik Degussa, F.C.: Fisher Chemical, L.G.: Lange, M.B.: MicroBioTests, M.K.: Merck, M.Q.: Milli-Q Millipore, P.R.: Panreac, S.A.: Sigma Aldrich.

## 2.2. Experimental set-ups

### 2.2.1. Laboratory-scale set-ups

#### A. Catalyst preparation

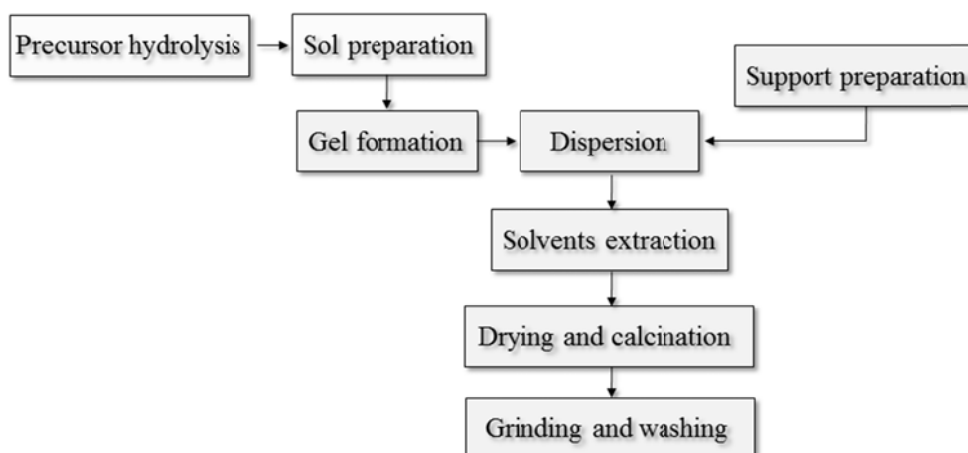


**Figure 2.1.** Main steps of the sol-gel procedures followed for the catalysts preparation

Figure 2.1. shows a simplified scheme indicating the main steps of the synthesis procedures followed for the preparation of  $\text{TiO}_2$  catalysts, both powdered and supported on activated carbon.

Hydrolysis of titania precursor (described in Chapters V and VI) was carried out under reflux in a single-neck round-bottom flask (Labbox) provided with a vertical coil condenser (Pobel). The flask was placed inside a tap water bath heated in a Selecta Agimatic-E (640 W, 2.8 A) hot plate-magnetic stirrer (see Figure 2.2.). Hydrolysis at room temperature (described in Chapter VII) was performed in a glass-made beaker with magnetic stirring.

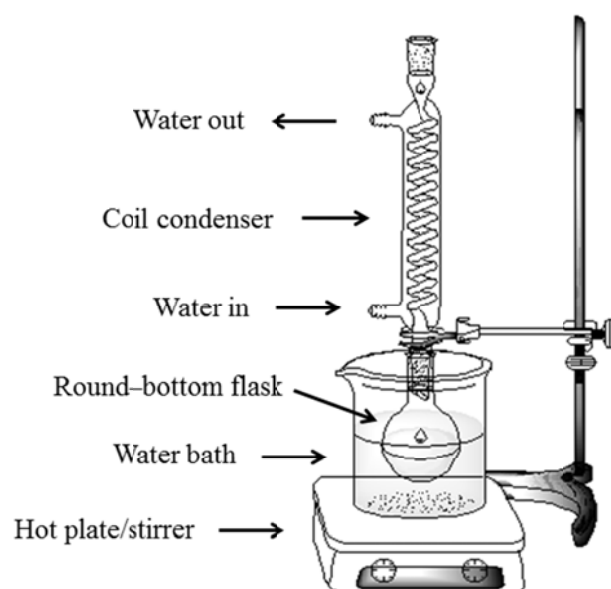


**Figure 2.2.** Reflux set-up for the hydrolysis of titania precursor

If needed, the dispersion of titania particles obtained after hydrolysis (sol) was washed with water and/or ethanol in a beaker under magnetic stirring. After each washing stage, the titania particles were separated by centrifugation in an Alresa centrifuge (200 W, 50 Hz), filtrated by a Millipore vacuum pump (WP6 122050, 230 V, 50 Hz) using Startorius Stedim cellulose nitrate filters (0.45  $\mu\text{m}$ ).

Activated carbon magnetization (described in Chapters V and VI) was carried out by incipient wetness impregnation adding dropwise an iron-containing solution to carbon grains spread in a flat beaker or crystallizer (Labbox). Then a thermal



treatment was carried out in a Hobersal vertical split tubular furnace (TR-23, 1500 W) in a nitrogen atmosphere (see Figure 2.3.)

Magnetized carbon nanotubes were dried in a Selecta Conterm convection oven (2000201, 150 L, 2 kW), manually grinded with an agate mortar and sieved in the case of activated carbon and dispersed into the titania sols. This dispersion was carried out in an Elmasonic S-60H ultrasound bath (37 Hz, 550 W, 5.75 L) provided with temperature and time controllers.

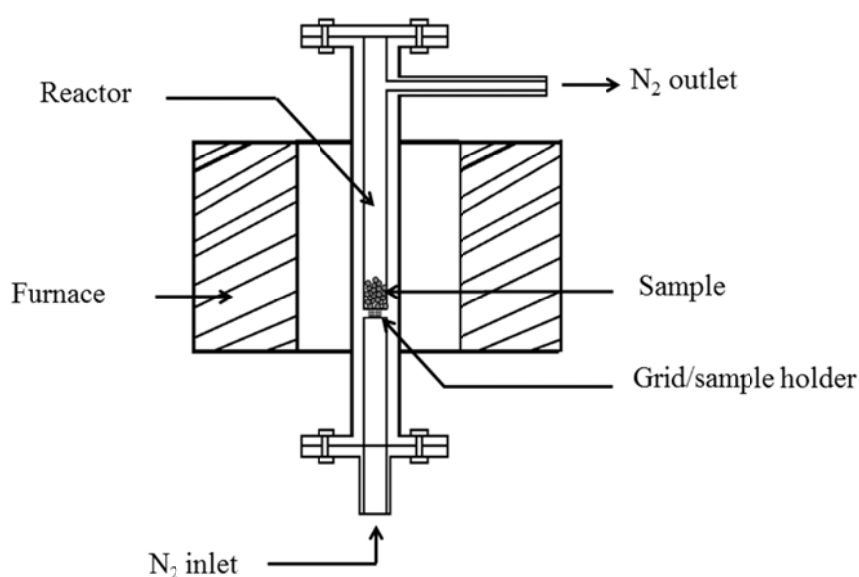


**Figure 2.3.** Scheme of the split tubular furnace used in the thermal treatment of the activated carbon support

To remove other solvents and volatile components from the catalysts, extraction was carried out in a Büchi rotary evaporator (kRvr 65/45, 50 Hz) provided with an OVAN thermostatic bath (100-12L, 1.2 kW, 50/60 Hz) and a DINKO vacuum pump (D-95, 130 W). A Raypa electric furnace (HM-9MP, 3 kW, P.I.D. control, thermocouple type K) was used for the calcination of the catalysts.

Final washing of magnetic carbon catalysts was performed by manual stirring of an aqueous suspension of the catalysts.

For a more detailed description on the catalysts preparation and operation conditions, please see Experimental Section of Chapters V, VI and VII.

### B. Solar simulator for photoactivity tests

Figure 2.4. shows a picture of the experimental set-up used to study the degradability of water contaminants by means of solar-driven processes (e.g., photolysis, photocatalytic oxidation and photocatalytic ozonation) at laboratory scale.

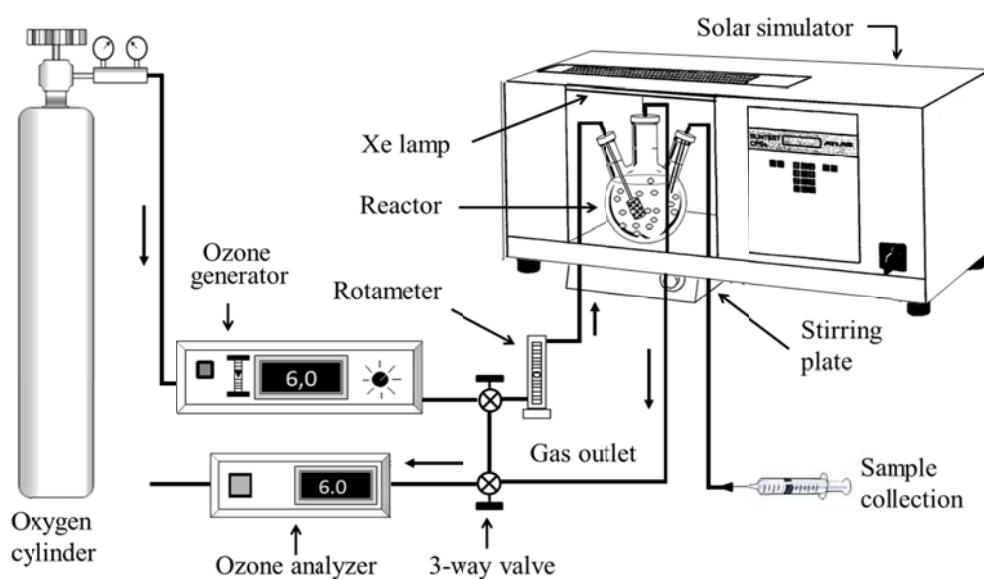


**Figure 2.4.** Laboratory-scale set-up for photoactivity tests

A Suntest CPS+ solar simulator (Atlas) was used to conduct the solar photoactivity tests at laboratory scale. The solar simulator is provided with an air-cooled Xe lamp equipped with quartz and glass filters so that the emission is restricted to wavelengths over 300 nm. The output light intensity was set to  $550 \text{ W m}^{-2}$  (average global solar radiation in a sunny day) and the temperature of the system was kept between 25 and 40°C throughout the experiments.

If needed, a laboratory-scale ozone generator (COM-AD, Anseros) was used to produce ozone from an oxygen stream. The oxygen-ozone mixture was fed to the reactor at a constant flowrate as controlled by a rotameter (Gilmont Instruments) and bubbled into the solution through a diffuser.

Two different reactors were used for the photoactivity tests, depending on the volume of solution considered: a 1-litre glass-made cylindrical reactor (10.7 cm internal diameter) and a 250-mL Pyrex-made 3-neck round-bottom flask (8.8 cm

outer diameter). In any case the reactor was provided with three ports designed for input and output of gas and aqueous sampling. The reactor was placed into the solar simulator chamber and seated on a magnetic stirring plate. First, the reactor was charged with the aqueous solution to be treated. Then, if used, the catalyst was added and the flow of oxygen or oxygen/ozone was started. An ozone analyzer (GM, Ozomat) was used to continuously monitor the ozone concentration in the inlet and outlet gas streams. Aqueous samples were withdrawn at intervals and kept for analysis. The duration of the experiments depended on the treatment goal (e.g. removal or mineralization of the target compound).

### 2.2.2. Pilot-scale solar plant

Experiments of treatability of a mixture of emerging contaminants of water were carried out using a pilot-scale solar plant which comprises a compound parabolic collector (CPC) used as solar photo-reactor (Ecosystem Environmental Services SA) and an ozonation system. Experiments were run in Badajoz, Spain (38°52'43" N, 6°58'15" W).

The photo-reactor is equipped with 4 borosilicate glass tubes (32 mm external diameter, 1.4 mm thickness, 750 mm length), anodized aluminum reflectors tilted 45 degrees and two gas feeding points which consist of two borosilicate glass-made porous plates situated at the entrance of two of the reactor tubes. The photo-reactor total area is 0.25 m<sup>2</sup> and the exposed volume is 1.8 L. The reactor is also provided with a polypropylene tank where the sample to be treated is loaded and from which it is continuously recirculated to the tubes during the reaction time. The tank also favors the gas-liquid separation. A broadband UV radiometer (290-370 nm, Acadus 85-PLS) tilted at the same inclination that the reactor was used to monitor the solar UV light supplied to the system. Figure 2.5. shows a picture of the CPC photo-reactor used in the pilot plant.

The ozonation system comprises an air compressor (Pintuc Extreme 3), an ozone generator (OZVa 1200E, ProMinent), a gas flow controller (MC-10SLPM-D, Alicat Scientific), two ozone analyzers (Anseros Ozomat, RTI-6000-GM and GM-6000-PRO) and an ozone destructor (CAT-1500 72258, Anseros).



**Figure 2.5.** CPC photo-reactor used in pilot scale experiments

A detailed scheme of the CPC photo-reactor and the whole pilot plant can be seen, respectively, in Figure 3.1. (Chapter III) and Figure 4.2. (Chapter IV).

## 2.3. Analytical methods

---

### 2.3.1. Concentration of pollutants in water

The quantitative analysis of water pollutants was carried out by high-performance liquid chromatography (HPLC). For that purpose, two HPLC apparatus were used:

- An Elite LaChrom HPLC (Hitachi) equipped with a programmable high pressure pump (L-2130), a degasser, an autosampler (L-2200), a diode array detector (L-2450), a C-18 column (150 mm × 3 mm internal diameter, 5 μm particle size, Phenomenex) and EZChrom Elite Data System Software.
- An Agilent 1100 Series HPLC (Hewlett Packard) equipped with a vacuum degasser (G1322A), an isocratic pump (G1310A), an autosampler (G1313A), a variable wavelength detector (G1314A), a Kromasil C18 column (150 mm × 4 mm internal diameter, 5 μm particle size, Teknokroma) and ChemStation Software.

In all cases, a binary mixture of acetonitrile (solvent A) and 0.1% (v/v) phosphoric acid aqueous solution (solvent B) was used as mobile phase. Table 2.2 summarizes the conditions of each method used to analyze the compound concentrations.

**Table 2.2.** Conditions of the HPLC methods used

Method	Conditions	Analyte	Retention time/ Detection wavelength (min/nm)	LOD×10 <sup>2</sup> (mg L <sup>-1</sup> )	HPLC apararat.
1	Isocratic elution at 1.0 mL min <sup>-1</sup> , 15% solvent A.	ACE	2.9/244	0.6	A.G.
2	Isocratic elution at 0.65 mL min <sup>-1</sup> , 15% solvent A.	CAF	5.5/275	0.1	A.G.
		ANT	11.2/240	0.3	
		MTP	16.0/225	0.1	
3	Isocratic elution at 1.0 mL min <sup>-1</sup> , 50% solvent A.	pCBA	3.5/250	0.3	A.G.
		BIS	3.9/220	0.4	
		TST	4.6/250	1.2	
4	Isocratic elution at 0.50 mL min <sup>-1</sup> , 15% solvent A.	MTP	4.1/225	7.1	E.L.
5	Gradient elution at 1.0 mL min <sup>-1</sup> . Solvent A was linearly varied 40-25% in 12.5 min, then 25-40% in 7.5 min and kept at 40% for 10 min.	DIU	10.0/220	6.5	A.G.
		MCPA	15.2/220	4.3	
		TBA	23.2/220	1.9	
		OPP	25.8/220	4.2	

E.L.: Elite LaChrom, A.G.: Agilent, LOD: Detection limit [1].

### 2.3.2. Identification of degradation intermediates

The detection of metoprolol (MTP) degradation products was carried out using a high performance liquid chromatography coupled with mass spectrometry equipment. The chromatographic system was an Agilent 1260 series equipment consisting of an infinity micro degasser, a binary pump, a HiP-ALS SL+ autosampler and a TCC SL thermostatted column compartment. The mass detector was an Agilent 6520 Accurate-Mass Q-TOF-LC/MS operating in the 4 GHz high-resolution mode, using an electrospray ion source Dual ESI. High purity nitrogen was used as nebulizer gas (30 psi, 350°C and 10 L min<sup>-1</sup>).

Electrospray conditions were as follows: positive mode; skimmer voltage, 65 V; octapole RF, 750 V; fragmentor, 175 V. Mass acquisition range (*m/z*) and capillary for MTP were 70–3200 and 3500 V, while for TBA 30-1000 and 2000V.

MTP intermediates were separated using a Zorbax SB-C18 column (3.5 μm, 150 mm long, 4.6 mm diameter) with a gradient elution at 0.2 mL min<sup>-1</sup> of a binary mixture of acetonitrile and acidified water (25 mM formic acid) from 10 to 100% of acetonitrile in 40 min with 15 min of equilibration.

Data were acquired and processed using Agilent Mass Hunter Workstation Software (version B.03.01). Accurate mass measurements were carried out using

double calibration introducing together with the chromatograph flow a standard solution containing the internal reference compounds purine and HP-921 (hexakis(1H,1H,3H-tetrafluoropropoxy)phosphazine),  $m/z$  121.0509 and 922.0098, respectively.

### 2.3.3. Total organic and inorganic carbon (TOC, IC)

A TOC-V<sub>SCH</sub> Shimadzu carbon analyzer was used for the determination of total organic and inorganic carbon (TOC and IC, respectively). This instrument measures the total carbon and total inorganic carbon in a liquid sample, and then, the total organic carbon is computed as the difference between these two measurements as described in ASTM standard D7573-09 [2].

Total carbon analysis is carried out by heating the sample up to 680°C in an oxygen-rich atmosphere inside a combustion tube filled with a platinum catalyst (Pt/Al<sub>2</sub>O<sub>3</sub>). Then, the carbon dioxide generated by oxidation is cooled, dehumidified, and analyzed using an infrared gas analyzer (NDIR). Finally, the total carbon content in the sample is obtained through comparison with a calibration curve. The inorganic carbon content is determined by acidifying the sample with 25% H<sub>3</sub>PO<sub>4</sub> so that conditions in which the carbonate and bicarbonate present in the sample are converted into CO<sub>2</sub>, which is sent to the NDIR detector for the signal to be processed. According to the manufacturer, the detection limit is 50 µg L<sup>-1</sup>.

TOC measurement was used to compute the mineralization degree, i.e. TOC removal percentage, according to equation (2.1)

$$\text{Mineralization degree}_t = \frac{\text{TOC}_0 - \text{TOC}_t}{\text{TOC}_0} \times 100 \quad (2.1)$$

where TOC<sub>0</sub> and TOC<sub>t</sub> are the organic carbon content at the start of reaction and at time t, respectively.

### 2.3.4. Dissolved ozone concentration

Ozone concentration in water was measured by the colorimetric method of Bader and Hoigné [3]. In this method, aqueous ozone concentration is quantified by allowing it to react stoichiometrically with a brightly-coloured dye (indigo trisulfonate) which when oxidised by ozone leads to a colourless product. Then, as

the dye has a strong light absorbance at 600 nm, the ozone concentration can be computed from the difference in light absorbance between the oxidized sample and a blank sample prepared under identical conditions but adding ultrapure water as test sample. Typically, to determine the ozone concentration in a liquid sample, 2 mL indigo trisulfonate solution were mixed with 2 mL of the test sample. This mixture was transferred to a 1-cm quartz cell and its absorbance at 600 nm was measured.

According to the Beer's Law and in the absence of any other species that absorb radiation under 600 nm, there is a linear relationship between the decrease in absorbance of the solution and the ozone concentration in the sample, as indicated in equation (2.2):

$$C_{O_3} = \frac{\Delta A_{600nm}}{\varepsilon_{600nm} b} \frac{V_{dye} + V_{sample}}{V_{sample}} \quad (2.2)$$

where  $C_{O_3}$  is the ozone concentration in the sample (in mol L<sup>-1</sup>),  $\Delta A_{600nm}$  is the difference in absorbance between the oxidized dye solution and a blank,  $\varepsilon_{600nm}$  is the dye molar absorptivity at 600 nm ( $2 \times 10^4$  L mol<sup>-1</sup> cm<sup>-1</sup>),  $b$  is the cell path length,  $V_{dye}$  and  $V_{sample}$  are the volume of dye solution and added sample, respectively. According to the authors, this method presents 2% precision and a detection limit of  $10^{-7}$  mol L<sup>-1</sup> for absorbance measurements in 5 cm cell. In this work, 1 cm cell was used so that detection limit was  $5 \times 10^{-7}$  mol L<sup>-1</sup>.

The indigo trisulfonate solution was prepared by mixing 900 mL of a buffer solution (containing 28 and 35 g L<sup>-1</sup> of KH<sub>2</sub>PO<sub>4</sub> and H<sub>3</sub>PO<sub>4</sub>, respectively) and 100 mL of dye stock solution (containing 0.6 and 2.3 g L<sup>-1</sup> indigo trisulfonate and H<sub>3</sub>PO<sub>4</sub>, respectively). This mixture is stable for about 4 months when stored in the dark between 2 and 8°C.

It was confirmed that hydrogen peroxide and Fe(III) do not interfere with the method.

### 2.3.5. Gas-phase ozone concentration

Ozone in gas phase was monitored by means of ozone analyzers. The functional principle is based on photometric determination of ozone according to its UV light absorption at 253.7 nm. A fraction of the gas stream is irradiated by a low pressure Hg lamp inside an optical absorption cell. Thus, the light attenuation of the transmitted beam is used to determine the ozone concentration according to the

Beer's Law. This equipment is designed to work at pressures up to 2 bars and has a measuring range of 0-50 mg L<sup>-1</sup> O<sub>3</sub>.

### 2.3.6. Total dissolved iron concentration

Total iron concentration was determined by the ferrozine method [4] which is based on the reduction of total Fe(III) to Fe(II) and further formation of a purple complex with the ferrozine reagent which can be analyzed by spectrophotometry at 565 nm. In this work, the Spectroquant ® iron test kit (Merck) was used to determining the total iron concentration in solution.

Typically, 5 mL of test sample were mixed with 3 drops of Spectroquant ® reagent. Fifteen minutes after being prepared, the mixture was transferred to an 1 cm quartz cell and its absorbance at 565 nm was measured. Then, the Beer's Law was applied to determine the iron concentration in the sample according to equation (2.3):

$$C_{\text{Fe}} = \frac{\Delta A_{565\text{nm}}}{\epsilon_{565\text{nm}} b} \quad (2.3)$$

where  $C_{\text{Fe}}$  is the iron concentration in the sample (in mol L<sup>-1</sup>),  $\Delta A_{565\text{nm}}$  is the difference in absorbance between the test sample and a blank (prepared using ultrapure water as test sample),  $\epsilon_{565\text{nm}}$  is the iron complex molar absorptivity at 565 nm ( $2.704 \times 10^4$  L mol<sup>-1</sup> cm<sup>-1</sup>) and  $b$  is the cell path length.

### 2.3.7. Iron (II) concentration

Aqueous Fe(II) was measured colorimetrically at 510 nm by complexation with 1,10-phenanthroline in acidic medium [5]. The resulting reddish orange complex absorbs light in the range 380-580 nm with a maximum at 510 nm. To carry out this analysis, 1.5 mL glacial acetic acid (0.1 mol L<sup>-1</sup>), 1 mL 1,10-phenanthroline (0.2 wt%) and 5 mL of the test sample were mixed. This mixture was stirred and then 1 mL NH<sub>4</sub>F (2 mol L<sup>-1</sup>) was added. After 20 min, the mixture was transferred to an 1 cm quartz cell and its absorbance at 510 nm was measured. Finally, given Beer's Law, in the absence of any species that absorbs radiation at 510 nm, the concentration of Fe (II) in the sample was computed by equation (2.4):



$$C_{\text{Fe(II)}} = \frac{\Delta A_{510\text{nm}}}{\varepsilon_{510\text{nm}}} \frac{V_{\text{acetic}} + V_{\text{phenant.}} + V_{\text{sample}} + V_{\text{NH}_4\text{F}}}{b V_{\text{sample}}} \quad (2.4)$$

where  $C_{\text{Fe(II)}}$  is the iron concentration in the sample (in  $\text{mol L}^{-1}$ ),  $\Delta A$  is the difference in absorbance between the test sample and a blank (prepared using ultrapure water as test sample),  $\varepsilon_{510\text{nm}}$  is the complex molar absorptivity at 510 nm ( $1.102 \times 10^4 \text{ L mol}^{-1} \text{ cm}^{-1}$ ),  $b$  is the cell path length and  $V_{\text{acetic}}$ ,  $V_{\text{phenant.}}$ ,  $V_{\text{sample}}$  and  $V_{\text{NH}_4\text{F}}$  are, respectively, the volume of acetic acid, 1,10-phenantroline, test sample and  $\text{NH}_4\text{F}$  added.

### 2.3.8. Hydrogen peroxide concentration

Two methods for aqueous hydrogen peroxide quantification depending on the expected concentrations were used.

For samples having hydrogen peroxide concentrations higher than  $6.5 \times 10^{-5} \text{ mol L}^{-1}$ , the Eisenberg colorimetric method was used [6]. This method is based on the formation of pertitanic acid by the reaction between hydrogen peroxide and a titanium sulfonate reagent. The pertitanic acid, which is yellow in color, is stable for at least 6 hours and can be colorimetrically measured at 405 nm. Thus, to determine the hydrogen peroxide in a sample, 0.5 mL of commercial titanium(IV) oxysulfate in sulfuric acid solution were mixed with 4.5 mL of the test sample. Then, the mixture was allowed to stand for 5 minutes, transferred to an 1 cm quartz cell and its absorbance at 405 nm was measured. Finally, the hydrogen peroxide concentration was calculated using the equation (2.5):

$$C_{\text{H}_2\text{O}_2} = \frac{\Delta A_{405\text{nm}}}{\varepsilon_{405\text{nm}}} \frac{V_{\text{reagent}} + V_{\text{sample}}}{b V_{\text{sample}}} \quad (2.5)$$

where  $C_{\text{H}_2\text{O}_2}$  is the hydrogen peroxide concentration (in  $\text{mol L}^{-1}$ ),  $\Delta A_{405\text{nm}}$  is the difference in absorbance between the test sample and a blank (prepared with ultrapure water),  $\varepsilon_{405\text{nm}}$  is the pertitanic acid molar absorptivity at 405 nm ( $720 \text{ L mol}^{-1} \text{ cm}^{-1}$ ),  $b$  is the cell path length and  $V_{\text{reagent}}$  and  $V_{\text{sample}}$  are respectively, the volume of titanium(IV) oxysulfate reagent and test sample added.

For samples with hydrogen peroxide concentrations below  $6.5 \times 10^{-5} \text{ mol L}^{-1}$ , the colorimetric method proposed by Masschelein was used [7]. This method is based on the stoichiometric oxidation of Co(II) to Co(III) by hydrogen peroxide and the subsequent formation of a cobalt (III)-bicarbonate complex having maximum

absorbance at 260, 440 and 635 nm. Due to the Co(III)-bicarbonate complex high molar absorptivity at 260 nm, hydrogen peroxide determination is usually carried out at this wavelength. Typically, 0.5 mL Co(II) chloride solution (16.1 g  $\text{CoCl}_2 \cdot 6\text{H}_2\text{O}$   $\text{L}^{-1}$ ), 0.5 mL sodium hexametaphosphate (10 g  $\text{L}^{-1}$ ), 1 mL of test sample and 10 mL of saturated sodium bicarbonate solution were mixed. The mixture was agitated and after 15 minutes its absorbance at 260 nm was determined using an 1-cm path length-quartz cell. Since at 260 nm the organic content present in the test sample can interfere in the analysis, it is also necessary to prepare a second mixture replacing the 0.5 mL cobalt (II) chloride 6-hydrate solution by 0.5 mL ultrapure water. In the same way, two blanks using ultrapure water as test sample were prepared. Thus, applying the Beer's Law, the concentration of hydrogen peroxide in the sample can be determined using the following expression:

$$C_{\text{H}_2\text{O}_2} = \frac{\Delta A_{\text{Co-260nm}} - \Delta A_{\text{H}_2\text{O-260nm}}}{\epsilon_{260\text{nm}} b} \frac{V_{\text{Co/H}_2\text{O}} + V_{\text{metaphosp.}} + V_{\text{sample}} + V_{\text{bicarbon.}}}{V_{\text{sample}}} \quad (2.6)$$

where  $C_{\text{H}_2\text{O}_2}$  is the hydrogen peroxide concentration (in  $\text{mol L}^{-1}$ ),  $\Delta A_{\text{Co-260nm}}$  is the difference in absorbance between the test samples and blank prepared with cobalt (II) chloride,  $\Delta A_{\text{H}_2\text{O-260nm}}$  is the difference in absorbance between the test samples and blank prepared without cobalt (II) chloride,  $\epsilon_{260\text{nm}}$  is the cobalt(III)-bicarbonate complex molar absorptivity at 260 nm ( $2.665 \times 10^4 \text{ L mol}^{-1} \text{ cm}^{-1}$ ),  $b$  is the cell path length,  $V_{\text{Co/H}_2\text{O}}$  is the volume cobalt (II) chloride solution (or ultrapure water),  $V_{\text{metaphosp.}}$ ,  $V_{\text{sample}}$  and  $V_{\text{bicarbon.}}$  are the added volume of sodium hexametaphosphate, test sample and saturated sodium bicarbonate solutions, respectively.

The detection limit of the method is reported to be approximately  $3 \times 10^{-7} \text{ mol L}^{-1}$ .

### 2.3.9. Dissolved boron concentration

Boron in solution was photometrically determined at 410 nm by complexation with azomethine-H [8]. Typically, 5 ml sample, 4 ml buffer-masking solution (which was a mixture of 500 ml of a 0.5 wt% ammonium acetate solution, 125 mL glacial acetic acid, 6.7 g ethylenediamine tetraacetic acid and 60 mL of a 80 wt% thioglycolic acid solution) and 2 ml of azomethine-H solution (containing 9 and 2 g  $\text{L}^{-1}$  azomethine-H monosodium salt and L-ascorbic acid, respectively) were mixed. The mixture was allowed to stand in the dark for 1-2 h and transferred to an 1-cm quartz cell. Then its absorbance at 410 nm was measured and the boron concentration was obtained through comparison with a calibration curve. This method follows the Beer's Law up to 3 mg B  $\text{L}^{-1}$ .

### 2.3.10. Biological oxygen demand

The biological oxygen demand (BOD) was analyzed by measuring the oxygen consumption by bacteria while oxidizing the sample in a 5-day test period [9], using a ST-OxiTop<sup>®</sup> device. Activated sludge from a municipal wastewater treatment plant (Badajoz, Spain) was used as inoculum. An electronic pressure sensor is used to monitor the air pressure in an airtight bottle containing the sample and continually stirred during a 5-day incubation period. As the microorganisms consume organic matter present in the water, the air pressure inside the container is reduced since the bacteria use oxygen and release carbon dioxide. The CO<sub>2</sub> is subsequently absorbed by sodium hydroxide pellets placed in a cup of a septum sealed nozzle of the container. This causes a pressure drop inside the container.

To carry out this analysis, 432 mL of previously conditioned sample (pH adjusted to 6.5–7.5, filtered to remove catalyst particles if used, and mixed with 1% v/v of catalase solution (containing 0.01 wt% catalase from bovine liver) to quench hydrogen peroxide if used) was introduced together with 1 mL of activated sludge into an Oxitop<sup>®</sup> container provided with a pressure sensor and a septum sealed nozzle to introduce 3–4 NaOH pellets. Thereafter, the container was sealed, placed for five days into a temperature controlled incubator at 20°C and magnetically stirred. After the incubation period, the pressure sensor was used to convert the saved pressure drop data into mg L<sup>-1</sup> of oxygen.

### 2.3.11. Chemical oxygen demand

The analysis of the chemical oxygen demand (COD) was carried out by the closed reflux-colorimetric method [10]. In this procedure the sample is oxidized with potassium dichromate in sulfuric acid. The reaction is carried out at 148 °C using silver sulfate as a catalyst. The interference due to the possible presence of chloride ions is avoided by adding mercury sulfate to the reaction medium, which precipitates as mercuric chloride, HgCl<sub>2</sub>. The reduction of Cr(VI) to Cr(III) is then photometrically evaluated by the reduction in the yellow coloration of the mixture.

COD analysis was carried out using commercial LCK 414 kits (Lange) which are valid for a COD determination in the range 5–60 mg L<sup>-1</sup> O<sub>2</sub>. To carry out this test 2 mL of sample were added to a kit cuvette (containing a mixture of potassium dichromate, sulfuric acid, silver sulfate and mercury sulfate). Then the cuvette was introduced in a Lange thermoreactor (LT200), preheated up to 148°C and then kept at this temperature for 2 hours. After this time the cuvette was allowed to reach

room temperature and the COD value was analyzed using a Lange DR2800 spectrophotometer which directly provides the COD value.

### 2.3.12. Acute toxicity

Acute toxicity Daphnia tests were conducted following the commercial test kit DAPHTOXKIT F<sup>TM</sup> (MicroBioTests) using the water flea *D. Magna*. These tests were performed in accordance with testing conditions prescribed by OECD Guideline for Daphnia sp. acute immobilisation test [11]. Prior toxicity tests, the water sample was prepared by adjusting its pH to 6.5–7.5, filtration to remove catalyst particles, and mixing with 1% v/v of catalase solution (containing 0.01 wt% catalase from bovine liver).

Ephippia were incubated into a petri dish with a pre-aerated freshwater medium (prepared with standard solutions of NaHCO<sub>3</sub>, CaCl<sub>2</sub>·2H<sub>2</sub>O, MgSO<sub>4</sub>·7H<sub>2</sub>O and KCl provided by MicroBioTests) for 72 h at 20°C under continuous illumination of 6000 lux of light intensity at the top of the petri dish. After this hatching period and 2 h prior to being collected for the test, the neonates were fed with Spirulina microalgae suspension (MicroBioTests). Then, 20 actively swimming neonates were selected to be used in the analysis. The water sample to be assayed was divided into four replicates of 10 mL placed in a multiwall plate. Five neonates were added to each replicate. Immobility was observed after 48 h at 20°C in the dark. Immobilisation of the animals leads to their death because of inherent impossibility of capturing food. Potassium dichromate was the reference chemical used.

### 2.3.13. Turbidity

Turbidity of water was measured by the nephelometric method [12] using a HI 93414 turbidimeter (Hanna) with a measuring range from 0 to 1000 NTU (Nephelometric Turbidity Units). The HI 93414 turbidimeter includes a tungsten filament lamp to irradiate a water sample contained in a glass-made cuvette, and two photodetectors located at 90 and 180 degrees to the incident light path to measure respectively, the scattered and transmitted light. Then the microprocessor of the instrument calculates from the signals that reach the two detectors, the NTU value, using an effective algorithm.

To carry out the analysis the instrument was previously calibrated using standard suspensions supplied by Hanna Instruments.

### 2.3.14. Conductivity

Conductivity of the samples was measured by potentiometry [13] with a Crison 524 conductimeter. This device is a microprocessor based instrument which directly displays the sample conductivity on screen. This instrument is calibrated with standard suspensions of 1413 and 12.88  $\mu\text{S cm}^{-1}$  (25°C) supplied by Crison. Measurement accuracy was 3%.

### 2.3.15. Phenolic nature intermediates

Total phenolic content in the solution was determined by the method proposed by Singleton and Rossi [14], consisting in the oxidation of phenolic compounds by the Folin-Ciocalteu reagent, which is a mixture of phosphotungstic ( $\text{H}_3\text{PW}_{12}\text{O}_{40}$ ) and phosphomolybdic acid ( $\text{H}_3\text{PMo}_{12}\text{O}_{40}$ ). This reaction leads to the formation of mixture of tungsten ( $\text{W}_8\text{O}_{23}$ ) and molybdenum oxides ( $\text{Mo}_8\text{O}_{23}$ ) whose absorbance at 740 nm is proportional to the phenolic content in the sample. If present, Fe(II) ions can interfere with this analysis since it is oxidized to Fe (III) by the Folin-Ciocalteu reagent, therefore this interference is taken into account in the expression used to determine phenolic content.

Typically, 4 mL of test sample were mixed with 0.4 mL water and 0.4 mL Folin-Ciocalteu reagent, led to stand for 6 min, mixed with 3.2 mL  $\text{Na}_2\text{CO}_3$  solution (20 wt%) and after 30 min transferred to an 1-cm quartz cell to measure its absorbance at 740 nm. Simultaneously, Fe(II) concentration in the test sample was measured as indicated in item 2.3.7. Then, the equation (2.7) was applied to determine the phenolic compounds concentration in terms of bisphenol A equivalents (i.e. expressed as if all phenols were derived from bisphenol A since it is the compound having the mayor signal among the compounds used in this work).

$$C_{\text{Phenolyc}} = \frac{\Delta A_{740\text{nm}} - \varepsilon_{\text{Fe(II)/740nm}} C_{\text{Fe(II)}} b}{\varepsilon_{740\text{nm}} b} \frac{V_{\text{H}_2\text{O}} + V_{\text{Folin}} + V_{\text{sample}} + V_{\text{Na}_2\text{CO}_3}}{V_{\text{sample}}} \quad (2.7)$$

where  $C_{\text{Phenolyc}}$  is the phenolic compounds concentration (in mol BIS  $\text{L}^{-1}$ ),  $\Delta A_{740\text{nm}}$  is the difference in absorbance between the test sample and a blank (prepared with ultrapure water),  $\varepsilon_{740\text{nm}}$  is the molar absorptivity at 740 nm of phenolic compounds in terms of BIS ( $15200 \text{ L mol}^{-1} \text{ cm}^{-1}$  [15]),  $\varepsilon_{\text{Fe(II)/740nm}}$  is the molar absorptivity at 740 nm of species formed from Fe(II) in the solution ( $1983 \text{ L mol}^{-1} \text{ cm}^{-1}$  [15]),  $C_{\text{Fe(II)}}$  is the Fe(II) concentration (in mol  $\text{L}^{-1}$ ),  $b$  is the cell path length and  $V_{\text{H}_2\text{O}}$ ,  $V_{\text{Folin}}$ ,  $V_{\text{sample}}$  and  $V_{\text{Na}_2\text{CO}_3}$  are respectively, the volume of water, Folin reagent, test sample and sodium carbonate added.

### 2.3.16. Ions (phosphate, nitrate, sulfate and chloride) concentration

A 881 compact IC Pro ion chromatography apparatus (Metrohm) equipped with a Metrosep A Supp 7 anion column (150 x 4 mm diameter, 5  $\mu\text{m}$  particle size) thermostated at 45°C and a Metrohm conductivity detector was used to measure the anion content of water samples. A mixture of  $\text{Na}_2\text{CO}_3$  solution and ultrapure water was eluted at 0.7  $\text{mL min}^{-1}$  for 50 min varying the  $\text{Na}_2\text{CO}_3$  concentration from 0.6 to 14.6 mM. Chemical suppression was carried out using 250 mM  $\text{H}_2\text{SO}_4$  solution. Quantification was performed, prior calibration with standards, using MagIC Net 2.4 S.

The retention times for fluoride, chloride, nitrate, phosphate, and sulfate species were, 6.95, 12.81, 25.23, 35.16, and 36.36 min, respectively.

### 2.3.17. pH and temperature

pH measurement was performed by potentiometry using a GLP 21+ pH meter and a 5331 model electrode (equipped in the CPC photo-reactor), both provided by Crison and with a pH measuring range between 0 and 14. The electrodes were daily calibrated with buffer solutions of pH 4.01, 7.00 and 9.21 (Crison). These pH electrodes comprise integrated temperature sensors.

## 2.4. Catalyst characterization

---

### 2.4.1. X-ray diffraction (XRD)

In this work, the XRD technique was used to determine the crystalline phases present in the catalysts prepared. The X-ray diffraction patterns obtained from the catalysts were also used to determine the crystalline sizes of the phases found in them.

This analysis was carried out using a Bruker D8 Advance XRD diffractometer with a  $\text{Cu K}\alpha$  radiation ( $\lambda = 0.1541 \text{ nm}$ ) and a linear VANTEC detector. The data were collected from  $2\theta = 20^\circ$  to  $70^\circ$  at a scan rate of  $0.02 \text{ s}^{-1}$  and 1 s per point.

To carry out this analysis a solid catalyst sample, previously pulverized into fine powder and homogenized in an agate mortar, was compressed into a pellet using a manual hydraulic press and subjected to XRD analysis. During this analysis, the detector which is scanned around the sample along a detection circle, records the

angles at which the sample lattice planes families diffract the X-ray beams and the intensities of those diffractions. In this way, a characteristic two-dimensional pattern (diffraction intensity vs. angular position) is obtained and used as a fingerprint to determine the crystalline phases present in the sample by comparing the experimental pattern with those recorded in the database of the ICDD (International Centre for Diffraction Data) [16, 17].

The Scherrer's equation (2.8) was used to calculate the mean size of the most important single crystal nanoparticles found in the samples [18].

$$d = \frac{K \lambda}{\beta \cos\theta} \quad (2.8)$$

In equation (2.8)  $d$  is the crystallite size,  $K$  is a numerical factor frequently referred to as the crystallite-shape factor,  $\lambda$  is the wavelength of the X-rays,  $\beta$  is the width (full-width at half-maximum) of the X-ray diffraction peak in radians and  $\theta$  is the Bragg angle. In the absence of detailed shape information,  $K = 0.9$  is a good approximation [19].

In this work, the crystallite size for titania was calculated from the peak whose Miller indices are (1 0 1) while for magnetite or maghemite it was calculated from the peak with Miller indices (3 1 1) using the Scherrer's equation.

#### 2.4.2. X-ray photoelectron spectroscopy (XPS)

The surface chemical composition of the catalysts was evaluated by XPS. This analysis was carried out with a  $K\alpha$  Thermo Scientific apparatus equipped with an Al  $K\alpha$  ( $h\nu = 1486.68$  eV) X-ray source, using a voltage of 12 kV under vacuum ( $2 \times 10^{-7}$  mbar). Binding energies were calibrated relative to the C1s peak from carbon samples at 284.6 eV.

The samples (which were prepared in similar way as indicated for XRD analysis) were irradiated with energetic X-rays causing the emission of photoelectrons from the samples surfaces. The photoelectron kinetic energy ( $E_k$ ), which is measured during the analysis by an electron energy detector, is given by the Einstein's photoelectric law (equation (2.9) [20]):

$$E_k = h\nu + E_b \quad (2.9)$$

where  $h\nu$  is the energy of the incident radiation and  $E_b$  the binding energy of the electron in a particular level. If the incident photon is sufficiently energetic, many different levels in the sample may be ionized and thus a spectrum is produced [21].

The resulting XPS peaks were curve-fitted to a combination of Gaussian and Lorentzian functions using XPSPEAK Software with a Shirley type background for peak analysis. From the binding energy and intensity of a photoelectron peak, the elemental identity, chemical state and quantity of each element were determined.

Atomic ratio calculation was carried out from the peak areas and using Wagner atomic sensitivity factors [22] by the formula (2.10):

$$\frac{n_x}{n_y} = \frac{A_{p-x}/S_x}{A_{p-y}/S_y} \quad (2.10)$$

where  $n_x/n_y$  is the atomic ratio between elements  $x$  and  $y$  on the catalyst surface,  $A_p$  the peak area of each element and  $S$  the relative sensitivity factor based on empirical data.

### 2.4.3. Nitrogen adsorption-desorption isotherms

Catalyst textural parameters determined from nitrogen adsorption-desorption isotherms obtained using an Autosorb 1 apparatus (Quantachrome) at  $-196^\circ\text{C}$ .

Prior to analysis, the samples were outgassed at  $250^\circ\text{C}$  for 12 h under high vacuum ( $<10^{-4}$  Pa). Adsorption isotherms were obtained measuring the amount of nitrogen adsorbed onto the catalysts while the system relative pressure,  $P/P_0$ , was increased. And desorption isotherms were obtained from the amount of nitrogen removed from the catalysts as relative pressure was reduced. The recorded data during the experiment was processed with AS1Win<sup>TM</sup> 2.01 Software to determine the BET and surface areas and, the micropore volume.

BET area was determined by software using the method developed by Brunauer, Emmett and Teller [23] which is based on equation (2.11):

$$\frac{1}{V(P_0/P-1)} = \frac{1}{V_m C} + \frac{C-1}{V_m C} \left( \frac{P}{P_0} \right) \quad (2.11)$$



where  $V$  is the volume of gas adsorbed at a given relative pressure,  $P/P_0$ ,  $V_m$  the volume of gas required to form a complete unimolecular adsorbed layer and  $C$  a constant which is related to the heat of adsorption. A plot of  $1/[V(P_0/P-1)]$  against  $P/P_0$  should give a straight line whose intercept and slope are  $1/V_m C$  and  $(C-1)/V_m C$ , respectively. Thus from the slope and intercept  $V_m$  and  $C$  can be calculated [23]. When nitrogen is used the BET area,  $S_{\text{BET}}$ , is calculated from  $V_m$  by the expression (2.12) [24]:

$$S_{\text{BET}} = 4.37 V_m \quad (2.12)$$

where  $S_{\text{BET}}$  is in  $\text{m}^2 \text{g}^{-1}$  and  $V_m$  in  $\text{mL g}^{-1}$ . Accordingly, in this work the isotherm experimental data corresponding to relative pressures approximately between 0.03 and 0.15, was used for the  $S_{\text{BET}}$  computation.

The external area,  $S_{\text{EXT}}$ , was determined by the  $t$  method using the adsorption branch of the experimental isotherms. For this, a plot of the volume of gas adsorbed against a standard non-porous solid multilayer thickness,  $t$ , calculated by the Halsey's equation (2.12) [25] at every  $P/P_0$  value was prepared:

$$t = m \left( \frac{n}{\ln(P/P_0)} \right)^x \quad (2.13)$$

In equation (2.13)  $t$  is the adsorbate multilayer thickness (in  $\text{\AA}$ ),  $m$  the adsorbate monolayer thickness,  $n$  the Halsey equation numerator, and  $x$  the Halsey exponent. For nitrogen adsorption at  $-196^\circ\text{C}$ , the parameters  $m$ ,  $n$  and  $x$  can be assumed as  $3.54 \text{ \AA}$ ,  $-5$  and  $1/3$ , respectively. The slope of the linear portion of  $V$  vs.  $t$  curve was used to compute  $S_{\text{EXT}}$  according to equation (2.14) [24]:

$$V = \frac{S_{\text{EXT}}}{15.47} t \quad (2.14)$$

where  $V$ ,  $t$  and  $S_{\text{EXT}}$  are in  $\text{cm}^3 \text{g}^{-1}$ ,  $\text{\AA}$  and  $\text{m}^2 \text{g}^{-1}$ , respectively. Then the micropore surface,  $S_{\text{MICRO}}$ , can be calculated by equation (2.15):

$$S_{\text{MICRO}} = S_{\text{BET}} - S_{\text{EXT}} \quad (2.15)$$

Finally, the volume of micropores was determined calculating the intercept,  $i$ , of the  $V$  vs.  $t$  plot by extrapolating the linear portion with of the curve and then applying the expression (2.16):

$$V_{\text{MICRO}} = i \times 0.001547 \quad (2.16)$$

where  $V_{\text{MICRO}}$  and  $i$  are in  $\text{cm}^3 \text{g}^{-1}$ .

Nitrogen adsorption-desorption isotherms of the catalysts additionally allowed the classification of the type of solid (micro, meso and macroporous) according to the IUPAC's standards [23].

#### 2.4.4. Inductively coupled plasma

Inductively coupled plasma (ICP) was used to measure the Fe, Ti and B content in the catalysts. Additionally, this technique was used to monitor any leaching of Fe and Ti from the catalysts.

Throughout the research two ICP equipment were used. An ICP coupled with mass spectrometry (ICP-MS) NexION 300D (Perkin-Elmer) was used to analyze the iron content of the catalysts and, as well, to measure iron and titanium in solution. An ICP coupled with an optical emission spectrometry (ICP-OES) Optima 3300DV (Perkin-Elmer) was used to measure the B content in bulk catalysts.

Liquid samples were analyzed without additional preparation, while solid samples were previously digested in acidic medium assisted by microwaves. During analysis the samples were injected into Ar gas plasma and excited by a strong magnetic field. In the case of ICP-OES analysis, the excited elements and ions present in the samples emitted photons at a characteristic wavelength while returning to ground state. The total number of photons is directly proportional to the concentration of the originating element in the sample [26]. Therefore, the wavelengths of the photons were used to identify the elements present in the samples and their concentration. In ICP-MS analysis the plasma is used to generate positively charged ions which are directed to a mass spectrometer where they are distinguished by their mass-to-charge ratio [27].

#### 2.4.5. SQUID Magnetometry

Magnetic properties of the catalysts were measured in a Quantum Design MPMS XL-7 Superconducting Quantum Interference Device (SQUID).

In this analysis, the sample is slowly moved through a superconducting pick-up loop. The magnetic moment of the sample induces a magnetic flux change in the

pick-up coils. This change in magnetization generates a current in the pick-up loop around the sample. The SQUID output voltage is then recorded as a function of the sample position and is used to calculate the actual magnetic moment of the sample. The SQUID is computer controlled and for this work, the magnetization measurements were performed at room temperature as a function of applied magnetic field (M versus H).

The maximum possible magnetization or saturation magnetization, which represents the maximum induced magnetic moment that can be obtained in the sample was determined from the magnetization curve (M-H) as the asymptotical maximum value of M as H field increases [28,29].

#### 2.4.6. Diffuse reflectance UV-Vis spectroscopy (DR-UV-Vis)

The band gap in doped semiconductors was calculated via diffuse reflectance UV-Vis spectroscopy (DR-UV-Vis) using an UV-Vis-NIR Cary 5000 spectrophotometer (Varian-Agilent Technologies) equipped with an integrating sphere device.

UV-Visible spectra of the samples in the range 200-900 nm were recorded. This information was used to compute the semiconductor band gap applying the expression proposed by Tauc (2.17) [30]:

$$(\alpha h\nu)^{1/n} = C(h\nu - E_g) \quad (2.17)$$

where  $\alpha$  is an absorption coefficient (dimensionless),  $h$  the Planck's constant ( $4.135 \times 10^{-15}$  eV s),  $\nu$  the frequency of incident photons (in  $s^{-1}$ ),  $E_g$  the band gap (in eV),  $C$  a proportional constant (band tailing parameter),  $n$  is an index which can have different values as 1/2, 1/3, 2 and 3, such as direct allowed, direct forbidden, indirect allowed and indirect forbidden transitions, respectively.

Accordingly, for semiconductors like  $TiO_2$ , indirect and direct band-to-band allowed transitions are possible [31], which can be verified graphically by plotting  $(\alpha h\nu)^{1/n}$  vs.  $h\nu$  [32]. The absorption coefficient is calculated by the expression (2.18):

$$\alpha = -\ln(R) \quad (2.18)$$

where  $R$  is the reflectance expressed as a decimal. Finally, by plotting  $(\alpha h\nu)^2$  vs.  $h\nu$  and extrapolating the linear portion to the photon energy axis, when  $(\alpha h\nu)^2 = 0$  and  $h\nu = E_g$ , the semiconductor band gap was determined [33].

#### 2.4.7. Fourier transform infrared spectroscopy (FTIR)

Identification of functional groups present in the catalysts was performed by FTIR. Spectra of the samples were obtained on a Nicolet iS10 spectrometer using KBr wafers containing about. Data were acquired in the wavenumber range 400-4000  $\text{cm}^{-1}$  using 32 scans with a resolution of 4  $\text{cm}^{-1}$  and processed using OMNIC Software.

A solid mixture of sample and KBr, containing 0.01 g sample, is homogenized and pressed to obtain a pellet. Then an infrared light beam is passed through the pellet and the molecules contained in the sample absorb the photons whose vibration frequency corresponds to those of their chemical bonds. A detector measures the intensity of the transmitted beam to plot an infrared spectrum showing the transmission vs. wavenumber which is used as a fingerprint for identification of the type of functional groups in the sample [34].

#### 2.4.8. Scanning electron microscopy-Energy dispersive X-ray analysis (SEM-EDX)

The morphology of catalyst particles was characterized by scanning electron microscopy (SEM) using a Hitachi S-4800 apparatus working at 20-30 kV accelerating voltage and 500-2000 magnification. In addition, the catalyst was examined by means of energy dispersive X-ray analysis (EDX) to determine the distribution of Ti and Fe in the particles. For that purpose, a SSD detector XFlash 5010 (Bruker), working at 5 kV accelerating voltage and 500-2000 magnification was used.

In this analysis the sample is scanned by a high focussed electron beam producing low energy secondary electrons, backscattered electrons and X-rays. Then, by the measurement of the secondary electrons intensity a high resolution image of the sample topography is constructed. Additionally, the X-rays emitted from the sample are used to do an elemental analysis of it [35].

### 2.5. References

---

- [1] J.N. Miller, J.C. Miller, *Estadística y quimiometría para química analítica*, Prentice Hall, Pearson Educación, S.A., Madrid, 2002.

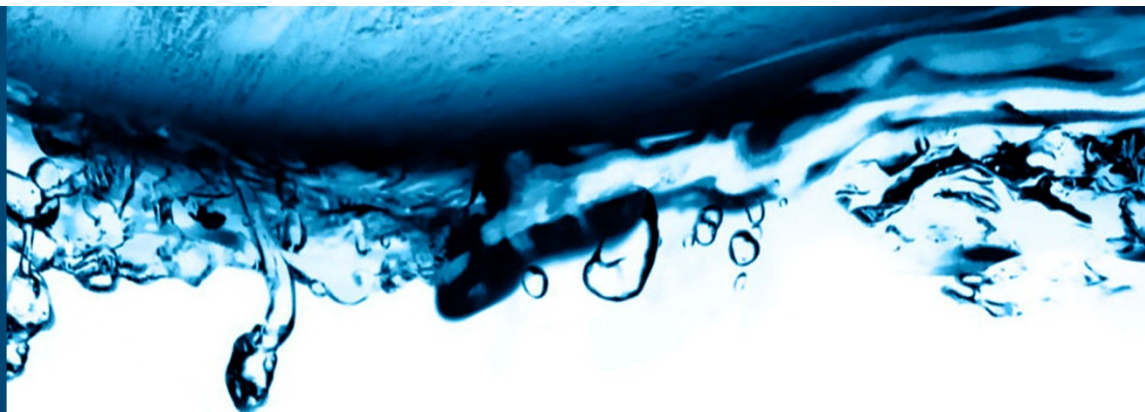
- [2] ASTM. *D7573-09, Standard test method for total carbon and organic carbon in water by high temperature catalytic combustion and infrared detection*, 2009, DOI: 10.1520/D7573-09.
- [3] H. Bader, J. Hoigné, *Determination of ozone in water by indigo method*, *Water Res.* 15 (1981) 449–456.
- [4] L.L. Stookey, *Ferrozine-A new spectrophotometric reagent for iron*, *Anal. Chem.* 42 (1970) 779–781.
- [5] Y. Zuo, *Kinetics of photochemical/chemical cycling of iron coupled with organic substances, in cloud and fog droplets*, *Geochim. Cosmochim. Ac.* 59 (1995) 3123–3130.
- [6] G. Eisenberg, *Colorimetric determination of hydrogen peroxide*, *Ind. Eng. Chem. Anal. Ed.* 15 (1943) 327–328.
- [7] W. Masschelein, M. Denis, R. Ledent, *Spectrophotometric determination of residual hydrogen peroxide*, *Water Sewage Works* 124 (1977) 69–72.
- [8] F.J. López, E. Giménez, F. Hernández, *Analytical study on the determination of boron in environmental water samples*, *Fresenius J. Anal. Chem.* 346 (1993) 984-987.
- [9] APHA-AWWA-WEF. *5210B: Biochemical Oxygen Demand (BOD)*, in: *Standard methods for the examination of water and wastewater*, 21th Edition, Washington DC, 2005.
- [10] APHA-AWWA-WEF. *5220: Chemical Oxygen Demand (COD)*, in: *Standard methods for the examination of water and wastewater*. 21th Edition, Washington DC, 2005.
- [11] OECD. *Test No. 202: Daphnia sp. Acute immobilisation test*, in: *OECD Guidelines for the testing of chemicals*, Section 2, OECD Publishing, 2004.
- [12] APHA-AWWA-WEF. *2130: Turbidity*, in: *Standard methods for the examination of water and wastewater*, 21th Edition, Washington DC, 2005.
- [13] APHA-AWWA-WEF. *2510: Conductivity*, in: *Standard methods for the examination of water and wastewater*, 21th Edition, Washington DC, 2005.
- [14] V. Singleton, J. Rossi. *Colorimetry of total phenolic with phosphomolybdic-phosphotungstic acid reagents*. *Am. J. Enol. Viticult.* 16 (1965) 144-158.
- [15] G. Fernández, *Degradación de bisfenol A en agua mediante procesos fotocatalíticos con luz negra y luz solar*, PhD dissertation, Universidad de Extremadura (2011).

- [16] B. Fultz, J. Howe, *Transmission electron microscopy and diffractometry of materials, graduate texts in physics*, Springer-Verlag Berlin, 2013.
- [17] B.B. He, U. Preckwinkel, K.L. Smith, *Fundamentals of two-dimensional x-ray diffraction (XRD<sup>2</sup>)*, in: *Advances in X-ray analysis*, International centre for diffraction data, 2000.
- [18] U. Holzwarth, N. Gibson, *The Scherrer equation versus the Debye-Scherrer equation*, *Nat. Nanotechnol.* 6 (2011) 534.
- [19] H.P. Klug, L.E. Alexander, *X-ray diffraction procedures for polycrystalline and amorphous materials*, 2nd. Edition, John Wiley & Sons, 1974.
- [20] C.R. Brundle, J.F. Watts, J. Wolstenholme, *X-ray photoelectron and auger electron spectroscopy*, in *Ewing's analytical instrumentation handbook*, 3rd Edition, CRC Press, New York, 2005.
- [21] A.M. Venezia, *X-ray photoelectron spectroscopy (XPS) for catalysts characterization*, *Catal. Today* 77 (2003) 359–370.
- [22] C.D. Wagner, L.E. Davis, M.V. Zeller, J.A. Taylor, R.H. Raymond, L.H. Gale, *Empirical atomic sensitivity factors for quantitative analysis by electron spectroscopy for chemical analysis*, *Surf. Interf. Anal.* 3 (1981) 211-225.
- [23] S. Brunauer, P. Emmett, E. Teller, *Adsorption of gases in multimolecular Layers*, *J. Am. Chem. Soc.* 60 (1938) 309–319.
- [24] B.C. Lippens, B.G. Linsen, J.H.D. Boer, *Studies on pore systems in catalysts I. The adsorption of nitrogen; Apparatus and calculation*, *J. Catal.* 3 (1964) 32-37.
- [25] M.I.D. Albani, C.P. Arciprete, *A study of pore size distribution and mean pore size on unsupported gamma-alumina membranes prepared by modifications introduced in the alkoxide hydrolysis step*, *J. Membr. Sci.* 69 (1992) 21-28.
- [26] X. Hou, B.T. Jones, *Inductively coupled plasma/optical emission spectrometry*, in: *Encyclopedia of Analytical Chemistry*, John Wiley & Sons Ltd, 2000.
- [27] A. Farhat, F. Ahmad, H. Arafat, *Analytical techniques for boron quantification supporting desalination processes: A review*, *Desalination* 310 (2013) 9–17.
- [28] R. Nagendran, N. Thirumurugan, N. Chinnasamy, M.P. Janawadkar, C.S. Sundar, *Development of high field SQUID magnetometer for magnetization studies up to 7 T and temperatures in the range from 4.2 to 300 K*, *Rev. Sci. Instrum.* 82, 015109 (2011).

- [29] K. Gramm, L. Lundgren, O. Beckman, *SQUID magnetometer for magnetization measurements*, Phys. Script. 13 (1976) 93-95.
- [30] A. Ibrahim, S.K.J. Al-Ani, *Models of optical absorption in amorphous semiconductors at the absorption edge - a review and re-evaluation*, Czech J. Phys. 44 (1994) 785-797.
- [31] K. Charette, K.Y.S. Ng, J. Zhu, S.O. Salley, D. Deng, *Gram-scale synthesis of high-temperature (900°C) stable anatase TiO<sub>2</sub> nanostructures assembled by tunable building subunits for safer lithium ion batteries*, RSC Adv. 4 (2014) 2557-2562.
- [32] P. Malliga, J. Pandiarajan, N. Prithivikumar, K. Neyvasagam, *Influence of film thickness on structural and optical properties of sol – gel spin coated TiO<sub>2</sub> thin film*, J. Appl. Phys. 6 (2014) 22-28.
- [33] F.A. Mir, *Transparent wide band gap crystals follow indirect allowed transition and bipolaron hopping mechanism*, Results in Physics 4 (2014) 103-104.
- [34] N. Jaggi, D.R. Vij, *Fourier transform infrared spectroscopy*, in: *Handbook of applied solid state spectroscopy*, Springer Science+Business Media, 2006.
- [35] J.M. Rodenburg, *Electron microscopy and analysis 1997: Proceedings of the institute of physics electron microscopy and analysis group conference, Cavendish Laboratory, University of Cambridge*, Institute of Physics Publishing, Bristol, 1997.







## Chapter III

### Paper 1:

Application of solar photocatalytic ozonation for the degradation of emerging contaminants in water in a pilot plant

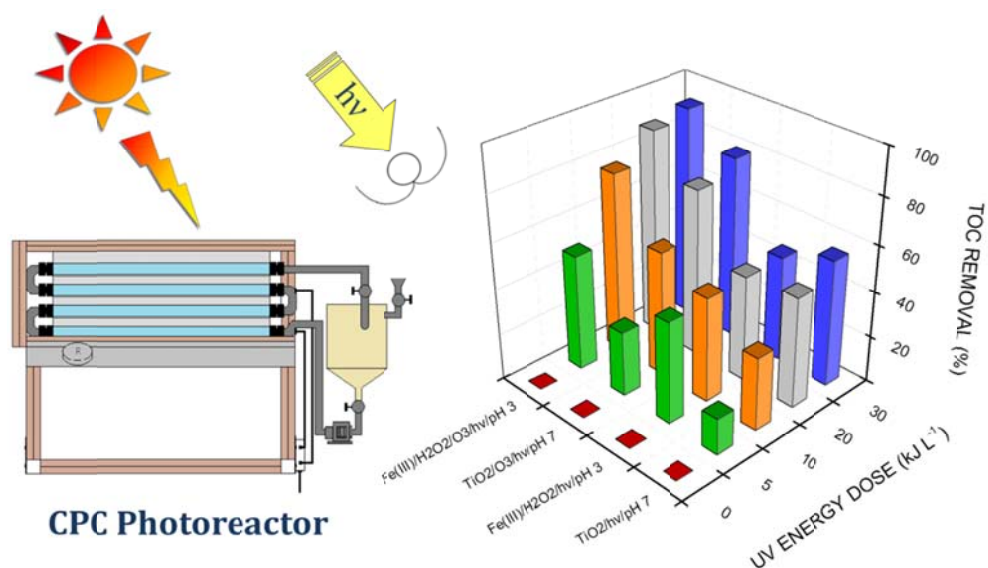
Diego H. Quiñones<sup>1</sup>, Pedro M. Álvarez<sup>1</sup>, Ana Rey<sup>1</sup>, Sandra Contreras<sup>2</sup>, Fernando J. Beltrán<sup>1</sup>

<sup>1</sup> Departamento de Ingeniería Química y Química Física, Facultad de Ciencias, Universidad de Extremadura, Av. de Elvas s/n, 06071 Badajoz (Spain)

<sup>2</sup> Departament d'Enginyeria Química, Universitat Rovira i Virgili, Campus Sescelades, Av. Països Catalans 26, 43007 Tarragona (Spain)

Chemical Engineering Journal, 260 (2015) 399-410





### 3.1. Abstract

Aqueous mixtures of six commonly detected emerging contaminants (acetaminophen, antipyrine, bisphenol A, caffeine, metoprolol and testosterone), selected as model compounds, were treated by different solar-driven photochemical processes including photolysis, photocatalytic oxidation with Fe(III) or TiO<sub>2</sub>, photo-Fenton and single, photolytic and photocatalytic ozonations. Experiments were carried out in a compound parabolic collector photoreactor. It was found that photolysis and photocatalytic oxidation using Fe(III) are not effective for the complete removal of the selected contaminants, while TiO<sub>2</sub> photocatalysis, photo-Fenton, single, photolytic and photocatalytic ozonations can rapidly remove them and decrease total organic carbon to some extent. The combination of photocatalytic oxidation and ozonation considerably enhances the system efficiency by reducing the ozone demand and energy requirements to completely remove the contaminants. Results also demonstrate that, at the operational conditions applied in this work, the contaminant removal and mineralization by ozone processes takes place in the slow kinetic regime, therefore the application of the ozone combined processes studied instead of single ozonation is recommended. Kinetic considerations on the application of solar photocatalytic processes for mineralization have been also assessed.

**Keywords:** Compound parabolic collector, emerging compound, ozonation kinetic regime, photocatalytic ozonation, synergy.

### 3.2. Introduction

---

Nowadays a great number of pharmaceuticals and personal care products, commonly known as emerging contaminants (ECs), are being detected in aqueous systems such as rivers, lakes, streams, aquifers and wastewater treatment plant influents and effluents. These compounds are considered potentially hazardous as some are ubiquitous, persistent to conventional wastewater treatments and biologically active, many of them with recognized endocrine disruption functions [1,2].

Advanced Oxidation Processes (AOPs) constitute an alternative for the degradation of ECs. AOPs are physicochemical processes based on the generation of hydroxyl radicals ( $\cdot\text{OH}$ ) under mild experimental conditions. The hydroxyl radical has a non-selective, high oxidizing power ( $E^\circ = 2.8\text{V}$  vs. SHE), which makes it able to mineralize almost any organic molecule, yielding  $\text{CO}_2$  and inorganic ions [3].

Heterogeneous photocatalytic oxidation, being one of the most applied AOPs, involves the absorption in a semiconductor particle of photons of energy ( $h\nu$ ) equal to or exceeding the band gap energy ( $E_g$ ) of the semiconductor, resulting in the excitation of an electron ( $e^-_{\text{CB}}$ ) from the valence band to the conduction band and, therefore, in the generation of a positive hole ( $h^+_{\text{VB}}$ ) in the valence band. Electron/hole pairs might further trigger a process leading to the generation of  $\cdot\text{OH}$  and, as a result, to the degradation of pollutants. Titanium dioxide is, so far, the most extensively used photocatalyst due to its high chemical stability, its non-toxicity, its relatively low cost and its highly oxidizing power in solar-driven processes as it is capable to absorb UV radiation from the solar spectrum [3]. Likewise, homogeneous photocatalytic systems using iron-based catalysts have been widely applied. Thus, Fe(III) photocatalytic oxidation can generate iron (III) aqua complexes, primarily  $\text{Fe}(\text{OH})^{2+}$ , which undergoes photolysis under radiation of  $\lambda > 300\text{ nm}$  to yield  $\cdot\text{OH}$  radicals. Moreover, if hydrogen peroxide is added, the resulting system, known as photo-Fenton, enhances the generation of hydroxyl radicals through the decomposition of  $\text{H}_2\text{O}_2$ . Iron-based catalysts are not toxic, easily available and can be efficiently used at acidic conditions [4,5].

Ozonation has also been extensively used in water treatment. Ozone is a selective oxidant ( $E^\circ = 2.07\text{V}$  vs. SHE in acidic medium and  $1.27\text{V}$  vs. SHE in alkaline medium), which can react directly with many organic compounds. In addition, it can also decompose, especially at alkaline conditions, into hydroxyl radicals [6].

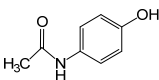
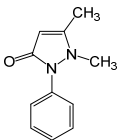
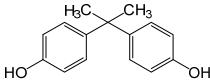
It is well known that the combination of various AOPs may lead to an enhanced production of  $\cdot\text{OH}$  radicals and other oxidizing species and, as consequence, to

faster degradation pollutants. In this sense, photocatalytic ozonation, which involves the combination of photocatalytic oxidation and ozonation, can be a promising treatment method [7]. Some previous studies have already shown that synergistic effect might occur when photocatalysis and ozonation are carried out simultaneously [8,9].

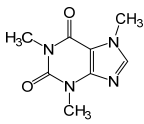
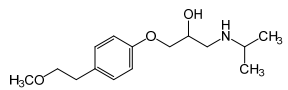
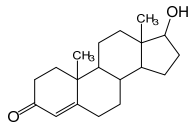
In this work, various AOPs, such as ozonation, photolytic ozonation, Fe(III) photocatalytic oxidation, photo-Fenton, TiO<sub>2</sub> photocatalytic oxidation and the combination of some of them have been applied to degrade aqueous mixtures of six ECs under solar illumination and process performance has been compared. The ECs used have been acetaminophen (ACE), antipyrine (ANT), bisphenol A (BIS), caffeine (CAF), metoprolol (MTP) and testosterone (TST). Their chemical structures, common uses and some reported data on their detection in water bodies are summarized in Table 3.1.

Previous works have addressed the abatement of ECs in water using solar-driven photocatalysis [10–12] and ozonation [13–15]. However, to the best of our knowledge, only three works have been published so far dealing with solar photocatalytic ozonation at pilot scale [16–18]. The present work is focused on a study on the kinetic aspects concerning these AOPs, such as oxidation pathways, ozone reaction regimes of absorption and apparent reaction rate constants, as well as on the synergistic effect of some solar-driven combined processes.

**Table 3.1.** Chemical structures, common uses and occurrence in water bodies of the ECs used in this work

Compound	Chemical structure	Common uses	Detected in
ACE		Analgesic, antiinflammatory	WWTP influents and effluents (up to 1534 ng L <sup>-1</sup> ) [1], groundwater (up to 1890 ng L <sup>-1</sup> ) [19], surface waters (up to 10000 ng L <sup>-1</sup> ) [20,21].
ANT		Antipyretic, analgesic	WWTP influents (up to 72 ng L <sup>-1</sup> ) and effluents (up to 58 ng L <sup>-1</sup> ) [15], and surface waters (up to 752 ng L <sup>-1</sup> ) [21].
BIS		Plasticizer	WWTP effluents (up to 3642 ng L <sup>-1</sup> ) [22], surface waters (up to 12000 ng L <sup>-1</sup> ) [20], and paper industry effluents (up to 370000 ng L <sup>-1</sup> ) [23].

**Table 3.1. (continued)** Chemical structures, common uses and occurrence in water bodies of the ECs used in this work

Compound	Chemical structure	Common uses	Detected in
CAF		Stimulant	WWTP influents (up to 230000 ng L <sup>-1</sup> ) [24] and effluents (up to 1589 ng L <sup>-1</sup> ) [15], and surface waters (up to 6000 ng L <sup>-1</sup> ) [20].
MTP		β-blocker	WWTP effluents and surface waters (both up to 2200 ng L <sup>-1</sup> ) [25].
TST		Steroid hormone	WWTP effluents (up to 4.9 ng L <sup>-1</sup> ) [22] and surface waters (up to 214 ng L <sup>-1</sup> ) [20].

### 3.3. Materials and methods

#### 3.3.1 Chemicals

Unbuffered ultrapure water (18.2 MΩ cm) obtained from a Milli-Q water purification system provided with a Quantum ultrapure cartridge (Millipore S.A) was used to prepare aqueous solutions of the six selected ECs, all of them purchased from Sigma–Aldrich. Solutions containing the target ECs were stored in the dark at room temperature and were found to be stable for several weeks. Hydrogen peroxide (30% w/v) was acquired from Panreac.

Iron (III) perchlorate hydrate (Sigma–Aldrich) was used as Fe(III) source in homogeneous Fe(III) photocatalytic oxidation experiments while AEROXIDE® TiO<sub>2</sub> P25 (Degussa-Evonik) was used as catalyst in heterogeneous photocatalytic oxidation experiments.

Chemically pure (>99%) sodium chloride, sodium sulfate, sodium carbonate, sodium nitrate and sodium phosphate 12-hydrated, all of them supplied by Panreac, were used in some experiments. Other laboratory reagents used throughout the experiments were sodium thiosulfate pentahydrate (Merck), potassium indigo-trisulfonate (Sigma–Aldrich), acetonitrile (Fisher Scientific), phosphoric acid (85%, Fisher Scientific), titanium(IV) oxysulfate-sulfuric acid solution (Sigma–Aldrich), hydrochloric acid (37%, Acros Organics) and sodium hydroxide (Panreac).

### 3.3.2. Experimental set-up

A compound parabolic collector (CPC) was used as photo-reactor. The reactor was assembled by Ecosystem Environmental Services S.A. (Spain) and equipped with 4 borosilicate glass tubes (32 mm external diameter, 1.4 mm thickness, 750 mm length), anodized aluminum reflectors tilted 45 degrees and, inlets and outlets for the gases (see Figure 3.1.). The total collector surface is 0.25 m<sup>2</sup> and the illuminated volume is 1.8 L. A broadband UV radiometer (290-370 nm, Acadus 85-PLS) tilted at the same angle of the CPC was used to measure the solar instantaneous and accumulated UV light absorbed. A laboratory ozone generator (OZVa 1200E, ProMinent) was used for the production of ozone from an air stream supplied by a compressor (Extreme 30, Pintuc). A precision gas flow controller (Alicat Scientific) set to 0.67 L min<sup>-1</sup> was used to continuously feed the inlet gas that was bubbled through two porous plates situated at two of the reactor tubes. The pH of the aqueous solution was controlled at set point values by means of an automatic pH control system. GM-6000-RTI and GM-6000-PRO ozone analyzers (Anseros) were used to monitor the ozone concentration in the inlet and outlet gas streams, respectively.

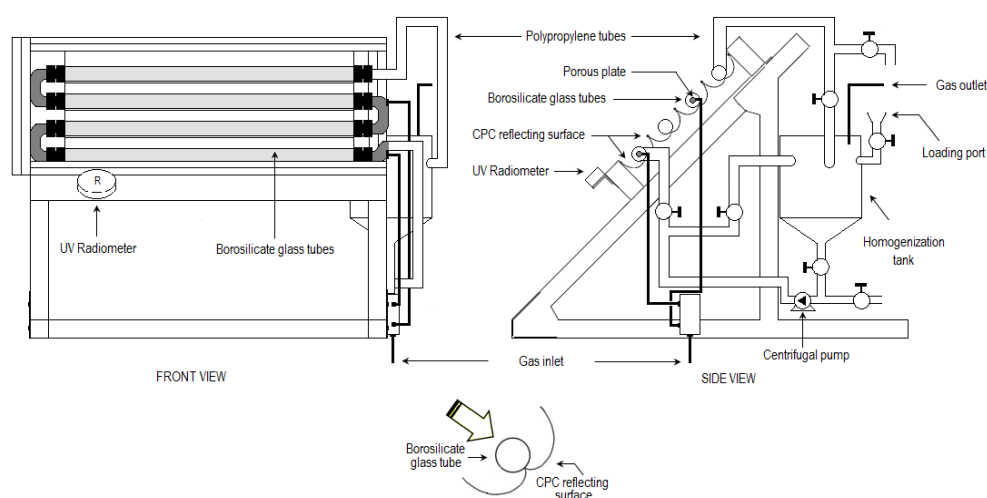


**Figure 3.1.** Scheme of the CPC photo-reactor

### 3.3.3. Experimental procedure

Semi-batch mode experiments were carried out in Badajoz, Spain (38°52'43" N, 6°58'15" W) under sunlight and at ambient temperature. Typically, a reservoir tank was first loaded with 5 L of the aqueous solution of ECs and the required amount

of catalyst was added afterwards. Then, the solution was recirculated through the CPC by a centrifugal pump at a flow rate of  $8.7 \text{ L min}^{-1}$  so that the flux pattern inside the tubes was turbulent (the Reynolds number was 7550). For the first 30 min, the CPC tubes were kept covered to avoid sunlight illumination. This time was enough to reach the adsorption equilibrium of ECs onto  $\text{TiO}_2$  (if used). After that, the CPC was uncovered and the gas feeding was started. Also, if needed, hydrogen peroxide was added at this point. Reaction samples were withdrawn at intervals through a sampling port to determine the ECs concentration, the remaining total organic carbon (TOC), and the concentrations of hydrogen peroxide, ozone and Fe(II). The ozone concentration in the outlet gas stream was also continuously monitored with in-line ozone analyzers.

The initial concentration for each compound was  $10^{-5} \text{ mol L}^{-1}$  (i.e. in  $\text{mg L}^{-1}$ , 1.51 ACE, 1.88 ANT, 2.28 BIS, 1.94 CAF, 2.67 MTP and 2.88 TST). These starting concentrations were selected to improve the chemical analysis accuracy and facilitate a kinetic comparative study of the mineralization. The initial Fe(III) and  $\text{TiO}_2$  concentrations were  $2.79$  and  $200 \text{ mg L}^{-1}$ , respectively, and the initial  $\text{H}_2\text{O}_2/\text{Fe(III)}$  mass ratio was 6.09. Depending on the type of experiment being carried out, the gas inlet was either air or an air-ozone mixture ( $13 \text{ mg L}^{-1}$  ozone). These experimental conditions were chosen from previous works [7,26,27] where they resulted very appropriate to study the removal and mineralization of water pollutants. Experiments using iron-based systems were conducted at pH 3 while  $\text{TiO}_2$ -based systems were at pH 7.

### 3.3.4. Analytical methods

Some samples taken from the reactor during the course of experiments using ozone were immediately bubbled with helium to remove residual ozone. Likewise, excess hydrogen peroxide in samples could be quenched by adding an aliquot of concentrated sodium thiosulfate solution. These procedures avoided further ozone and/or hydrogen peroxide reactions while samples were kept before ECs and TOC analyses. It was checked that no volatile organic compounds were removed as a result of helium bubbling. Prior to analysis, the samples were filtered by a  $0.22 \mu\text{m}$  PET filtering membrane (Chromafil Xtra).

The concentration of the compounds was analyzed by high-performance liquid chromatography with an Agilent 1100 Series HPLC apparatus (Hewlett Packard) equipped with a Kromasil C18 column ( $150 \text{ mm} \times 4 \text{ mm}$  internal diameter,  $5 \mu\text{m}$  particle size, Teknokroma) as stationary phase. ANT, CAF and MTP were analyzed with  $0.65 \text{ mL min}^{-1}$  flow of a 3:17 (v/v) acetonitrile (solvent A) and 0.1%



(v/v) phosphoric acid solution (solvent B) mixture and 240, 275 and 225 nm, respectively, as detection wavelengths. BIS and TST were analyzed using a 50% mixture of solvents A and B at 1 mL min<sup>-1</sup> and 220 and 250 nm, respectively, as detection wavelengths. ACE was analyzed with a 3:17 (v/v) mixture of solvents A and B at 1 mL·min<sup>-1</sup> and 244 nm wavelength detection.

Total organic carbon (TOC) was measured using a TOC-VSCH analyzer (Shimadzu) equipped with an ASI-V autosampler.

Dissolved ozone concentration was spectrophotometrically measured at 600 nm by the indigo method [28]. Hydrogen peroxide at concentrations below 2.21 ppm ( $6.5 \times 10^{-5}$  mol L<sup>-1</sup>) was measured by photometry at 260 nm using the cobalt-bicarbonate method proposed by Masschelein [29] while for higher H<sub>2</sub>O<sub>2</sub> concentrations the Eisenberg colorimetric method was followed [30]. Aqueous Fe(II) was colorimetrically measured at 510 nm by complexation with ortho-phenantroline [31]. All the spectrophotometric measurements were carried out in a Helios- $\alpha$  UV/Vis spectrophotometer (ThermoSpectronic).

### 3.4. Results and discussion

---

#### 3.4.1. Preliminary experiments

To determine whether the selected ECs formed solar-photoactive iron complexes at the experimental conditions used in this work, aqueous solutions of each target compound and mixtures of each of them and Fe(III) were prepared at pH 3 and their UV-vis spectra were recorded. It was found that the spectra of each compound and that of its corresponding mixture with Fe(III) were identical, which means that no photoactive iron complexes were formed. Figure 3.S1. of the supplementary material shows the absorption spectra of these solutions for wavelengths between 200 and 500 nm (no absorption was observed at wavelengths above the plotted range).

#### 3.4.2. Target compounds depletion and total organic carbon removal

Aqueous solutions containing a mixture of the six ECs were subjected to various AOPs. The oxidation systems applied were: photolysis (hv), Fe(III)-photocatalytic oxidation (Fe(III)/hv), photo-Fenton (Fe(III)/H<sub>2</sub>O<sub>2</sub>/hv), ozonation (O<sub>3</sub>), photolytic ozonation (O<sub>3</sub>/hv), Fe(III)-photocatalytic ozonation (Fe(III)/O<sub>3</sub>/hv), photo-Fenton-based photocatalytic ozonation (Fe(III)/H<sub>2</sub>O<sub>2</sub>/O<sub>3</sub>/hv), TiO<sub>2</sub> photocatalytic oxidation (TiO<sub>2</sub>/hv), and TiO<sub>2</sub> photocatalytic ozonation (TiO<sub>2</sub>/O<sub>3</sub>/hv). Figure 3.2. shows the

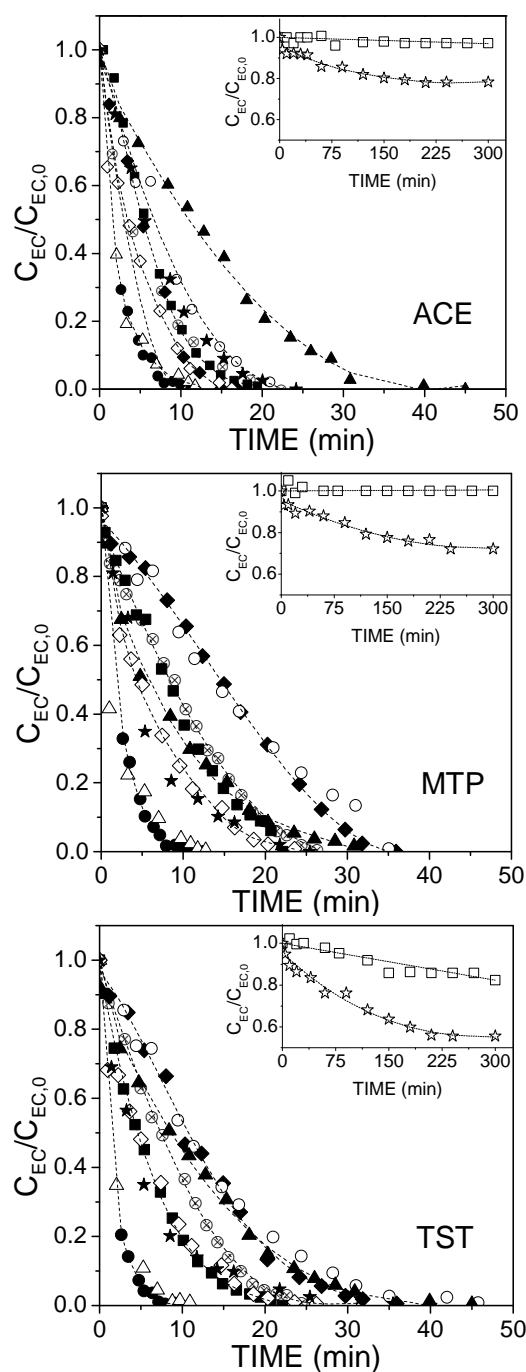


**Figure 3.2.** Evolution of the normalized concentration ( $C_{EC}/C_{EC,0}$ ) for ACE, MTP and TST. Experimental conditions: Mixture of six ECs ( $10^{-5}$  mol L $^{-1}$  each),  $C_{Fe(III)} = 2.79$  mg L $^{-1}$ ,  $H_2O_2/Fe(III) = 6.09$  (mass),  $C_{TiO_2} = 200$  mg L $^{-1}$ ,  $Q_g = 0.67$  L min $^{-1}$ ,  $C_{O_3,g} = 13$  mg L $^{-1}$ , average incident UVA solar radiation  $41.2$  W m $^{-2}$ . Symbols: hv ( $\square$ ), Fe(III)/hv/pH 3 ( $\star$ ), Fe(III)/H $_2$ O $_2$ /hv/pH 3 ( $\bullet$ ), O $_3$ /pH 3 ( $\blacklozenge$ ), O $_3$ /hv/pH 3 ( $\otimes$ ), Fe(III)/O $_3$ /hv/pH 3 ( $\blacksquare$ ), Fe(III)/H $_2$ O $_2$ /O $_3$ /hv/pH 3 ( $\triangle$ ), TiO $_2$ /hv/pH 7 ( $\blacktriangle$ ), O $_3$ /pH 7 ( $\circ$ ), O $_3$ /hv/pH 7 ( $\star$ ), TiO $_2$ /O $_3$ /hv/pH 7 ( $\diamond$ ).

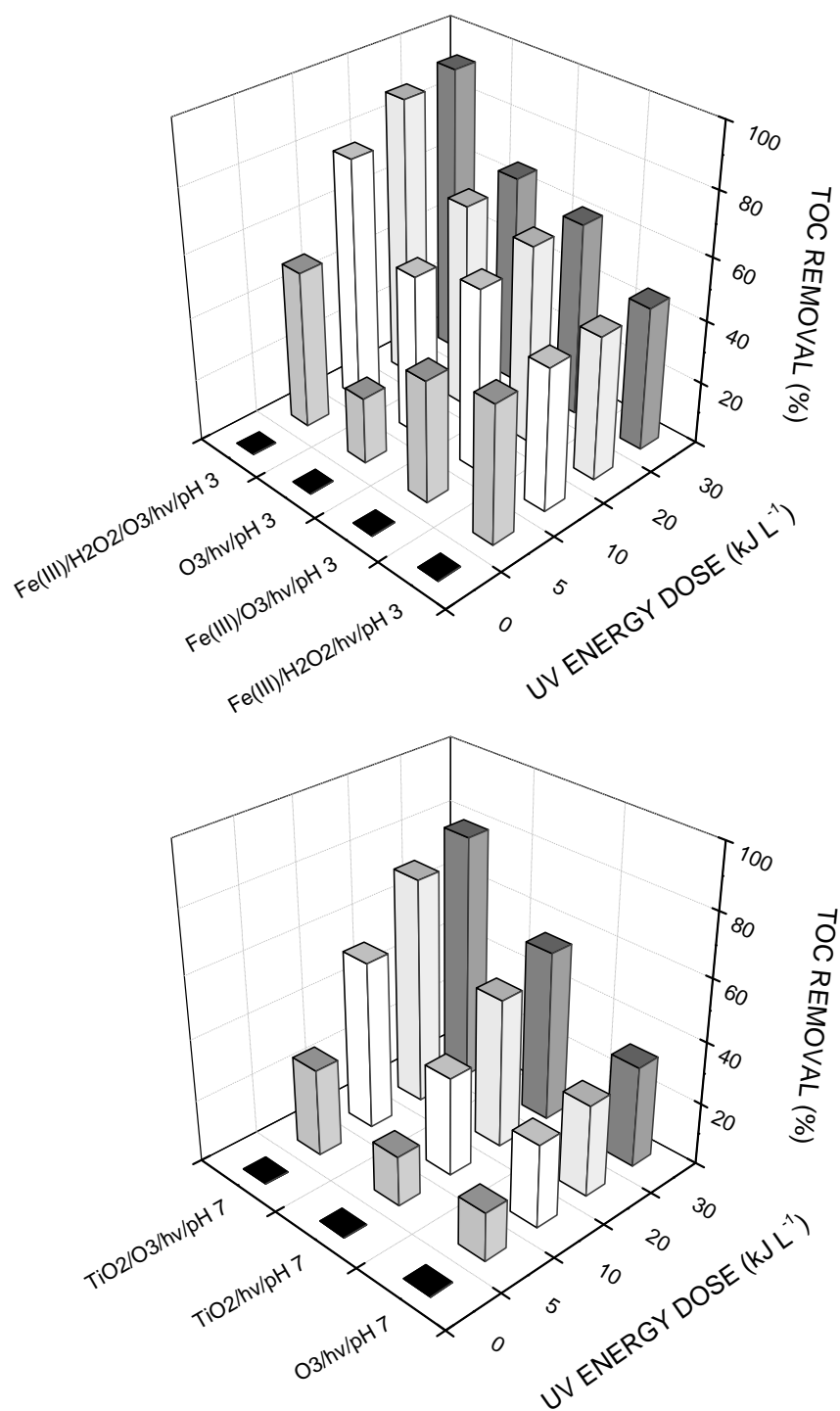


**Figure 3.3.** Evolution of the TOC removal vs. UV dose for systems at pH 3 (upper graph) and 7 (lower graph). Experimental conditions: Mixture of six ECs ( $10^{-5}$  mol L<sup>-1</sup> each),  $C_{\text{Fe(III)}} = 2.79$  mg L<sup>-1</sup>,  $\text{H}_2\text{O}_2/\text{Fe(III)} = 6.09$  (mass),  $C_{\text{TiO}_2} = 200$  mg L<sup>-1</sup>,  $Q_g = 0.67$  L min<sup>-1</sup>,  $C_{\text{O}_3,\text{g}} = 13$  mg L<sup>-1</sup>, average incident UVA solar radiation 41.2 W m<sup>-2</sup>.

concentration profiles during the course of these experiments for ACE, MTP and TST as an example. It should be notice that the compounds concentrations were normalized with respect to their corresponding initial concentrations.

Also, the TOC evolution vs. supplied solar energy is shown in Figure 3.3. for the experiments for which fast TOC removal was observed. Figure 3.S2. of the supplementary material shows the correlation between solar energy dose and irradiation time.

All solar experiments were started around midday in order to have similar radiation conditions. Thus, as can be seen in Figure 3.S2., the energy supplied during the first 90 min of irradiation was quite similar for all the experiments. Differences in the accumulated energy with time among experiments were only noticeable at longer reaction times.

#### A. ECs adsorption onto TiO<sub>2</sub>

As stated in the experimental section, when TiO<sub>2</sub> was used as catalyst, adsorption of ECs was allowed for 30 min in the dark. This time was proven long enough to reach adsorption equilibrium. It was found that barely 2-6% of the initial amount of ECs was adsorbed onto TiO<sub>2</sub>.

#### B. Photolysis

None of the ECs investigated but TST was removed by direct photolysis. This fact was expected since solar radiation under 290 nm does not reach Earth's surface as it is mostly retained by gases in the atmosphere [32] and target ECs do not absorb radiation above 300 nm significantly (Figure 3.S1.). Additionally, CPC borosilicate tubes only cut off radiation with wavelengths below 300 nm. However, TST was partially photo-degraded (14%) by solar radiation (see Figure 3.2.). As discussed elsewhere [33] this is likely due to the fact that TST can absorb radiation of wavelengths below 360 nm (molar absorptivity,  $\epsilon$ , around  $110 \text{ L mol}^{-1} \text{ cm}^{-1}$  and quantum yield,  $\Phi$ , at 313 nm of  $2.4 \times 10^{-3}$ ), giving rise to  $n \rightarrow \pi^*$  transition of its carbonyl group. Despite partial removal of TST, direct photolysis ( $h\nu$ ) did not lead to mineralization at all (not shown).

#### C. Photocatalytic oxidation

Table 3.2. summarizes the main reactions involved in the AOPs used in this work. In the photocatalytic oxidation with Fe(III)/ $h\nu$ , compound oxidation occurs by the formation of aqua complexes, mainly Fe(OH)<sup>2+</sup> (see reaction (3.1)), which can

undergoes photolysis under UV radiation ( $\lambda > 300$  nm) to give hydroxyl radicals as shown in reaction (3.2). The quantum yield of  $\text{Fe}(\text{OH})^{2+}$  photolysis is 0.14 at 313 nm and 0.017 at 360 nm [34].

**Table 3.2.** Reactions involved in the AOPs applied

Reaction		Kinetic constants	Ref.
$\text{Fe}^{3+} + \text{H}_2\text{O} \rightleftharpoons \text{Fe}(\text{OH})^{2+} + \text{H}^+$	(3.1)		[34]
$\text{Fe}(\text{OH})^{2+} \xrightarrow{h\nu} \text{Fe}^{2+} + \cdot\text{OH}$	(3.2)	$1.2 \times 10^{-3} \text{ s}^{-1}$	[34]
$\text{Fe}^{2+} + \text{H}_2\text{O}_2 \longrightarrow \text{Fe}^{3+} + \text{OH}^- + \cdot\text{OH}$	(3.3)	$63 \text{ M}^{-1} \text{ s}^{-1}$	[35]
$\text{H}_2\text{O}_2 \xrightarrow{h\nu} 2\cdot\text{OH}$	(3.4)		[36]
$\text{H}_2\text{O}_2 + \cdot\text{OH} \longrightarrow \text{HO}_2\cdot + \text{H}_2\text{O}$	(3.5)	$3 \times 10^7 \text{ M}^{-1} \text{ s}^{-1}$	[36]
$\text{Fe}^{3+} + \text{HO}_2\cdot \longrightarrow \text{O}_2 + \text{Fe}^{2+} + \text{H}^+$	(3.6)	$3.3 \times 10^5 \text{ M}^{-1} \text{ s}^{-1}$	[36]
$\text{O}_3 + \text{OH}^- \longrightarrow \text{HO}_2\cdot + \text{O}_2^{\cdot-}$	(3.7)	$70 \text{ M}^{-1} \text{ s}^{-1}$	[37]
$\text{O}_3 + \text{O}_2^{\cdot-} \longrightarrow \text{O}_3^{\cdot-} + \text{O}_2$	(3.8)	$1.6 \times 10^9 \text{ M}^{-1} \text{ s}^{-1}$	[37]
$\text{O}_3 + \cdot\text{OH} \longrightarrow \text{HO}_4\cdot$	(3.9)	$2 \times 10^9 \text{ M}^{-1} \text{ s}^{-1}$	[37]
$\text{O}_3 + \text{H}_2\text{O} \xrightarrow{h\nu} \text{O}_2 + \text{H}_2\text{O}_2$	(3.10)		[38]
$\text{Fe}^{2+} + \text{O}_3 \longrightarrow \text{FeO}^{2+} + \text{O}_2$	(3.11)	$8.2 \times 10^5 \text{ M}^{-1} \text{ s}^{-1}$	[39]
$\text{FeO}^{2+} \longrightarrow \text{Fe}^{3+} + \cdot\text{OH} + \text{OH}^-$	(3.12)	$1.3 \times 10^{-2} \text{ M}^{-1} \text{ s}^{-1}$	[39]
$\text{FeO}^{2+} + \text{Fe}^{2+} + 2\text{H}^+ \longrightarrow 2\text{Fe}^{3+} + \text{H}_2\text{O}$	(3.13)	$1.4 \times 10^5 \text{ M}^{-1} \text{ s}^{-1}$	[39]
$\text{TiO}_2 \xrightarrow{h\nu \leq 390 \text{ nm}} \text{e}^-_{\text{CB}} + \text{h}^+_{\text{VB}}$	(3.14)		[3]
$\text{h}^+_{\text{VB}} + \text{OH} \longrightarrow \cdot\text{OH}$	(3.15)		[3]
$\text{O}_2 + \text{e}^-_{\text{CB}} \longrightarrow \text{O}_2^{\cdot-}$	(3.16)		[3]
$\text{O}_3 + \text{e}^-_{\text{CB}} \longrightarrow \text{O}_3^{\cdot-}$	(3.17)	$3.6 \times 10^{10} \text{ M}^{-1} \text{ s}^{-1}$	[40]
$\text{O}_3^{\cdot-} + \text{H}^+ \longrightarrow \text{HO}_3\cdot$	(3.18)		[3]
$\text{HO}_3\cdot \longrightarrow \text{O}_2 + \cdot\text{OH}$	(3.18b)		[3]

According to Figure 3.2., the Fe(III)/hv system led to partial degradation of the ECs. ECs conversion was between 15 and 30%, except for TST. For this latter, a higher conversion (45%) was reached as a result of the contribution of direct photolysis as discussed above. The Fe(III)/hv system, however, was not able to mineralize the ECs to any extent (not shown).

The addition of H<sub>2</sub>O<sub>2</sub> to Fe(III)/hv system gives rise to the well-known oxidation system called photo-Fenton. In this system, H<sub>2</sub>O<sub>2</sub> accelerates the  $\cdot$ OH production via reactions (3.3) and (3.4) (see Table 3.2.). Additionally, hydrogen peroxide can react with  $\cdot$ OH to form hydroperoxyl radicals (reaction (3.5) in Table 3.2.), which, in turn, can reduce Fe(III) to Fe(II) (reaction (3.6) in Table 3.2.). The average quantum yield for H<sub>2</sub>O<sub>2</sub> photolysis between 200 and 400 nm is 1.11 [36].

As seen in Figure 3.2., the application of photo Fenton process led to removals of the ECs higher than 99%. This points out the greater efficiency of the photo-Fenton process in the generation of oxidizing species compared to the Fe(III)/hv system. However, once about 50% TOC removal was reached, no further mineralization was observed, as can be seen in (Figure 3.3.). It should be notice that when c.a. 50% TOC removal was achieved all the added H<sub>2</sub>O<sub>2</sub> had been consumed. These results demonstrate that the target ECs can be degraded by radical species. However, a greater concentration of free radicals is needed to obtain complete ECs depletion and degrade their intermediates, thus achieving a great level of ECs mineralization.

#### D. Ozonation and photolytic ozonation

The application of single ozonation in the absence of solar radiation led to a complete removal of the ECs. Since ozone reacts selectively with compounds having unsaturated moieties (double or triple carbon bonds) or aromatic rings with substituent groups that activate the ozone electrophilic reactions, it was expected that the ECs studied here were removed by direct ozonation [41]. Table 3.S1. of the supplementary material shows some literature data on pK<sub>a</sub> of the ECs and rate constants of the reactions of the ECs with ozone ( $k_{O_3}$ ) and hydroxyl radicals ( $k_{OH\cdot}$ ). Also, points of ozone attack to ECs molecules are presented. All the ECs, except ANT, have pK<sub>a</sub> values higher than 9 so at the pH values applied in this work (3 and 7) they are mainly in their neutral forms (>99.6%). ANT, on the other hand, would be mostly in its deprotonated form (>97.5%). Thus, their reactivity towards the ozone molecule is supposedly independent on the pH. However, it is worth mentioning that some important deviations were found in the values of  $k_{O_3}$  reported in the literature. Thus, for instance, the reported values for ACE at acidic

conditions ranged from  $10^3$  (pH 3) to  $10^5$  (pH 2) even though at both pHs ACE is present in water in its neutral form. These differences might be attributed to the kinetic procedure the authors followed to determine the rate constants. Despite this fact, these rate data might be useful to discuss the results of this work.

The experimental results indicate that CAF, MTP and TST have low reactivity towards ozone compared to the other ECs investigated, as it took longer times (around 30–35 min) for them to be completely removed at both pH 3 and 7. In Table 3.S1., the  $k_{O_3}$  values that best fit the experimental results of this work have been underlined. ACE, ANT and BIS were completely eliminated after c.a. 15–25 min ozonation time.

Single ozonation led to mineralization percentages of 7% (pH 3) and 14% (pH 7). As a selective oxidant, ozone can remove the parent compounds and transform them into intermediates that may be recalcitrant to ozone attack, especially small oxygenated species, short chain acids and alcohols, thus not high mineralization capability was expected for this system [42]. The application of ozone produces a high accumulation of  $H_2O_2$  due to the breaking of aromatic rings and unsaturated groups and as a consequence, an increase in the ozone decomposition rate, as indicated in reactions (3.7–3.9) (see Table 3.2.) [37]. At pH 7, ozone decomposition likely goes through reaction (3.7), which could explain the higher mineralization single ozonation reaches.

The application of ozone in the presence of radiation ( $O_3/h\nu$ ), both at pH 3 and 7, led to an enhancement of the ECs degradation and mineralization rates. This improvement is likely due to a partial depletion of ozone under UVB ( $290 < \lambda < 315$  nm) radiation directly yielding  $H_2O_2$  as shown in reaction (3.10) [38].

The generated hydrogen peroxide undergoes photolysis to yield  $\cdot OH$  radicals (as in reaction (3.4) in Table 3.2.) which, consequently, favors the production of more reactive oxygen species as indicated in reactions (3.8–3.10) (see Table 3.2.). These radicals are likely the main responsible species for the ECs mineralization.

It is worth mentioning that during the course of solar experiments, the temperature of the aqueous solution increases gradually from c.a. 20 °C (typical initial value) up to c.a. 35°C. This favored the ECs degradation rates since ozone reaction rates increase with temperature as reported elsewhere [43]. Although an increase of the reaction temperature reduces the ozone solubility, the increase of the kinetic energy of the molecules has likely a stronger effect on the compound degradation.

The depletion profiles observed during single ozonation experiments for BIS, CAF, MTP and TST show an induction stage which was not observed in the rest of the ozone processes. This induction stage is likely due to a competitive use of ozone between the parent compounds and their primary degradation intermediates. Intermediates formed during the first stages of reaction might still present available moieties that could react fast with ozone [44]. As the reaction continues, ozone-refractory byproducts are expected to be formed (i.e. carboxylic acids), thus favoring the removal of parent compounds, which are more prone to react with ozone. In contrast, photolytic ozonation and other ozonation led to a higher concentration of free radicals, thus avoiding the accumulation of ozone-consuming intermediates, which would explain the absence of the induction period observed. This can also hold for other ozone combined oxidation systems.

### E. Photocatalytic ozonation

If present, Fe(II) species can decompose  $O_3$  to yield  $\cdot OH$  through the pathway indicated by reactions (3.11) and (3.12) (see Table 3.2.) [39]. However,  $\cdot OH$  generation through this way can be affected if reaction (3.13) takes place.

As a general trend, the presence of Fe(III) exerted a positive effect on ECs removal rates. However, in the case of ACE, which reacts fast with ozone, Fe(III) did not affect the removal rate. With regard to ECs mineralization, similar TOC conversion was observed for both Fe(III)/ $O_3/h\nu$  and  $O_3/h\nu$  systems (63-67%) likely due to reaction (3.13) as Fe(II) was always detected in the medium.

The Fe(III)/ $H_2O_2/O_3/h\nu$  system may have synergistic effect due to catalytic ozone decomposition. Accordingly, this system led to a high mineralization degree (93%). However, ECs depletion profiles were very close to those of Fe(III)/ $H_2O_2/h\nu$ , which suggests that the dominant mechanism for these processes is the radical-mediated degradation due to the contribution of photo-Fenton reactions to increase the concentration of hydroxyl radicals.

### F. $TiO_2$ systems

The mechanism on photo-induced oxidation of organic compounds mediated by  $TiO_2$  is well known and it has been widely discussed [3].  $TiO_2$  can absorb photons with wavelength higher or equal to its band gap, thus promoting electrons from the valence to the conduction band generating electronic vacancies (holes,  $h^+_{VB}$ ) at the valence band (reaction (3.14) in Table 3.2.). Then, the promoted electrons ( $e^-_{CB}$ ) and the holes participate in reduction-oxidation reactions producing a series of free radicals (see reactions (3.15) and (3.16) in Table 3.2.).



The ozone molecule is able to accept electrons from the surface of TiO<sub>2</sub> to give the ozonide ion radical, O<sub>3</sub><sup>•-</sup> (reaction (3.17)), which, in turn, forms hydroxyl radicals according to reactions (3.18) and (3.18b) and also diminishes the recombination of electron-hole pairs.

In this work TiO<sub>2</sub>/hν and TiO<sub>2</sub>/O<sub>3</sub>/hν systems have been investigated at pH 7. Although TiO<sub>2</sub> photocatalytic oxidation at pH 7 was more efficient to remove the ECs than the Fe(III)/hν system at pH 3, it must be mentioned that the photo-Fenton system allowed initial degradation rates higher than the TiO<sub>2</sub>/hν system. However, ECs mineralization through photo-Fenton stopped when hydrogen peroxide was consumed as discussed above. Hence, eventually, the TiO<sub>2</sub>/hν system led to a higher level of mineralization (63%). Photo-Fenton-mediated photocatalytic ozonation was also found to be more efficient than the corresponding TiO<sub>2</sub> system at pH 7, which reached 81% ECs mineralization.

### 3.4.3. Synergistic effect assessment

The results discussed above confirm the synergistic effect when combining some oxidizing systems. This effect was specially observed in terms of ECs mineralization. For instance, single ozonation and Fe(III)/hν did not lead to significant mineralization while their simultaneous application allowed a high TOC removal.

The quantification of the synergy in terms of ECs degradation rates, ECs mineralization degree and ozone consumption is summarized in Table 3.3. This evaluation was carried out by calculating the synergy index, SI, adapted from Shin et al [16]:

$$SI = \frac{P_{\text{combined AOPs}}}{P_{\text{AOP1}} + P_{\text{AOP2}}} \quad (3.19)$$

where P represents the value of a given parameter such as the mineralization degree or the apparent degradation rate constant. A synergy index around 1 indicates a weak synergism so that the combined system performance is additive, i.e. there is not an apparent improvement by the joint application of various AOPs compared to the individual processes. A SI higher than 1 indicates that the combined process has positive synergic effect, while a SI lower than 1 means a negative effect.

In Table 3.3. the parameter  $\eta$  represents the ozone consumption rate per mg TOC removed (which is to be discussed more extensively below),  $k_{ACE}$ ,  $k_{MTP}$  and  $k_{TST}$  are the apparent pseudo-first order constants for ACE, MTP and TST depletion calculated, as example, from the data plotted in Figure 3.2.

As observed in Table 3.3., in all cases, mineralization was improved by combination of processes. This was especially noticeable for  $O_3/h\nu$  (at pH 3 and 7) and  $Fe(III)/O_3/h\nu$  (pH 3).  $Fe(III)$  systems presented a higher SI for TOC removal compared to  $TiO_2/O_3/h\nu$  (pH 7) system, likely due to the different species formed in  $Fe(III)$  systems.

Regarding SI for the pseudo-first order degradation rate constant of ACE, MTP and TST removal, photolytic ozonation (at pH 3 and 7) and  $Fe(III)$ -photocatalytic ozonation (at pH 3) enhanced the compounds degradation rate considerably. However, SI was found to be around 1 for both photo-Fenton (at pH 3) and  $TiO_2$  based (at pH 7) photocatalytic ozonations.

With respect to SI for ozone consumption,  $\eta$ , values lower than 1 has to be interpreted as a positive result since they mean less ozone requirements for the combined process compared to the required ozone rate to remove a given amount of TOC for the individual processes.

**Table 3.3.** Synergy index (SI).

Combined system	Individual AOPs	TOC removal	$k_{ACE}$	$k_{MTP}$	$k_{TST}$	$\eta$
$O_3/h\nu/pH\ 3$	$O_3 + h\nu$ (pH 3)	9.6	1.7	3.1	1.6	0.13
$Fe(III)/O_3/h\nu/pH\ 3$	$Fe(III)/h\nu + O_3$ (pH 3)	9.0	1.0	3.8	2.6	0.14
$Fe(III)/O_3/H_2O_2/h\nu/pH\ 3$	$Fe(III)/H_2O_2/h\nu + O_3$ (pH 3)	1.7	0.8	0.9	0.7	0.05
$O_3/h\nu/pH\ 7$	$O_3 + h\nu$ (pH 7)	2.4	1.0	2.6	2.3	0.14
$TiO_2/O_3/h\nu/pH\ 7$	$TiO_2/h\nu + O_3$ (pH 7)	1.1	1.0	0.9	1.0	0.10

$k_{ACE}$ ,  $k_{MTP}$  and  $k_{TST}$  represent the apparent pseudo-first order constant for ACE, MTP and TST removal rate while  $\eta$  is the parameter representing the ozone consumption per mg TOC removed.

### 3.4.4. Ozone consumption

Efficient use of ozone is a key factor in ozonation systems as it reduces operational costs. According to our experimental results, the simultaneous application of ozonation and other AOPs leads to a positive impact in terms of ozone requirements for ECs mineralization.

Determination of ozone mass transfer rate to the water phase where ozone reacts with the organic matter can be accomplished by first applying an ozone mass balance in the water. For the semicontinuous perfectly mixed photoreactor used in this work, the ozone mass balance can be expressed as follows:

$$V \frac{dC_{O_3}}{dt} = N_{O_3} - r_{O_3} V \quad (3.20)$$

where  $V$  is the volume of the reacting system,  $dC_{O_3}/dt$  represents the accumulation rate of ozone in the water phase,  $r_{O_3}V$  the ozone consumed rate accounting for direct and indirect reactions to degrade the organic matter and  $N_{O_3}$  is the ozone absorption rate. In the tubes where ozonation experiments were carried out, the accumulation rate of ozone in the gas phase can be considered negligible [45]. Since the gas flow rate was kept constant the ozone absorption rate equals the difference between the ozone gas rates at the reactor inlet and outlet:

$$N_{O_3} = Q_g (C_{O_3,g \text{ in}} - C_{O_3,g \text{ out}}) \quad (3.21)$$

where  $Q_g$  is the gas flow rate,  $C_{O_3,g \text{ in}}$  and  $C_{O_3,g \text{ out}}$  are the ozone concentrations in the gas at the reactor inlet and outlet, respectively. Taking into account that  $V$  was also constant, after substitution of equation (3.21) in equation (3.20), variable separation and integration, the ozone balance can be expressed as follows:

$$V \left( C_{O_3}(t) + \int_0^t r_{O_3} dt \right) = Q_g \left( \int_0^t C_{O_3,g \text{ in}} dt - \int_0^t C_{O_3,g \text{ out}} dt \right) \quad (3.22)$$

where  $C_{O_3}$  is the concentration of ozone in water. Therefore, the mole ratio between the ozone consumed and TOC removed in a period of time was calculated as  $z_G$ :

$$z_G(t) = \frac{Q_g \left( \int_0^t C_{O_3,g \text{ in}} dt - \int_0^t C_{O_3,g \text{ out}} dt \right) - VC_{O_3}(t)}{V (C_{TOC_0} - C_{TOC_t})} \quad (3.23)$$

In equation (3.23),  $C_{\text{TOC}0}$  and  $C_{\text{TOC}t}$  stand for the organic carbon content at the beginning of the ozonation and after a time  $t$  of reaction, respectively. Using experimental data the parameter  $z_G$  at different times was calculated by applying equation (3.23) and a numerical integration method. Figure 3.4. shows the results obtained expressed as  $\text{mg O}_3 \text{ mg}^{-1} \text{ TOC}$ . The curves are plotted from 60 min irradiation when all the parent compounds had already been eliminated and only refractory byproducts remained, whose concentration slowly diminished with time.

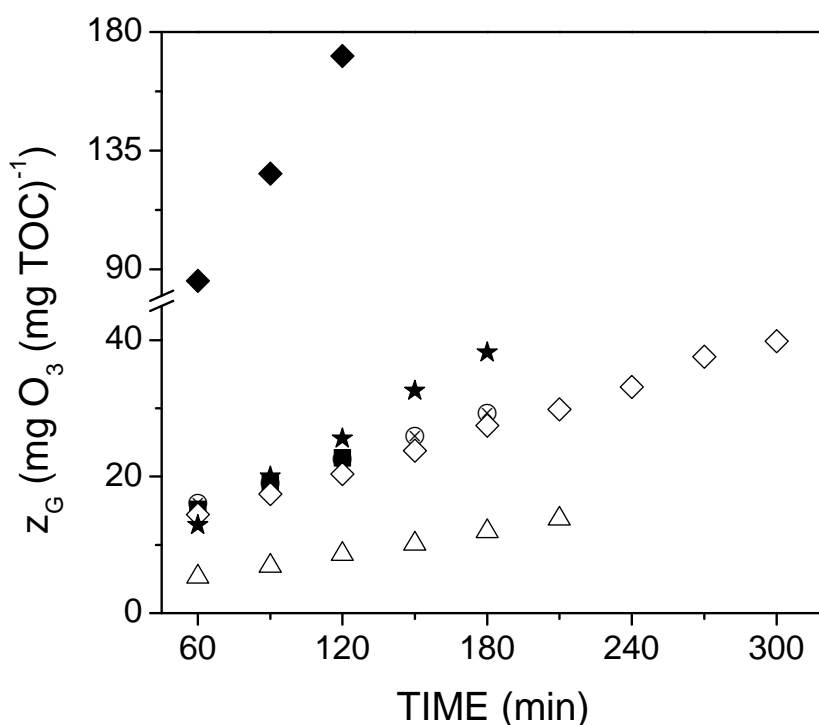


**Figure 3.4.** Consumption of ozone per mass of TOC removed. Experimental conditions: Mixture of six ECs ( $10^{-5} \text{ mol L}^{-1}$  each),  $C_{\text{Fe(III)}} = 2.79 \text{ mg L}^{-1}$ ,  $\text{H}_2\text{O}_2/\text{Fe(III)} = 6.09$  (mass),  $C_{\text{TiO}_2} = 200 \text{ mg L}^{-1}$ ,  $Q_g = 0.67 \text{ L min}^{-1}$ ,  $C_{\text{O}_3, \text{g}} = 13 \text{ mg L}^{-1}$ , average incident UVA solar radiation  $41.2 \text{ W m}^{-2}$ . Symbols:  $\text{O}_3/\text{pH } 3$  (◆),  $\text{O}_3/\text{h}\nu/\text{pH } 3$  (⊗),  $\text{Fe(III)/O}_3/\text{h}\nu/\text{pH } 3$  (■),  $\text{Fe(III)/H}_2\text{O}_2/\text{O}_3/\text{h}\nu/\text{pH } 3$  (△),  $\text{O}_3/\text{h}\nu/\text{pH } 7$  (★),  $\text{TiO}_2/\text{O}_3/\text{h}\nu/\text{pH } 7$  (◇).

The slope of each curve, defined here as  $\eta$ , gives an estimation of the average rate of ozone ( $\text{mg min}^{-1}$ ) that is required to eliminate 1 mg of TOC. Values of  $\eta$  were found to be 1.47, 0.19, 0.214, 0.205, 0.145 and  $0.069 \text{ mg O}_3 \text{ mg}^{-1} \text{ TOC min}^{-1}$  for  $\text{O}_3$  at pH 3,  $\text{O}_3/\text{h}\nu$  at pH 3,  $\text{Fe(III)/O}_3/\text{h}\nu$  at pH 3,  $\text{O}_3/\text{h}\nu$  at pH 7,  $\text{TiO}_2/\text{O}_3/\text{h}\nu$  at pH 7 and  $\text{Fe(III)/H}_2\text{O}_2/\text{O}_3/\text{h}\nu$  at pH 3, respectively. Then, to remove a given amount of

organic matter, ozone consumption is 10.1 or 21.3 fold higher if simple ozonation is used compared to the use of  $\text{TiO}_2/\text{O}_3/\text{hv}$  (at pH 7) or  $\text{Fe(III)}/\text{H}_2\text{O}_2/\text{O}_3/\text{hv}$  (at pH 3) systems, respectively. Furthermore, in the case of simple ozonation the application of large quantities of ozone does not guarantee to reach the desired TOC conversion, since as previously discussed, ozonation efficiency is affected by the accumulation of refractory products.

### 3.4.5. Effect of inorganic species

Different inorganic species present in wastewater may affect AOP removal rates. Thus, the effect of the presence of inorganic compounds in the aqueous matrix, such as nitrate, phosphate, chloride, carbonate and sulfate ions was also studied. These species were added to the aqueous solution at concentration levels commonly found in WWTP effluents [15, 46]. Thus, a new series of experiments was carried out in the presence of  $\text{Cl}^-$ ,  $\text{SO}_4^{2-}$ ,  $\text{CO}_3^{2-}$ ,  $\text{NO}_3^-$  and  $\text{PO}_4^{3-}$  at 79, 107, 270, 55 and 6  $\text{mg L}^{-1}$ , respectively. The AOPs applied were  $\text{Fe(III)}/\text{H}_2\text{O}_2/\text{O}_3/\text{hv}/\text{pH}$  3 and  $\text{TiO}_2/\text{O}_3/\text{hv}/\text{pH}$  7.

Figure 3.S3. and 3.S4. of the supplementary material show, respectively, the normalized ECs depletion profiles and TOC conversion with time obtained compared to the results without ionic species. On the other hand, Figure 3.S5. presents the variation of the accumulated UV dose with time for the solar systems applied. As it is seen from Figure 3.S5. UV radiation received was similar for all the experiments during the first 150 min reaction time. Thus, comparison among these experiments can only be made for this reaction period. Under the conditions investigated the effect of these ionic species is observed to be negative. When applying the  $\text{TiO}_2/\text{O}_3/\text{hv}/\text{pH}$  7 system, the presence of ions delayed for about 20 minutes the time to remove the target ECs at 99% level. Also, ECs mineralization rates were diminished. These results suggest that in the  $\text{TiO}_2$ -based systems the presence of the selected anions reduces the active surface of the semiconductor exerting a scavenging effect on radical production.

Similar comments can be applied to the  $\text{Fe(III)}/\text{H}_2\text{O}_2/\text{O}_3/\text{hv}/\text{pH}$  3 system, though anionic species apparently affected the oxidation rates in a lesser extent. As this process was carried out at pH 3, carbonate ions were quickly transformed into carbonic acid, which was released through the outlet gas stream as  $\text{CO}_2$ . However the final ECs mineralization was diminished in the presence of mineral anionic species.

### 3.4.6. Kinetic aspects of AOP systems investigated

Finally, a kinetic evaluation of the ECs mineralization processes was carried out. The kinetic studies of the AOP systems have been classified here according to the pH of water (3 or 7) and focuses on TOC removal since the AOPs involve many different reactions, most of them with the participation of free radical entities and intermediate compounds of different nature, with mass transfer and chemical steps.

First, the mass balance equation corresponding to the reactor used has to be known. This largely depends on the type of flow the water has through the reactor. In this work, given the turbulent flow regime and the recirculation flow, perfect mixing has been assumed. On the other hand, whether or not ozone was fed, a non-stationary regimen holds (batch or semi-batch CPC photo-reactor) so that the mass balance of TOC (as surrogate parameter that undergoes reaction) is:

$$\frac{dC_{\text{TOC}}}{dt} = r_{\text{TOC}} \quad (3.24)$$

where  $r_{\text{TOC}}$  is the rate of TOC removal due to all possible reactions: direct ozonation, direct photolysis and hydroxyl radical oxidation. This rate term, obviously, depends on the type of AOP system applied.

#### A. AOP systems at pH 3

The AOP processes applied at pH 3 were Fe(III)/hv, Fe(III)/H<sub>2</sub>O<sub>2</sub>/hv, Fe(III)/O<sub>3</sub>/hv and Fe(III)/O<sub>3</sub>/H<sub>2</sub>O<sub>2</sub>/hv and, for comparative reasons, hv, O<sub>3</sub>, O<sub>3</sub>/hv. For the most complex AOP system (Fe(III)/O<sub>3</sub>/H<sub>2</sub>O<sub>2</sub>/hv), equation (3.24) becomes:

$$\frac{dC_{\text{TOC}}}{dt} = -[k_{\text{UV}} + k_{\text{O}_3}C_{\text{O}_3} + k_{\text{HO}}C_{\text{HO}}]C_{\text{TOC}} \quad (3.25)$$

where the three terms on the right hand side of equation (3.25) correspond to the potential contributions of direct photolysis ( $k_{\text{UV}}$ ), direct ozonation ( $k_{\text{O}_3}$ ) and hydroxyl radical oxidation ( $k_{\text{HO}}$ ). In this work, in addition to ozone direct ozone reactions and direct photolysis, it is assumed that no other free radicals or short-living fast-reacting species different than hydroxyl radicals are active oxidants, which is in accordance with most of the published works reporting on the AOP systems considered here. However, according to our experimental results (see Figure 3.3.), though TST was partially removed by direct photolysis, no TOC removal was observed in single photolysis experiments so that  $k_{\text{UV}}$  can be removed

from equation (3.25). In the ozone-free AOPs, the rate term due to direct ozonation is zero, so that for Fe(III)/hv and Fe(III)/H<sub>2</sub>O<sub>2</sub>/hv systems, equation (3.25) can be simplified to:

$$\frac{dC_{\text{TOC}}}{dt} = -k_{\text{HO}} C_{\text{HO}} C_{\text{TOC}} \quad (3.26)$$

In equation (3.26), the concentration of hydroxyl radicals depends on the initiation reactions of the mechanism that leads to the appearance of these free radicals (see reactions in Table 3.2.) and this also depends on the type of AOP. Thus, the kinetics of each AOP system needs a particular discussion.

### Fe(III)/hv system

For Fe(III)/hv system the concentration of hydroxyl radicals, C<sub>OH</sub>, can be expressed as a function of the Fe(III) concentration and the radiation flux. Thus, TOC removal rate can be expressed as follows:

$$\frac{dC_{\text{TOC}}}{dt} = -k_{\text{HO}} k_{\text{Fe(III)-UV}} C_{\text{Fe(III)}} C_{\text{TOC}} = -k_{\text{T1}} C_{\text{Fe(III)}} C_{\text{TOC}} \quad (3.27)$$

where  $k_{\text{Fe(III)-UV}}$  is an apparent rate constant that takes into account the effect of the radiation flux. However, no significant TOC removal was observed when the Fe(III)/hv system was applied so that  $k_{\text{T1}}$  can be considered negligible.

### Fe(III)/H<sub>2</sub>O<sub>2</sub>/hv system

In the Fe(III)/H<sub>2</sub>O<sub>2</sub>/hv system, it can be assumed that the photo-Fenton reaction is the main pathway producing hydroxyl radicals. Photo-Fenton reaction develops because of the formation of Fe(II) as a result of Fe(III) aqua complexes photolysis. Then, Fe(II) reacts with the added hydrogen peroxide to form <sup>•</sup>OH radicals. According to this, equation (3.26) is transformed into (3.28):

$$\frac{dC_{\text{TOC}}}{dt} = -k_{\text{HO}} k_{\text{Fenton}} C_{\text{Fe(II)}} C_{\text{H2O2}} C_{\text{TOC}} = -k_{\text{T2}} C_{\text{Fe(II)}} C_{\text{H2O2}} C_{\text{TOC}} \quad (3.28)$$

From equation (3.28) one has:

$$\ln \frac{C_{\text{TOC}}}{C_{\text{TOC0}}} = -k_{\text{T2}} \int_0^t C_{\text{Fe(II)}} C_{\text{H2O2}} dt \quad (3.29)$$

The integral in equation (3.29) was numerically solved from experimental values of concentrations of Fe(II) and hydrogen peroxide. Then, from the linear regression of equation (3.29), a value of  $4.34 \times 10^5 \text{ L mol}^{-1} \text{ min}^{-1}$  was obtained for  $k_{T2}$  ( $R^2 = 0.97$ ).

### Ozone systems

For ozone systems, equation (3.26) is only valid if the regime of ozone absorption is slow. In the ozonation experiments carried out at pH 3 ozone was always detected in solution, which is a strong indication of slow kinetic regime [41]. Nevertheless, the kinetic regime of ozonation reactions was determined by the computation of the Hatta number (Ha). This parameter allows the quantification of the relative importance of mass transfer and chemical reaction rates in heterogeneous gas-liquid systems.

For a second order irreversible reaction between a gaseous compound A and the liquid compound B, Ha is defined as follows:

$$Ha = \frac{(k D_A C_B)^{1/2}}{k_L} \quad (3.30)$$

where  $k$ ,  $D_A$ ,  $k_L$  and  $C_B$  are the rate constant of the reaction referred to compound A, the diffusivity of A in the liquid phase, the individual liquid side mass transfer coefficient and the concentration of compound B (TOC in this case), respectively. Here, Hatta determination was carried out considering a global reaction of ozone with TOC as shown later. However, the apparent second order rate constant  $k$  is needed.

Equation (3.26) is directly applied to ozone systems. For the most complex ozone AOP systems studied at pH 3, Fe(III)/O<sub>3</sub>/H<sub>2</sub>O<sub>2</sub>/hv, equation (3.26), taking into account equation (3.28), is as follows:

$$\frac{dC_{TOC}}{dt} = -[k_{T2} C_{Fe(II)} C_{H2O2} + k_D C_{O3} + k_{T3} C_{O3}] C_{TOC} \quad (3.31)$$

In equation (3.31) the two new terms,  $k_D C_{O3}$  and  $k_{T3} C_{O3}$ , are due to the reactions of TOC with ozone (direct reactions) and with the fraction of hydroxyl radicals that comes from ozone decomposition initiation-promotion reactions (see Table 3.2.). The apparent rate constant  $k_{T3}$  is the result of applying the  $R_{CT}$  concept [47]. Accordingly, the concentration of hydroxyl radicals in ozone systems can be



expressed as a function of the ozone concentration and  $R_{CT}$ , proposed to relate both ozone and hydroxyl radical concentrations. Thus:

$$k_{T3} = k_{HO} R_{CT} \quad (3.32)$$

with

$$C_{HO} = R_{CT} C_{O_3} \quad (3.33)$$

- *O<sub>3</sub> and O<sub>3</sub>/hν systems.*

In these systems, equation (3.31) reduces to:

$$\frac{dC_{TOC}}{dt} = -k'_T C_{O_3} C_{TOC} \quad (3.34)$$

where

$$k'_T = k_D + k_{T3} \quad (3.35)$$

Hence, for iron-free ozone systems TOC removal rate was assumed to be due to a surrogate general reaction between ozone and TOC, with  $k'_T$  as the apparent second order rate constant referred to TOC removal rate. However, for Ha determination the rate constant to be used must be referred to the ozone removal rate ( $k$  in equation (3.30)). According to the stoichiometric ratio, this rate constant is defined as follows:

$$k_T = z_G k'_T \quad (3.36)$$

where the global stoichiometric coefficient  $z_G$  expressed as mole of O<sub>3</sub> consumed per mole of TOC depleted, can be calculated with equation (3.23). Then, equation (3.37) is obtained:

$$\frac{dC_{TOC}}{dt} = -\frac{k_T}{z_G} C_{O_3} C_{TOC} \quad (3.37)$$

Integrating equation (3.37) one yields:

$$\ln \frac{C_{\text{TOC}}}{C_{\text{TOC},0}} = -k_T \int_0^t \frac{C_{\text{O}_3}}{Z_G} dt \quad (3.38)$$

Values of  $k_T$  for single and photolytic ozonation were then calculated from linear regression ( $R^2 > 0.98$ ) of experimental data according to equation (3.38), and were found to be 855 and 2190  $\text{M}^{-1}\text{min}^{-1}$ , respectively. Next,  $H_a$  was determined from equation (3.30) the surrogate ozone-TOC reaction. In equation (3.30),  $D_{\text{O}_3}$  and  $k_L$  were taken as  $1.4 \times 10^{-9} \text{ m}^2 \text{ s}^{-1}$  [48] and  $4 \times 10^{-4} \text{ m s}^{-1}$  [49], respectively. In all cases,  $H_a$  was found to be much lower than 0.3, which confirmed that the general TOC-ozone reactions developed in the slow kinetic regime, thus validating the TOC balance equation applied. At first sight, this means that both direct and hydroxyl radical reactions compete for TOC removal, which means that ozone combined systems could be useful technologies to mineralize ECs in water. However, given the values of  $k_T$  from ozonation alone and  $\text{O}_3/\text{h}\nu$  systems, it can be concluded that hydroxyl radical oxidation is the main way of TOC removal.

▪ *Fe(III)/O<sub>3</sub>/hν and Fe(III)/O<sub>3</sub>/H<sub>2</sub>O<sub>2</sub>/hν systems*

In Fe(III)/O<sub>3</sub>/hν systems, equation (3.31) could be applied. Once variables are separated and after equation integration, it becomes:

$$\ln \frac{C_{\text{TOC}}}{C_{\text{TOC},0}} + k_{T2} \int_0^t C_{\text{Fe(II)}} C_{\text{H}_2\text{O}_2} dt = -k_T \int_0^t \frac{C_{\text{O}_3}}{Z_G} dt \quad (3.39)$$

Since  $k_{T2}$  is known, the linear regression analysis of equation (3.39) led to the new values of  $k_T$  that were 2200 and 2960  $\text{L mol}^{-1} \text{ min}^{-1}$  for the Fe(III)/O<sub>3</sub>/hν and Fe(III)/O<sub>3</sub>/H<sub>2</sub>O<sub>2</sub>/hν systems, respectively (see Figure 3.5. for the plot corresponding to the Fe(III)/O<sub>3</sub>/H<sub>2</sub>O<sub>2</sub>/hν system). Again, Hatta values were found to be lower than 0.3, which confirmed the slow kinetic regime for ozone reactions. By comparing processes on the basis of  $k_T$  values, Table 3.4. shows that the single ozonation system is less effective in mineralizing ECs than the other three ozone-based AOP systems studied. The Fe(III)/H<sub>2</sub>O<sub>2</sub>/O<sub>3</sub>/hν system, with the highest rate constant value for ozone systems, leads to the highest TOC conversion, as expected. Also, since reactions were carried out at pH 3 it is likely that hydroxyl radical formation comes from ozone photolysis, ozone-Fe(II) and photo-Fenton reactions rather than from the ozone-hydrogen peroxide reaction (ozone only reacts with the ionic form of hydrogen peroxide). Note that Fe(II) is formed from the photolysis of Fe(III) complex.

### B. AOP systems at pH 7

Only iron-free ozonation systems were studied at pH 7, that is,  $O_3$ ,  $O_3/h\nu$ ,  $TiO_2/h\nu$  and  $TiO_2/O_3/h\nu$ . Equation (3.25) has been modified to be applied to  $TiO_2$  systems. Thus, the contribution of the photocatalytic oxidation to the global mineralization rate has been considered using a Langmuir-type expression [50]. Accordingly, equation (3.40) has been obtained:

$$\frac{dC_{TOC}}{dt} = - \left[ k_{UV} + \frac{k_i C_{O_3}}{1 + \sum (K_i C_i)} + k_{O_3} C_{O_3} + k_{HO} C_{HO} \right] C_{TOC} \quad (3.40)$$

where  $\sum K_i C_i$  represents the contribution of equilibria of adsorbing species. As discussed above, direct photolysis ( $k_{UV}$ ) can be neglected since no mineralization was achieved by direct photolysis. Also, as also mentioned before, ECs adsorption on the  $TiO_2$  surface was weak and, as a result, their corresponding adsorption equilibrium constants must be very low. Accordingly and considering the adsorption of water on the  $TiO_2$  surface, the denominator of the Langmuir term in equation (3.40) can be reduce to  $K_{H_2O} C_{H_2O}$ . Hence, Langmuir term finally reduces to:

$$\frac{k_i C_{O_3}}{K_{H_2O} C_{H_2O}} \approx k_{UV-Cat} C_{O_3} \quad (3.41)$$

Finally, TOC mass balance equation (3.40) also becomes as equation (3.38) that holds for all ozone AOP systems at pH 7. Accordingly, integrated equation (3.38) has been applied to experimental data of all ozone AOP systems studied at pH 7. As an example, Figure 3.5. shows the plot of  $\ln(C_{TOC}/C_{TOC,0})$  versus the integral of the ozone concentration global stoichiometric ratio over the reaction time corresponding to a  $TiO_2/O_3/h\nu$  experiment taken as an example. As it is seen, experimental data are situated around a straight line. Least squares fitting led a value for  $k_T$  of  $1.30 \times 10^4 \text{ L mol}^{-1} \text{ min}^{-1}$ . In the case of  $O_3$  and  $O_3/h\nu$  systems, values of  $k_T$  were found to be 739 and  $1.13 \times 10^4 \text{ L mol}^{-1} \text{ min}^{-1}$ , respectively. Hatta numbers were in all cases lower than 0.3 then ozone absorption regimes was also slow.

With regard to the  $TiO_2/h\nu$  system, TOC mass balance reduces to equation (3.42):

$$\frac{dC_{TOC}}{dt} = - \frac{k_i C_{O_2} C_{TOC}}{1 + \sum (K_i C_i)} \approx -k'_{UV-Cat} C_{TOC} \quad (3.42)$$

which is an apparent pseudo first order kinetics. Accordingly, the slope of the straight line resulting from a plot of  $\ln(C_{\text{TOC}}/C_{\text{TOC},0})$  against time is  $-k'_{\text{UV-Cat}}$  that, after least squares analysis, was found to be  $4.68 \times 10^{-3} \text{ min}^{-1}$ .

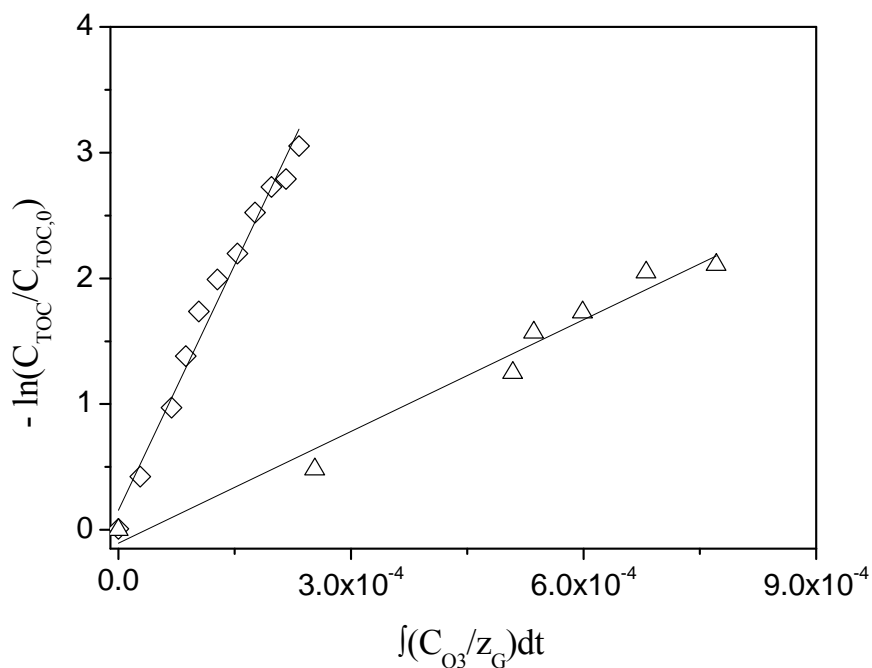


**Figure 3.5.**  $\ln(C_{\text{TOC}}/C_{\text{TOC},0})$  versus the integral of the ozone concentration global stoichiometric ratio over the reaction time for Fe(III)/H<sub>2</sub>O<sub>2</sub>/O<sub>3</sub>/hv/pH 3 (Δ) and TiO<sub>2</sub>/O<sub>3</sub>/hv/pH 7 (◇) systems.

In Table 3.4, the values for  $k_T$  are also summarized. All rate constants from Table 3.4, have to be used with caution and cannot be directly compared since they are related to different mechanisms. However they are useful to determine for the AOPs systems involving both ozone and Fe(III), the contribution of these species. Thus, the parameter %RI is defined as the relative importance (as percentage) of a given pathway. For the ozone pathway is as follows:

$$\%RI = \frac{(k_D + k_{T3})C_{\text{O}_3}}{k_{\text{UV}} + k_{T1}C_{\text{Fe(III)}} + k_{T2}C_{\text{Fe(II)}}C_{\text{H}_2\text{O}_2} + (k_D + k_{T3})C_{\text{O}_3}} \times 100 \quad (3.43)$$

The numerator in equation (3.43) can also be changed to  $k_{UV}$ ,  $k_{T1}C_{Fe(III)}$  or  $k_{T2}C_{Fe(II)}C_{H_2O_2}$  to evaluate, respectively, the %RI of the contributions due to direct photolysis, Fe(III) complex photodissociation and photo-Fenton reaction. However, as above mentioned direct photolysis and Fe(III) photolysis do not lead to mineralization. Thus, using the information depicted in Table 3.4. and experimental data, for the Fe(III)/O<sub>3</sub>/H<sub>2</sub>O<sub>2</sub>/hv/pH 3 system, application of equation (3.43) leads to the following conclusions: during the first seconds of reaction, the main contribution to the mineralization process corresponds to the photo-Fenton reaction. This is because, at the start of reaction, hydrogen peroxide is at its highest concentration and ozone concentration is low. Some minutes later, because of the ozone accumulation and hydrogen peroxide partial consumption, the %RI of ozone-involving mechanisms increases. Therefore, contribution of ozone processes to mineralization increases with the increasing reaction time, accounting for 72% of mineralization after 5 min reaction and for 98% after 1 hour.

**Table 3.4.** Apparent mineralization rate constants<sup>a</sup>

System	Rate constant
hv	$k_{UV} = 0$ <sup>b</sup>
Fe(III)/hv/pH 3	$k_{T1}^c = 0$ <sup>b</sup>
Fe(III)/H <sub>2</sub> O <sub>2</sub> /hv/pH 3	$k_{T2}^d = 4.34 \times 10^5$
TiO <sub>2</sub> /hv/pH 7	$k_{UV-cat}^e = 4.68 \times 10^{-3}$ <sup>b</sup>
O <sub>3</sub> /pH 3	$k_T^f = 8.55 \times 10^2$
O <sub>3</sub> /hv/pH 3	$k_T^f = 2.19 \times 10^3$
Fe(III)/O <sub>3</sub> /hv/pH 3	$k_T^g = 2.20 \times 10^3$
Fe(III)/O <sub>3</sub> /H <sub>2</sub> O <sub>2</sub> /hv/pH 3	$k_T^g = 2.96 \times 10^3$
O <sub>3</sub> /pH 7	$k_T^f = 7.39 \times 10^2$
O <sub>3</sub> /hv/pH 7	$k_T^f = 1.13 \times 10^4$
TiO <sub>2</sub> /O <sub>3</sub> /hv/pH 7	$k_T^f = 1.30 \times 10^4$

<sup>a</sup>Units are L mol<sup>-1</sup>min<sup>-1</sup> unless indicated. <sup>b</sup>min<sup>-1</sup>. <sup>c</sup>From equation (3.27). <sup>d</sup>From equation (3.29). <sup>e</sup>From equation (3.42). <sup>f</sup>From equation (3.38). <sup>g</sup>From equation (3.39).

### 3.5. Conclusions

---

The following conclusions were reached in this work:

- Solar photolysis and photocatalytic oxidation using Fe(III) are not effective for the complete removal of the selected contaminants. However, the use of H<sub>2</sub>O<sub>2</sub> enhances their degradation rates and mineralization.
- Although the application of single ozonation can lead to the complete removal of the ECs, it does not lead to a significant mineralization. On the other hand, the application of ozonation and solar irradiation leads to an improvement of the mineralization degree.
- The joint application of ozonation and photocatalysis has a synergistic effect, which is shown by the increases in the initial degradation and mineralization rates and the decrease in the ozone consumption.
- In the ozone-based AOPs systems, ECs mineralization takes place in the slow kinetic regime, which means that the indirect oxidation by hydroxyl radical is an important contribution to the overall degradation process.
- The adjustment of experimental data to apparent pseudo-first order reaction models allows TOC conversion kinetics to be simulated for the AOPs applied. Also, contribution of ozone processes to mineralization can also be estimated.

### 3.6. Supplementary information

---

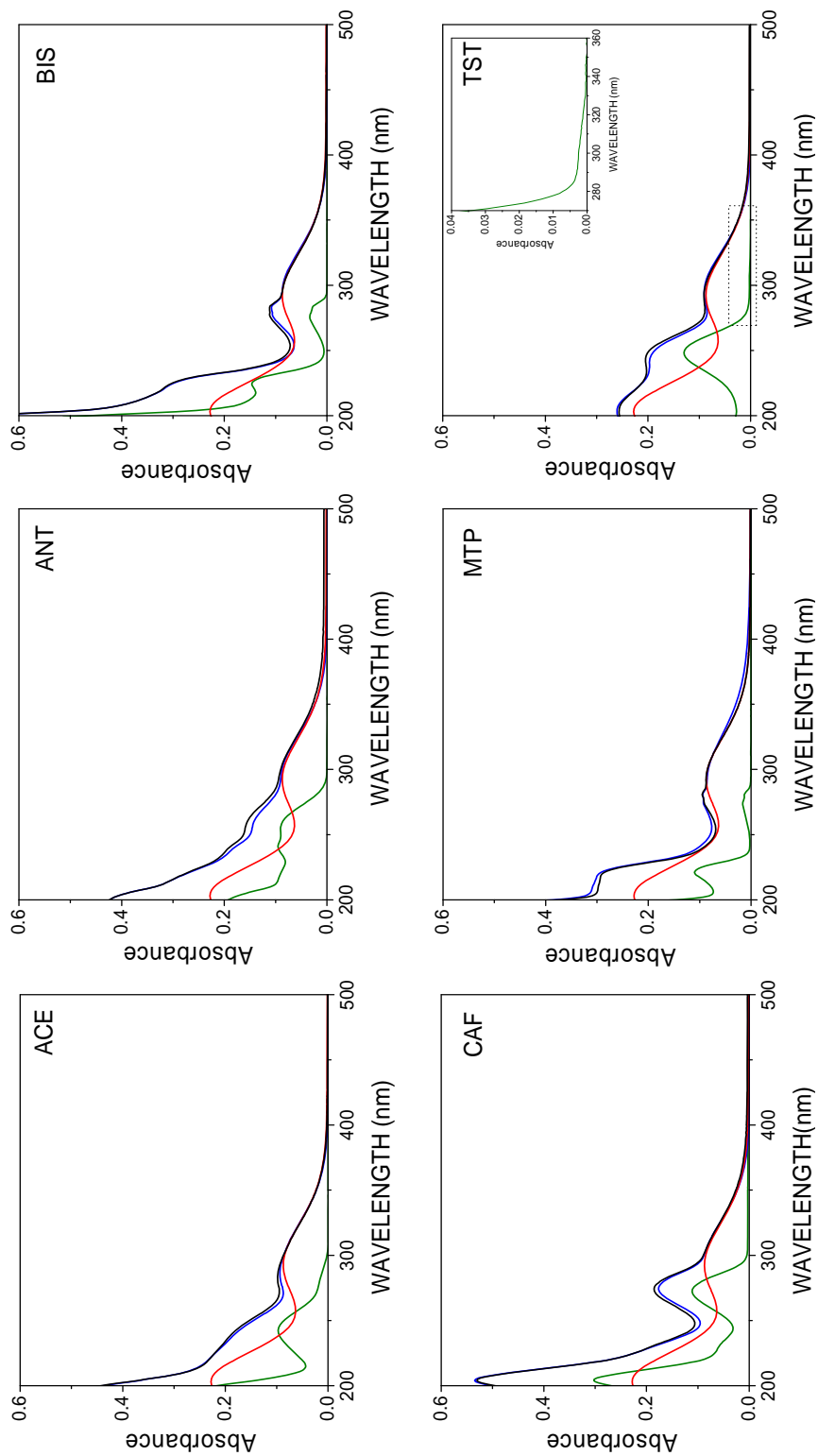


**Figure 3.S1.** Absorption spectra of the target compounds and Fe(III) in ultrapure water  
 Compound (green), Fe(III) solution (red), Prepared mixture (compound and Fe(III)) (blue), Sum of compound and Fe(III) spectra (black)  
 $C_{\text{compound}} = 10^{-5} \text{ mol L}^{-1}$ ,  $C_{\text{Fe(III)}} = 2.79 \text{ mg L}^{-1}$

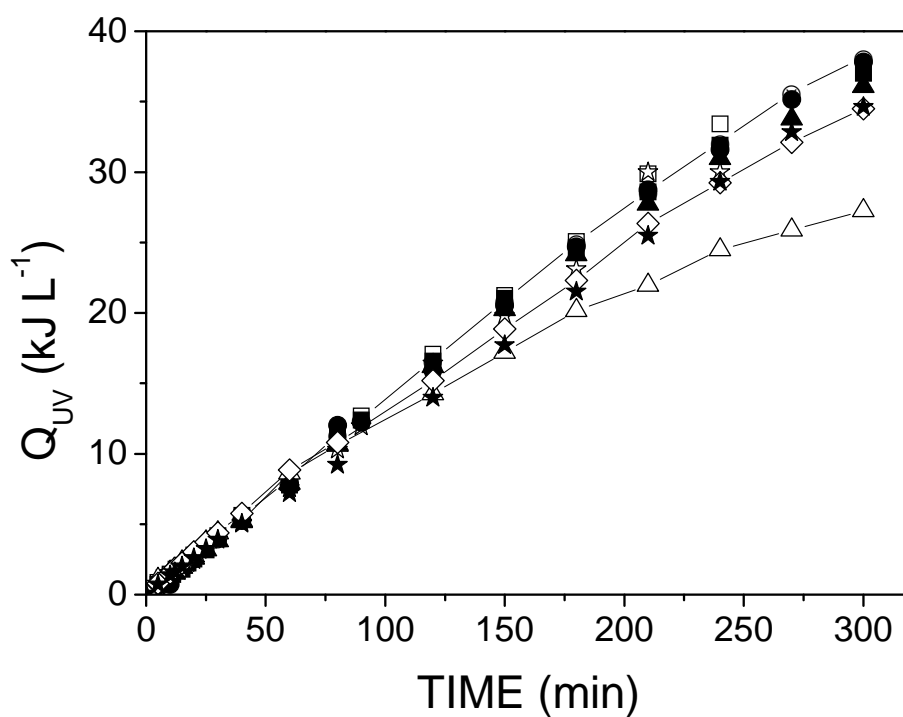


**Figure 3.S2.** Evolution of the accumulated UV dose with time for the solar systems applied in this work. Experimental conditions: Mixture of six ECs ( $10^{-5}$  mol L $^{-1}$  each),  $C_{\text{Fe(III)}} = 2.79$  mg L $^{-1}$ ,  $\text{H}_2\text{O}_2/\text{Fe(III)} = 6.09$  (mass),  $C_{\text{TiO}_2} = 200$  mg L $^{-1}$ ,  $Q_g = 0.67$  L min $^{-1}$ ,  $C_{\text{O}_3, \text{g}} = 13$  mg L $^{-1}$ , average incident UVA solar radiation 41.2 W m $^{-2}$ . Symbols: hv (□), Fe(III)/hv/pH 3 (☆), Fe(III)/H $_2$ O $_2$ /hv/pH 3 (●), O $_3$ /hv/pH 3 (⊗), Fe(III)/O $_3$ /hv/pH 3 (■), Fe(III)/H $_2$ O $_2$ /O $_3$ /hv/pH 3 (△), TiO $_2$ /hv/pH 7 (▲), O $_3$ /hv/pH 7 (★), TiO $_2$ /O $_3$ /hv/pH 7 (◇).



**Table 3.S1.** Literature reported kinetic constants for the reaction between target ECs with ozone and hydroxyl radicals.

Compound	pK <sub>a</sub>	k <sub>O<sub>3</sub></sub> app, L mol <sup>-1</sup> s <sup>-1</sup>	k <sub>OH</sub> , L mol <sup>-1</sup> s <sup>-1</sup>	Ozone attack points
ACE	9.4 [51]	<u>2.1-2.9×10<sup>5</sup></u> , <u>3.58×10<sup>5</sup></u> (pH 2, WW) [52], 2.37×10 <sup>3</sup> (pH 3) [13], <u>2.70×10<sup>5</sup></u> (pH 7, WW) [52]	2.20×10 <sup>9</sup> (pH 5.5) [13], 9.80×10 <sup>9</sup> (pH 7) [53], 1.70×10 <sup>9</sup> [54]	
ANT	1.4 [51]	<u>1.3-1.8×10<sup>5</sup></u> , <u>4.07×10<sup>5</sup></u> (pH 2, WW) [52], <u>6.15×10<sup>5</sup></u> (pH 7, WW) [53]	5.20×10 <sup>9</sup> [55], 4.86×10 <sup>9</sup> [56]	
BIS	9.6, 10.2 [57]	<u>4.8×10<sup>4</sup></u> (pH 2)[58], <u>1.3×10<sup>4</sup></u> (pH 2)[59], <u>2.70×10<sup>5</sup></u> (pH 7, WW) [52], <u>1.71×10<sup>5</sup></u> (pH 7) [58]	3.30×10 <sup>9</sup> [60], 1.10×10 <sup>10</sup> [61], 1.01×10 <sup>10</sup> [62], 1.02×10 <sup>10</sup> [63], 1.55×10 <sup>10</sup> [64], 1.70×10 <sup>10</sup> [65]	
CAF	10.4 [51]	2.1-2.9×10 <sup>4</sup> , 1.75×10 <sup>4</sup> , <u>1.16×10<sup>3</sup></u> (pH 2, WW) [52], <u>6.95×10<sup>2</sup></u> (pH 6.3) [66], 2.49×10 <sup>4</sup> (pH 7, WW) [52]	5.90×10 <sup>9</sup> [67], 7.30×10 <sup>9</sup> [68]	
MTP	9.7 [51]	<u>3.72×10<sup>2</sup></u> (pH 2, WW) [52], 6.2-8.7×10 <sup>4</sup> (pH 2, WW) [52], <u>2.39×10<sup>2</sup></u> (pH 2.5) [69], 2.49×10 <sup>3</sup> (pH 7, WW) [52], 1.40×10 <sup>3</sup> (pH 7) [69]	7.30×10 <sup>9</sup> [70], 6.83×10 <sup>9</sup> [71], 8.39×10 <sup>9</sup> [72]	
TST	17.4 <sup>a</sup> [73]	4.80×10 <sup>2</sup> (pH 2-8) <sup>b</sup> [74]	N.D.	

WW: wastewater matrix, N.D. No data published, <sup>a</sup> Estimated by software (SPARC), <sup>b</sup> Rate constants for the reaction between TST with ozone are not known and the reported value in Table 3.S1. corresponds to the ozone-progesterone reaction. This is because TST and progesterone have similar structure and moieties and it has been assumed, to have similar reactivity with ozone. Underlined values are considered the most appropriated ones for fitting experimental results in this work (see section 3.4.2.D of main text).

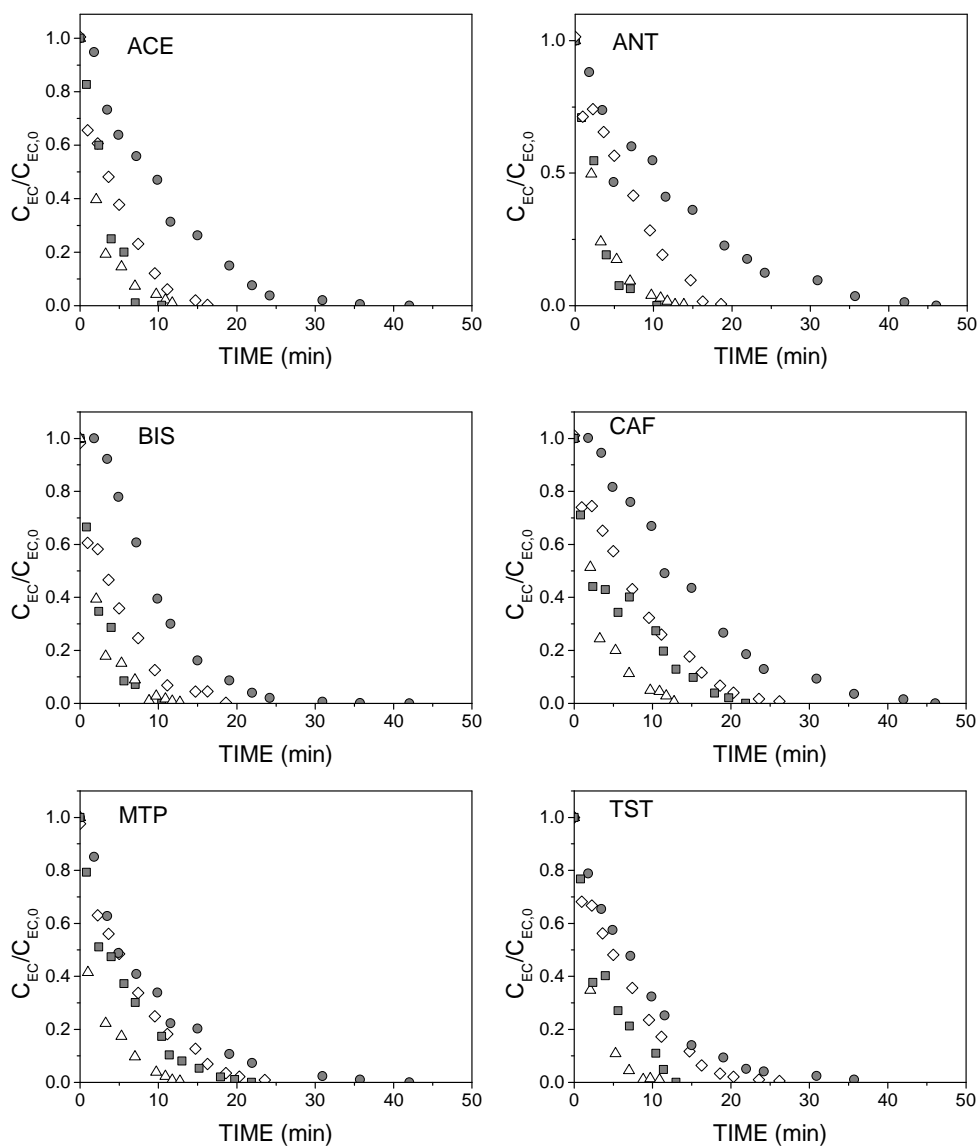


**Figure 3.S3.** Dimensionless normalized concentration of ECs ( $C_{EC}/C_{EC,0}$ ) with time. Experimental conditions: Mixture of six ECs ( $10^{-5}$  mol L $^{-1}$  each),  $C_{Fe(III)} = 2.79$  mg L $^{-1}$ ,  $H_2O_2/Fe(III) = 6.09$  (mass),  $C_{TiO_2} = 200$  mg L $^{-1}$ ,  $Q_g = 0.67$  L min $^{-1}$ ,  $C_{O_3,g} = 13$  mg L $^{-1}$ ,  $C_{Cl} = 79$  mg L $^{-1}$ ,  $C_{SO_4} = 107$  mg L $^{-1}$ ,  $C_{CO_3} = 270$  mg L $^{-1}$ ,  $C_{NO_3} = 55$  mg L $^{-1}$ ,  $C_{PO_4} = 6$  mg L $^{-1}$ . Symbols: Fe(III)/H $_2$ O $_2$ /O $_3$ /hv/ultrapure water/pH 3 ( $\Delta$ ), Fe(III)/H $_2$ O $_2$ /O $_3$ /hv/presence of ionic species/pH 3 ( $\blacksquare$ ), TiO $_2$ /O $_3$ /hv/ultrapure water/pH 7 ( $\diamond$ ), TiO $_2$ /O $_3$ /hv/presence of ionic species/pH 7 ( $\bullet$ ).

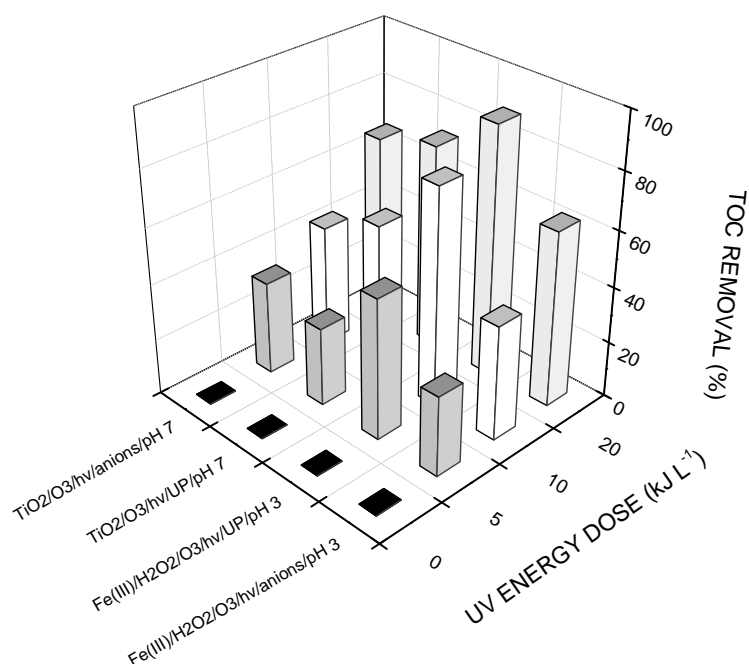


**Figure 3.S4.** Evolution of the normalized TOC content vs. UV dose for the systems. Experimental conditions: Mixture of six ECs ( $10^{-5}$  mol L<sup>-1</sup> each),  $C_{\text{Fe(III)}} = 2.79$  mg L<sup>-1</sup>,  $\text{H}_2\text{O}_2/\text{Fe(III)} = 6.09$  (mass),  $C_{\text{TiO}_2} = 200$  mg L<sup>-1</sup>,  $Q_g = 0.67$  L min<sup>-1</sup>,  $C_{\text{O}_3, \text{g}} = 13$  mg L<sup>-1</sup>,  $C_{\text{Cl}} = 79$  mg L<sup>-1</sup>,  $C_{\text{SO}_4} = 107$  mg L<sup>-1</sup>,  $C_{\text{CO}_3} = 270$  mg L<sup>-1</sup>,  $C_{\text{NO}_3} = 55$  mg L<sup>-1</sup>,  $C_{\text{PO}_4} = 6$  mg L<sup>-1</sup>.

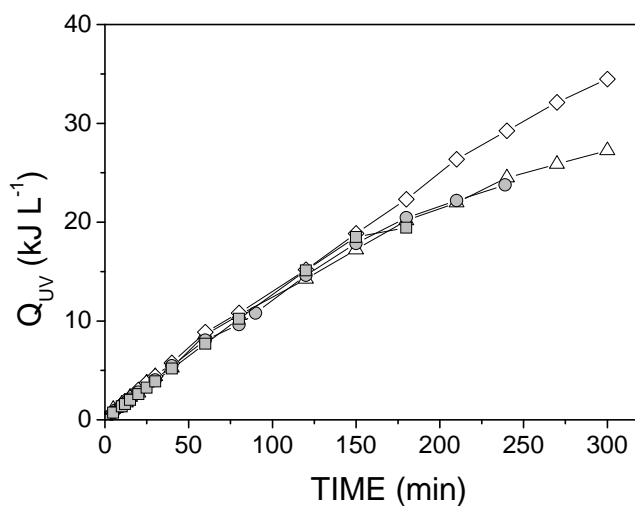


**Figure 3.S5.** Evolution of the accumulated UV dose with time for the systems shown in Fig 4.S4. Experimental conditions: Mixture of six ECs ( $10^{-5}$  mol L<sup>-1</sup> each),  $C_{\text{Fe(III)}} = 2.79$  mg L<sup>-1</sup>,  $\text{H}_2\text{O}_2/\text{Fe(III)} = 6.09$  (mass),  $C_{\text{TiO}_2} = 200$  mg L<sup>-1</sup>,  $Q_g = 0.67$  L min<sup>-1</sup>,  $C_{\text{O}_3, \text{g}} = 13$  mg L<sup>-1</sup>,  $C_{\text{Cl}} = 79$  mg L<sup>-1</sup>,  $C_{\text{SO}_4} = 107$  mg L<sup>-1</sup>,  $C_{\text{CO}_3} = 270$  mg L<sup>-1</sup>,  $C_{\text{NO}_3} = 55$  mg L<sup>-1</sup>,  $C_{\text{PO}_4} = 6$  mg L<sup>-1</sup>. Symbols: Fe(III)/H<sub>2</sub>O<sub>2</sub>/O<sub>3</sub>/hv/ultrapure water/pH 3 (△), Fe(III)/H<sub>2</sub>O<sub>2</sub>/O<sub>3</sub>/hv/presence of ionic species/pH 3 (□), TiO<sub>2</sub>/O<sub>3</sub>/hv/ultrapure water/pH 7 (◇), TiO<sub>2</sub>/O<sub>3</sub>/hv/presence of ionic species/pH 7 (●).

### 3.7. Acknowledgements

---

Authors thank the financial support received from Spanish Ministerio de Economía y Competitividad (MINECO) and ERDF Funds through the projects CTQ2009/13459-C05-05 and CTQ2012-35789-C02-01. D. H. Quiñones thanks the MINECO the concession of a predoctoral FPI grant.

### 3.8. References

---

- [1] B. Kasprzyk-Hordern, R.M. Dinsdale, A.J. Guwy, *The removal of pharmaceuticals, personal care products, endocrine disruptors and illicit drugs during wastewater treatment and its impact on the quality of receiving waters*, Water Res. 43 (2009) 363-380.
- [2] R.U. Halden, *Ecological and human health considerations, in: contaminants of emerging concern in the environment*, ACS Symposium Series, American Chemical Society, Washington DC, 2010.
- [3] S. Malato, P. Fernández-Ibáñez, M.I. Maldonado, J. Blanco, W. Gernjak, *Decontamination and disinfection of water by solar photocatalysis: Recent overview and trends*, Catal. Today 147 (2009) 1-59.
- [4] M. Vedrenne, R. Vasquez-Medrano, D. Prato-Garcia, B.A. Frontana-Uribe, M. Hernandez-Esparza, J.M. de Andrés, *A ferrous oxalate mediated photo-Fenton system: Toward an increased biodegradability of indigo dyed wastewaters*, J. Hazard. Mater. 243 (2012) 292-301.
- [5] A.P.S. Batista, R.F.P. Nogueira, *Parameters affecting sulfonamide photo-Fenton degradation – Iron complexation and substituent group*, J. Photochem. Photobiol. A Chem. 232 (2012) 8–13.
- [6] X. Zhang, P. Chen, F. Wu, N. Deng, J. Liu, T. Fang, *Degradation of 17 $\alpha$ -ethinylestradiol in aqueous solution by ozonation*, J. Hazard. Mater. 133 (2006) 291–298.
- [7] E.M. Rodríguez, G. Márquez, E.A. León, P.M. Álvarez, A.M. Amat, F.J. Beltrán, *Mechanism considerations for photocatalytic oxidation, ozonation and photocatalytic ozonation of some pharmaceutical compounds in water*, J. Environ. Manage. 127 (2013) 114-124.
- [8] U. von Gunten, *Ozonation of drinking water: Part I. Oxidation kinetics and product formation*, Water Res. 37 (2003) 1443–1467.
- [9] L. Sánchez, X. Domènech, J. Casado, J. Peral, *Solar activated ozonation of phenol and malic acid*, Chemosphere 50 (2003) 1085–1093.

- [10] N. Klamerth, N. Miranda, S. Malato, A. Agüera, A.R. Fernández-Alba, M.I. Maldonado, J.M. Coronado, *Degradation of emerging contaminants at low concentrations in MWTPs effluents with mild solar photo-Fenton and TiO<sub>2</sub>*, *Catal. Today* 144 (2009) 124–130.
- [11] N. Miranda-García, S. Suárez, B. Sánchez, J.M. Coronado, S. Malato, M.I. Maldonado, *Photocatalytic degradation of emerging contaminants in municipal wastewater treatment plant effluents using immobilized TiO<sub>2</sub> in a solar pilot plant*, *Appl. Catal. B-Environ.* 103 (2011) 294–301.
- [12] A. Bernabeu, R.F. Vercher, L. Santos-Juanes, P.J. Simón, C. Lardín, M.A. Martínez, J.A. Vicente, R. González, C. Llosá, A. Arques, A.M. Amat, *Solar photocatalysis as a tertiary treatment to remove emerging pollutants from wastewater treatment plant effluents*, *Catal. Today* 161 (2011) 235–240.
- [13] R. Andreozzi, V. Caprio, R. Marotta, D. Vogna, *Paracetamol oxidation from aqueous solutions by means of ozonation and H<sub>2</sub>O<sub>2</sub>/UV system*, *Water Res.* 37 (2003) 993–1004.
- [14] M. Umar, F. Roddick, L. Fan, H.A. Aziz, *Application of ozone for the removal of bisphenol A from water and wastewater – A review*, *Chemosphere* 90 (2013) 2197–2207.
- [15] R. Rosal, A. Rodríguez, J.A. Perdígón-Melón, A. Petre, E. García-Calvo, M.J. Gómez, A. Agüera, A.R. Fernández-Alba, *Occurrence of emerging pollutants in urban wastewater and their removal through biological treatment followed by ozonation*, *Water Res.* 44 (2010) 578–588.
- [16] D. Shin, M. Jang, M. Cui, S. Na, J. Khim, *Enhanced removal of dichloroacetonitrile from drinking water by the combination of solar-photocatalysis and ozonation*, *Chemosphere* 93 (2013) 2901–2908.
- [17] T. Oyama, T. Otsu, Y. Hidano, T. Koike, N. Serpone, H. Hidaka, *Enhanced remediation of simulated wastewaters contaminated with 2-chlorophenol and other aquatic pollutants by TiO<sub>2</sub>-photoassisted ozonation in a sunlight-driven pilot-plant scale photoreactor*, *Solar Energy* 85 (2011) 938–944.
- [18] G. Márquez, E.M. Rodríguez, F.J. Beltrán, P.M. Álvarez, *Solar photocatalytic ozonation of a mixture of pharmaceutical compounds in water*, *Chemosphere* 113 (2014) 71–78.
- [19] M.S. Fram, K. Belitz, *Occurrence and concentrations of pharmaceutical compounds in groundwater used for public drinking-water supply in California*, *Sci. Total Environ.* 409 (2011) 3409–3417.
- [20] D.W. Kolpin, E.T. Furlong, M.T. Meyer, E.M. Thurman, S.D. Zaugg, L.B. Barber, H.T. Buxton, *Pharmaceuticals, hormones, and other organic*

- wastewater contaminants in U.S. streams, 1999–2000: A national reconnaissance*, Environ. Sci. Technol. 36 (2002) 1202-1211.
- [21] Y. Valcárcel, S. González Alonso, J.L. Rodríguez-Gil, R.R. Maroto, A. Gil, M. Catalá, *Analysis of the presence of cardiovascular and analgesic/anti-inflammatory/antipyretic pharmaceuticals in river- and drinking-water of the Madrid Region in Spain*, Chemosphere 82 (2011) 1062–1071.
- [22] E. Drewes, J. Hemming, S.J. Ladenburger, J. Schauer, W. Sonzogni, *An assessment of endocrine disrupting activity changes during wastewater treatment through the use of bioassays and chemical measurements*, Water Environ. Res. 77 (2005) 12–23.
- [23] H. Fukazawa, K. Hoshino, T. Shiozawa, H. Matsushita, Y. Terao, *Identification and quantification of chlorinated bisphenol-A in wastewater from wastepaper recycling plants*, Chemosphere 44 (2001) 973–979.
- [24] T. Heberer, K. Reddersen, A. Mechlinski, *From municipal sewage to drinking water: fate and removal of pharmaceutical residues in the aquatic environment in urban areas*, Water Sci. Technol. 46 (2002) 81–88.
- [25] T.A. Ternes, *Analytical methods for the determination of pharmaceuticals in aqueous environmental samples*, Trends Anal. Chem. 20 (2001) 419.
- [26] P.M. Álvarez, E.M. Rodríguez, G. Fernández, F.J. Beltrán, *Degradation of bisphenol A in water by Fe(III)/UVA and Fe(III)/polycarboxylate/UVA photocatalysis*, Water Sci. Technol. 61 (2010) 2717-2722.
- [27] C. Minero, E. Pelizzetti, S. Malato, J. Blanco, *Large solar plant photocatalytic water decontamination: effect of operational parameters*, Solar Energy 56 (1996) 421–428.
- [28] H. Bader, J. Hoigné, *Determination of ozone in water by the indigo method*, Water Res. 15 (1981) 449-456.
- [29] W. Masschelein, M. Denis, R. Ledent, *Spectrophotometric determination of residual hydrogen peroxide*, Water Sewage Works 124 (1977) 69–72.
- [30] G. Eisenberg, *Colorimetric determination of hydrogen peroxide*, Ind. Eng. Chem. Anal. Ed. 15 (1943) 327–328.
- [31] Y. Zuo, *Kinetics of photochemical/chemical cycling of iron coupled with organic substances in cloud and fog droplets*, Geochim. Cosmochim. Ac. 59 (1995) 3123-3130.
- [32] J.L. Lean, *Short term, direct indices of solar variability*, Space Sci Rev. 94 (2000) 39–51.

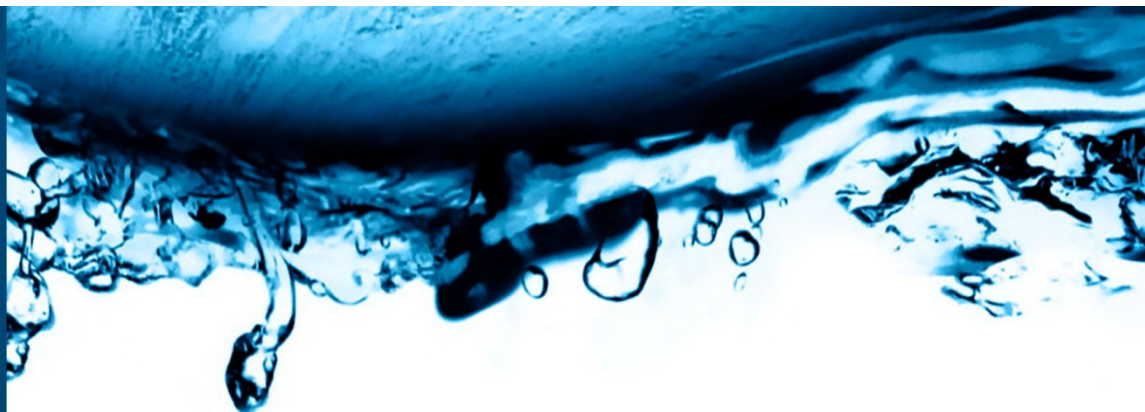
- [33] E. Vulliet, M. Falletta, P. Marote, T. Lomberget, J.O. Païssé, M.F. Grenier-Loustalo, *Light induced degradation of testosterone in waters*, *Sci. Total Environ.* 408 (2010) 3554–3559.
- [34] B. Faust, J. Hoigne, *Photolysis of iron(III)-hydroxy complexes as sources of hydroxyl radicals in clouds, fog and rain*, *J. Atmos. Environ.* 24A (1990) 79–89.
- [35] J. Jeong, J. Yoon, *pH effect on OH radical production in photo/ferrioxalate system*, *Water Res.* 39 (2005) 2893–2900.
- [36] S. Goldstein, D. Aschengrau, Y. Diamant, J. Rabani, *Photolysis of aqueous H<sub>2</sub>O<sub>2</sub>: Quantum yield and applications for polychromatic UV actinometry in photoreactors*, *Environ. Sci. Technol.* 21 (2007) 7486–7490.
- [37] G.R. Peyton, W.H. Glaze, *Destruction of pollutants in water with ozone in combination with ultraviolet radiation. 3 Photolysis of aqueous ozone*, *Environ. Sci. Technol.* 22 (1988) 761–767.
- [38] J. Staehelin, R.E. Buehler, J. Hoigne, *Ozone decomposition in water studied by pulse radiolysis. 2. Hydroxyl and hydrogen tetroxide (HO<sub>4</sub>) as chain intermediates*, *J. Phys. Chem.* 88 (1984) 5999–6004.
- [39] T. Loegager, J. Holcman, K. Sehested, T. Pedersen, *Oxidation of ferrous ions by ozone in acidic solutions*, *Inorg. Chem.* 31 (1992) 3523–3529.
- [40] D. Bahnemann, E.J. Hart, *Rate constants of the reaction of the hydrated electron and hydroxyl radical with ozone in aqueous solution*, *J. Phys. Chem.* 86 (1982) 252–255.
- [41] F.J. Beltrán, *Ozone reaction kinetics for water and wastewater systems*, Lewis Publishers, CRC Press. Boca Raton, Florida USA, 2003.
- [42] S.J. Khan, H.S. Weinberg, *Characterisation of carbonyl byproducts of drinking water ozonation*, *Wat. Sci. & Technol.* 7 (2007) 95–100.
- [43] X.B. Zhang, W.Y. Dong, W. Yang, *Decolorization efficiency and kinetics of typical reactive azo dye RR2 in the homogeneous Fe(II) catalyzed ozonation process*, *Chem. Eng. J.* 233 (2013) 14–23.
- [44] C. Decoret, J. Royer, B. Legube, M. Doré, *Experimental and theoretical studies of the mechanism of the initial attack of ozone on some aromatics in aqueous medium*, *Environ. Technol. Lett.* 5 (1984) 207–221.
- [45] F.J. Beltrán, J.M. Encinar, J.F. García-Araya, *Modelling industrial wastewater ozonation in bubble contactors. 2: Scale-up from bench to pilot plant*, *Ozone-Sci. Eng.* 17 (1996) 379–398.

- [46] A. Espejo, A. Aguinaco, A.M. Amat, F.J. Beltrán, *Some ozone advanced oxidation processes to improve the biological removal of selected pharmaceutical contaminants from urban wastewater*, J. Environ. Sci. Health. A 49 (2014) 410–421.
- [47] M.S. Elovitz, U. von Gunten, *Hydroxyl radical/ozone ratios during ozonation processes. I. The  $R_{ct}$  concept*, Ozone-Sci. Eng. 21 (1999) 239-260.
- [48] P.N. Johnson, R.A. Davis, *Diffusivity of ozone in water*, J. Chem. Eng. Data 41 (1996) 1485-1487.
- [49] G.R. Cokelet, J.W. Hoopes, T. Vermeulen, *Advances in Chemical Engineering*, Volume 11, Academic Prerss, New York USA, 1981.
- [50] F.J. Beltrán, A. Aguinaco, J.F. García-Araya, A. Oropesa, *Ozone and photocatalytic processes to remove the antibiotic sulfamethoxazole from water*, Water Res. 42 (2008) 3799-3808.
- [51] I. Muñoz, M.J. Gómez, A. Molina-Díaz, M.A.J. Huijbregts, A.R. Fernández-Alba, E. García-Calvo, *Ranking potential impacts of priority and emerging pollutants in urban wastewater through life cycle impact assessment*, Chemosphere 74 (2008) 37–44.
- [52] F.J. Rivas, J. Sagasti, A. Encinas, O. Gimeno, *Contaminants abatement by ozone in secondary effluents. Evaluation of second order rate constants*, J Chem. Technol. Biotechnol. 86 (2011) 1058–1066.
- [53] R.H. Bisby, N. Tabassum, *Properties of the radicals formed by one-electron oxidation of acetaminophen—a pulse radiolysis study*, Biochem. Pharmacol. 37 (1988) 2731–2738.
- [54] L. Yang, L.E. Yu, M.B. Ray, *Photocatalytic oxidation of paracetamol: dominant reactants, intermediates, and reaction mechanisms*, Environ. Sci. Technol. 43 (2009) 460–465.
- [55] Y. Chen, C. Hu, X. Hu, J. Qu, *Indirect photodegradation of amine drugs in aqueous solution under simulated sunlight*, Environ. Sci. Technol. 43 (2009) 2760–2765.
- [56] F. Yuan, C. Hu, X. Hu, J. Qu, M. Yang, *Degradation of selected pharmaceuticals in aqueous solution with UV and UV/H<sub>2</sub>O<sub>2</sub>*, Water Res. 43 (2009) 1766 – 1774.
- [57] M. Deborde, S. Rabouan, J.P. Duguet, B. Legube, *Kinetics of aqueous ozone-induced oxidation of some endocrine disruptors*, Environ. Sci. Technol. 39 (2005) 6086–6092.



- [58] T. Garoma, S. Matsumoto, *Ozonation of aqueous solution containing bisphenol A: Effect of operational parameters*, J. Hazard. Mater. 167 (2009) 1185–1191.
- [59] J. Lee, H. Park, J. Yoon, *Ozonation characteristics of bisphenol A in water*, Environ. Technol. 24 (2003) 241–248.
- [60] E. Felis, S. Ledakowicz, J.S. Miller, *Degradation of bisphenol A using UV and UV/H<sub>2</sub>O<sub>2</sub> processes*, Water Environ. Res. 83 (2011) 2154–2158.
- [61] B. Gozmen, M.A. Oturan, N. Oturan, O. Erbatır, *Indirect electrochemical treatment of bisphenol A in water via electrochemically generated Fenton's reagent*, Environ. Sci. Technol. 37 (2003) 3716–3723.
- [62] Z. Manjun, *Determination of photochemically-generated reactive oxygen species in natural water*, J. Environ. Sci. 21 (2009) 303–306.
- [63] E.J. Rosenfeldt, K.G. Linden, *Degradation of endocrine disrupting chemicals bisphenol A, ethinyl estradiol, and estradiol during UV photolysis and advanced oxidation processes*, Environ. Sci. Technol. 38 (2004) 5476–5483.
- [64] N. Nakatani, N. Hashimoto, H. Sakugawa, *An evaluation of hydroxyl radical formation in river water and the potential for photodegradation of bisphenol A*, Geo. Soc. S. P. 9 (2004) 233–242.
- [65] M. Sánchez-Polo, M.M.A. Daiem, R. Ocampo-Pérez, J. Rivera-Utrilla, A.J. Mota, *Comparative study of the photodegradation of bisphenol A by HO<sup>•</sup>, SO<sub>4</sub><sup>•-</sup> and CO<sub>3</sub><sup>•-</sup>/HCO<sub>3</sub><sup>•</sup> radicals in aqueous phase*, Sci. Total Environ. 463–464 (2013) 423–431.
- [66] R. Broséus, S. Vincent, K. Aboulfadl, A. Daneshvar, S. Sauvé, B. Barbeau, M. Prévost, *Ozone oxidation of pharmaceuticals, endocrine disruptors and pesticides during drinking water treatment*, Water Res. 43 (2009) 4707–4717.
- [67] X. Shi, N. S. Dalal, *Antioxidant behaviour of caffeine. Efficient scavenging of hydroxyl radicals*, Fd. Chem. Toxic 29 (1991) 1–6.
- [68] T.P.A. Devasagayam, J.P. Kamat, Hari Mohan, P.C. Kesavan, *Caffeine as an antioxidant: inhibition of lipid peroxidation induced by reactive oxygen species*, BBA-Biomembranes 1282 (1996) 63–70.
- [69] F.J. Benitez, J.L. Acero, F.J. Real, G. Roldán, *Ozonation of pharmaceutical compounds: Rate constants and elimination in various water matrices*, Chemosphere 77 (2009) 53–59.
- [70] J. Benner, E. Salhi, T. Ternes, U. von Gunten, *Ozonation of reverse osmosis concentrate: Kinetics and efficiency of beta blocker oxidation*, Water Res. 42 (2008) 3003–3012.

- [71] F.J. Benitez, F.J. Real, J.L. Acero, G. Roldan, *Removal of selected pharmaceuticals in waters by photochemical processes*, J. Chem. Technol. Biotechnol. 84 (2009) 1186–1195.
- [72] W. Song, W.J. Cooper, S.P. Mezyk, J. Greaves, B.M. Peake, *Free radical destruction of  $\beta$ -blockers in aqueous solution*, Environ. Sci. Technol. 42 (2008) 1256–1261.
- [73] Y. Yoon, P. Westerhoff, S.A. Snyder, E. C. Wert, *Nanofiltration and ultrafiltration of endocrine disrupting compounds, pharmaceuticals and personal care products*, J. Membr. Sci. 270 (2006) 88–100.
- [74] E. Barron, M. Deborde, S. Rabouan, P. Mazellier, Bernard Legube, *Kinetic and mechanistic investigations of progesterone reaction with ozone*, Water Res. 40 (2006) 2181–2189.



## Chapter IV

### Paper 2:

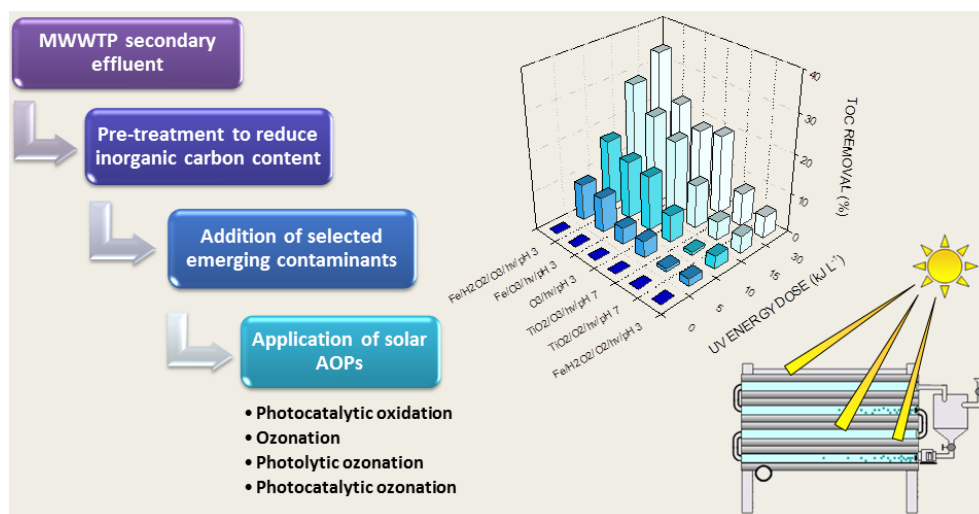
Removal of emerging contaminants from municipal WWTP secondary effluents by solar photocatalytic ozonation. A pilot-scale study.

Diego H. Quiñones<sup>1</sup>, Pedro M. Álvarez<sup>1</sup>, Ana Rey<sup>1</sup>, Fernando J. Beltrán<sup>1</sup>

<sup>1</sup> Departamento de Ingeniería Química y Química Física, Facultad de Ciencias, Universidad de Extremadura, Av. de Elvas s/n, 06071 Badajoz (Spain)

Submitted for publication in: Separation and Purification Technology





#### 4.1. Abstract

Ozonation, solar photocatalytic oxidation and a combination of both systems, known as solar photocatalytic ozonation, has been studied to treat a secondary effluent from a municipal wastewater treatment plant containing a selection of six emerging contaminants (acetaminophen, antipyrine, bisphenol A, caffeine, metoprolol and testosterone). Fe(III), Fenton reagent and TiO<sub>2</sub> were used in photocatalytic experiments, which were conducted in a pilot-scale compound parabolic collector photo-reactor using solar radiation as energy source. Emerging contaminants were completely removed by most of the solar photocatalytic treatments applied, showing the ozone-based systems at pH 3 higher reaction rates than other solar photocatalytic oxidation systems. However, the organic matter mineralization level achieved was limited (< 35% TOC removal) even after the application of solar photocatalytic ozonation, for which an enhanced generation of hydroxyl radicals was measured in experiments carried out in the presence of the hydroxyl radical probe p-chlorobenzoic acid. *Daphnia Magna* bioassays were used to test toxicity of samples before and after their treatment, showing that samples subjected to solar photocatalytic ozonation were less toxic than the mixture of emerging contaminants in the secondary effluent. Finally, a simplified estimation of operating costs shows some solar photocatalytic ozonation processes advantageous over the solar photo-Fenton system.

**Keywords:** Domestic wastewater, emerging contaminant, solar photocatalytic ozonation, toxicity.

## 4.2. Introduction

---

The development of advanced analytical techniques has allowed the detection of emerging contaminants (ECs) in aquatic environments revealing a worldwide issue [1]. Many of these compounds, which are incorporated into the sewage system through domestic and industrial drains, have been found to be recalcitrant to the biological and physicochemical processes typically applied in wastewater treatment plants (WWTP). As a result, they remain in treated wastewaters being discharged into natural waters bodies (rivers, lakes, seas and streams) [1,2].

The EC group includes a wide variety of compounds such as pharmaceuticals, personal care products, hormones, industrial additives and household chemicals. Usually, their metabolites and degradation products are also included in this category of pollutants [2]. Most of the ECs are bio-accumulative, have endocrine disrupting effects and can cause health and mutagenic effects on living beings that benefit from aquatic systems [3,4].

This situation is leading to stringent regulations on wastewater management [3,5], though most of the ECs are not yet regulated [6]. Advanced oxidation processes (AOPs) can be considered as potential effective alternatives for the treatment of ECs in water. This is so because AOPs, characterized by the generation of short-life reactive species such as the hydroxyl radical ( $\cdot\text{OH}$ ), can completely degrade a wide range of water contaminants, transforming them into less harmful species. Since the application of AOPs to treat wastewaters leads to better quality effluents, wastewater recycling can be considered as a management option [7].

Currently, ozonation processes are applied in wastewater treatment as disinfectant, oxidant of organic pollutants and pre or post-treatment of other unit operations (as coagulation, flocculation, biological oxidation, etc) [8]. However, its use implies high operating costs due to ozone production. Moreover, although ozone itself can remove most of the organic compounds present in domestic wastewaters, due to its selective nature, it is not usually able to mineralize them, remaining ozonation by-products in the effluents. If combined with other agents, such as UV light and/or catalysts, significant improvements in the level of organic matter mineralization and the efficiency on the use of ozone can be achieved. Such enhancements were observed in a previous work where a first approach to the application, at pilot-scale, of solar photocatalytic ozonation assisted by Fe(III), Fe(III)/H<sub>2</sub>O<sub>2</sub> and TiO<sub>2</sub> to remove selected ECs from water was carried out [9]. As part of our continuing work on solar photocatalytic ozonation, here the treatment method has been applied to degrade ECs in a secondary effluent from a municipal WWTP. The use of solar

radiation instead of UV lamps may drastically reduce the operating cost associated with the treatment system [10].

### 4.3. Materials and methods

#### 4.3.1. Secondary effluent samples

First, secondary effluent samples from a municipal WWTP (Badajoz, Spain) were collected and their pH was lowered to 3 by adding concentrated hydrochloric acid solution while bubbling air to remove their carbonate and bicarbonate content, which have been found to be detrimental for the efficiency of AOPs since these species can scavenge hydroxyl radicals [11]. The main characteristics of the secondary effluent samples after this pretreatment are summarized in Table 4.1.

**Table 4.1.** Main characteristics of the secondary effluent samples used in this work (after pH adjustment treatment)

Parameter	Value
Inorganic carbon (mg L <sup>-1</sup> )	0.3 ± 0.2
Total organic carbon (mg L <sup>-1</sup> )	20.0 ± 2.1
pH	3.0 ± 0.1
BOD <sub>5</sub> (mg L <sup>-1</sup> )	10 ± 3
COD (mg L <sup>-1</sup> )	58.6 ± 3.5
Turbidity (NTU)	7.8 ± 1.1
Conductivity (μS cm <sup>-1</sup> )	1330 ± 9
PO <sub>4</sub> <sup>3-</sup> (mg L <sup>-1</sup> )	10.4 ± 1.0
SO <sub>4</sub> <sup>2-</sup> (mg L <sup>-1</sup> )	63.6 ± 0.5
Cl <sup>-</sup>	294.7 ± 4.6
NH <sub>4</sub> <sup>+</sup> (mg L <sup>-1</sup> )	2.5 ± 0.6
NO <sub>3</sub> <sup>-</sup> (mg L <sup>-1</sup> )	5.7 ± 0.8

Acetaminophen (ACE), antipyrine (ANT), bisphenol A (BIS), caffeine (CAF), metoprolol (MET) and testosterone (TST), purchased from Sigma–Aldrich and used as received, were the ECs selected as target compounds for this work. Secondary effluent samples were spiked with 200 μg L<sup>-1</sup> of each compound. Additionally, p-chlorobenzoic acid (pCBA, Merck) was used as hydroxyl radical probe compound in some experiments. The chemical structures of all these compounds are shown in Figure 4.1.

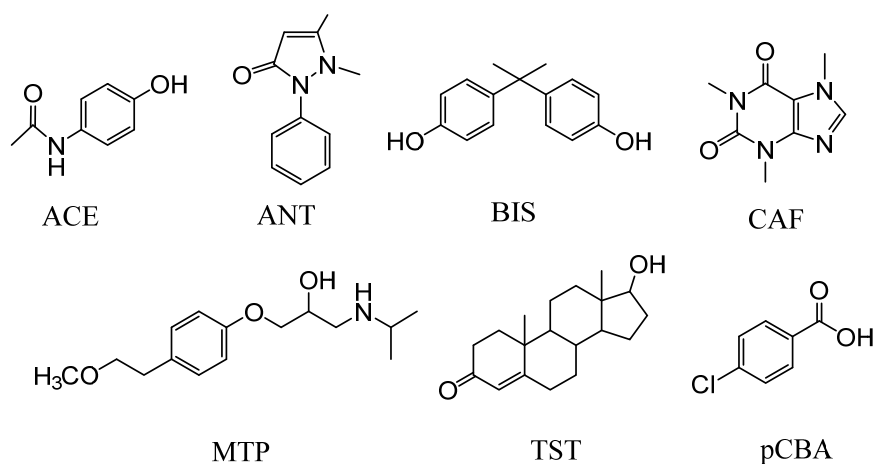


**Figure 4.1.** Chemical structures of the chemical compounds used in this work

### 4.3.2. Experimental set-up and procedure

Experiments were conducted at ambient temperature in a pilot-scale solar plant located in Badajoz, Spain (38°52'43" N, 6°58'15" W). The solar plant consists mainly of an air compressor (Pintuc Extreme 3), an ozone generator (OZVa 1200E, ProMinent) and a compound parabolic collector (CPC, Ecosystem-Environmental Services S.A.) operated in semi-batch mode. Additionally, the plant was equipped with measurement devices (e.g., ozone analyzers) and controllers as shown in Figure 4.2. Thus, the CPC inlet gas stream is regulated by a precision gas flow controller (MC-10SLPM-D, Alicat Scientific) while two ozone analyzers (GM-6000-RTI and GM-6000-PRO, Anseros) were used to monitor the ozone concentration in the inlet and outlet gas streams, respectively.

The CPC used as photo-reactor consisted of four borosilicate-glass tubes (32 mm external diameter, 1.4 mm thickness, 750 mm length, ~90% transmittance) connected in series (total irradiated volume of 1.8 L) reflected by involute-type mirrors (320 G electropolished aluminum, 0.25 m<sup>2</sup> reflection surface), which were mounted on a fixed platform tilted 45°. The reactor also had two ports for inlet and outlet of gas, a reservoir tank of 7 L total capacity and connecting tubing and valves. The pH of the aqueous solution in the tank was automatically controlled at set-point values (i.e., 3 or 7) by an in-line pH control system provided with WP1000-P1/8S4-J4-C Welco pumps to feed hydrochloric acid or sodium hydroxide solutions to the system. The photo-reactor was also equipped with a Pt-100 probe and a broadband UV radiometer (Acadus 85-PLS) to record continuously the temperature and the incident UV radiation ( $\lambda < 400$  nm), respectively.



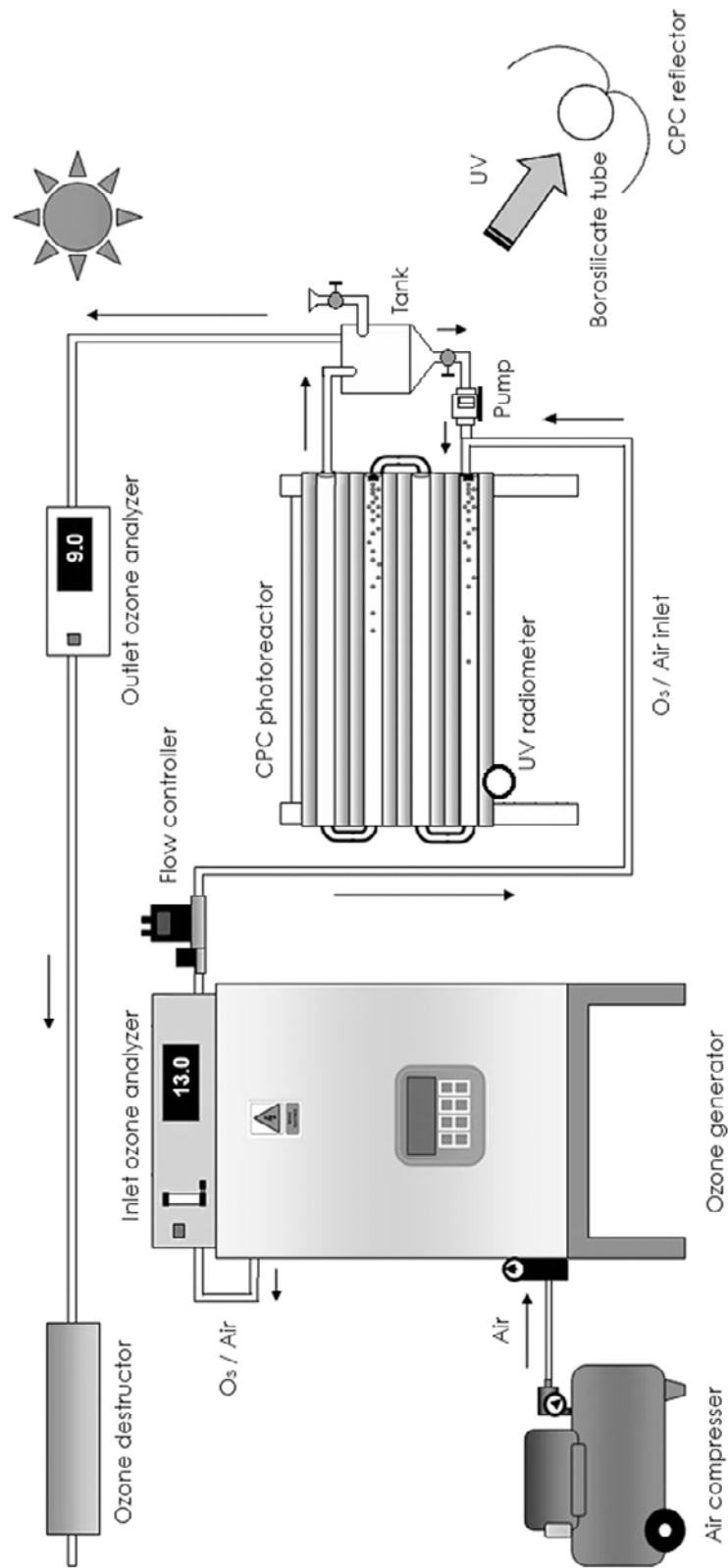


**Figure 4.2.** Simplified scheme of the solar pilot plant used in this work

Radiation data were acquired as instantaneous and accumulated UV energy (Proasis DCS-Win 3.55 software, Design Instruments S.A.). In a typical experiment, the photo-reactor reservoir tank was first loaded with 5 L of the secondary effluent containing a mixture of ECs and the required amount of catalyst (Fe(III) or TiO<sub>2</sub>) was added afterwards. Initial concentrations of catalysts were as follows: 2.8 mg L<sup>-1</sup> of Fe(III) as iron(III) perchlorate hydrate (Sigma–Aldrich) or 200 mg L<sup>-1</sup> of TiO<sub>2</sub> Aeroxide ® P25 (Evonik Industries). After adding the catalyst, the solution was recirculated through the CPC by a centrifugal pump at a flow rate of 8.7 L min<sup>-1</sup> so that the flux pattern inside the tubes was turbulent ( $Re > 7500$ ). The CPC tubes were kept covered to avoid sunlight illumination for the first 30 min of each experiment (dark stage). This time was used for homogenization purposes and it was enough to reach the adsorption equilibria of ECs onto TiO<sub>2</sub> (if used). After that, the CPC was uncovered and a continuous gas flow (0.67 L min<sup>-1</sup> flow rate) was supplied to the reactor. Also, if needed, hydrogen peroxide (Panreac) was added at this point to the CPC system. The gas stream entering the CPC tube was either air or an ozone-air mixture (c.a. 13 mg L<sup>-1</sup> ozone). Experiments lasted 5 hours plus the 30 min of the dark stage. During the whole course of the experiment liquid samples were withdrawn from the reactor at intervals through a sampling port to determine the EC concentration, total organic carbon (TOC), and the concentrations of hydrogen peroxide, ozone and iron. Also, the concentration of phenolic compounds was analyzed in some liquid samples. In addition, biodegradability (i.e. the ratio between the 5-day biochemical oxygen demand and the chemical oxygen demand, BOD<sub>5</sub>/COD ratio) and ecotoxicity (*Daphnia Magna* assay) was measured in selected samples.

#### 4.3.3. Analytical methods

Samples taken during the course of experiments using ozone were immediately bubbled with helium to remove residual ozone. Likewise, excess hydrogen peroxide in samples was quenched by adding an aliquot of concentrated sodium thiosulfate solution. These procedures, which did not alter the organic content of the samples, avoided further ozone and/or hydrogen peroxide reactions while samples were kept before ECs and other organic content analyses. Prior to analysis, the samples were filtered through a 0.45 µm PET filtering membrane (Chromafil Xtra). Samples used in ecotoxicity tests were withdrawn from the photo-reactor, bubbled with helium if ozone was used, mixed with catalase solution (0.1 g·L<sup>-1</sup> bovine liver, 3390 units mg<sup>-1</sup> solid, Sigma–Aldrich) to eliminate the residual H<sub>2</sub>O<sub>2</sub>, neutralized and filtered through a 0.45 µm cellulose nitrate filtering membrane (Sartorius Stedim) before analysis. Samples used to analyze the dissolved ozone concentration were withdrawn from the reactor and, without any further pretreatment, analyzed immediately by the indigo method [12].

An Agilent 1100 Series HPLC (Hewlett Packard) equipped with a Kromasil C18 column (5  $\mu\text{m}$  particle size, 150 mm length, 4 mm diameter, Teknokroma) as stationary phase was used to measure compounds concentration. A binary mixture of acetonitrile and 0.1% v/v phosphoric acid aqueous solution was used as mobile phase. ANT, CAF and MET were analyzed at 240, 275 and 225 nm detection wavelength respectively, using a 15% acetonitrile mobile phase eluted at 0.65 mL  $\text{min}^{-1}$ . BIS, TST and pCBA were analyzed at 220 and 250 nm (for the latter two) with a 50% acetonitrile mobile phase at 1 mL  $\text{min}^{-1}$ . ACE was analyzed with a 15% acetonitrile mobile phase at 1 mL  $\text{min}^{-1}$  and 244 nm as detection wavelength. A Shimadzu TOC-V<sub>SCH</sub> analyzer equipped with an infrared detector was used to measure the total, inorganic and organic carbon content. An ion chromatography apparatus (881 compact IC pro, Metrohm) equipped with a Metrosep A Supp 7 column (150 mm length, 4 mm diameter) was used to measure phosphate, sulfate, nitrate, chloride and ammonium in the secondary effluent samples. Hydrogen peroxide was measured by the Eisenberg method [13]. Total phenolic content in solution was determined by the method proposed by Singleton and Rossi [14] and expressed as mg BIS  $\text{L}^{-1}$ . Dissolved Fe(II) was measured as indicated by Zuo [15]. COD was measured by the dichromate method using the Lange cuvette test while the BOD<sub>5</sub> was determined measuring the oxygen consumed during a 5-day incubation period [16] using ST-OxiTop® devices. Acute toxicity tests were conducted with Daphtoxkit F™ magna toxicity test kits (MicroBioTests) using water flea *Daphnia Magna* according to OECD Guidelines [17]. pH, conductivity and turbidity of samples were measured using a GLP 21+ pHmeter (Crison), a 524 conductivity meter (Crison) and a HI 93414 turbidity meter (Hanna Instruments), respectively.

## 4.4. Results and discussion

---

### 4.4.1. ECs depletion and TOC removal

Samples of the MWWTP secondary effluent containing a mixture of the six above-mentioned ECs were subjected to the following treatments at pH 3: single photolysis (exposure to sunlight without reagents and/or catalyst), ozonation in the dark ( $\text{O}_3$ ), photolytic ozonation ( $\text{O}_3/\text{light}$ ), Fe(III)-based photocatalytic oxidation (Fe(III)/ $\text{O}_2/\text{light}$ ), Fe(III)-based photocatalytic ozonation (Fe(III)/ $\text{O}_3/\text{light}$ ), photo-Fenton (Fe(III)/ $\text{H}_2\text{O}_2/\text{O}_2/\text{light}$ ) and photo-Fenton-based photocatalytic ozonation (Fe(III)/ $\text{H}_2\text{O}_2/\text{O}_3/\text{light}$ ). For comparison purposes, also  $\text{TiO}_2$ -based photocatalytic oxidation ( $\text{TiO}_2/\text{O}_2/\text{light}$ ),  $\text{TiO}_2$  photocatalytic ozonation ( $\text{TiO}_2/\text{O}_3/\text{light}$ ) and ozonation ( $\text{O}_3$ ) processes were applied at pH 7.

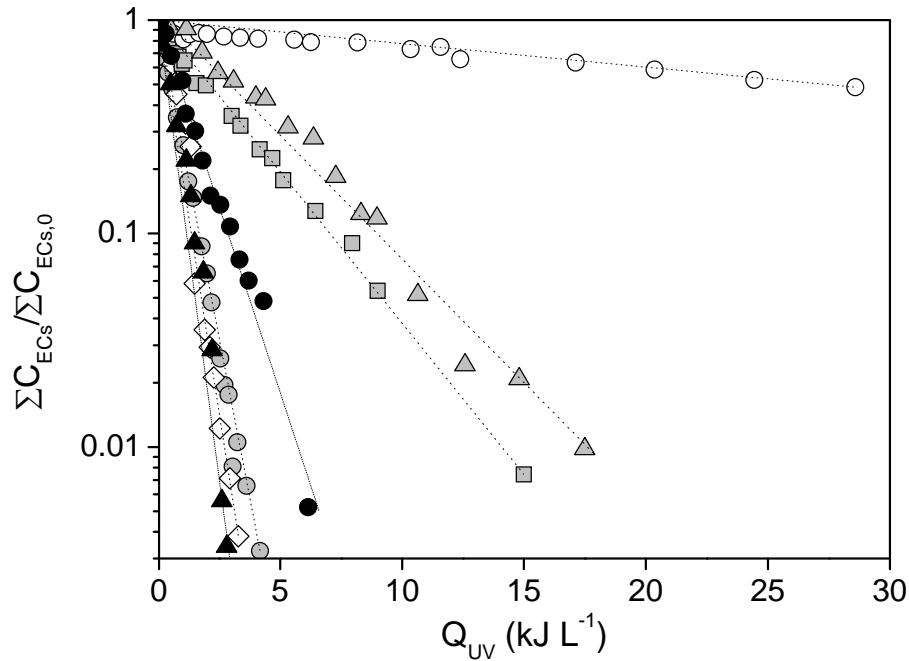
Single photolysis was not able to degrade the ECs. Thus, only TST was removed to some extent by single photolysis (34% removal after 5h irradiation, which meant 33 kJ L<sup>-1</sup> UV radiation supplied). Fe(III) photocatalytic oxidation experiments only led to EC removal percentages between 26% (ANT) and 43% (TST) after 5 h treatment (39 kJ L<sup>-1</sup> UV radiation dose). However, complete removal of ECs was achieved in photo-Fenton experiments in less than 90 min reaction time (8 kJ·L<sup>-1</sup> UV radiation dose) and in single ozonation experiments at pH 3 and 7 in about 25 min (c.a. 28 mg O<sub>3</sub> L<sup>-1</sup>) and 45 min (c.a. 100 mg O<sub>3</sub> L<sup>-1</sup>), respectively. Moreover, systems involving ozone and solar radiation (i.e. O<sub>3</sub>/light, Fe(III)/O<sub>3</sub>/light and Fe(III)/H<sub>2</sub>O<sub>2</sub>/O<sub>3</sub>/light) were able to eliminate, at pH 3, the ECs faster (20-30 min) and with UV doses lower than 6 kJ L<sup>-1</sup>. Among them, the Fe(III)/H<sub>2</sub>O<sub>2</sub>/O<sub>3</sub>/light system was observed to be the most efficient, leading to complete removal of ECs with UV radiation and ozone doses of about 2 kJ L<sup>-1</sup> and 19 mg L<sup>-1</sup>, respectively. TiO<sub>2</sub> photocatalytic experiments, carried out at pH 7, also led to the complete disappearance of the ECs but they required higher UV radiation doses than photo-Fenton and photocatalytic ozonation experiments performed at pH 3. Thus, TiO<sub>2</sub> photocatalytic oxidation experiments (TiO<sub>2</sub>/O<sub>2</sub>/light) absorbed about 15.7 kJ L<sup>-1</sup> of UV radiation (c.a. 2 h of irradiation) to eliminate the parent ECs while in TiO<sub>2</sub>/O<sub>3</sub>/light experiments the consumptions of UV light and ozone were about 12 kJ L<sup>-1</sup> and 37 mg L<sup>-1</sup>, respectively (c.a. 40 min of simultaneous irradiation and ozonation).

Figure 4.3. shows a comparison of the efficiency of some of the solar treatment systems applied in this work in terms of the use of radiation to remove the selected ECs. The delivered UV radiation per volume unit,  $Q_{UV,n}$ , as represented in Figure 4.3. was computed using the equation (4.1) [18]:

$$Q_{UV,n} = Q_{UV,n-1} + (t_n - t_{n-1}) \overline{UV}_{G,n} \frac{A}{V} \quad (4.1)$$

where  $t_n$  is elapsed irradiation time until sample  $n$ ,  $\overline{UV}_{G,n}$  is the average incident UV radiation in the period  $t_{n-1} - t_n$ ,  $V$  is the total reaction volume and  $A$  is the illuminated reactor surface. As it can be seen in Figure 4.3., the treatment systems involving ozone were the most efficient in removing the selected ECs while the Fe(III)/O<sub>2</sub>/light system was the one that required the highest UV radiation dose to remove the ECs. Also, it is apparent from Figure 4.3. that, in all cases, the ECs depletion profiles followed a pseudo first-order kinetics with respect to the UV radiation dose. Accordingly, equation (4.2) was found to be satisfactory fulfilled:

$$\ln \left( \frac{\sum C_{EC,0}}{\sum C_{EC}} \right) = k_{UV} Q_{UV} \quad (4.2)$$



**Figure 4.3.** Plot of  $\Sigma C_{ECs,0}/\Sigma C_{ECs}$  against the UV radiation dose ( $Q_{UV}$ ) for some experiments. Experimental conditions: EC concentration =  $200 \mu\text{g L}^{-1}$ , each; Applied ozone =  $520 \text{ mg h}^{-1}$ ;  $C_{Fe(III),0} = 2.8 \text{ mg L}^{-1}$ ; Initial  $\text{H}_2\text{O}_2/\text{Fe(III)}$  mass ratio = 6.1;  $C_{TiO_2,0} = 200 \text{ mg L}^{-1}$ . Symbols: ( $\odot$ )  $\text{O}_3/\text{light}/\text{pH } 3$ , ( $\circ$ )  $\text{Fe(III)}/\text{O}_2/\text{light}/\text{pH } 3$ , ( $\diamond$ )  $\text{Fe(III)}/\text{O}_3/\text{light}/\text{pH } 3$ , ( $\square$ )  $\text{Fe(III)}/\text{H}_2\text{O}_2/\text{O}_2/\text{light}/\text{pH } 3$ , ( $\blacktriangle$ )  $\text{Fe(III)}/\text{H}_2\text{O}_2/\text{O}_3/\text{light}/\text{pH } 3$ , ( $\triangle$ )  $\text{TiO}_2/\text{O}_2/\text{light}/\text{pH } 7$ , ( $\bullet$ )  $\text{TiO}_2/\text{O}_3/\text{light}/\text{pH } 7$ . Lines: linear regression ( $R^2 > 0.96$ )

The value of the pseudo-first order reaction rate constant,  $k_{UV}$ , was used to estimate the time required to remove 99% of the initial concentration of ECs ( $t_{99}$ ) at a given average incident UV irradiation ( $\overline{UV}_G$ ). Thus equation (4.3) was applied.

$$t_{99} = \frac{\ln(100)}{k_{UV}} \frac{V}{\overline{UV}_G A} \quad (4.3)$$

where  $A$  and  $V$  are the reactor irradiation area and the reaction volume, respectively. Experimental data from single ozonation experiments, carried out in absence of radiation, were satisfactorily fitted to equation (4.4):

$$\ln\left(\frac{\Sigma C_{EC,0}}{\Sigma C_{EC}}\right) = k t \quad (4.4)$$

where  $k$  is the apparent pseudo first order rate constant for total ECs depletion and  $t$  is the irradiation time. In accordance with this,  $t_{99}$  was estimated by the expression (4.5):

$$t_{99} = \frac{\ln(100)}{k} \quad (4.5)$$

Table 4.2. shows the values of the pseudo first-order rate constants for the various treatment systems derived from experimental data (for conditions see the legend of Figure 4.3.) and  $t_{99}$  values computed either by equation (4.3) considering an average incident UV irradiation of  $30 \text{ W} \cdot \text{m}^{-2}$ , which is the typical average UV flux in a sunny day [18] or by equation (4.5).

**Table 4.2.** Pseudo first-order rate constants and estimated depletion time for 99% total EC concentration removal for the AOPs studied in this work

System applied	$k_{UV}$ (L $\text{kJ}^{-1}$ ) <sup>a</sup> or $k$ ( $\text{min}^{-1}$ ) <sup>b</sup>	$t_{99}$ (min)
O <sub>3</sub> /light/pH 3	1.438 <sup>a</sup>	36 <sup>c</sup>
Fe(III)/O <sub>2</sub> /light/pH 3	0.021 <sup>a</sup>	2344 <sup>c</sup>
Fe(III)/O <sub>3</sub> /light/pH 3	1.476 <sup>a</sup>	35 <sup>c</sup>
Fe(III)/H <sub>2</sub> O <sub>2</sub> /O <sub>2</sub> /light/pH 3	0.325 <sup>a</sup>	158 <sup>c</sup>
Fe(III)/H <sub>2</sub> O <sub>2</sub> /O <sub>3</sub> /light/pH 3	1.501 <sup>a</sup>	34 <sup>c</sup>
TiO <sub>2</sub> /O <sub>2</sub> /light/pH 7	0.258 <sup>a</sup>	198 <sup>c</sup>
TiO <sub>2</sub> /O <sub>3</sub> /light/pH 7	0.975 <sup>a</sup>	60 <sup>c</sup>
O <sub>3</sub> /pH 3	0.110 <sup>b</sup>	42 <sup>d</sup>
O <sub>3</sub> /pH 7	0.069 <sup>b</sup>	67 <sup>d</sup>

<sup>a</sup> Calculated by equation (4.2); <sup>b</sup> Calculated by equation (4.4); <sup>c</sup> Calculated by equation (4.3), assuming  $\overline{UV}_G = 30 \text{ W m}^{-2}$ ,  $V = 5 \text{ L}$  and  $A = 0.25 \text{ m}^2$ ; <sup>d</sup> Calculated by equation (4.5)

As far as TOC removal is concerned, Figure 4.4. shows, for selected experiments, the evolution of TOC conversion as a function of the UV energy supplied. It should be mentioned here that the overall TOC in the wastewater samples subjected to treatment was composed of TOC from occurring compounds in the secondary effluent (average TOC =  $20 \text{ mg L}^{-1}$ ) and TOC from added ECs (TOC =  $0.83 \text{ mg L}^{-1}$ ). Accordingly, about 96% of TOC in the samples to be treated was due to the organics present in the MWWTP secondary effluent.

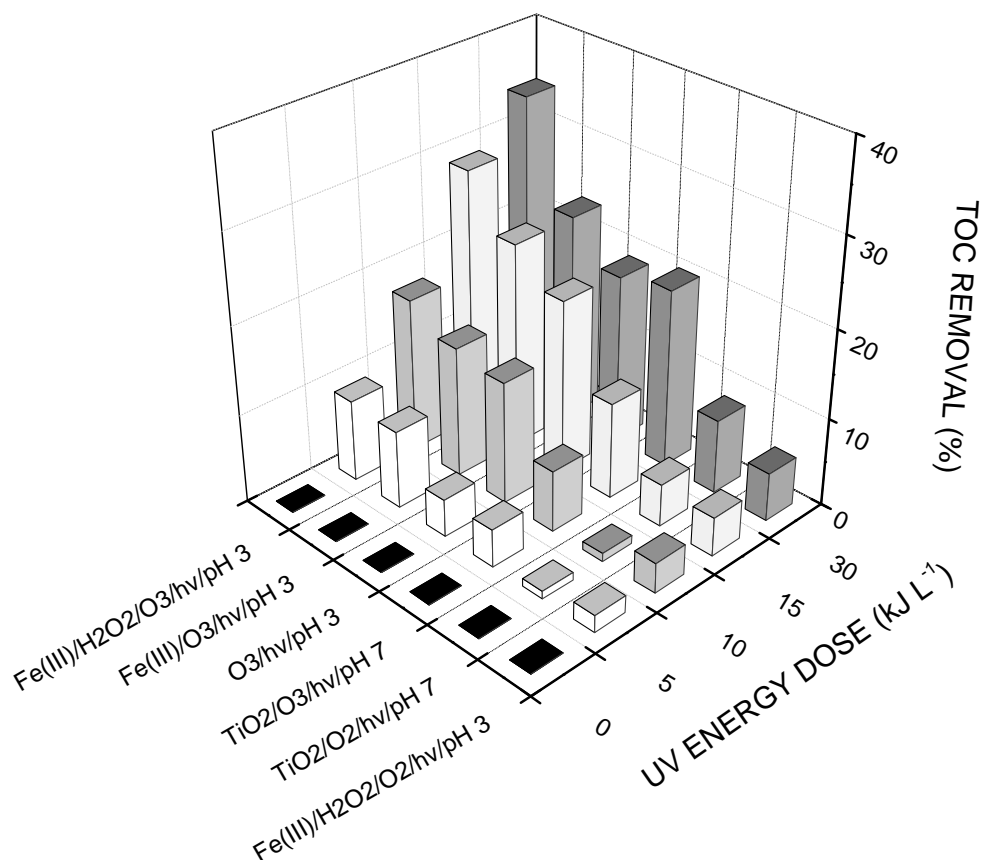


**Figure 4.4.** TOC removal vs UV energy dose for some experiments. Experimental conditions: EC concentration =  $200 \mu\text{g L}^{-1}$ , each; Applied ozone =  $520 \text{ mg h}^{-1}$ ;  $C_{\text{Fe(III),0}} = 2.8 \text{ mg L}^{-1}$ ; Initial  $\text{H}_2\text{O}_2/\text{Fe(III)}$  mass ratio = 6.1;  $C_{\text{TiO}_2,0} = 200 \text{ mg L}^{-1}$ .

As it can be observed in Figure 4.4., TOC removal was far from being complete (<35% TOC removal) in any of the experiments carried out despite the high average incident radiation, which was ranged between  $35$  and  $46 \text{ W m}^{-2}$  (i.e., cumulative UV radiation dose in 5-h experiments was higher than  $30 \text{ kJ L}^{-1}$ ). Nevertheless, it should be mentioned that COD removals (up to 70%) were greater than TOC removals in all cases. Thus, the COD/TOC ratio decreased from the initial value of about 3 to final values of 1.5-2, suggesting that the oxidation progressed to yield organic products which were recalcitrant and, therefore, difficult to degrade. Under the experimental conditions applied in this work, low TOC removal (< 5%) was observed after the application of ozonation in the dark ( $\text{O}_3$ ), both at pH 3 and 7, and the  $\text{Fe(III)}/\text{O}_2/\text{light}$  (pH 3) system (results not shown). Photocatalytic ozonation systems (i.e.,  $\text{Fe(III)}/\text{O}_3/\text{light}$  and  $\text{Fe(III)}/\text{H}_2\text{O}_2/\text{O}_3/\text{light}$ ) at pH 3, however, were much more effective leading to 20-35% TOC conversion

(see Figure 4.4.). In  $\text{TiO}_2$  photocatalytic experiments (pH 7), it was observed an initial period where the TOC removal negligible followed by a period of higher TOC conversion up to reach 8% ( $\text{TiO}_2/\text{O}_2/\text{light}$ ) and 20% ( $\text{TiO}_2/\text{O}_3/\text{light}$ ) removals after the 5-h treatment. The induction period in  $\text{TiO}_2$  catalytic systems could be ascribed to the formation of agglomerates catalyst crystallites or to the adsorption of some inorganic ions on the catalyst surface [19].

For comparative purposes, TOC experimental data were fitted to a first-order kinetic equation. Figure 4.5. shows the apparent first order rate constant,  $k_{\text{TOC,app}}$ , computed for the different systems applied as well as the average incident radiation measured during each experiment.

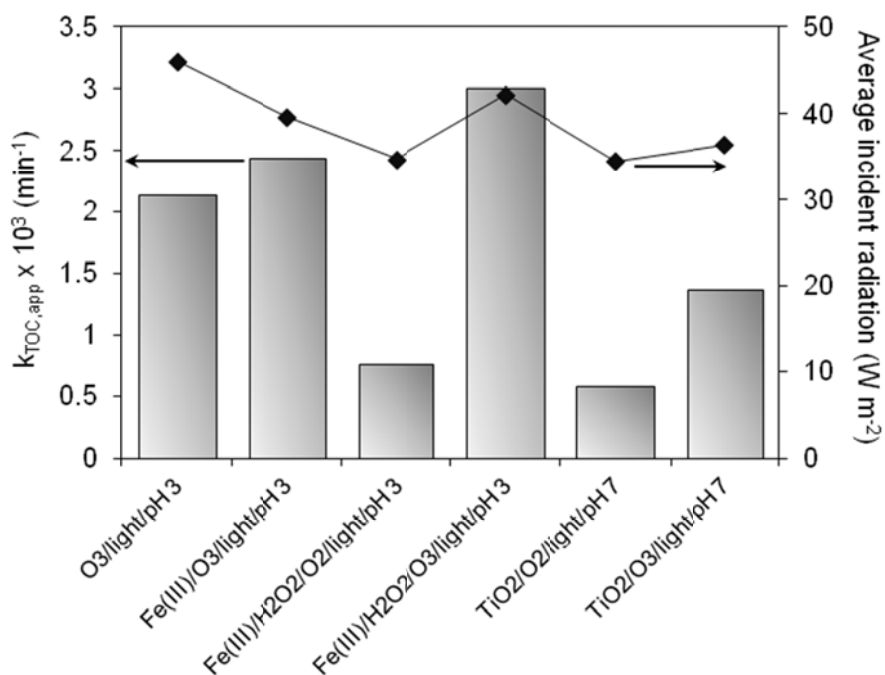


**Figure 4.5.** Apparent mineralization rate constant and average incident radiation for some experiments. Experimental conditions: EC concentration =  $200 \mu\text{g L}^{-1}$ , each; Applied ozone =  $520 \text{ mg h}^{-1}$ ;  $C_{\text{Fe(III),0}} = 2.8 \text{ mg L}^{-1}$ ; Initial  $\text{H}_2\text{O}_2/\text{Fe(III)}$  mass ratio = 6.1;  $C_{\text{TiO}_2,0} = 200 \text{ mg L}^{-1}$ .

As it can be deduced from Figure 4.5., the mineralization (i.e., TOC removal) rate constants followed the order:  $\text{Fe(III)/H}_2\text{O}_2/\text{O}_3/\text{light}$  (pH 3) >  $\text{Fe(III)/O}_3/\text{light}$  (pH 3) >  $\text{Fe(III)/H}_2\text{O}_2/\text{O}_2/\text{light}$  (pH 3) >  $\text{TiO}_2/\text{O}_3/\text{light}$  (pH 7) >  $\text{TiO}_2/\text{O}_2/\text{light}$  (pH 7). Single ozonation (pH 3 and 7), single photolysis (pH 3) and  $\text{Fe(III)/O}_2/\text{light}$  (pH 3) experiments led to very low values of  $k_{\text{TOC,app}}$  ( $< 5 \times 10^{-4} \text{ min}^{-1}$ ) as limited TOC



removal (<5%) was observed after the 5-h experiments. The Fe(III)/H<sub>2</sub>O<sub>2</sub>/O<sub>3</sub>/light system, which showed the highest mineralization rate constant, was also the most efficient system in terms of use of energy (7.5 kJ per mg of TOC removed). Fe(III)/O<sub>3</sub>/light (pH 3) and TiO<sub>2</sub>/O<sub>3</sub>/light (pH 7) experiments showed similar energy efficiencies, ranging between 14.5 and 16.8 kJ per mg of TOC removed. Accordingly, these systems led to similar mineralization degrees (19-23% TOC removal). Photocatalytic oxidation systems such as Fe(III)/H<sub>2</sub>O<sub>2</sub>/O<sub>2</sub>/light (pH 3) and TiO<sub>2</sub>/O<sub>2</sub>/light (pH 7) required more UV energy to remove each mg of TOC (90 and 35 kJ·mg<sup>-1</sup>, respectively) and led to lower mineralization levels (6-9% TOC removal) than the photocatalytic ozonation systems tested.

#### 4.4.2. Hydroxyl radical exposure

In the applied systems the depletion of the pollutants might take place mainly by three pathways: photolysis, direct reaction with molecular ozone, and oxidation by hydroxyl radicals. Taking into account those contributions, the degradation of each compound can be expressed by the equation (4.6):

$$\frac{dC_{EC}}{dt} = -\left(k_{\text{phot.}} + k_{\text{OH}}C_{\text{OH}} + k_{\text{O}_3}C_{\text{O}_3}\right)C_{\text{EC}} \quad (4.6)$$

In equation (4.6),  $k_{\text{phot.}}$  is the first order rate constant for compound photolysis,  $k_{\text{OH-EC}}$  and  $k_{\text{O}_3\text{-EC}}$  are the rate constants for the reaction of each EC with the hydroxyl radical and dissolved ozone, respectively;  $C_{\text{EC}}$ ,  $C_{\text{OH}}$  and  $C_{\text{O}_3}$  are the concentration of ECs, hydroxyl radicals and ozone, respectively. After integration and variable separation, the following expression is obtained:

$$\ln\left(\frac{C_{\text{EC},0}}{C_{\text{EC}}}\right) = k_{\text{phot.}} \int_0^t dt + k_{\text{OH}} \int_0^t C_{\text{OH}} dt + k_{\text{O}_3} \int_0^t C_{\text{O}_3} dt \quad (4.7)$$

where  $\int C_{\text{OH}} dt$  and  $\int C_{\text{O}_3} dt$  are the corresponding hydroxyl radicals and ozone exposures.

Hydroxyl radical exposure is thought to have a high impact on the mineralization of organic compounds in the secondary effluent (both added ECs and naturally occurring compounds) through the AOPs studied because direct photolysis and single ozonation at pH 3, where low concentration of  $\cdot\text{OH}$  is expected, did not lead to significant TOC removals (< 2%).

The hydroxyl radical exposure can be calculated using pCBA as a probe compound [20] because of its high reactivity with  $\cdot\text{OH}$  ( $k_{\text{OH}} = 5 \times 10^9 \text{ L mol}^{-1} \text{ s}^{-1}$  [21]) and negligible reactivity with ozone ( $k_{\text{O}_3} < 0.15 \text{ L mol}^{-1} \text{ s}^{-1}$  [22]). In addition, aqueous pCBA does not absorb radiation beyond 290 nm wavelength and, therefore, pCBA does not undergo direct photolysis under solar irradiation (i.e.,  $k_{\text{phot}} \sim 0$ ). Accordingly, the  $\cdot\text{OH}$  exposure can be calculated by equation (4.8):

$$\int_0^t C_{\text{OH}} dt = \frac{\ln\left(\frac{C_{\text{pCBA},0}}{C_{\text{pCBA}}}\right)}{k_{\text{OH}}} \quad (4.8)$$

Figure 4.6. shows the  $\cdot\text{OH}$  exposure during the first minutes of experiments of degradation of ECs in the secondary effluent in the presence of pCBA.

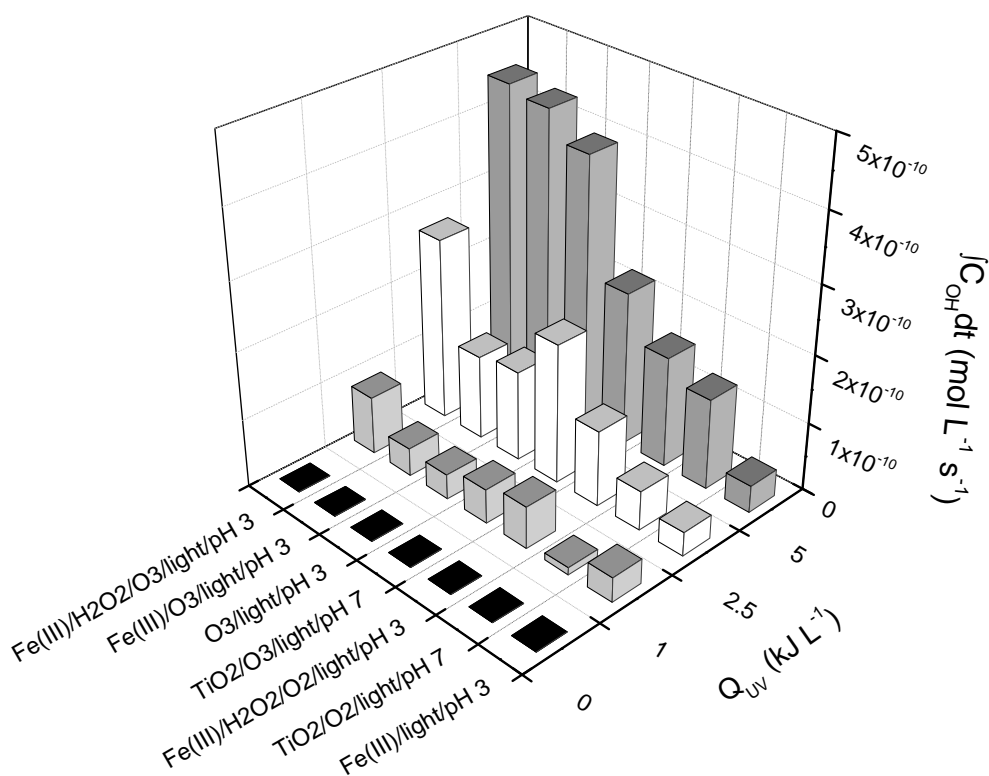


**Figure 4.6.** Hydroxyl radical exposure during the first irradiation minutes for the some experiments. Experimental conditions: EC concentration=  $200 \mu\text{g L}^{-1}$ , each; applied ozone =  $520 \text{ mg h}^{-1}$ ;  $C_{\text{Fe(III),0}} = 2.8 \text{ mg L}^{-1}$ ; Initial  $\text{H}_2\text{O}_2/\text{Fe(III)}$  mass ratio = 6.1;  $C_{\text{TiO}_2,0} = 200 \text{ mg L}^{-1}$ .

It can be seen that the  $\cdot\text{OH}$  exposure increased with the UV radiation dose for any of the system tested. For a given radiation dose, the ozone/light systems (pH 3) led to higher  $\cdot\text{OH}$  production than those systems carried out in the absence of ozone. The Fe(III)/H<sub>2</sub>O<sub>2</sub>/O<sub>3</sub>/light (pH 3) system can be highlighted as that leading to the highest  $\cdot\text{OH}$  exposure and, as a result, the highest TOC removal after 5-h treatment (35%).

#### 4.4.3. Phenolic intermediates

Given the molecular structures of the selected ECs (see Figure 4.1.) as well as those of other organic compounds typically present in MWWTP secondary effluents, some of the primary intermediates expected to be formed during their oxidation are phenolic compounds. Figure 4.7. shows the concentration of phenolic compounds during the course of selected experiments.

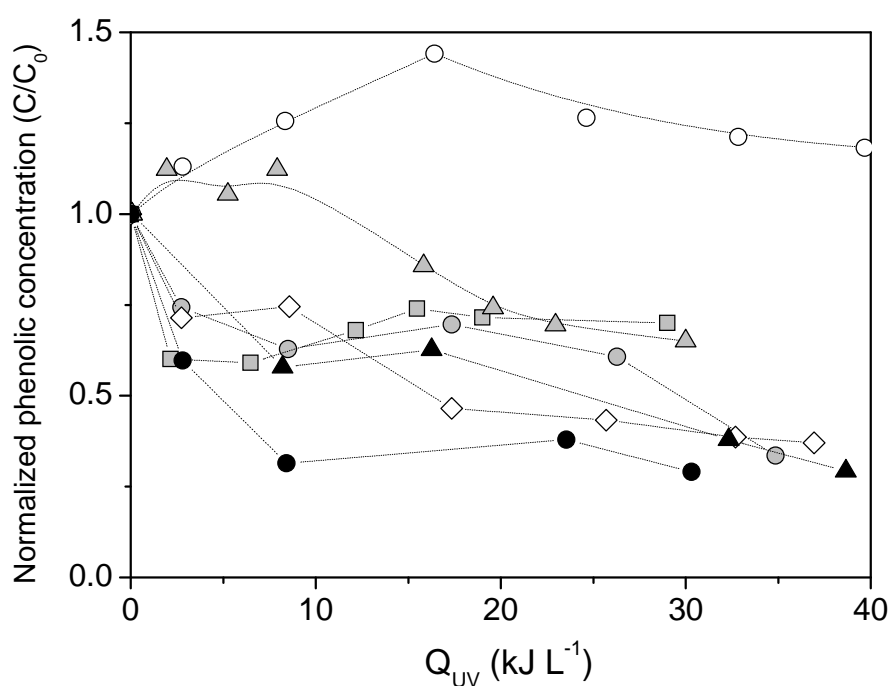


**Figure 4.7.** Evolution of the phenolic concentration with the dose of UV radiation during the course of some photocatalytic experiments. Experimental conditions: EC concentration = 200  $\mu\text{g L}^{-1}$ , each; applied ozone = 520  $\text{mg h}^{-1}$ ;  $C_{\text{Fe(III),0}} = 2.8 \text{ mg L}^{-1}$ ; Initial H<sub>2</sub>O<sub>2</sub>/Fe(III) mass ratio = 6.1;  $C_{\text{TiO}_2,0} = 200 \text{ mg L}^{-1}$ . Symbols: (○) O<sub>3</sub>/light/pH 3, (◊) Fe(III)/O<sub>3</sub>/light/pH 3, (◻) Fe(III)/H<sub>2</sub>O<sub>2</sub>/O<sub>2</sub>/light/pH 3, (▲) Fe(III)/H<sub>2</sub>O<sub>2</sub>/O<sub>3</sub>/light/pH 3, (△) TiO<sub>2</sub>/O<sub>2</sub>/light/pH 7, (●) TiO<sub>2</sub>/O<sub>3</sub>/light/pH 7.

As can be seen, during the first minutes of reaction, an increase in the phenolic compounds concentration was observed in Fe(III)/O<sub>2</sub>/light (pH 3) and TiO<sub>2</sub>/O<sub>2</sub>/light (pH 7) experiments, which clearly indicates that rates of formation of these species are higher than rates of consumption. As shown in Figure 4.6., these systems are, among the studied, those that led to the lowest hydroxyl radical exposures and, as a consequence, showed the lowest organic matter degradation rates. Thus, accumulation of phenolic intermediates was more pronounced during the course of these experiments. On the other hand, photolytic ozonation and photocatalytic ozonation systems, which led to the formation of hydroxyl radicals to a significant extent (see Figure 4.6.), were more effective in removing the phenolic content of samples. Thus, no accumulation of phenolic substances was observed throughout the course of these experiments and percentages of removal after the 5-h experiments were around 60-75% as it is apparent from Figure 4.7. The Fe(III)/H<sub>2</sub>O<sub>2</sub>/O<sub>2</sub>/light (pH 3) system was also able to remove phenolic compounds to some extent, though no more than 30% removal was achieved after 5 hours of experiment. Finally, single ozonation systems (pH 3 and 7, not shown in Figure 4.7) led to 45-50% removal of the initial phenolic content after 5 h of treatment.

#### 4.4.4. Biodegradability measurements

The ratio BOD<sub>5</sub>/COD in samples before and after the experiments was measured to assess changes in biodegradability. It was found that samples taken after the 5-h treatments had BOD<sub>5</sub>/COD ratios ranged from 0.15 to 0.47. Since the initial BOD<sub>5</sub>/COD value was 0.17 (see Table 4.1.), it can be concluded that, in general, the AOPs tested enhanced the biodegradability of samples. Particularly, the Fe(III)/H<sub>2</sub>O<sub>2</sub>/O<sub>3</sub>/light (pH 3) system led to a 2.5-fold increase of the BOD<sub>5</sub>/COD ratio.

#### 4.4.5. Toxicity tests

One important aspect about the application of AOPs is the possible formation of toxic intermediates or by-products, which could be even more toxic than the compounds initially present in the samples. Toxicity bioassays of some selected reaction samples were assessed using acute *D. Magna*. For this purpose, samples were taken from the reactor at a time when complete ECs removal was almost achieved (i.e, t<sub>99</sub> as defined in equations (4.3) or (4.5)) and after the 5-h experiments. Figure 4.8. shows the results of immobilization of *D. Magna* after 48 hours exposure. It should be mentioned here that no data for t<sub>99</sub> are reported for the Fe(III)/O<sub>2</sub>/light (pH 3) system since no complete removal of ECs could be achieved after 5 hours of application of this treatment (see Table 4.2.).

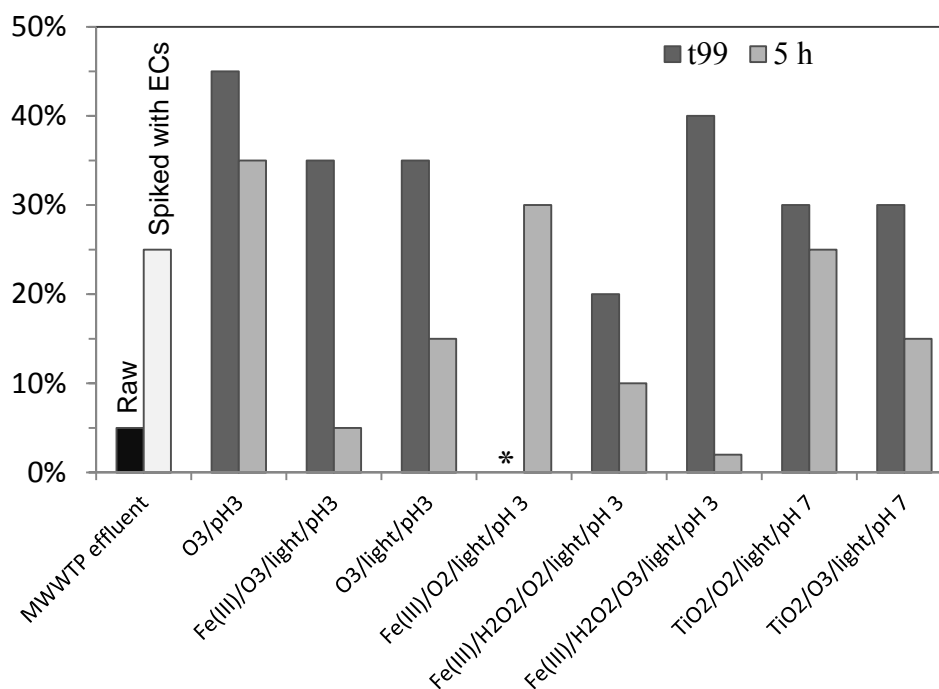


**Figure 4.8.** Toxicity towards *D. magna* of samples at different reaction times during the course of some experiments. Experimental conditions: EC concentration =  $200 \mu\text{g L}^{-1}$ , each; Applied ozone =  $520 \text{ mg h}^{-1}$ ;  $C_{\text{Fe(III),0}} = 2.8 \text{ mg L}^{-1}$ ; Initial  $\text{H}_2\text{O}_2/\text{Fe(III)}$  mass ratio = 6.1;  $C_{\text{TiO}_2,0} = 200 \text{ mg L}^{-1}$ . (\*) Not measured, as  $t_{99}$  was greater than 5 hours

The results of toxicity bioassays show an increase of toxicity after the addition of ECs to the secondary effluent. Also, changes in sample toxicity were observed during the course of the photocatalytic experiments. As a rule, toxicity of samples increased at the beginning of the photocatalytic treatment, likely as a result of the accumulation of phenolic and other toxic intermediates and then decreased. This result is in agreement with that reported for the removal of other ECs by ozonation and solar photocatalytic ozonation with  $\text{TiO}_2$  [23,24]. Toxicity removal below the baseline level (i.e., 25% inhibition) was only observed when a large degree of TOC removal (i.e., mineralization) was achieved. This applies especially for the  $\text{Fe(III)/O}_3/\text{light/pH } 3$  and  $\text{Fe(III)/H}_2\text{O}_2/\text{O}_3/\text{light/pH } 3$  photocatalytic ozonation systems.

#### 4.4.6. Influence of the H<sub>2</sub>O<sub>2</sub>/Fe(III) ratio

The Fe(III)/H<sub>2</sub>O<sub>2</sub>/O<sub>3</sub>/light treatment at pH 3 has been proved so far as a good choice for the treatment of the secondary effluent contaminated with the ECs, as complete removal of ECs, high mineralization of organic matter (i.e., 35 % TOC removal) and great removal of phenolic compounds (i.e., 71 % removal) was achieved after 5 h of treatment (i.e., 38.7 kJ L<sup>-1</sup> radiation dose). In addition, the effluent from the treatment did not show toxicity towards *D. Magna* (i.e., < 5% inhibition) and presented a favourable BDO<sub>5</sub>/COD ratio. A key parameter of the process performance and the process efficiency for this AOP is the H<sub>2</sub>O<sub>2</sub>/Fe(III) ratio. To study the effect of this variable a series of experiments were carried out at varying mass ratios in the range 6.1–18.3. Following results of Table 4.3., where some process performance parameters are presented, the best H<sub>2</sub>O<sub>2</sub>/Fe(III) mass ratio, in the range considered here, was 12.2. Although, the greater H<sub>2</sub>O<sub>2</sub>/Fe(III) ratio the faster EC removal observed (i.e., lower t<sub>99</sub>) the TOC removal rate was the highest when applying 12.2 H<sub>2</sub>O<sub>2</sub>/Fe(III) mass ratio. The lower TOC removal rate obtained at the highest H<sub>2</sub>O<sub>2</sub>/Fe(III) mass ratio compared to the optimum is likely to be a consequence of the hydroxyl radical scavenger character of hydrogen peroxide.

**Table 4.3.** Evaluation of the effect of the H<sub>2</sub>O<sub>2</sub>/Fe(III) ratio on the performance of the Fe(III)/H<sub>2</sub>O<sub>2</sub>/O<sub>3</sub>/light treatment at pH 3

H <sub>2</sub> O <sub>2</sub> /Fe(III) mass ratio	6.1	12.2	18.3
k <sub>TOC</sub> × 10 <sup>3</sup> (min <sup>-1</sup> )	3.01	3.32	2.58
% TOC removal	35	42.6	39.6
% Phenolic compounds removal	70.8	75.4	73.1
radiation dose (kJ·L <sup>-1</sup> )	38.7	24.3	28.6
t <sub>99</sub> (min)	34	22	18

Experimental conditions: EC concentration= 200 µg L<sup>-1</sup>, each; applied ozone = 520 mg h<sup>-1</sup>; C<sub>Fe(III),0</sub> = 2.8 mg L<sup>-1</sup>; overall radiation dose ~30 kJ L<sup>-1</sup>; treatment time = 5 h.

#### 4.4.7. Simplified comparison of operating costs

Operating an efficient and cost-effective treatment process is the goal of every successful MWWTP. Therefore, before process development and scale-up economic analysis must be considered. In this work a simplified economic comparison of operating costs associated with the investigated treatment process is

presented. The economic analysis accounts for the cost of the main reagents and/or catalysts used (i.e., iron(III), hydrogen peroxide and titanium dioxide) according to vendors (Proquiman and Quimidroga, Spain) as well as that of the electricity (Red Eléctrica de España, Spain) to power the air compressor, the ozone generator and the CPC reactor of the pilot-plant used in this work. Pre-treatment costs (e.g., pH adjustment) have not been accounted for. As basis for the evaluation, experimental conditions used throughout this investigation have been considered. Also, two criteria have been used: (1) operating costs to reach complete removal of ECs; (2) operating costs to remove 20% of the TOC of the secondary effluent. Results are shown, as relative cost, in Table 4.4. Relative cost of the solar photo-Fenton process has been set as 1 as this is, so far, the best known solar photo-catalytic treatment process. Recently, Durán et al. [25] estimated an operating cost of 1.56 € m<sup>-3</sup> for the treatment of a secondary effluent from a MWWTP contaminated with antipyrine by a solar photo-Fenton method at semi-industrial scale.

**Table 4.4.** Estimated relative operating costs of the AOPs studied at pilot-plant scale

Treatment system	Relative cost	
	Objective: Complete EC removal	Objective: 20% TOC removal
O <sub>3</sub> /light/pH 3	0.32	0.62
Fe(III)/O <sub>3</sub> /light/pH 3	0.32	0.46
Fe(III)/H <sub>2</sub> O <sub>2</sub> /light/pH 3	1.00	1.00
Fe(III)/O <sub>2</sub> /light/pH 3	14.28	*
O <sub>3</sub> /pH 3	0.38	*
Fe(III)/H <sub>2</sub> O <sub>2</sub> /O <sub>3</sub> /light/pH 3	0.35	0.44
TiO <sub>2</sub> /light/pH 7	2.57	1.92
TiO <sub>2</sub> /O <sub>3</sub> /light/pH 7	1.88	1.25

Notes: Fe(III)/H<sub>2</sub>O<sub>2</sub>/O<sub>2</sub>/light has been chosen as reference system (relative cost = 1); Experimental conditions as indicated in Figure 4.3.

(\*) Not calculated, as very low mineralization (<2.5%) was achieved in 5 hours by the treatment method at the conditions applied.

From the results of Table 4.4. it is apparent that the systems which involve the use of ozone, except the TiO<sub>2</sub>/O<sub>3</sub>/light (pH 7) system, are the most economic choices

when the goal is just the 99% removal of the ECs with relative costs ranging from 0.32 to 0.38. On the other hand, the operating cost of the Fe(III)/O<sub>2</sub>/light/pH 3 system is the highest due to the long treatment time needed to remove the ECs (see Table 4.2.). If the treatment goal is also to remove TOC to some extent (i.e., 20% TOC removal) the solar photocatalytic ozonation systems using iron or iron and H<sub>2</sub>O<sub>2</sub> have the lowest operating costs while the use of TiO<sub>2</sub> as catalyst increases significantly the cost due to the expensiveness of this material.

## 4.5. Conclusions

---

From the results of this study, it can be concluded that iron-mediated solar photocatalytic ozonation can be a suitable method to degrade ECs in secondary effluents from MWWTPs. The ECs used in this investigation (acetaminophen, antipyrine, bisphenol A, caffeine, metoprolol and testosterone) were easily removed by ozone but the organic matter in the effluent was difficult to mineralize (TOC removal < 35%) at the experimental conditions applied. In any case, solar photocatalytic ozonation processes were shown to be more efficient than single ozonation and single photocatalytic oxidation systems in terms of TOC removal due to an enhanced generation of hydroxyl radicals. Treated effluents after the application of solar photocatalytic ozonation showed low toxicity towards *D. Magna* and higher biodegradability than the non-treated secondary effluent. Finally, a simplified estimation of operating costs reveals that some solar photocatalytic ozonation processes (e.g., Fe(III)/O<sub>3</sub>/light/pH 3 and Fe(III)/H<sub>2</sub>O<sub>2</sub>/O<sub>3</sub>/light/pH 3) can be cheaper than the solar photo-Fenton system.

## 4.6. Acknowledgements

---

This study was supported by Spanish Ministerio de Economía y Competitividad (MINECO) and European Regional Development Funds through the projects CTQ2009/13459-C05-05 and CTQ2012-35789-C02-01. D. H. Quiñones is grateful to MINECO for the concession of a predoctoral FPI grant.

## 4.7. References

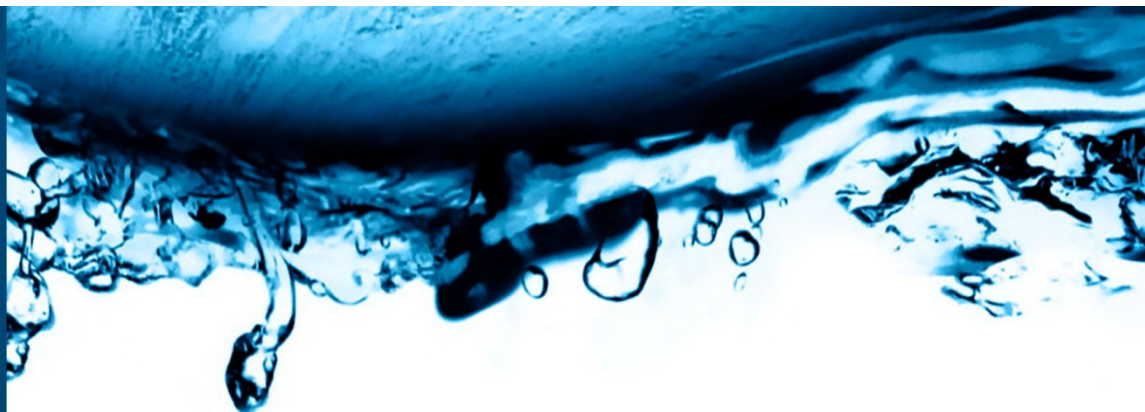
---

- [1] M. Stuart, D. Lapworth, E. Crane, A. Hart, *Review of risk from potential emerging contaminants in UK groundwaters*, *Sci. Total Environ.* 446 (2012) 1–21.



- [2] C. Mukhopadhyay, A. Mason, *Smart sensors for real-time water quality monitoring*, Springer, New York USA, 2013.
- [3] T. Deblonde, C. Cossu-Leguille, P. Hartemann, *Emerging pollutants in wastewater: A review of the literature*, *Int. J. Hyg. Environ. Health* 214 (2011) 442–448.
- [4] N. Bolong, A.F. Ismail, M.R. Salim, T. Matsuura, *A review of the effects of emerging contaminants in wastewater and options for their removal*, *Desalination* 239 (2009) 229–246.
- [5] M.H.Y. Lau, K.M.Y. Leung, S.W.Y. Wong, H. Wang, Z.G. Yan, *Environmental policy, legislation and management of persistent organic pollutants (POPs) in China*, *Environ. Pollut.* 165 (2012) 182–192.
- [6] P. Verlicchi, A. Galletti, M. Petrovic, D. Barceló, *Hospital effluents as a source of emerging pollutants: An overview of micropollutants and sustainable treatment options*, *J. Hydrol.* 389 (2010) 416–428.
- [7] Z. Liu, Y. Kanjo, S. Mizutani, *Removal mechanisms for endocrine disrupting compounds (EDCs) in wastewater treatment — physical means, biodegradation, and chemical advanced oxidation: A review*, *Sci. Total Environ.* 407 (2009) 731–748.
- [8] F.J. Beltrán, *Ozone reaction kinetics for water and wastewater systems*, Lewis Publishers, CRC Press, Boca Raton, Florida USA, 2003.
- [9] D.H. Quiñones, P.M. Álvarez, A. Rey, S. Contreras, F. J. Beltrán, *Application of solar photocatalytic ozonation for the degradation of emerging contaminants in water in a pilot plant*, *Chem. Eng. J.* 260 (2015) 399–410.
- [10] L. Prieto-Rodríguez, I. Oller, N. Klamerth, A. Agüera, E.M. Rodríguez, S. Malato, *Application of solar AOPs and ozonation for elimination of micropollutants in municipal wastewater treatment plant effluents*, *Water Res.* 15 (2013) 1521–1528.
- [11] I. Gultekin, N.H. Ince, *Degradation of reactive azo dyes by UV/H<sub>2</sub>O<sub>2</sub>: Impact of radical scavengers*, *J. Environ. Sci. Health A Tox. Hazard. Subst. Environ. Eng.* 39 (2004) 1069–1081.
- [12] H. Bader, J. Hoigné, *Determination of ozone in water by the indigo method*, *Water Res.* 15 (1981) 449–456.
- [13] G. Eisenberg, *Colorimetric determination of hydrogen peroxide*, *Ind. Eng. Chem. Anal. Ed.* 15 (1943) 327–328.
- [14] V. Singleton, J. Rossi, *Colorimetry of total phenolic with phosphomolybdic-phosphotungstic acid reagents*, *Am. J. Enol. Viticult.* 16 (1965) 144–158.
- [15] Y. Zuo, *Kinetics of photochemical/chemical cycling of iron coupled with organic substances in cloud and fog droplets*, *Geochim. Cosmochim. Ac.* 59 (1995) 3123–3130.

- [16] APHA-AWWA-WEF. *5210B: Biochemical Oxygen Demand (BOD)*, in: *Standard methods for the examination of water and wastewater*, 21th Edition, Washington DC, 2005.
- [17] OECD. *Test No. 202: Daphnia sp. Acute immobilisation test*, OECD Guidelines for the testing of chemicals, Section 2, OECD Publishing, 2004.
- [18] S. Malato, J. Blanco, A. Vidal, D. Alarcón, M.I. Maldonado, J. Cáceres, W. Gernjak, *Applied studies in solar photocatalytic detoxification: An overview*, Sol. Energy 75 (2003) 329–336.
- [19] E. V. Savinkina, L. N. Obolenskaya, G. M. Kuz'micheva, A. V. Dorokhov, A. Yu. Tsivadze, *A new  $\eta$ -titania-based photocatalyst*, Dokl. Phys. Chem. 441 (2011) 224-226.
- [20] M.S. Elovitz, U. von Gunten, *Hydroxyl radical/ozone ratios during ozonation processes. I. The Rct concept*, Ozone-Sci. Eng. 21 (1999) 239–260.
- [21] G.V. Buxton, C.L. Greenstock, W.P. Helman, A.B. Ross, *Critical review of rate constants for reactions of hydrated electrons, hydrogenatoms and hydroxyl radicals in aqueous solution.*, J. Phys. Chem. Ref. Data 17 (1988) 513-886.
- [22] D.C.C. Yao, W.R. Haag, *Rate constants for direct reactions of ozone with several drinking water contaminants*, Water Res. 25 (1991) 761–773.
- [23] G. Márquez, E.M. Rodríguez, F.J. Beltrán, P.M. Álvarez, *Solar photocatalytic ozonation of a mixture of pharmaceutical compounds in water*, Chemosphere 113 (2014) 71-78.
- [24] G. Márquez, E.M. Rodríguez, M. I. Maldonado, P.M. Álvarez, *Integration of ozone and solar  $TiO_2$ -photocatalytic oxidation for the degradation of selected pharmaceutical compounds in water and wastewater*, Sep. Purif. Technol. 136 (2014) 18-26.
- [25] A. Durán, J.M. Monteagudo, I. Sanmartín, A. Valverde, *Solar photodegradation of antipyrine in a synthetic WWTP effluent in a semi-industrial installation*, Sol. Energ. Mat. Sol. C. 125 (2014) 215–222.



## Chapter V

### Paper 3:

#### Simulated solar-light assisted photocatalytic ozonation of metoprolol over titania-coated magnetic activated carbon

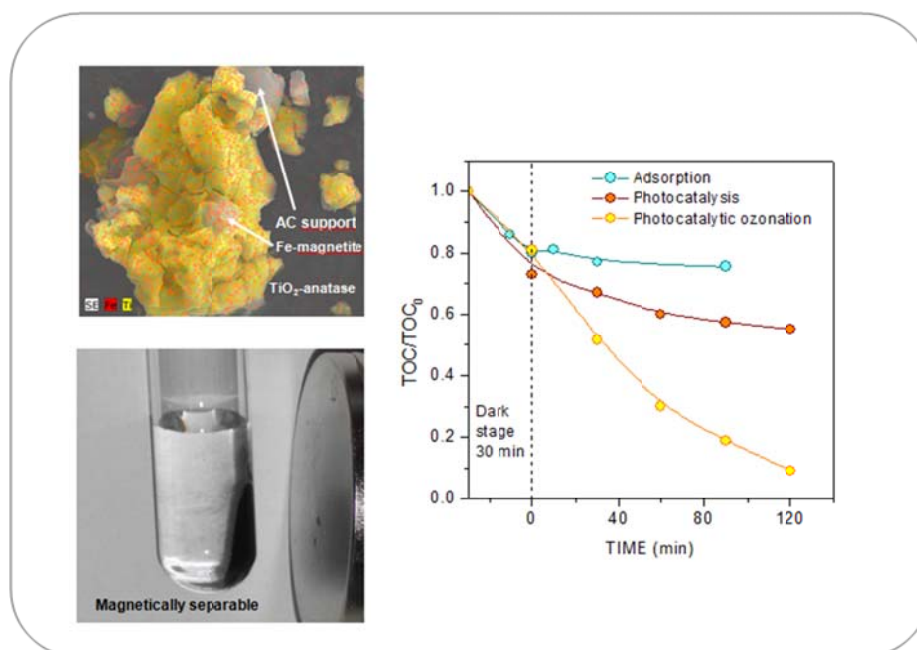
Ana Rey<sup>1</sup>, Diego H. Quiñones<sup>1</sup>, Pedro M. Álvarez<sup>1</sup>, Fernando J. Beltrán<sup>1</sup>, Pawel K. Plucinski<sup>2</sup>

<sup>1</sup> Departamento de Ingeniería Química y Química Física, Facultad de Ciencias, Universidad de Extremadura, Av. de Elvas s/n, 06071 Badajoz (Spain)

<sup>2</sup> Department of Chemical Engineering, University of Bath, BA2 7AY Bath (United Kingdom)

Applied Catalysis B: Environmental, 111-112 (2012) 246-253





## 5.1. Abstract

A magnetically separable photocatalyst consisting of magnetic porous activated carbon with attached anatase TiO<sub>2</sub> particles has been prepared and tested for the degradation of metoprolol (MTP) in aqueous solution. The synthesized photocatalyst (TiFeC) was characterized by nitrogen adsorption, XRD, FTIR, SEM, EDX and SQUID magnetometer. The obtained catalyst with a TiO<sub>2</sub> composition of 61 wt% (mostly anatase) had moderate surface area (BET surface of 331 m<sup>2</sup> g<sup>-1</sup>) and volume of micropores and exhibited magnetic properties with saturation magnetization of 1.6 emu g<sup>-1</sup> and neither remanent magnetization nor coercivity. The photocatalytic activity of TiFeC samples was tested by degrading MTP by simulated solar photocatalytic ozonation. The results were compared to those obtained with a commercial titania (Degussa P25) and by photolytic ozonation (i.e., absence of catalyst). Complete MTP removal and more than 60% TOC conversion were achieved after 3h of photocatalytic ozonation of an aqueous solution containing as much as 50 mg L<sup>-1</sup> MTP initial concentration. The reusability and stability of the catalyst were tested through a series of five photocatalytic ozonation experiments. Minor amounts of iron and titanium were leached out from the catalyst and the catalytic activity decreased to a very low extent with the reuse of the catalyst.

**Keywords:** Magnetic catalyst, ozone, pharmaceuticals, solar photocatalysis, water treatment.

## 5.2. Introduction

---

Solar photocatalytic detoxification of water and wastewater is an emerging area of research and commercial development as it may be considered as one of the most cost effective treatment technologies in regions of high incoming solar radiation [1,2]. Solar photocatalytic detoxification is a relatively new clean technology to remove toxic and persistent pollutants in water and wastewater by focusing sunlight onto a reactor through which the contaminated water is flowing in the presence of a catalyst. Among candidates for solar photocatalysis, TiO<sub>2</sub> in the form of anatase is the most suitable material for industrial use at present because it is a non-toxic material with high chemical stability, low cost and high oxidation power. It is a semiconductor with a band gap of about 3.2 eV allowing absorption of UV light with wavelengths below 387.5 nm (about 5% of solar spectrum) to generate electron-hole pairs ( $e^-_{CB}/h^+_{VB}$ ) on the catalyst surface. Electron-hole pairs, in turn, trigger a series of reactions generating free-radicals (mainly hydroxyl radicals,  $\cdot\text{OH}$ ), which are very efficient non-selective oxidizers of water pollutants, both chemical compounds and microorganisms (disinfection). Solar TiO<sub>2</sub> photocatalysis is receiving great attention for water and wastewater remediation and it has been extensively investigated for the removal of organic recalcitrant pollutants as for example, pharmaceuticals [3-6], dyes [7] or pesticides [8] as well as to inactivate pathogenic microorganisms such as *Escherichia coli* [9].

Given the concern over the risk posed by the presence of pharmaceutical compounds in water bodies, and hence the possible impacts on public health and aquatic ecosystems a great deal of research is being carried out on technologies for the removal of these compounds [10-12]. In general, pharmaceutical compounds are hardly biodegradable so they are not eliminated by conventional treatment at wastewater treatment plants (WWTPs) and, as a consequence, they are frequently reported to be present in WWTP effluents at ng L<sup>-1</sup> and even µg L<sup>-1</sup> concentration levels [13]. Although solar TiO<sub>2</sub> photocatalysis has been found effective for the removal of different pharmaceutical compounds from aqueous solution, to achieve complete mineralization long reaction times are needed because of the formation of a number of intermediates which, frequently, are hard to degrade [2].

In this work, with the aim of enhancing process performance regarding mineralization rate of complex organic molecules such those of pharmaceutical compounds, solar photocatalytic ozonation has been applied. Photocatalytic ozonation, which is the combination of TiO<sub>2</sub> photocatalysis and ozonation, is a promising advanced oxidation technology capable of producing much larger number of hydroxyl radicals than single ozonation or TiO<sub>2</sub> photocatalysis. In the combined process, the recombination of electron-hole pairs on the TiO<sub>2</sub> surface is

reduced with respect to single  $\text{TiO}_2$  photocatalysis as electrons are captured by ozone generating a new via of hydroxyl radicals formation and, therefore, increasing the oxidation rate [14, 15]. Most of the photocatalytic ozonation studies conducted to date make use of  $\text{TiO}_2$  suspensions and UV lamps from low to high pressure [16-18]. In spite of the great degradation rates found for the studied pollutants, two drawbacks of the process can be considered: (1) the use of UV lamps as a source of radiation can make the process expensive for commercial applications; (2) the separation of  $\text{TiO}_2$  catalyst in suspension after the reaction is a major obstacle. To overcome these problems, in this work simulated solar radiation has been used as UV light source and a  $\text{TiO}_2$  magnetic activated carbon photocatalyst has been synthesized and applied. Literature reports on the preparation of various types of magnetic  $\text{TiO}_2$  photocatalysts, which can be easily recovered by the application of an external magnetic field [19-23]. Among them,  $\text{TiO}_2$  magnetic activated carbon catalysts have shown a high activity in the photo-degradation of phenol and dyes [24, 25], but no study has been found on their use in photocatalytic ozonation process.

In this work, we have prepared and characterized a  $\text{TiO}_2$  magnetic activated carbon catalyst with enhanced photocatalytic activity to mineralize complex organic pollutants in water such as the pharmaceutical compound metoprolol tartrate (MTP). MTP (see Figure 5.1. for structure) is a  $\beta$ -blocker used for several cardiovascular diseases which has been frequently detected in surface waters and effluents from sewage treatment plants [26-27]. The  $\text{TiO}_2$  magnetic activated carbon catalyst has been tested in both solar photocatalysis and solar photocatalytic ozonation and compared with the efficiency of commercial  $\text{TiO}_2$  powder (Degussa P25), which is a standard material in the field of photocatalytic reactions.

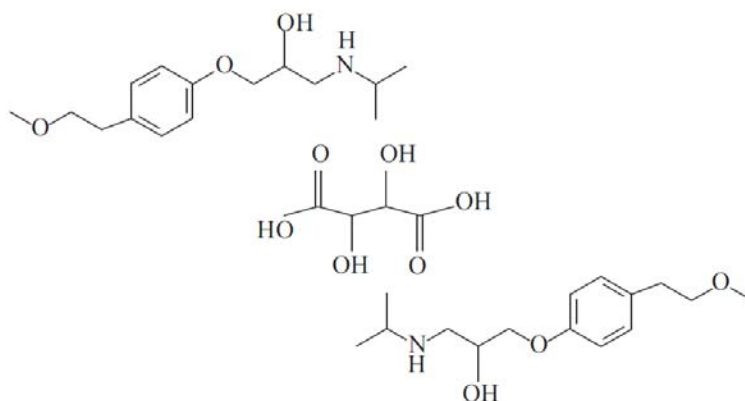


**Figure 5.1.** Molecular structure of metoprolol tartrate

## 5.3. Experimental section

---

### 5.3.1. Preparation of catalyst

First, a magnetically separable activated carbon (FeC) was prepared following the method reported by Fuertes and Tartaj [28]. In a typical preparation, 10 g of a meso-microporous activated carbon (Darco 12-20, Sigma Aldrich) were impregnated with 8.7 mL of ferric nitrate ( $923 \text{ g L}^{-1}$ ) in ethanol solution to obtain about 12 wt% Fe in the final product. Once the solution was adsorbed onto the activated carbon, the sample was dried at  $90^\circ\text{C}$  for 2 h. After that, it was impregnated with 150 mmol of ethylene glycol. The impregnated activated carbon was then transferred into an oven where it was heated in nitrogen at  $350^\circ\text{C}$  for 2 h. After cooling to room temperature in nitrogen, the magnetic activated carbon sample was milled into powder ( $d_p < 125 \mu\text{m}$ ).

Titania coated magnetic activated carbon (TiFeC) was prepared by the sol-gel method reported by Ao et. al. [24]. First, 25.5 mL of titanium (IV) butoxide (97%, Aldrich) were diluted with 8.2 mL of isopropanol (>99%, Aldrich), and the mixture was added dropwise to 205 mL of distilled water at pH 2 (adjusted with  $\text{HNO}_3$  65%, Panreac) under vigorous stirring. The solution was kept under stirring and refluxed at  $75^\circ\text{C}$  for 24 h and, thereafter, transferred to a rotary evaporator where excess alcohol was removed by heating at  $80^\circ\text{C}$  under vacuum, thus obtaining a titania sol. Finally, 3 g of the prepared magnetic activated carbon (FeC) were dispersed in the titania sol and subjected to ultrasonic treatment for 1 h. After evaporation to dryness under vacuum at  $80^\circ\text{C}$  on a rotary evaporator, the residue sample was repeatedly washed with distilled water until no total organic carbon (TOC) was detected in the supernatant and then separated from the liquid fraction by an external magnet to select only the magnetic particles. The TiFeC catalyst thus prepared was dried at  $100^\circ\text{C}$  overnight.

### 5.3.2. Catalyst characterization

Surface areas and pore structure of the activated carbon used as support (AC), the magnetic activated carbon (FeC) and the TiFeC catalyst were obtained from nitrogen adsorption-desorption isotherms at  $-196^\circ\text{C}$  acquired with a Autosorb 1 apparatus (Quantachrome). Before measurements, the samples were outgassed at  $250^\circ\text{C}$  for 12 h under high vacuum ( $< 10^{-4} \text{ Pa}$ ). The isotherms were analyzed by BET equation and t-plot to obtain BET and external surface areas, respectively. X-Ray diffraction (XRD) patterns were collected with a Bruker D8 Advance XRD diffractometer with a  $\text{CuK}_\alpha$  radiation ( $\lambda = 0.1541 \text{ nm}$ ). The data were collected



from  $2\theta = 20^\circ$  to  $70^\circ$  at a scan rate of  $0.02^\circ \cdot \text{s}^{-1}$  and 1 s per point. FTIR spectra were obtained on a Nicolet iS10 spectrometer using KBr wafers containing about 0.01 g sample. Data were acquired in the wavelength range  $400\text{--}4000 \text{ cm}^{-1}$  using 32 scans with a resolution of  $4 \text{ cm}^{-1}$ . The morphology of catalyst particles was characterized by scanning electron microscopy (SEM) using a Hitachi S-4800 apparatus working at 20–30 kV accelerating voltage and 500–2000 magnification. In addition, the catalyst was examined by means of energy dispersive X-ray analysis (EDX) to determine the distribution of Ti and Fe in the particles. For that purpose, a SSD detector XFlash 5010 (Bruker), working at 5 kV accelerating voltage and 500–2000 magnification was used. The iron content of the TiFeC catalyst was analyzed by inductively coupled plasma with an ICP-MS NexION 300D (Perkin-Elmer) after acidic microwave digestion of the sample. The amount of  $\text{TiO}_2$  on the catalyst was estimated from the mass residue after combustion of the sample in air at  $900^\circ\text{C}$ , taking into account the amount of iron on the sample. Magnetic measurements were performed using a Quantum Design MPMS XL-7 Superconducting Quantum Interference Device (SQUID). The magnetic moment  $M$  was measured as function of applied magnetic field  $H$  at room temperature.

### 5.3.3. Photocatalytic experiments

Photocatalytic experiments were carried out using a commercial solar simulator (Suntest CPS, Atlas) provided with a 1500 W air cooled xenon arc lamp whose emission was restricted to  $\lambda > 300 \text{ nm}$  by means of quartz and glass cut-off filters. The irradiation intensity was  $550 \text{ W} \cdot \text{m}^{-2}$ . The chamber of the solar simulator was maintained at about  $30^\circ\text{C}$  throughout the experiments. The experiments were carried out in semi-batch mode using a glass-made agitated tank as reactor provided with gas inlet, gas outlet and liquid sampling ports. Ozone was produced in a laboratory ozone generator (Anseros Ozomat Com AD-02) from pure oxygen and continuously fed to the reactor. In a typical photocatalytic ozonation experiment, the reactor was loaded with 250 mL of an aqueous solution of metoprolol tartrate (>99% Sigma) (MTP) and a given mass of catalyst. The suspension was stirred in the dark for 30 min before switching on the lamp and feeding ozone to the reactor. Ozone ( $20 \text{ L h}^{-1}$  gas flow rate and  $6 \text{ mg L}^{-1}$  concentration) was bubbled into the solution through a diffuser placed at the bottom of the reactor. Liquid samples were periodically withdrawn from the reactor and filtered through a  $0.2 \mu\text{m}$  PTFE filter to remove photocatalyst particles prior to analysis. In addition to photocatalytic ozonation experiments using TiFeC, experiments of single adsorption (i.e., absence of radiation and ozone), single ozonation (i.e., absence of radiation and catalyst), catalytic ozonation (i.e., absence of radiation), photolytic ozonation (i.e., absence of catalyst),  $\text{TiO}_2$  photocatalysis

(i.e., absence of ozone) and photocatalytic ozonation with Degussa P25 (comparative purpose) were carried out. Also photocatalytic experiments varying initial concentration of MTP (10-50 mg L<sup>-1</sup>) were completed to examine the effect of contaminant concentration. To test the stability of the TiFeC catalyst, several consecutive experiments were carried out recovering the catalyst particles by using a magnet.

The concentration of MTP was analysed by high-performance liquid chromatography (HP 1100 Series chromatograph) using a Kromasil C-18 column (5  $\mu$ m, 150 mm long., 4 mm diameter) as stationary phase and 0.65 mL min<sup>-1</sup> of 15:85 acetonitrile:acidic water (0.1% phosphoric acid) as mobile phase. An UV detector set at 225 nm was used for detection. TOC was measured using a Shimadzu TOC-V<sub>SCH</sub> analyzer. Aqueous ozone was measured by following the indigo method [29] using a Helios- $\alpha$  UV/Vis spectrophotometer set at 600 nm. Ozone in the gas phase was continuously monitored by means of an Anseros Ozomat GM-6000Pro analyzer. Iron and titanium in solution were analyzed by means of inductively coupled plasma using a Perkin Elmer NexION 300D ICP-MS apparatus.

## 5.4. Results and discussion

### 5.4.1. Characterization of TiO<sub>2</sub> magnetic activated carbon

Table 5.1. summarizes composition, some textural parameters (BET and external surface areas) and saturation magnetization of the prepared TiFeC catalyst, the impregnated activated carbon (FeC) and the activated carbon used as support itself.

**Table 5.1.** Properties of the TiFeC catalyst and precursors

	Fe (wt%)	TiO <sub>2</sub> (wt%)	S <sub>BET</sub> (m <sup>2</sup> g <sup>-1</sup> )	S <sub>EXT</sub> (m <sup>2</sup> g <sup>-1</sup> )	V <sub>MICRO</sub> (cm <sup>3</sup> g <sup>-1</sup> )	M <sub>S</sub> (emu g <sup>-1</sup> )
TiFeC	4.7	61	331	65	0.163	1.56
FeC	12.0	---	552	61	0.253	---
AC	3.7	---	640	51	0.299	---

It can be seen that the TiO<sub>2</sub> mass composition of the TiFeC catalyst is somewhat lower than expected (i.e., 66 wt%) likely due to the loss of some TiO<sub>2</sub> during the washing steps of the synthesis procedure. The amount of iron in the TiFeC catalyst, about 5 wt%, is in good agreement with the Fe mass composition of the activated

carbon used as support and the amount of iron added during the preparation of the magnetically separable activated carbon (FeC).

Figure 5.2. shows the nitrogen adsorption-desorption isotherms of the activated carbon support and the FeC and TiFeC samples. All the three samples show a typical type I isotherm characteristic of microporous materials with high uptake at very low relative pressures [30]. However, a drastic decrease in the volume adsorbed at low relative pressures was produced after impregnation (FeC sample) and TiFeC catalyst preparation. As a result, noticeable decreases in BET surface area and micropore volume were computed (see Table 5.1.). Such a loss of internal surface was most likely due to the blockage of some microporous as a consequence of iron species and  $\text{TiO}_2$  deposition [24]. The activated carbon used as support had a significant external surface area which was even increased upon TiFeC preparation likely due to the formation of new large pores (meso or macropores) by the aggregation of titania particles on the support.

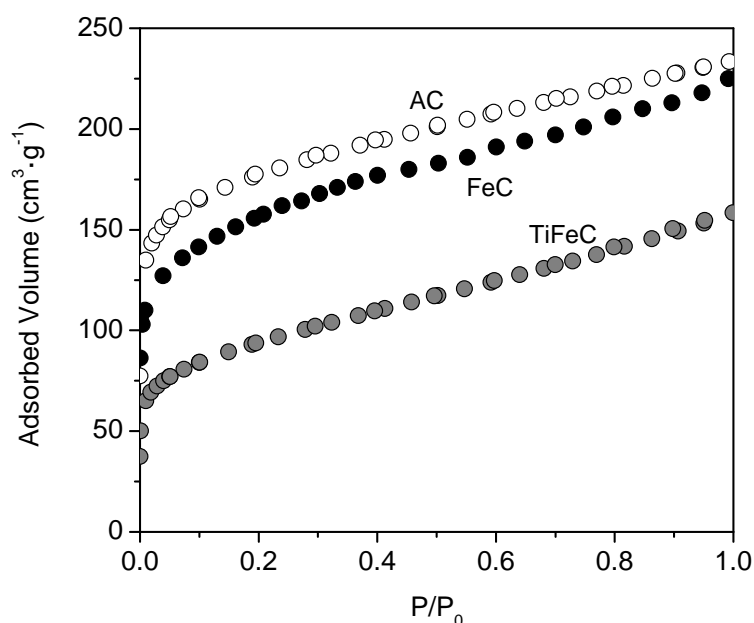


**Figure 5.2.**  $\text{N}_2$  adsorption-desorption isotherms of AC support, FeC and TiFeC catalyst

Figure 5.3. shows the XRD patterns of the activated carbon support and the TiFeC catalyst. In the diffractogram of the activated carbon (AC) two broad peaks at  $2\theta = 26^\circ$  and  $43^\circ$  can be distinguished corresponding to characteristic graphite diffraction peaks. The peaks width, which is characteristic of amorphous carbon materials, together with the absence of other (hkl) peaks suggests low dimensions of the graphitic domains. It can also be noticed the presence of a sharp diffraction

peak at  $26.6^\circ$  corresponding to  $\text{SiO}_2$ -quartz reflection, and others at  $21.9^\circ$ ,  $36.0^\circ$  and  $62.0^\circ$  which are likely due to  $\text{SiO}_2$ -cristoballite structures. XRD pattern of the TiFeC sample shows the characteristic peaks of anatase at  $25.4^\circ$ ,  $38.0^\circ$ ,  $48.0^\circ$ ,  $54.7^\circ$  and  $63.0^\circ$ . From the (1 0 1) peak the anatase crystallite size was calculated to be 4.7 nm after application of the Scherrer equation. Regarding the structure of iron species present in the catalyst, very small and wide characteristic diffraction peaks ( $30.4^\circ$ ,  $35.7^\circ$ ,  $43.4^\circ$  and  $57.4^\circ$ ) of magnetite or maghemite can be observed. In fact, both iron species have very similar XRD patterns so the XRD results do not allow one to distinguish one species from another. Finally, some  $\text{SiO}_2$  peaks can also be observed in the diffractogram of TiFeC.

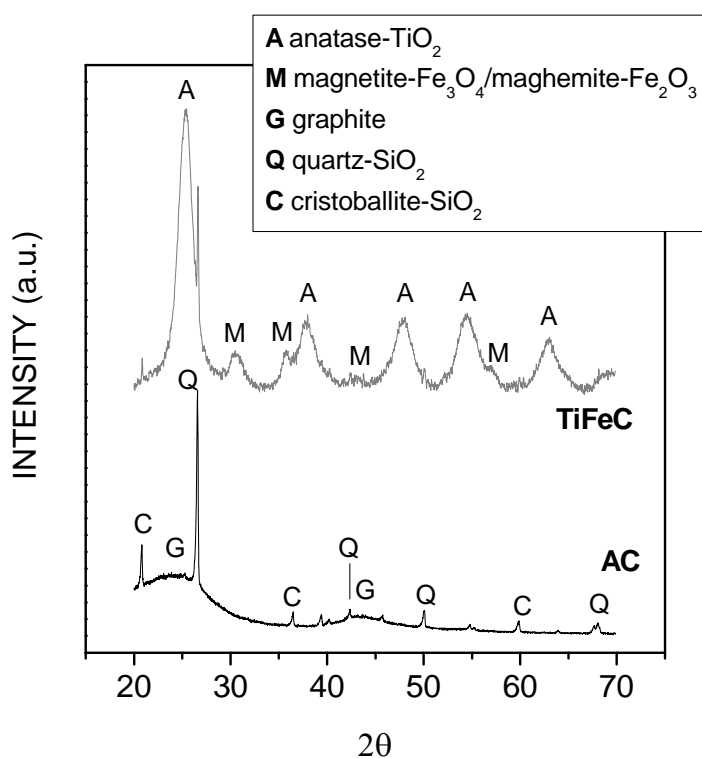


**Figure 5.3.** XRD patterns of the AC support and TiFeC catalyst

Figure 5.4. shows the FTIR spectra recorded for activated carbon and TiFeC samples. In the spectrum of activated carbon (AC), the broad band in the  $3200\text{--}3600\text{ cm}^{-1}$  region can be assigned to the stretching vibration of  $\text{--OH}$  groups present as phenolic surface groups [31]. In the TiFeC sample this band is also attributable to  $\text{TiO}_2\text{--OH}$  bonds [32, 33]. The AC sample exhibits overlapped bands in the region  $1700\text{--}1550\text{ cm}^{-1}$  which are generally accepted to be due to absorption of quinone and other carbonyl groups ( $\text{--C=O}$  structures) and stretching vibration of

aromatic structures [31]. The broad band centred at about  $1100\text{ cm}^{-1}$  in the spectrum of the activated carbon can be assigned primarily to ether structures (-C-O-C-) [31,34]. In the TiFeC spectrum, the broad band observed at  $600\text{ cm}^{-1}$  can be due to Ti-O stretching vibration and the peak at  $1620\text{ cm}^{-1}$  may correspond to bending vibration of OH groups of adsorbed water [35]. The sharp peak that can be seen at  $1385\text{ cm}^{-1}$  it is ascribable to the presence of nitrates ( $-\text{NO}_3^-$ ) on the catalyst surface [36], which would had been incorporated from the iron precursor during the synthesis of FeC. Finally, the peak located at  $1085\text{ cm}^{-1}$  could be assigned to Ti-O-C structures, suggesting a conjugation effect between bulk activated carbon and Ti-O bonds [37].

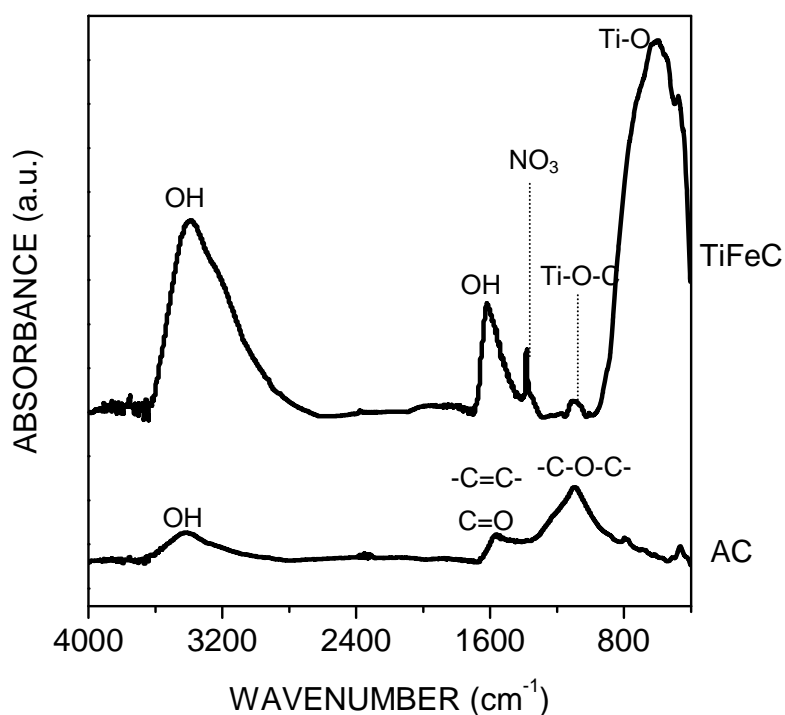


**Figure 5.4.** FTIR spectra of the AC support and TiFeC catalyst

The morphology of the catalyst particles has been investigated by SEM. Figure 5.5. (left) shows the SEM images at two different magnifications. It can be observed the non-uniform size of the catalyst particles, which were in any case lower than  $125\text{ }\mu\text{m}$ . The distribution of the Fe and Ti species was analyzed by means of energy dispersive X-ray analysis (EDX) by scanning the same area as shown in SEM images. Mapping results are shown in Figure 5.5. (right) where yellow and red areas correspond to Ti and Fe species, respectively. From these figures it is

apparent a uniform distribution of iron on the catalyst particles, whereas titanium was present in most of the particles with a less uniform concentration.

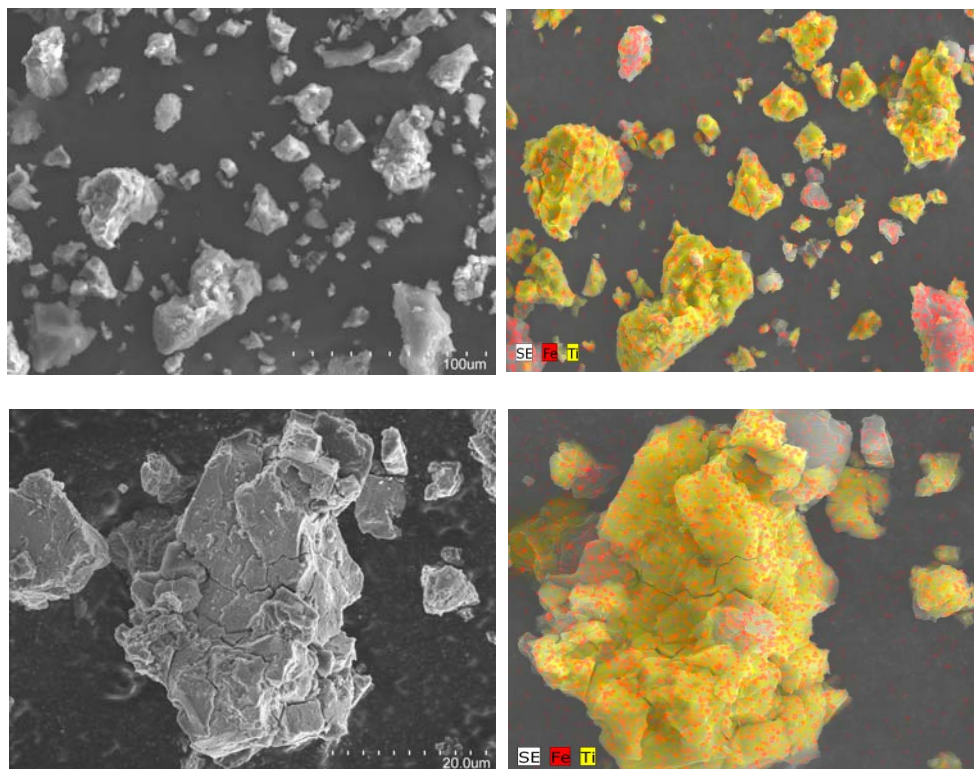


**Figure 5.5.** SEM images (left) and EDX mapping (right) for the TiFeC catalyst

Figure 5.6. illustrates the magnetization curve of the TiFeC catalyst. From it the value of saturation magnetization ( $M_S$ ) was calculated to be  $1.56 \text{ emu g}^{-1}$ . This value is similar to that reported by Ao et. al. [24]. However the saturation magnetization expected if all the iron was as magnetite was  $5.97 \text{ emu g}^{-1}$  taking into account the catalyst composition (Fe 4.7 wt%) and the saturation magnetization of bulk magnetite ( $92 \text{ emu g}^{-1}$ ). This fact suggests that a large amount of the iron incorporated to the catalyst is in a form other than magnetite. Nevertheless the catalyst could be easily separated from the solution with an external magnet as it has been illustrated in Figure 5.7. The sample showed almost zero coercivity and zero remanent magnetization, which indicates superparamagnetic behaviour of the catalyst particles. Accordingly, the particles did not aggregate being separated by a magnet and could be easily re-dispersed in solution for reusing.

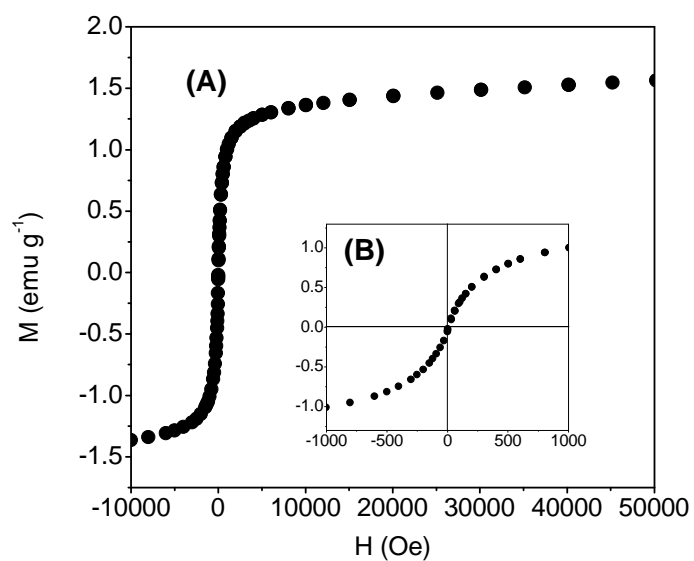


**Figure 5.6.** Magnetization vs. applied magnetic field at 25° C of TiFeC catalyst (left A) and (B) zoom of the -1000 to 1000 range.

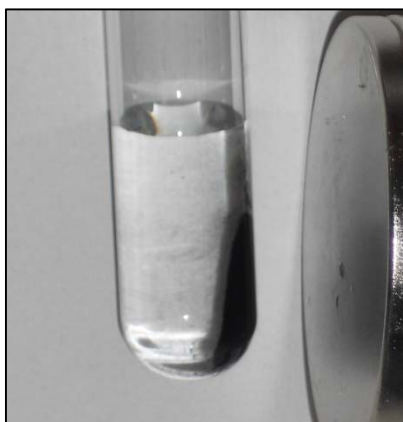


**Figure 5.7.** Illustration of the catalyst separation with a magnet

## 5.4.2. Photocatalytic activity

### A. Photodegradation of MTP

Figure 5.8A shows the evolution of MTP dimensionless concentration with time during the course of selected experiments. Two regions can be seen in the figure. First, a 30 min stage designated as dark stage (absence of radiation) where only

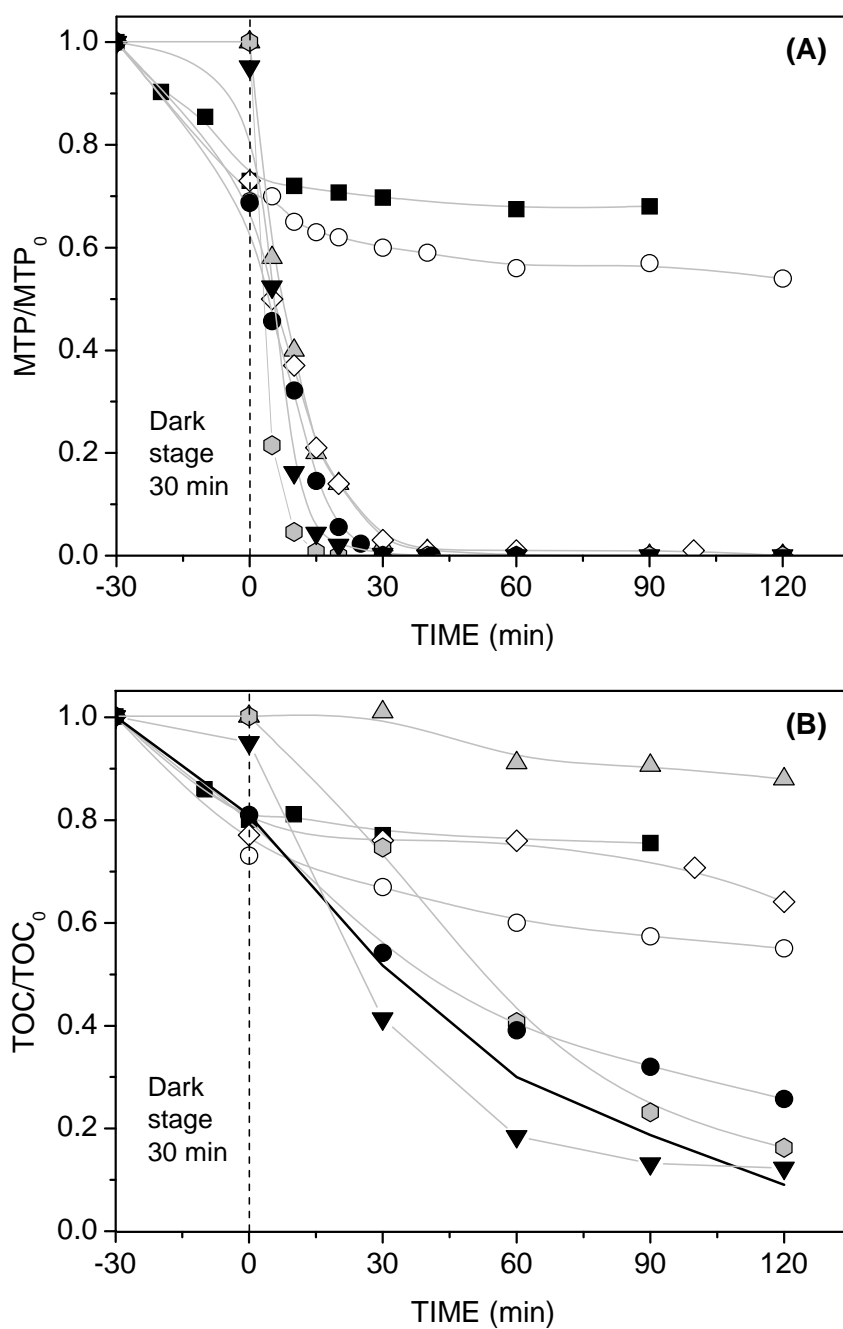


**Figure 5.8.** Variation of MTP (A) and TOC (B) dimensionless concentration with time.

Conditions:  $C_{MTP,L,0} = 10 \text{ mg L}^{-1}$ ,  $*C_{TiO_2,L} = 0.25 \text{ g L}^{-1}$  ( $C_{CAT,L} = 0.375 \text{ g L}^{-1}$ ),  $Q_g = 20 \text{ L h}^{-1}$ ,  $pH_0 = 6.5$ ,  $T = 30^\circ \text{ C}$ ,  $*C_{O_3,g} = 6 \text{ mg L}^{-1}$  (\*in the corresponding experiments).

Symbols: ■ adsorption, ○ photocatalysis, △ ozonation, ◇ catalytic ozonation, ⬡ photolytic ozonation, ● photocatalytic ozonation, ▼ P25-photocatalytic ozonation, — photocatalytic ozonation corrected



adsorption onto the catalyst took place, followed by a second stage where adsorption and/or oxidation reactions developed. From the adsorption curve it can be observed that about 25-30% of the MTP initially present in the aqueous solution was adsorbed onto the TiFeC catalyst at adsorption equilibrium. Also it can be seen that at the end of the dark stage, the concentration of MTP was close to the adsorption equilibrium value. Photocatalytic oxidation (TiFeC in the absence of ozone but radiation and oxygen) led to about 46% MTP removal after 2 h of irradiation while complete MTP removal was observed after 40 min reaction time in all the experiments when using ozone since this reacts relatively fast with MTP ( $k_{\text{O}_3\text{-MTP}} = 1.4 \times 10^3 \text{ L}^{-1} \text{ mol s}^{-1}$  at pH 7 [38]). Moreover, MTP concentration profiles were quite similar for single ozonation, catalytic ozonation and photocatalytic ozonation, suggesting that in these experiments MTP was mainly removed through direct ozonation reactions with little catalytic effect.

Table 5.2. shows the pseudo-first order apparent rate constant derived from Figure 5.8A. In agreement with the discussion above, it can be seen that  $k_{\text{app}}$  for the photocatalytic process (absence of ozone) was much lower than those for the ozone-based processes.

**Table 5.2.** Experimental pseudo-first order apparent rate constants for MTP depletion

Process	$k_{\text{app}}$ ( $\text{min}^{-1}$ )	$R^2$
Photocatalysis	0.005	0.97
Ozonation	0.121	0.98
Catalytic ozonation	0.110	0.98
Photolytic ozonation	0.319	0.99
Photocatalytic ozonation (TiFeC)	0.137	0.97
Photocatalytic ozonation (P25)	0.201	0.99

In Figure 5.8A the results of MTP degradation from a photocatalytic ozonation experiment with Degussa P25 are also shown. It is apparent that the catalytic activity of Degussa P25 was somewhat higher than that of the synthesized TiFeC catalyst. Thus, the computed  $k_{\text{app}}$  was 1.5 times higher for the P25 catalyzed process. Surprisingly, MTP removal by photolytic ozonation was faster than those achieved by any of the photo-catalyzed systems. This fact can be explained by

partial decomposition of ozone into hydroxyl radicals by photolysis at wavelengths near 300 nm [39].

Ozone consumptions within the processes are reported in Table 5.3. The presented data are the amounts of ozone consumed per mole of MTP degraded at 50% MTP removal, 98% MTP removal, and per mole of carbon at 50% TOC removal. From this table it is apparent that the least ozone-consuming process was the photocatalytic ozonation with Degussa P25. In fact, the amount of ozone used was about three times higher for the photocatalytic ozonation with TiFeC than with Degussa P25. This result suggests that in the presence of TiFeC much ozone is consumed through parallel reactions (i.e., ozonation of MTP by-products and catalyst surface oxidation) while Degussa P25 was a more efficient photocatalyst for degrading MTP by ozonation.

**Table 5.3.** Ozone consumption during all the O<sub>3</sub>-treatments with 10 mg L<sup>-1</sup> MTP initial concentration

Process	O <sub>3</sub> consumed/MTP degraded (mol/mol)		
	MTP 50%	MTP 98%	TOC 50%
Ozonation	2.26	6.29	----
Catalytic ozonation	3.70	8.74	1.68
Photolytic ozonation	3.42	5.24	1.43
Photocatalytic ozonation (TiFeC)	4.11	7.69	1.14
Photocatalytic ozonation (P25)	1.23	3.32	0.67

Regarding mineralization, Figure 5.8B. shows the time evolution of dimensionless TOC during the course of experiments. While single ozonation, single adsorption, catalytic ozonation and photocatalytic oxidation (without ozone) led to less than 50% TOC removal after 2 hours of experiment, greater mineralization levels were achieved by photocatalytic ozonation both with TiFeC or Degussa P25 and photolytic ozonation. It can be hypothesized that under the conditions studied, during photocatalytic ozonation hydroxyl radicals are formed on the photocatalyst surface [16]. Thus, intermediates from MTP ozonation could, in turn, be most

efficiently oxidized by hydroxyl radicals resulting in an enhanced mineralization [40].

It is important to recall here that a powdered carbon material subjected to ozonation in water may release organic carbon to water because of the reaction between ozone and surface groups of the activated carbon [41]. To assess whether or not TOC release was produced in our photocatalytic ozonation experiments with TiFeC, some experiments were carried out in ultrapure water (without MTP). TOC concentrations up to  $1.5 \text{ mg L}^{-1}$  were detected but this organic carbon is expected not to be an environmental problem because of its non-toxic nature and the fact that it can be removed by further ozonation [41]. In Figure 5.8B, the TOC profile for the TiFeC photocatalytic ozonation process has been re-plotted (solid line) by subtracting the TOC released from the actual TOC profile so that only the effect on MTP mineralization is shown. It can be seen now, that the photocatalytic effect of TiFeC on MTP mineralization was only slightly lower than that of Degussa P25.

From Figure 5.8B, it is also observed that great MTP mineralization was also achieved by photolytic ozonation (absence of catalyst). In a previous work, using a high-pressure mercury lamp with effective irradiation at 313 nm, high mineralization of the antibiotic sulfamethoxazole was also achieved by photolytic ozonation [42]. Up to our knowledge the degradation of water pollutants by solar photolytic ozonation has not been yet studied. Given the promising results obtained in this work it will be a subject of further work.

### **B. Influence of initial MTP concentration**

In order to study the effect of MTP initial concentration, some experiments (photocatalytic ozonation and photolytic ozonation) were carried out with 10 and  $50 \text{ mg L}^{-1}$  initial concentration of MTP. The time profiles of these experiments are depicted in Figure 5.9A for MTP and Figure 5.9B for TOC. As expected, higher reaction times were needed to reach complete MTP removal when using  $50 \text{ mg L}^{-1}$  MTP initial concentration. Regardless of the initial concentration used, MTP removal rates achieved by photocatalytic ozonation and photolytic ozonation were close to each other. However, regarding TOC degradation, while no great differences were observed at  $10 \text{ mg L}^{-1}$  initial concentration, at  $50 \text{ mg L}^{-1}$  initial concentration TOC degradation was faster by photocatalytic ozonation. Thus, for example TOC conversions after 3 h were 34% and 64% for photolytic ozonation and photocatalytic ozonation, respectively. Therefore, it can be concluded that the TiFeC catalyst enhanced the mineralization rate of MTP during photocatalytic ozonation in comparison to the photolytic ozonation.

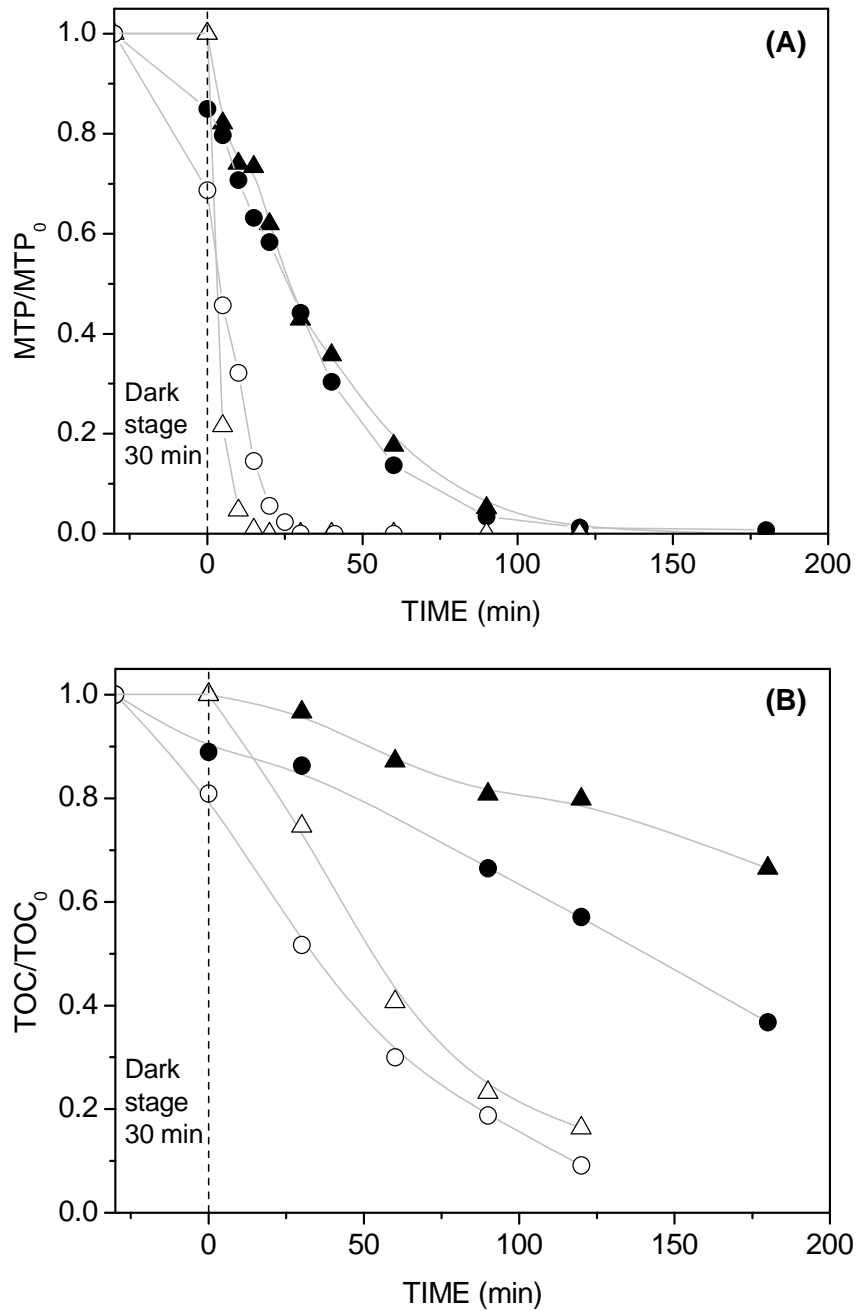


**Figure 5.9.** Variation of MTP (A) and TOC (B) dimensionless concentration with time.

Conditions:  $C_{MTP0} = 50 \text{ mg L}^{-1}$  (▲ photolytic ozonation, ● photocatalytic ozonation) and  $10 \text{ mg L}^{-1}$  (△ photolytic ozonation, ○ photocatalytic ozonation),  $*C_{TiO_2} = 0.25 \text{ g L}^{-1}$  ( $C_{CAT} = 0.375 \text{ g L}^{-1}$ ),  $Q_g = 20 \text{ L h}^{-1}$ ,  $pH_0 = 6.5$ ,  $T = 30^\circ \text{ C}$ ,  $C_{O_3,g} = 6 \text{ mg L}^{-1}$  (\*in the corresponding experiments)

### C. Catalyst stability and reusability

One of the key factors for the practical application of heterogeneous photocatalytic processes in water treatment is the recovery and reusability of the catalyst after the treatment. In this line, five consecutive runs were carried out with the TiFeC catalyst. In these experiments,  $50 \text{ mg L}^{-1}$  MTP initial concentration was used. After each two-hour run, the catalyst was separated with a magnet and the aqueous solution was removed from the reactor and replaced by a fresh MTP aqueous solution. Figure 5.10. shows some of the results obtained in terms of MTP and TOC conversions.

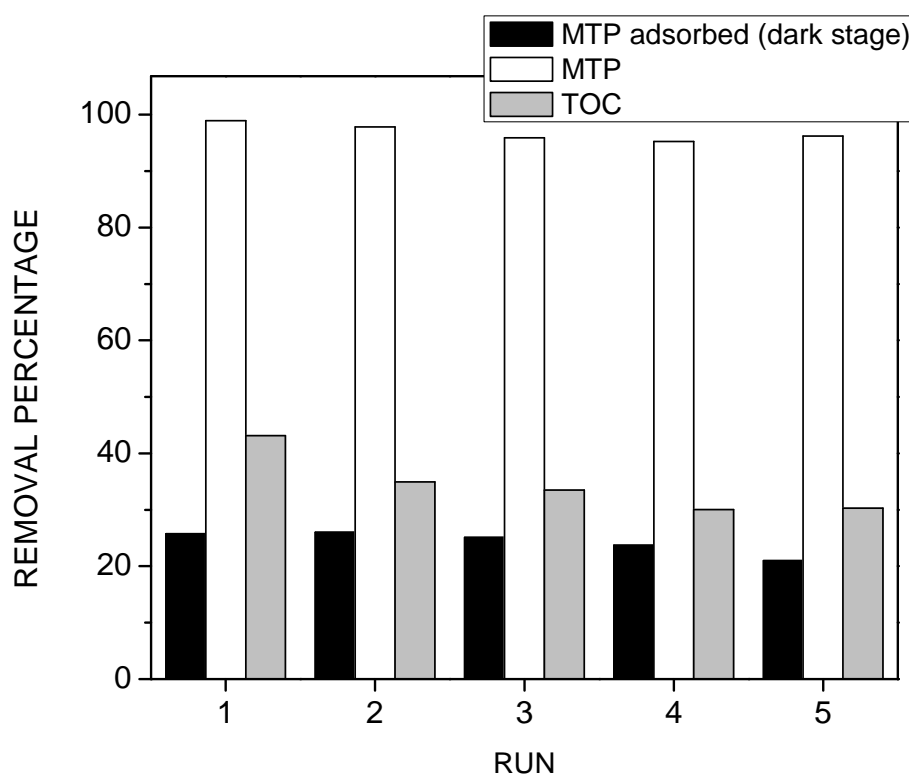


**Figure 5.10.** Initial adsorption, MTP and TOC conversion for consecutive photocatalytic ozonation runs with TiFeC catalyst. Conditions:  $C_{\text{MTP}0} = 50 \text{ mg L}^{-1}$ ,  $C_{\text{TiO}_2} = 0.25 \text{ g L}^{-1}$  ( $C_{\text{CAT}} = 0.375 \text{ g L}^{-1}$ ),  $Q_g: 20 \text{ L h}^{-1}$ ,  $\text{pH}_0 = 6.5$ ,  $T = 30^\circ \text{ C}$ ,  $C_{\text{O}_3, \text{g}} = 6 \text{ mg L}^{-1}$

First, it is seen that the adsorption capacity of the catalyst was barely affected throughout the series of experiments. Thus, MTP removed by adsorption during the initial dark stage was around 25% though slightly lower for the 4<sup>th</sup> and 5<sup>th</sup> run. This suggests that after each run the catalyst is free of adsorbed MTP which has been degraded by surface oxidation reactions. However, after a number of cycles some reaction by-products could remain on the catalyst surface, thus preventing MTP adsorption to some extent. Also, MTP conversion after 2 h, was kept practically constant around 95-98% for the whole series of experiments. However, TOC conversion decreased from 43% reached in the first run to 30-35% in the subsequent experiments, being always higher than the TOC conversion reached in a photolytic ozonation experiment (about 20%). Also, the amounts of Fe and Ti leached out from the catalyst were measured. Table 5.4. shows the element concentrations found in solution after each run. It can be seen that both Fe and Ti concentrations were low. Thus, from mass balances it was calculated that the percentages of titanium and iron leached out from the catalyst after the whole series of consecutive experiments were lower than 0.04% and 0.60%, respectively

**Table 5.4.** Ti and Fe lixiviation during photocatalytic ozonation runs with TiFeC catalyst

Run	1	2	3	4	5
Ti ( $\mu\text{g L}^{-1}$ )	<15	<10	<10	<10	<15
Fe ( $\mu\text{g L}^{-1}$ )	<25	<20	<20	<20	<20

## 5.5. Conclusions

This study focuses on the preparation of a titania-coated magnetic activated carbon (TiFeC) to be used in the removal of emerging contaminants from water by solar photocatalytic methods. The synthesized catalyst showed moderate surface areas and pore volume which allow adsorption of organic compounds to some extent.  $\text{TiO}_2$  crystallites attached to the activated carbon were in the form of anatase, thus showing high photocatalytic activity. Given its magnetic properties, catalyst particles were demonstrated to be easily separable by a magnet. Metoprolol (MTP) was chosen as model pollutant to test the photocatalytic activity of the synthesized catalyst. Solar photocatalytic ozonation resulted in higher MTP removal rate and TOC degradation than single adsorption, single ozonation and solar photocatalysis

without ozone. However, solar photolytic ozonation (without catalyst) effectiveness was comparable to that of solar photocatalytic ozonation when using a MTP initial concentration of  $10 \text{ mg L}^{-1}$ . Given this promising result, new research is being carried out in the application of solar photolytic ozonation for the degradation of other emerging contaminants and elucidation of reaction mechanisms. The TiFeC catalyst showed good stability (low Fe and Ti losses) and reusability. Although the TiFeC catalyst was not as effective as Degussa 25  $\text{TiO}_2$ , its easy separation by an external magnetic field makes it an interesting alternative material for solar photocatalytic processes.

## 5.6. Acknowledgements

---

This work has been financed by the Spanish Ministerio de Ciencia e Innovación (MICINN) and European Feder Funds through the project CTQ2009-13459-C05-05/PPQ. Authors acknowledge the SAIUEX service of the University of Extremadura for the characterization analyses. A. Rey thanks the University of Extremadura for a post-doctoral research grant. D. H. Quiñones thanks the MICINN for a FPI grant.

## 5.7. References

---

- [1] J. Blanco-Gálvez, P. Fernández-Ibañez, S. Malato-Rodríguez, *Solar photo catalytic detoxification and disinfection of water: Recent overview*, J. Sol. Energy Eng. 129 (2007) 4-15.
- [2] S. Malato, P. Fernández-Ibañez, M.I. Maldonado, J. Blanco, W. Gernjak, *Decontamination and disinfection of water by solar photocatalysis: Recent overview and trends*, Catal. Today 141 (2009) 1-59.
- [3] S. Malato, J. Cáceres, A. Agüera, M. Mezcuca, D. Hernando, *Degradation of imidacloprid in water by photo-Fenton and  $\text{TiO}_2$  photocatalysis at a solar pilot plant: A comparative study*, J. Vial, A.R. Fernández-Alba, Environ. Sci. Technol. 35 (2001) 4359-4366.
- [4] F. Méndez-Arriaga, S. Esplugas, J. Giménez, *Photocatalytic degradation of non-steroidal anti-inflammatory drugs with  $\text{TiO}_2$  and simulated solar irradiation*, Water Res. 42 (2008) 585-594.

- [5] T.E. Doll, F. ccH. Frimmel, *Photocatalytic degradation of carbamazepine, clofibric acid and iomeprol with P25 and Hombikat UV100 in the presence of natural organic matter (NOM) and other organic water constituents*, Water Res. 39 (2005) 403-411.
- [6] N. Miranda-García, S. Suárez, B. Sánchez, J. M. Coronado, S. Malato, M. I. Maldonado, *Photocatalytic degradation of emerging contaminants in municipal wastewater treatment plant effluents using immobilized TiO<sub>2</sub> in a solar pilot plant*, Appl. Catal. B-Environ. 103 (2011) 294-301.
- [7] B. Neppolian, H.C. Choi, S. Sakthivel, B. Arabindoo, V. Murugesan, *Solar light induced and TiO<sub>2</sub> assisted degradation of textile dye reactive blue 4*, Chemosphere 46 (2002) 1173-1181.
- [8] A. Arques, A.M. Amat, A. García-Ripoll, R. Vicente, *Detoxification and/or increase of the biodegradability of aqueous solutions of dimethoate by means of solar photocatalysis*, J. Hazard. Mater. 146 (2007) 447-452.
- [9] F.M. Salih, *Enhancement of solar inactivation of Escherichia coli by titanium dioxide photocatalytic oxidation*, J. Appl. Microbiol. 92 (2002) 920-926.
- [10] S. Baumgarten, H.F. Schroder, C. Charwath, M. Lange, S. Beier, J. Pinnekamp, *Evaluation of advanced treatment technologies for the elimination of pharmaceutical compounds*, Water Sci. Technol. 56 (2007) 1-8.
- [11] O.K. Dalrymple, D.H. Yeh, M.A. Trotz, *Removing pharmaceuticals and endocrine-disrupting compounds from wastewater by photocatalysis*, J. Chem. Technol. Biotechnol. 82 (2007) 121-134.
- [12] K. Ikehata, N. J. Naghashkar, M. G. El-Din, *Degradation of aqueous pharmaceuticals by ozonation and advanced oxidation processes: a review*, Ozone-Sci. Eng. 28 (2006) 353-414.
- [13] R. Rosal, A. Rodriguez, J.A. Perdigon-Melon, A. Petre, E. Garcia-Calvo, M.J. Gomez, A. Aguera, A.R. Fernandez-Alba, *Occurrence of emerging pollutants in urban wastewater and their removal through biological treatment followed by ozonation*, Water Res. 44 (2010) 578-588.
- [14] T.E. Agustina, H.M. Ang, V.K. Vareek, *A review of synergistic effect of photocatalysis and ozonation on wastewater treatment*, J. Photochem. Photobiol. C Photochem. Rev. 6 (2005) 264-273.
- [15] V. Augugliaro, M. Litter, L. Palmisano, J. Soria, *The combination of heterogeneous photocatalysis with chemical and physical operations: A tool for improving the photoprocess performance*, J. Photochem. Photobiol. C Photochem. Rev. 7 (2006) 127-144.



- [16] F.J. Beltrán, A. Aguinaco, J.F. García-Araya, *Mechanism and kinetics of sulfamethoxazole photocatalytic ozonation in water*, *Water Res.* 43 (2009) 1359-1369.
- [17] O. Gimeno, F. J. Rivas, F. J. Beltrán, M. Carbajo, *Photocatalytic ozonation of winery wastewaters*, *J. Agric. Food Chem.* 55 (2007) 9944-9950.
- [18] R. Rajeswari, S. Kanmani, *Degradation of pesticide by photocatalytic ozonation process and study of synergistic effect by comparison with photocatalysis and UV/ozonation processes*, *J. Adv. Oxid. Technol.* 12 (2009) 208-214.
- [19] D. Beydoun, R. Amal, G.K.C. Low, S. McEvoy, *Novel photocatalyst: Titania-coated magnetite. Activity and photodissolution*, *J. Phys. Chem. B* 104 (2000) 4387-4396.
- [20] D. Beydoun, R. Amal, *Implications of heat treatment on the properties of a magnetic iron oxide-titanium dioxide photocatalyst*, *Mater. Sci. Eng.* 94 (2002) 71-81.
- [21] S. Watson, J. Scott, D. Beydoun, R. Amal, *Implications of heat treatment on the properties of a magnetic iron oxide-titanium dioxide photocatalyst*, *J. Nanopart.* 7 (2005) 691-705.
- [22] S. Xu, W. Shangguan, J. Yuan, M. Chen, J. Shi, *Preparations and photocatalytic properties of magnetically separable nitrogen-doped TiO<sub>2</sub> supported on nickel ferrite*, *Appl. Catal. B-Environ.* 71 (2007) 177-184.
- [23] P. M. Álvarez, J. Jaramillo, F. López-Piñero, P. K. Plucinski, *Preparation and characterization of magnetic TiO<sub>2</sub> nanoparticles and their utilization for the degradation of emerging pollutants in water*, *Appl. Catal. B-Environ.* 100 (2010) 338-345.
- [24] Y. Ao, J. Xu, D. Fu, C. Yuan, *A simple route for the preparation of anatase titania-coated magnetic porous carbons with enhanced photocatalytic activity*, *Carbon* 46 (2008) 596-603.
- [25] S. Wang, S. Zhou, *Titania deposited on soft magnetic activated carbon as a magnetically separable photocatalyst with enhanced activity*, *Appl. Surf. Sci.* 256 (2010) 6191-6198.
- [26] V. Romero, N. de la Cruz, R. F. Dantas, P. Marco, J. Giménez, S. Esplugas, *Photocatalytic treatment of metoprolol and propranolol*, *Catal. Today* 161 (2011) 115-120.
- [27] V. Contardo-Jara, S. Pflugmacher, G. Nützmann, W. Kloas, C. Wiegand, *The  $\beta$ -receptor blocker metoprolol alters detoxification processes in the non-target organism *Dreissena polymorpha**, *Environ. Pollut.* 158 (2010) 2059-2066.

- [28] A. B. Fuertes, P. Tartaj, *A facile route for the preparation of superparamagnetic porous carbons*, Chem. Mater. 18 (2006) 1675–1679.
- [29] H. Bader, J. Hoigné, *Determination of ozone in water by the indigo method*, Water Res. 15 (1981) 449–456.
- [30] S. Brunauer, L.S. Deming, W.S. Deming, E. Teller, *On a theory of the van der Waals adsorption of gases*, J. Am. Chem. Soc. 62 (1940) 1723.
- [31] P. Serp, J. L. Figueiredo, *Carbon Materials for Catalysis*, John Wiley and Sons Inc., 2009.
- [32] T. López, J.A. Moreno, R. Gómez, X. Bokhimi, J.A. Wang, H. Yee-Madeira, G. Pecci, P. Reyes, *Characterization of iron-doped titania sol-gel materials*, J. Mater. Chem. 12 (2002) 714–718.
- [33] H. Jensen, A. Soloviev, Z. Li, E.G. Sogaard, *XPS and FTIR investigation of the surface properties of different prepared titania nano-powders*, Appl. Surf. Sci. 246 (2005) 239–249.
- [34] L.R. Radovic, *Chemistry and Physics of Carbon, A Series of Advances*, Volume 27, Marcel Dekker Inc., New York USA, 2001.
- [35] Y. Suda, T. Morimoto, *Molecularly adsorbed H<sub>2</sub>O on the bare surface of TiO<sub>2</sub> (rutile)*, Langmuir 3 (1987) 786–788.
- [36] M. Pakula, A. Swiatkowski, M. Walczyk, S. Biniak, *Voltammetric and FT-IR studies of modified activated carbon systems with phenol, 4-chlorophenol or 1,4-benzoquinone adsorbed from aqueous electrolyte solutions*, Colloids Surf. A Physicochem. Eng. Aspects 260 (2005) 145–155.
- [37] S.X. Liu, X.Y. Chen, X. Chen, *A TiO<sub>2</sub>/AC composite photocatalyst with high activity and easy separation prepared by a hydrothermal method*, J. Hazard. Mater. 143 (2007) 257–263.
- [38] F.J. Benitez, J.L. Acero, F.J. Real, G. Roldán, *Ozonation of pharmaceutical compounds: Rate constants and elimination in various water matrices*, Chemosphere 77 (2009) 53–59.
- [39] H. Taube, *Photochemical reactions of ozone in solution*, Trans. Faraday Soc. 53 (1957) 656–665.
- [40] J. Benner, T. A. Ternes, *Ozonation of metoprolol: Elucidation of oxidation pathways and major oxidation products*, Environ. Sci. Technol. 43 (2009) 5472–5480.
- [41] J. P. Pocostales, P. M. Álvarez, F. J. Beltrán, *Kinetic modeling of powdered activated carbon ozonation of sulfamethoxazole in water*, Chem. Eng. J. 164 (2010) 70–76.

- [42] F. J. Beltrán, A. Aguinaco, J. F. García-Araya, A. Oropesa, *Ozone and photocatalytic processes to remove the antibiotic sulfamethoxazole from water*, *Water Res.* 42 (2008) 3799–3808.





## Chapter VI

### Paper 4:

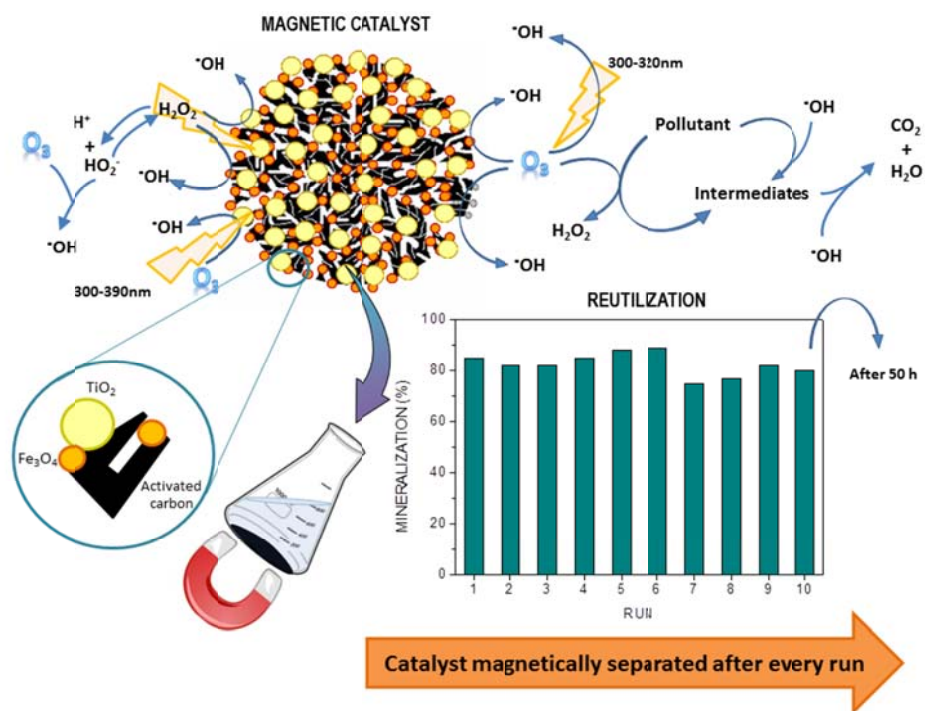
### Enhanced activity and reusability of TiO<sub>2</sub> loaded magnetic activated carbon for solar photocatalytic ozonation

Diego H. Quiñones<sup>1</sup>, Ana Rey<sup>1</sup>, Pedro M. Álvarez<sup>1</sup>, Fernando J. Beltrán<sup>1</sup>, Pawel K. Plucinski<sup>2</sup>

<sup>1</sup> Departamento de Ingeniería Química y Química Física, Facultad de Ciencias, Universidad de Extremadura, Av. de Elvas s/n, 06071 Badajoz (Spain)

<sup>2</sup> Department of Chemical Engineering, University of Bath, BA2 7AY Bath (United Kingdom)





## 6.1. Abstract

Magnetically separable photocatalysts with high activity under solar illumination were successfully synthesized from a commercial meso-to-microporous activated carbon. First magnetite and then titania (anatase) were deposited onto the activated carbon support by impregnation and sol-gel methods, respectively. Various catalyst samples were prepared with different iron and titania contents. The synthesized photocatalysts were characterized by nitrogen adsorption, XRD, SEM, EDX, ICP, XPS and SQUID magnetometer. Photocatalytic performance of some selected samples was examined under various irradiation conditions in the wavelength ranges of 300-800 nm, 320-800 nm and 390-800 nm. Metoprolol tartrate (MTP) in aqueous solution ( $50 \text{ mg L}^{-1}$ ) was chosen as target compound for catalytic activity tests. The most efficient catalyst had  $\text{TiO}_2$  and Fe mass compositions of 64 wt% and 9 wt%, respectively. It showed high activity in photocatalytic ozonation with complete removal of MTP in less than 2 h reaction time and 85% mineralization after 5 h. This catalyst was also easily separable due to its developed magnetic properties. Catalyst reusability and stability was proved to be rather good after completing a series of ten consecutive photocatalytic ozonation runs.

**Keywords:** Magnetic photocatalyst, metoprolol, photocatalytic ozonation, reusability, titania, water treatment.

## 6.2. Introduction

---

Given the global concern generated by the increasingly occurrence of emerging contaminants (ECs) in wastewater and aquatic environments, the research and development of novel water treatment technologies that can remove these compounds in a cost-efficient way is challenging.

Advanced oxidation processes (AOPs) involve the formation of highly reactive species, such as hydroxyl radical ( $\cdot\text{OH}$ ,  $E^\circ = 2.8\text{V}$  vs. SHE), which is capable of oxidizing most of the organic compounds in water [1]. Thus, various AOPs have demonstrated their ability to degrade many ECs transforming them into harmless products [2]. Among these AOPs, solar photocatalytic oxidation using  $\text{TiO}_2$  as catalyst is one of the most promising cost-effective alternatives since it is a method capable of completely degrade organic ECs up to  $\text{CO}_2$  and  $\text{H}_2\text{O}$  and also perform oxidative transformation of some inorganic compounds and deactivation of pathogenic microorganisms [3,4]. Recently, it has been shown that the combination of  $\text{TiO}_2$  and ozone under sunlight illumination (i.e., solar photocatalytic ozonation) can greatly enhance the ECs degradation rates achieved by the single processes (i.e., ozonation and solar photocatalytic oxidation). The reason for such behavior is likely due to the adsorption of ozone onto the  $\text{TiO}_2$  surface where it traps electrons promoted to the conduction band of the semiconductor, thus avoiding, to some extent, ineffective electron-hole recombination and generating ozonide radicals ( $\text{O}_3^-$ ), which can be further transformed into hydroxyl radicals [5-7].

A key factor in the development of solar photocatalytic ozonation processes for the removal of ECs from water is the use of a suitable photocatalyst. In a previous work, a  $\text{TiO}_2$  (anatase)-magnetic carbon composite (TiFeC) was synthesized and used for the degradation of metoprolol tartrate (MTP) [8]. MTP is a  $\beta$ -blocker pharmaceutical compound frequently found in effluents from sewage treatment plants [9,10]. After the treatment, the catalyst particles could be separated from the solution by an external magnet due to their superparamagnetic behavior, though their saturation magnetization was rather low ( $1.6 \text{ emu g}^{-1}$ ) compared to bulk magnetite ( $92 \text{ emu g}^{-1}$ ). Photocatalytic activity was fairly good though somewhat lower than that found for the commercially available catalyst AEROXIDE®  $\text{TiO}_2$  P25. As part of our ongoing work on photocatalytic ozonation, this paper is focused on the optimization of TiFeC catalysts to improve their photocatalytic activity, separability and reusability by means of the synthesis of catalysts with different magnetite and titanium dioxide loadings. Also, this paper gives some insights into the elucidation of the mechanism of solar photocatalytic oxidation taking into account the contribution of different pathways to the overall MTP degradation process as well as the main intermediates observed.



## 6.3. Experimental section

---

### 6.3.1. Catalyst preparation

Samples of magnetic photocatalysts were prepared following a method described previously, which comprises three main steps [11]. The first step was the synthesis of magnetic activated carbon particles (FeC) following the incipient wetness impregnation method reported by Fuentes and Tartaj [12]. Typically, 10 g of granular activated carbon (Darco 12-20, Sigma–Aldrich) were impregnated with an iron (III) nitrate ethanol solution. In order to have samples with different final iron content (10-30 wt% Fe), solutions of different concentrations (920-1190 g L<sup>-1</sup>) were used. Impregnated samples were dried at 90°C for 2 h and then 150 mmol of ethylene glycol was added to reduce Fe<sup>3+</sup> to Fe<sup>2+</sup>. Finally, the samples were subjected to heat treatment under nitrogen atmosphere at 350-550°C for 2-4 h. The particles thus obtained were milled and sieved so that only particles with size lower than 125 µm were selected.

The second stage was the synthesis of a TiO<sub>2</sub> nanosol. To prepare 1 g of TiO<sub>2</sub>, 4.3 mL of titanium (IV) butoxide (97%, Aldrich) were diluted in 1.4 mL of isopropanol (>99%, Aldrich) and the mixture was added dropwise to 34 mL of distilled water acidified at pH 2.0 with HNO<sub>3</sub> (65%, Panreac). The solution was stirred under reflux at 75°C for 24 h. Finally, the excess of alcohol was removed on a rotary evaporator operating at 80°C under vacuum, thus obtaining a TiO<sub>2</sub> nanosol. The final stage of the catalyst preparation was the dispersion of FeC particles in the TiO<sub>2</sub> nanosol under sonication for 1 h. Subsequently, the dispersion was dried under vacuum at 80°C. The residue was repeatedly washed with distilled water until no total organic carbon (TOC) was detected in the supernatant. After each washing step the particles were separated from the liquid phase by an external magnet so that the non-magnetic particles were discarded. Finally, the particles were dried at 100°C overnight and kept in a desiccator until further use in photocatalytic tests.

Table 6.1. shows the amounts of activated carbon (AC), Fe, FeC support and Ti and calcination conditions (step 1) used in the preparation of three magnetic catalysts selected for photocatalytic experiments.

**Table 6.1.** Preparation conditions used for the synthesis of three TiFeC catalysts selected for photocatalytic experiments

Catalyst sample	FeC magnetic support				TiFeC catalyst	
	AC (g)	Fe (g)	Calcination temperature (°C)	Calcination time (h)	FeC (g)	Ti (g)
TiFeC-1	10.0	1.1	350	2	3	3.6
TiFeC-2	10.0	4.3	450	3	3	7.2
TiFeC-3	10.0	4.3	550	4	3	7.2

### 6.3.2. Characterization of the catalysts

The characterization of the catalysts was carried out by N<sub>2</sub> adsorption-desorption, X-ray diffraction (XRD), scanning electron microscopy (SEM-EDX), X-ray photoelectron spectroscopy (XPS), inductively coupled plasma mass spectrometry (ICP-MS) and SQUID magnetometry.

BET surface area and pore structure of the AC used as support and the prepared photocatalysts were determined from their nitrogen adsorption-desorption isotherms obtained at -196°C using an Autosorb 1 apparatus (Quantachrome). Prior to analysis the samples were outgassed at 250°C for 12 h under high vacuum (<10<sup>-4</sup> Pa). The t-plot method was applied to obtain external surface area and micropore volume of samples.

The crystalline phases present in the catalysts and AC were inferred from their X-ray diffraction (XRD) patterns recorded using a Bruker D8 Advance XRD diffractometer with a CuK $\alpha$  radiation ( $\lambda = 0.1541$  nm). The data were collected from  $2\theta = 20^\circ$  to  $70^\circ$  at a scan rate of  $0.02$  s<sup>-1</sup> and 1 s per point.

The particle morphology of the catalysts was analyzed using a Hitachi S-4800 scanning electron microscope with 20–30 kV accelerating voltage and 500–2000 magnification. Catalysts were also examined by energy dispersive X-ray (EDX) in order to determine the distribution of Ti and Fe on the particles using a SSD detector XFlash 5010 (Bruker), with 5 kV accelerating voltage and 500–2000 magnification.

XPS spectra were obtained with a K $\alpha$  Thermo Scientific apparatus with an Al K $\alpha$  ( $h\nu=1486.68$  eV) X-ray source using a voltage of 12 kV under vacuum ( $2 \times 10^{-7}$  mbar). Binding energies were calibrated relative to the C1s peak from carbon

samples at 284.6 eV. The resulting XPS peaks were curve-fitted to a combination of Gaussian and Lorentzian functions using a Shirley type background for peak analysis.

The iron content of the catalysts was analyzed by inductively coupled plasma with an ICP-MS NexION 300D (Perkin-Elmer) after acidic microwave digestion of the samples. The content of TiO<sub>2</sub> was estimated from the residue of catalyst combustion in air at 900°C, taking into account the amount of iron and the ash content on the AC support used.

Magnetic properties of the materials were tested by magnetometry using a Quantum Design MPMS XL-7 Superconducting Quantum Interference Device (SQUID). The magnetic moment, *M*, was measured as function of the applied magnetic field, *H*, at room temperature.

### 6.3.3. Photocatalytic activity measurements

Metoprolol tartrate (>99% Sigma) (MTP) was used as target contaminant to test the catalytic activity of the synthesized materials in photocatalytic oxidation, photocatalytic ozonation, and catalytic ozonation experiments. In addition, experiments of adsorption of MTP onto AC and MTP ozonation, both in the darkness and under illumination (i.e., photolytic ozonation), were completed.

Photocatalytic experiments were carried out in semi-batch mode in a laboratory-scale system consisting of a 1 L glass-made cylindrical reactor with an internal diameter of 10.7 cm, provided with a gas inlet, a gas outlet and a liquid sampling port. The reactor was placed in the chamber of a commercial solar simulator (Suntest CPS, Atlas) provided with a 1500 W air-cooled Xe arc lamp with emission restricted to wavelengths over 300 nm because of the presence of quartz and glass cut-off filters. The irradiation intensity was kept at 550 W m<sup>-2</sup> and the temperature of the system was maintained between 25 and 40°C throughout the experiments. If required, a laboratory ozone generator (Anseros Ozomat Com AD-02) was used to produce a gaseous ozone-oxygen stream that was fed to the reactor. In that case, the ozone concentration was recorded on an Anseros Ozomat GM-6000Pro gas analyzer.

In a typical photocatalytic ozonation experiment, the reactor was first loaded with 750 mL of an aqueous solution containing 50 mg L<sup>-1</sup> MTP initial concentration. Then, 0.28 g of the catalyst were added and the suspension was stirred in the darkness for 30 min while bubbling air to the system. After this dark stage, the lamp was switched on and, simultaneously, a mixture of ozone-oxygen (6 mg L<sup>-1</sup>

ozone concentration) was fed to the reactor at a flow rate of 20 L h<sup>-1</sup>. The irradiation time for each experiment was 5 h. Samples were withdrawn from the reactor at intervals and filtered through a 0.2 μm PET membrane to remove the photocatalyst particles.

MTP adsorption (i.e., absence of radiation and ozone), MTP single ozonation (i.e., absence of radiation and catalyst), MTP catalytic ozonation (i.e., absence of radiation) and MTP photolytic ozonation (i.e., absence of catalyst) experiments were also carried out for comparative analysis. In addition, the ability of radiation to decompose ozone in the absence of MTP was tested. For that, the photoreactor was loaded with 750 mL of ozone saturated–ultrapure water ( $C_{O_3,0} \sim 1.6 \times 10^{-4}$  mol L<sup>-1</sup>) and the system was allowed to react either under illumination or in the dark for 10 min.

Some experiments were carried out supplementing the reaction device with specific filter sheets that selectively block UV radiation. To cut off all the wavelengths below 390 nm, a flexible polyester thin film (Edmund Optics) was used while a polyester film (Unipapel) was used to cut off UV radiation below 320 nm.

To test the reusability of a selected catalyst, ten consecutive photocatalytic ozonation experiments were carried out recovering the catalyst particles with an external magnet after each experiment and reusing them in the next run without further modification.

MTP concentration was analyzed by high-performance liquid chromatography HPLC-DAD (Hitachi, Elite LaChrom) using a Phenomenex C-18 column (5 μm, 150 mm long, 3 mm diameter) as stationary phase and 0.5 mL min<sup>-1</sup> of 15:85 acetonitrile:acidified water (0.1% phosphoric acid) as mobile phase (isocratic). An UV detector set at 225 nm was used for detection. MTP intermediates formed during different experiments were analyzed by HPLC-qTOF. Details of the analyses are given as supplementary information.

Total organic carbon (TOC) was measured using a Shimadzu TOC-V<sub>SCH</sub> analyzer. Aqueous ozone was measured by following the indigo method using a UV-Visible spectrophotometer (Evolution 201, Thermospectronic) set at 600 nm [13]. Ozone in the gas phase was continuously monitored by means of an Anseros Ozomat GM-6000Pro analyzer. Hydrogen peroxide concentration was determined photometrically by the cobalt/bicarbonate method, at 260 nm using a UV-Visible spectrophotometer (Evolution 201, Thermospectronic) [14]. Iron and titanium in solution were analyzed by inductively coupled plasma mass spectrometry using a Perkin Elmer NexION 300D ICP-MS apparatus.

## 6.4. Results and discussion

### 6.4.1. Characterization of the fresh catalysts

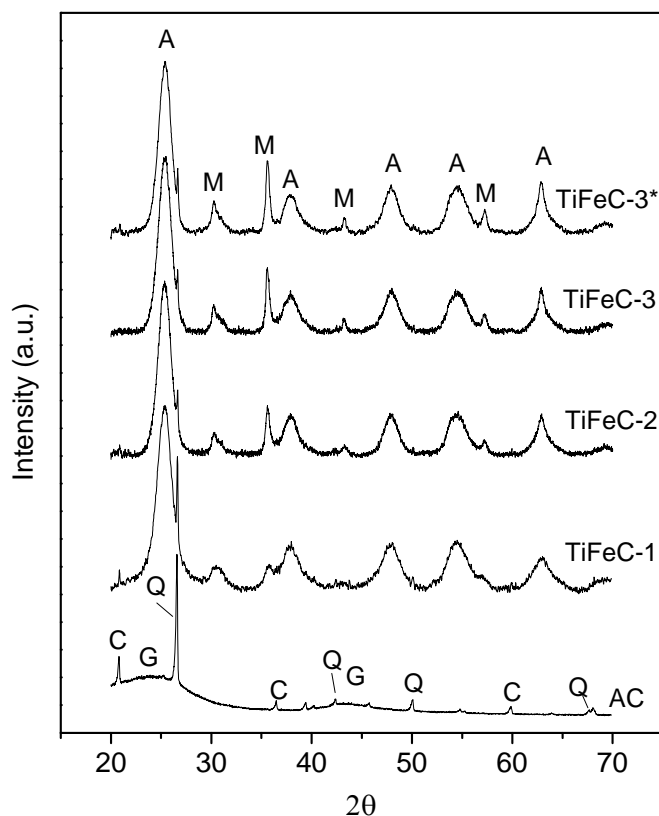
Table 6.2. summarizes the composition, crystallite sizes and main textural parameters of three selected TiFeC catalysts and the starting AC. Also, properties of a catalyst after being used in ten consecutive photocatalytic ozonation runs (namely TiFeC-3\*) are shown in Table 6.2. As it can be seen in Table 6.2., catalyst TiFeC-1 had lower Fe and TiO<sub>2</sub> contents than the catalysts TiFeC-2 and TiFeC-3 as a result of a lower metal loading during the preparation method (see Table 6.1.). The catalysts TiFeC-2 and TiFeC-3 had a similar content of TiO<sub>2</sub> and C but the amount of Fe in the latter was almost 20% higher than in the first. This suggests that calcination conditions (see Table 6.1.) play an important role in the fixation of Fe to the carbon surface. Regarding TiO<sub>2</sub> mass composition of the TiFeC catalysts, the final titania content of the catalysts was always somewhat lower than expected (i.e. 66 wt% for TiFeC-1 and 80 wt% for TiFeC-2 and TiFeC-3) likely due to the loss of some TiO<sub>2</sub> during the washing steps of the synthesis procedure.

**Table 6.2.** Bulk composition (wt%), XRD crystallite sizes and textural properties of TiFeC catalysts and the activated carbon used as support

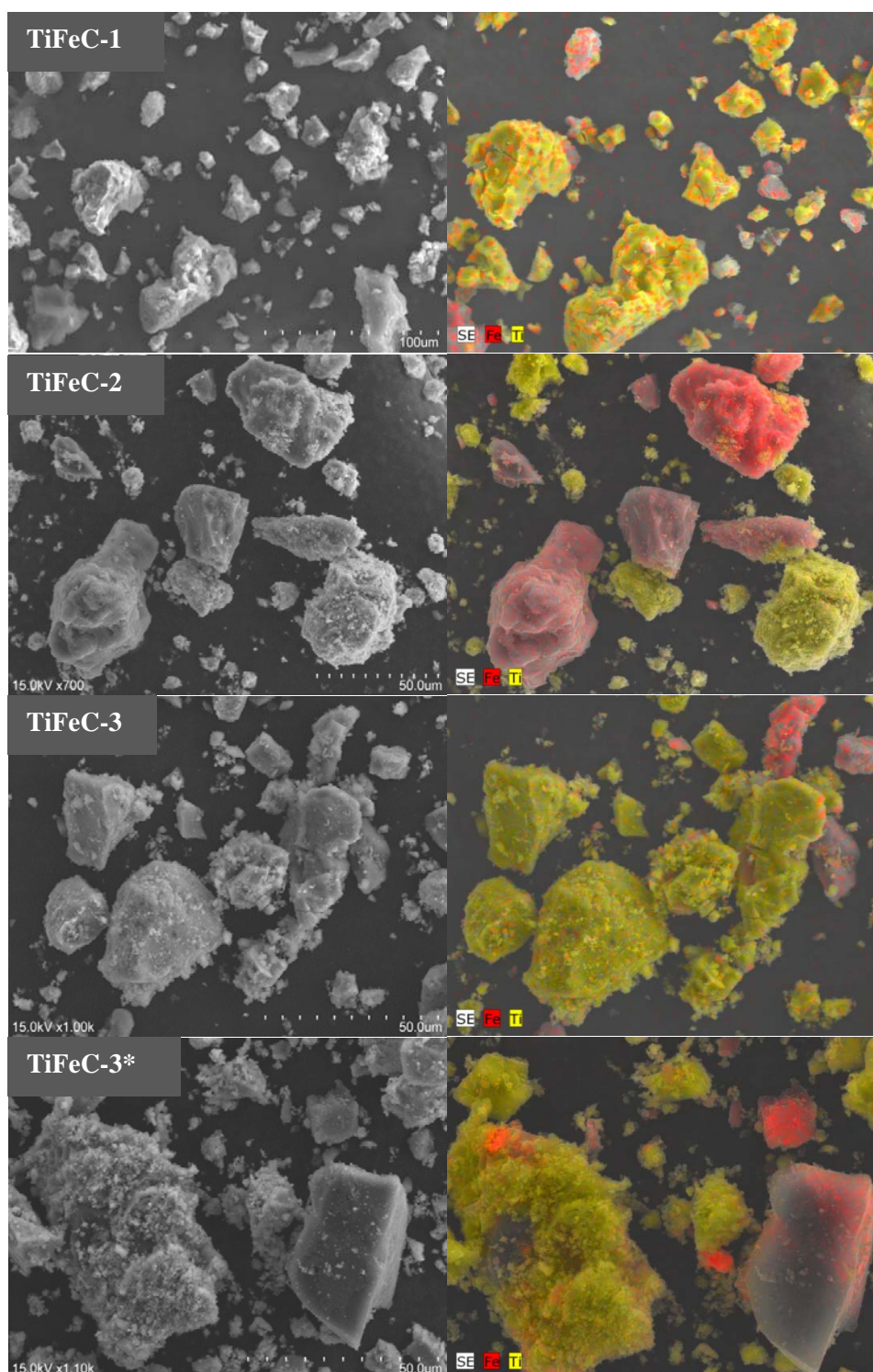
Sample	Fe (%)	TiO <sub>2</sub> (%)	C (%)	d <sub>A</sub> (nm)	d <sub>M</sub> (nm)	S <sub>BET</sub> (m <sup>2</sup> g <sup>-1</sup> )	S <sub>EXT</sub> (m <sup>2</sup> g <sup>-1</sup> )	V <sub>MICRO</sub> (cm <sup>3</sup> g <sup>-1</sup> )
AC	3.7	0	84.9	---	---	640	51	0.299
TiFeC-1	5.0	53.5	34.3	4.6	9.0	331	65	0.163
TiFeC-2	7.6	65.4	21.2	5.3	16.5	285	113	0.152
TiFeC-3	8.9	64.0	20.0	5.1	17.5	263	118	0.147
TiFeC-3*	n.m.	n.m.	n.m.	5.3	17.9	231	98	0.120

Figure 6.1. shows the XRD patterns obtained for the AC support and TiFeC catalysts. From the AC diffractogram, some characteristic diffraction peaks of graphite can be identified, as the two broad peaks at  $2\theta = 26$  and  $43^\circ$ . Other diffraction peaks are due to the presence of SiO<sub>2</sub>-quartz and SiO<sub>2</sub>-cristoballite particles which are common minerals in the activated carbon used in this work [8]. Regarding the TiO<sub>2</sub> structure, XDR patterns obtained for the three catalysts show

diffraction peaks at 25.4, 37.9, 47.9, 54.4 and 62.8° which confirm the presence of anatase in all cases. The anatase crystallite size,  $d_A$ , was calculated from the (101) diffraction peak using the Scherrer equation and the results are summarized in Table 6.2. It can be noticed a slight increase in the anatase particle size with the increasing content of  $\text{TiO}_2$  on the catalyst.  $\text{Fe}_3\text{O}_4$  magnetite or  $\gamma\text{-Fe}_2\text{O}_3$  maghemite species could also be identified (these two are indistinguishable by XRD) in the XRD patterns of the TiFeC catalysts with main reflection peaks at 30.2, 35.6, 43.1 and 57.0°. The intensity of the main peaks increases according to the sequence  $\text{TiFeC-1} < \text{TiFeC-2} < \text{TiFeC-3}$ , which is likely connected to the higher amount of iron loaded on the last two samples and the more drastic heat treatment carried out for their preparation. The magnetite-maghemite crystallite sizes were calculated by means of the Scherrer equation from the (311) diffraction peak. As can be seen in Table 6.2., the catalysts TiFeC-2 and TiFeC-3 exhibited a much larger crystallite size than the catalyst TiFeC-1.



**Figure 6.1.** XRD patterns of the AC support and some TiFeC catalysts. Crystalline phases detected: anatase (A), magnetite/maghemite (M), graphite (G), quartz (Q), cristoballite (C). TiFeC-3\* represents catalyst TiFeC-3 after being used in ten consecutive photocatalytic ozonation runs.



**Figure 6.2.** SEM images (left) and EDX mapping (right) for the TiFeC catalysts

BET area,  $S_{\text{BET}}$ , external surface area,  $S_{\text{EXT}}$ , and micropore volume,  $V_{\text{MICRO}}$ , were obtained from the nitrogen adsorption–desorption isotherms (not shown) and their values are presented in Table 6.2. All the samples showed type I isotherm, as it has already been reported for this type of samples [8], which is characteristic of microporous materials. The micropore volume of the prepared catalysts was much lower than that of the starting AC, which suggests that iron oxides and  $\text{TiO}_2$  might block some pore entrances of the AC [11]. On the other hand, the external surface areas of the catalysts were larger than that of the AC. This can be due to the generation of agglomerates of  $\text{TiO}_2$  on the surface of the AC, thus giving rise to the formation of new larger pores in the range of meso and macropores.

Figure 6.2. shows SEM images of the three catalysts and the distribution of Fe and Ti species by means of energy dispersive X-ray analysis (EDX). As can be seen in the images, the particle size distribution is wide with particles in the 5–125  $\mu\text{m}$  size range. A non-uniform distribution of Fe and Ti on all the three catalysts could be observed (see Figure 6.2., right). However, it is important to note that Fe can be found in all the particles analyzed since catalyst particles were magnetically separated after the washing steps in the catalyst preparation method.

Surface chemical composition of the catalysts was analyzed by XPS and the results are summarized in Table 6.3. and Figure 6.3. (only for catalyst TiFeC-3 as an example). XPS full spectra of the three catalysts confirmed the presence of C, Ti, O and Fe on their surface (see Figure 6.3A. for catalyst TiFeC-3). The surface composition of the catalysts (Table 6.3.) was calculated from peak areas and Wagner atomic sensitivity factors [15]. It can be noticed that all the catalyst presented fairly similar atomic surface Ti content though somewhat lower in catalyst TiFeC-2. On the other hand, the percentage of atomic surface Fe increased as bulk iron content of the catalysts was larger (see also Table 6.2.), being the highest on the catalyst TiFeC-3.

**Table 6.3.** XPS results of TiFeC catalysts

Sample	Surface composition (atomic %)				Fe 2p peaks position				Ti 2p peaks position	
	Ti (%)	O (%)	C (%)	Fe (%)	Fe 2p <sub>3/2</sub> (eV)	Fe 2p <sub>1/2</sub> (eV)	Sat-Fe <sup>2+</sup> (eV)	Sat-Fe <sup>3+</sup> (eV)	Ti 2p <sub>3/2</sub> (eV)	Ti 2p <sub>1/2</sub> (eV)
TiFeC-1	15.2	45.5	37.9	1.4	711.0	724.3	715.3	718.8	459.7	465.4
TiFeC-2	13.0	43.5	41.4	2.1	710.9	724.5	715.4	718.8	459.7	465.4
TiFeC-3	15.0	42.0	39.6	3.4	710.7	724.8	715.4	718.9	459.8	465.5
TiFeC-3*	16.9	45.4	32.6	5.1	712.0	725.1	n.d.	719.3	459.5	465.2



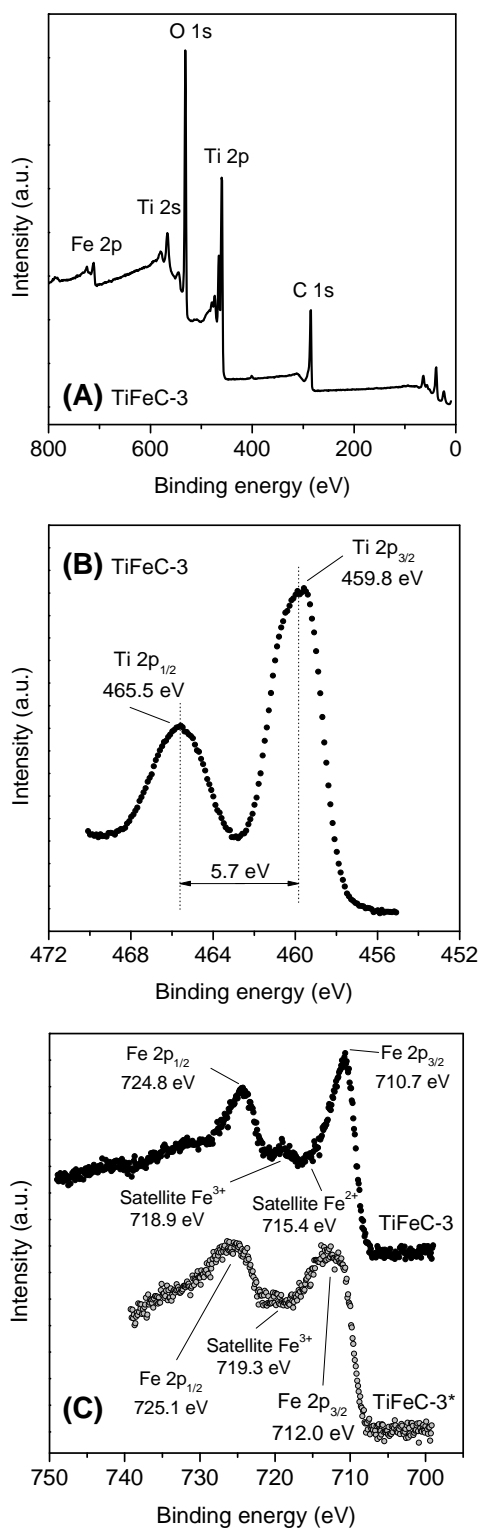


**Figure 6.3.** XPS full spectrum of catalyst TiFeC-3 (A), High-resolution XPS spectra of Ti2p (B) and Fe2p (C) spectral regions

Figure 6.3B. shows the high-resolution Ti 2p XPS spectrum for catalyst TiFeC-3. The binding energy peaks located at 459.8 and 465.5 eV can be attributed to the spin-orbit splitting of the Ti 2p components (Ti 2p<sub>3/2</sub> and Ti 2p<sub>1/2</sub>), with a difference in binding energy of ca. 5.7eV, which confirms the presence of Ti as Ti<sup>4+</sup> (TiO<sub>2</sub>) [16,17]. Similarly, Figure 6.3C. displays the high resolution Fe 2p XPS spectrum for catalyst TiFeC-3. The peak positions of Fe 2p<sub>3/2</sub> and Fe 2p<sub>1/2</sub> at ca. 710.7 and 724.8 eV, respectively, are consistent with the existence of magnetite (Fe<sub>3</sub>O<sub>4</sub>) [18,19]. On the other hand, the presence of satellite peaks at ca. 718.9 and 715.4 eV is attributable to the existence of Fe<sup>3+</sup> and Fe<sup>2+</sup> iron species, respectively [18]. Since it has been previously reported that Fe 2p<sub>3/2</sub> for pure Fe<sub>3</sub>O<sub>4</sub> does not have a satellite peak [20], the coexistence of other iron species such as maghemite ( $\gamma$ -Fe<sub>2</sub>O<sub>3</sub>) or FeO cannot be disregarded. Similar XPS results were found for the three fresh catalysts, as can be inferred from data in Table 6.3.

Due to the presence of magnetic iron species (magnetite and/or maghemite) in the catalysts, magnetization of the samples was analyzed and results are depicted in Figure 6.4. As expected, higher iron content led to higher saturation magnetization ( $M_s$ ) of the samples (see value for  $M_s$  in Figure 6.4.). The catalyst TiFeC-3, which was synthesized under the most drastic conditions in terms of temperature and time of the heat treatment and also had the highest iron content among the prepared catalysts (see Table 6.1.), is the one that presented the highest  $M_s$ . For this catalyst, the value of saturation magnetization was found to be 4.4 emu g<sup>-1</sup>.

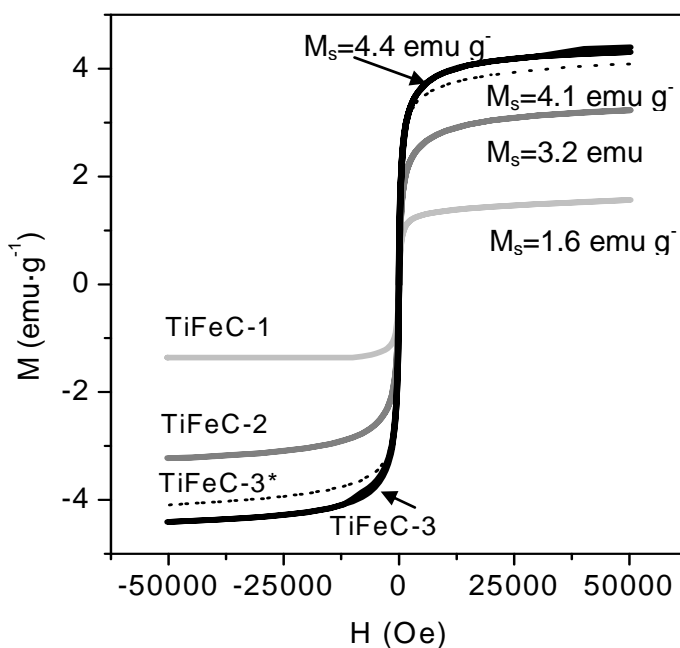


**Figure 6.4.** Magnetization vs. applied magnetic field at 25°C of TiFeC catalysts

Taking into account the iron content of this sample and considering that all iron could be converted into magnetite (bulk magnetite  $92 \text{ emu g}^{-1}$ ) a maximum  $M_s$  of  $12 \text{ emu g}^{-1}$  could be expected. However, it should be pointed out that magnetization of magnetite depends on the particle size and the particle distribution. Thus,  $M_s$  values lower than that of bulk magnetite (in the  $60\text{-}70 \text{ emu g}^{-1}$  range) have been found for magnetite particles of similar sizes of the crystallites found in TiFeC catalysts ( $\sim 10\text{-}20 \text{ nm}$ ) [21]. Also, magnetite readily reacts with oxygen to form maghemite, which has lower  $M_s$  than magnetite. Accordingly, partial oxidation of magnetite to maghemite in TiFeC catalysts is likely to take place. TiFeC-3 presented a much higher  $M_s$  value than TiFeC-1 and TiFeC-2, which could suggest a higher content of magnetic iron oxide (magnetite and maghemite) as also deduced from XRD and XPS results. This means that not only the iron content but also the heat treatment conditions (temperature and time) influences on the final content of magnetic iron oxide. It is also important to note that all the TiFeC catalysts showed zero coercivity and remanent magnetization indicating superparamagnetic behavior and thus the particles could be re-dispersed in solution for reuse after being separated by a magnet.

#### 6.4.2. Catalytic activity

The photoactivity of the synthesized catalysts was evaluated through simulated solar-light radiation (300-800 nm) photocatalytic oxidation and photocatalytic ozonation experiments aimed to degrade MTP. Some additional experiments were carried out to analyze the contributions of adsorption, direct ozonation and catalytic ozonation to the removal of MTP during the photocatalytic ozonation process. An initial concentration of MTP as high as  $50 \text{ mg L}^{-1}$  was used in the experiments, which allows us to analyze the effect of the catalysts in terms of mineralization (i.e. TOC depletion). Figure 6.5. shows the time evolution of MTP concentration and TOC during the course of some selected experiments.

As shown, MTP was adsorbed onto any of the catalysts surface to some extent, being the catalyst TiFeC-1 which presented the highest adsorption capacity (18% MTP removed after 5 h) while MTP uptake on catalysts TiFeC-2 and TiFeC-3 was only c.a. 12%. This result is in agreement with the highest BET surface area of TiFeC-1 (see Table 6.2.). It can be also noticed that in all cases adsorption equilibrium was practically reached in about 30 min, so relatively fast MTP adsorption took place.

Regarding photocatalytic oxidation, catalysts TiFeC-2 and TiFeC-3 were shown to be more efficient to degrade MTP than TiFeC-1 as it can be noticed in Figure 6.5. As seen in Figure 6.5., final MTP conversions obtained with catalysts TiFeC-2 and

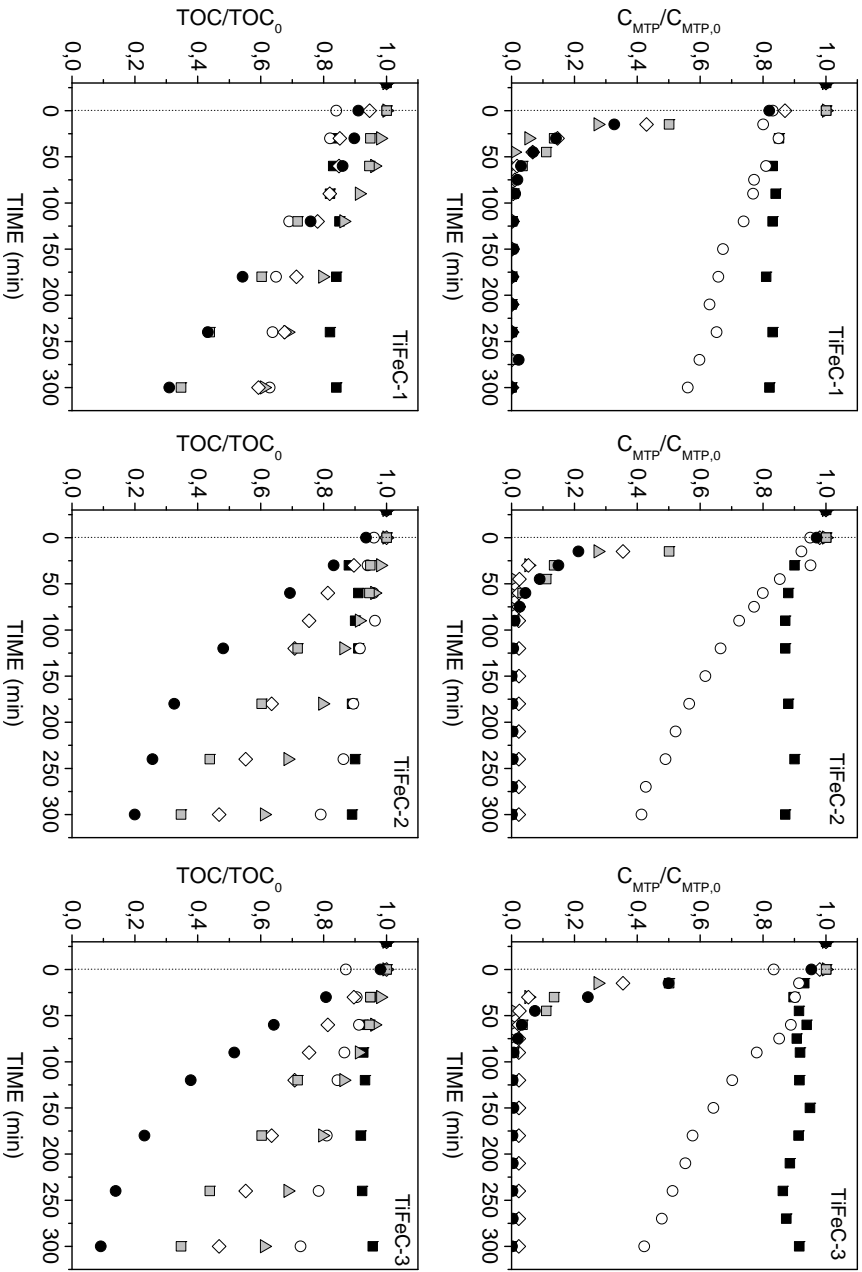


**Figure 6.5.** Evolution of dimensionless MTP concentration and TOC with time. Conditions:  $C_{MTP,0} = 50 \text{ mg L}^{-1}$ ,  $C_{CAT} = 375 \text{ mg L}^{-1}$ ,  $Q_g = 20 \text{ L h}^{-1}$ ,  $C_{O_3,g} = 6 \text{ mg L}^{-1}$ . Experiments: adsorption (■), photocatalytic oxidation (○), ozonation (△), catalytic ozonation (◇), photocatalytic ozonation (□), photocatalytic ozonation (●)

TiFeC-3 were ca. 60% while only 45% MTP conversion was reached when using the catalysts TiFeC-1. From these results, and taking into account the difference found in the TiO<sub>2</sub> content of the catalysts (TiFeC-2 and TiFeC-3 had a 10% more TiO<sub>2</sub> than TiFeC-1, see Table 6.2.), the removal efficiency of MTP may be mainly due to the oxidizing species generated by the photo-excitation of titania particles loaded onto the catalysts rather than to the adsorption capacity of the materials. Contribution of direct photolysis to the removal of MTP can also be ruled out as MTP does not absorb radiation at wavelength higher than 300 nm. From XPS results quite similar surface atomic Ti amounts were present on the three catalysts (Table 6.3.), accordingly it can be suggested that the simulated solar radiation could penetrate more than a few nanometers in samples (depth of XPS analysis), thus exciting TiO<sub>2</sub> particles located at deeper sites on the activated carbon. Contrary to MTP removal, TOC removal after 5 h was higher when using catalyst TiFeC-1 (c.a. 30% conversion) than in experiments using TiFeC-2 and TiFeC-3 (c.a. 20% conversion). This suggests that catalyst TiFeC-1 is able to absorb MTP degradation products to a higher extent than TiFeC-2 or TiFeC-3.

As can be observed in Figure 6.5., all the treatments using ozone (i.e. single ozonation, catalytic ozonation, photolytic ozonation and photocatalytic ozonation) led to much faster MTP degradation rates than the photocatalytic oxidation treatment regardless of the catalyst used. In all ozonation experiments MTP depletion rate was quite similar, which suggests that MTP removal occurs mainly through direct ozone reaction with low catalytic effect. Similar results have been observed previously for compounds that react fast with ozone, such as diclofenac and sulfamethoxazole [22]. MTP has also a relatively high rate constant for its reaction with ozone ( $k_{O_3-MTP} = 2.9 \times 10^2 \text{ L mol}^{-1} \text{ s}^{-1}$  at pH 6) [23]. Main differences among ozone processes were observed in mineralization profiles.

Single ozonation led to just about 40% TOC removal after the 5-hour reaction period. Ozone, despite being a strong oxidizing agent, reacts selectively primarily with aromatic and unsaturated compounds. As a result of direct ozonation of MTP non-aromatic and non-unsaturated intermediates compounds are formed (e.g., short-chain carboxylic acids), which react slowly with ozone. As a result, they are accumulated in water [24,25].

The presence of catalyst greatly improved mineralization rates compared to ozone alone. Thus, TOC conversion reached 40-50% and 70-90% after catalytic ozonation and photocatalytic ozonation experiments, respectively. Various catalytic and photolytic effects leading to the formation of hydroxyl radicals, which can unselectively oxidize organic compounds in water, can be addressed. First, in the absence of radiation (i.e., catalytic ozonation), ozone can be partially

transformed into hydroxyl radicals by the action of the activated carbon used as support [26–29] as well as the supported  $\text{TiO}_2$  [29,30] and iron oxides [29,31]. According to the results shown in Figure 6.5. it is apparent that the effects of metal oxides ( $\text{TiO}_2$  and/or iron oxides) were greater than that of the AC, as higher TOC conversions were achieved with catalyst TiFeC-2 and TiFeC-3, which had higher amounts of Ti and Fe in their composition than catalyst TiFeC-1. In the presence of radiation (i.e., photocatalytic ozonation), in addition to the aforementioned catalytic effects, ozone can absorb UV-photons to yield excited atomic oxygen species that further generate hydroxyl radicals [32,33]. Thus, as can be seen in Figure 6.5., 65% TOC conversion was reached in the photolytic ozonation experiment in contrast to 40% achieved in the single ozonation experiment carried out in the absence of radiation. In addition, the well-know photocatalytic effect of the semiconductor anatase must be considered. This effect can be greatly improved by the presence of ozone, which due to its electrophilic nature, is prone to trap the electrons from the semiconductor conduction band generating ozonide radicals, which are further transformed into additional  $\cdot\text{OH}$  [5,6]. Finally, iron oxides present in the catalysts could also play a photocatalytic role. Thus, as hydrogen peroxide can be generated from ozonation of MTP [24], iron oxides can catalyze photo-Fenton like reactions.

#### A. Effect of radiation wavelength

The results above show the importance of photolytic decomposition of ozone in the MTP mineralization rate. To evaluate the effect of the radiation wavelength in the photolytic ozonation process, some experiments were carried out using filters that selectively cut off particular wavelengths from the solar spectrum. Figure 6.6. shows the evolution of MTP concentration and TOC with time during photolytic ozonation experiments carried out with radiation of wavelengths ranging between 300-800, 320-800 and 390-800 nm. Results from a single ozonation experiment in the darkness are also shown.

As shown in Figure 6.6., MTP removal profiles were quite similar for all the experiments suggesting that MTP was mainly removed through direct reaction with ozone and the effect of radiation was negligible. However, from TOC results, it is evident that the 300-320 nm radiation enhanced the efficiency of TOC removal due to photolytic transformation of ozone into reactive oxygen species, which would eventually be transformed into in hydroxyl radicals [33].

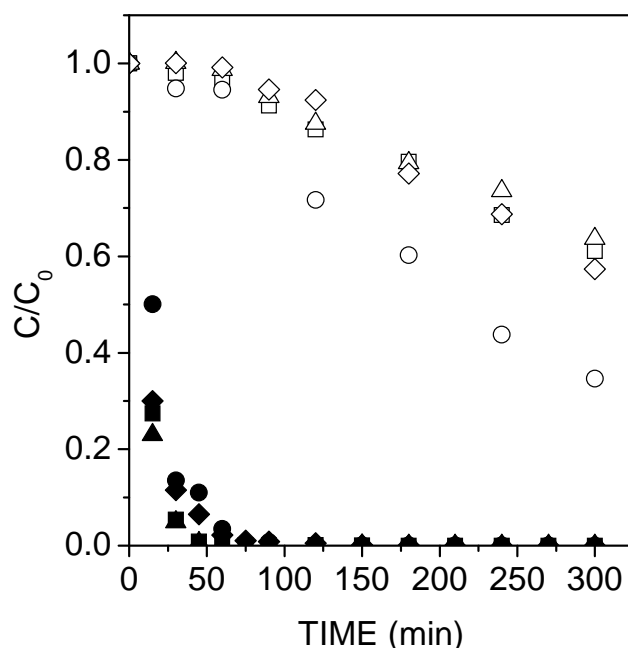


**Figure 6.6.** Evolution of dimensionless MTP concentration (solid symbols) and TOC (open symbols) with time. Conditions:  $C_{MTP_0} = 50 \text{ mg L}^{-1}$ , gas flow rate =  $20 \text{ L h}^{-1}$ ,  $C_{O_3,g} = 6 \text{ mg L}^{-1}$ . Experiments: ozonation (■,□), photolytic ozonation (300-800 nm) (●,○), photolytic ozonation (320-800 nm) (▲,△), photolytic ozonation (390-800 nm) (◆,◇)

To quantify the effect of different radiation wavelengths on the ozone decomposition, some experiments of ozone photolytic depletion from ozone saturated-ultrapure water were carried out. Aqueous ozone decomposition followed pseudo-first order kinetics:

$$-\frac{dC_{O_3}}{dt} = k_{app} C_{O_3} \quad (6.1)$$

Fitting results of experimental data to equation (6.1), the values summarized in Table 6.4. for the apparent rate constant were obtained. Since no great differences were found for the apparent rate constant in the darkness and under illumination with 320-800 and 390-800 nm radiation while  $k_{app}$  was much higher for the process under illumination with 300-800 nm radiation, it could be confirmed that the photolytic decomposition of ozone occurs primarily at wavelengths from 300 to 320 nm. Radiation wavelength over 320 nm does not significantly produce ozone photolysis and, therefore, did not improve MTP mineralization process performance. Photolytic decomposition of ozone has been also observed under

natural sunlight where a small fraction of radiation below 320 nm reaches the Earth surface and needs to be considered in solar-ozone processes.

**Table 6.4.** Experimental pseudo-first order apparent rate constants ( $k_{app}$ ) for  $O_3$  depletion in water at different wavelengths

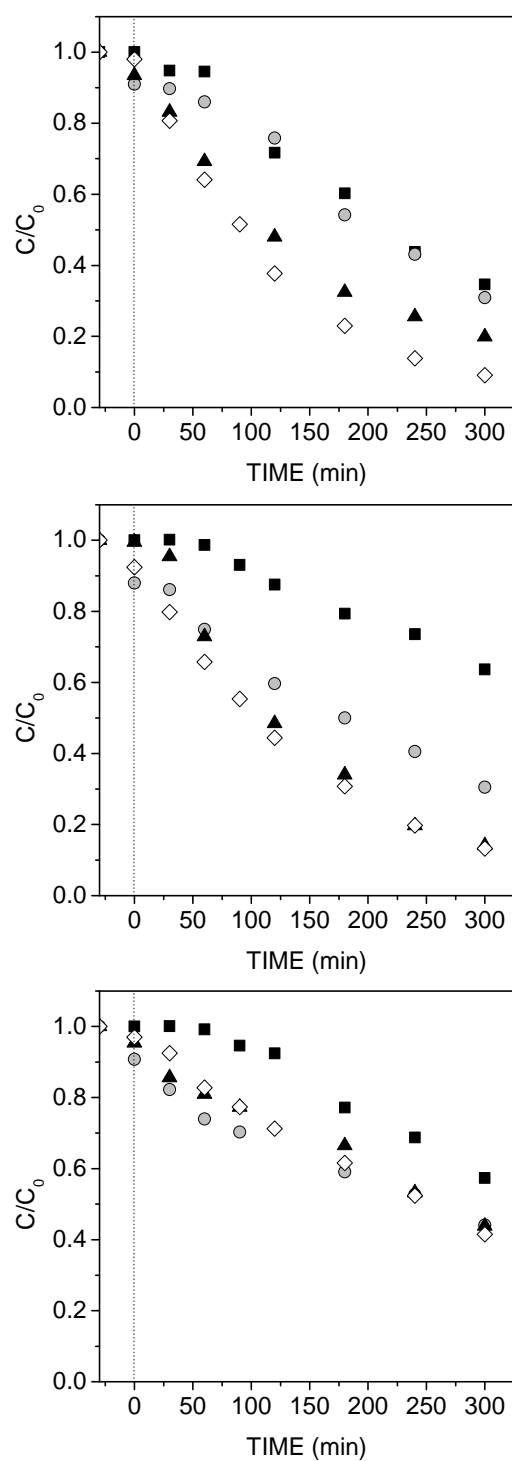
Conditions	$k_{app}$ ( $\text{min}^{-1}$ )	$R^2$
No radiation	0.071	0.995
390-800nm	0.068	0.995
320-800nm	0.083	0.996
300-800nm	0.123	0.997

Figure 6.7. shows the TOC profiles during some photocatalytic ozonation experiments carried out with different wavelength radiation and using TiFeC catalysts. Results from photolytic experiments (in the absence of catalyst) are also shown.

As a general trend, from Figure 6.7. it can be noticed that regardless of the radiation wavelength, the presence of any of the catalyst increased to some extent the MTP mineralization rate. When irradiated with 390-800 nm radiation (Figure 6. 7C.), the three catalysts led to similar mineralization degree. When compared with the results obtained in a catalytic ozonation experiment (Figure 6.5.), only slightly higher mineralization percentages were reached in the presence of the irradiated catalysts, suggesting that they have low activity under visible light irradiation.

Photocatalytic ozonation systems mediated by 300-800 and 320-800 nm radiation led to similar mineralization percentages with somewhat higher mineralization rate by using 300-800 nm radiation. These results are in contrast to photolytic ozonation that lost efficiency at 320-800 nm since the production of hydroxyl radicals from ozone photodissociation is minimized at wavelengths higher than 320 nm. Thus, when using 300-800 nm radiation, the catalytic effect of the synthesized materials can be masked by the ozone photolysis reaction, being preferable to use radiation of wavelength higher than 320 nm to evaluate the catalytic activity in the process studied (photocatalytic ozonation). In that sense, Figure 6.7B. shows that higher mineralization rates were obtained in the presence of the catalysts being TiFeC-2 and TiFeC-3 the catalysts with the best performance.





**Figure 6.7.** Evolution of TOC with time. Conditions:  $C_{MTP_0} = 50 \text{ mg L}^{-1}$ ,  $Q_g = 20 \text{ L h}^{-1}$ ,  $C_{O_{3,g}} = 6 \text{ mg L}^{-1}$ . Experiments: photolytic ozonation (■) and photocatalytic ozonation with TiFeC-1 (○), TiFeC-2 (▲), TiFeC-3 (◇)

## B. Simplified mechanistic approach

According to the above results, the reaction mechanism that takes place in the overall MTP photocatalytic ozonation process with a TiFeC catalyst could be explained as the sums of contributions and synergy of several processes (i.e. direct ozone reaction, ozone photolytic decomposition, heterogeneous photocatalysis, Fenton and photo-Fenton reactions, etc.). Figure 6.8. shows the time-evolution of dissolved ozone and hydrogen peroxide during single ozonation, catalytic ozonation and photocatalytic ozonation experiments carried out in the presence of catalyst TiFeC-3.

From Figure 6.8B. it can be noticed that ozone accumulated in solution during the single ozonation experiment reaching its maximum concentration at about 30 min reaction time, then slowly decreasing its concentration with time. A similar profile was observed during catalytic ozonation but with a slightly faster depletion rate. In contrast, in photocatalytic ozonation reaction, the maximum concentration of dissolved ozone was noticeably lower and a faster depletion rate was observed during the first 60 min, leading to a nearly steady concentration of about  $5 \times 10^{-6}$  mol L<sup>-1</sup>. The lowest values of dissolved ozone and the highest mineralization rate observed in the photocatalytic ozonation experiment suggest that besides direct MTP-O<sub>3</sub> reaction, or in lesser extent side reactions with catalyst surface (activated carbon or iron), O<sub>3</sub> was also consumed through its reaction with electrons on the TiO<sub>2</sub> surface improving MTP mineralization due to the generation of additional hydroxyl radicals [6,34].

Generation of hydrogen peroxide by direct ozonation of MTP has been previously proposed as a step of MTP degradation mechanism [35]. This has been confirmed experimentally in this work, as shown in Figure 6.8A. In contrast, H<sub>2</sub>O<sub>2</sub> concentration during the photocatalytic ozonation experiment was much lower likely due to the consumption of H<sub>2</sub>O<sub>2</sub> through surface photo-Fenton reactions (liquid bulk photo-Fenton reactions could be neglected as the concentration of iron in solution was rather low ca.  $1.5 \times 10^{-7}$  mol L<sup>-1</sup>) and/or its reaction on the TiO<sub>2</sub> surface as electron acceptor.

Intermediate compounds from MTP degradation during photocatalytic oxidation, ozonation and photocatalytic ozonation have been analyzed by HPLC-qTOF. Results show the generation of six main intermediates (MTP-133, MTP-237, MTP-239, MTP-253, MTP-283 and MTP-299) whose structure, name and other details can be found in the supplementary information. In general, they are large molecules which have been reported previously to be formed through O<sub>3</sub> and/or <sup>•</sup>OH attack to MTP [25, 35–38]

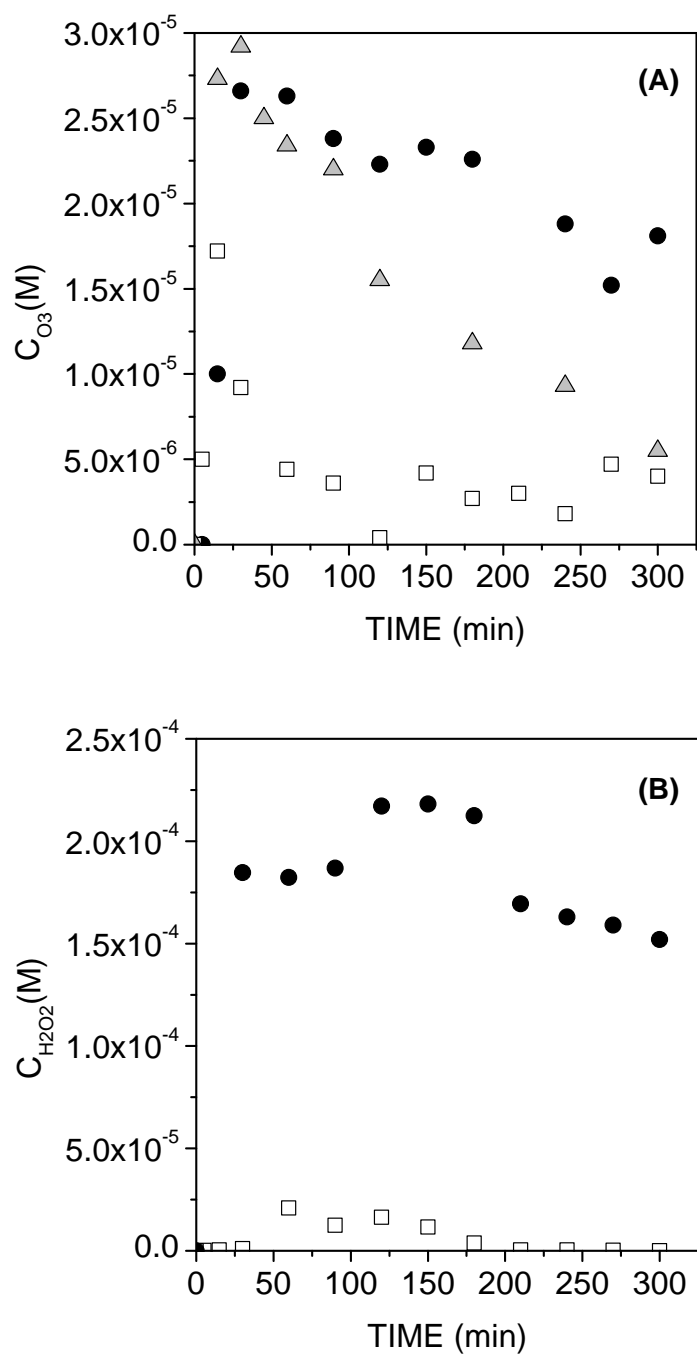


**Figure 6.8.** Evolution of dissolved ozone (A) and hydrogen peroxide (B) with time. Conditions:  $C_{MTP_0} = 50 \text{ mg L}^{-1}$ ,  $Q_g = 20 \text{ L h}^{-1}$ ,  $C_{O_3,g} = 6 \text{ mg L}^{-1}$ . Experiments: Single ozonation (●), catalytic ozonation (Δ) and photocatalytic ozonation with TiFeC-3 (□)

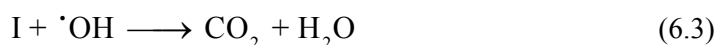
According to the findings of this work, it can be postulated that photocatalytic ozonation of MTP with TiFeC catalysts takes place through reactions (6.2) to (6.11), where ozone is the main species responsible for MTP disappearance and  $\cdot\text{OH}$  (on the catalyst surface or in solution) is the main responsible species for MTP mineralization.

MTP direct ozonation:

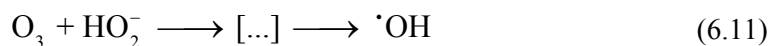
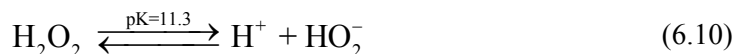
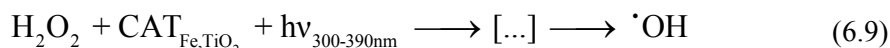
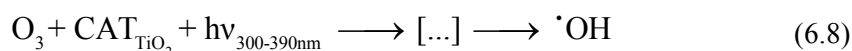
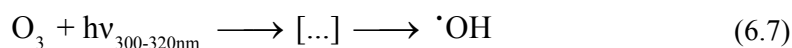
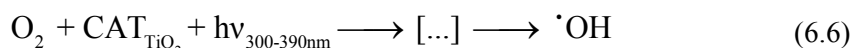
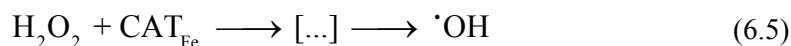
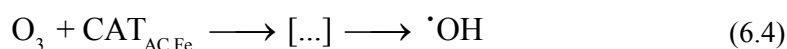


where I represents any intermediate or by-product of MTP oxidation pathway.

Hydroxyl radical attack to intermediate products:



Hydroxyl radical formation:



Reactions (6.4) to (6.9) and (6.11) involve intermediate steps that have been represented as [...]. Reaction (6.4) also involves the catalytic effect of activated carbon and iron in the catalyst in the ozone decomposition reaction; reaction (6.5) would be mainly due to Fenton like reaction due to the iron species in the catalyst surface; reaction (6.6) represents the conventional photocatalytic oxidation (with oxygen) set of reactions; (6.7) is the photolytic decomposition of ozone that has been proved to take place at wavelengths between 300-320 nm; reaction (6.8)

involves the role of ozone as electron acceptor on the  $\text{TiO}_2$  surface; reaction (6.9) considers, as a whole, the photo-Fenton reactions on the catalyst surface and the role of hydrogen peroxide as electron acceptor on the  $\text{TiO}_2$  surface; and reaction (6.11) groups the series of reactions that yield hydroxyl radical from the starting reaction between ozone and hydroperoxide ion.

The relative contribution of each step to the overall process would depend on the experimental reaction conditions (e.g., pH, ozone dose, radiation wavelength) and the catalyst structure and composition. This issue will be the subject of a future work.

### C. Catalyst reusability

Since catalyst TiFeC-3 showed the best catalytic performance and separability, further experiments were carried out to test its stability and reusability. Thus, a series of ten consecutive MTP photocatalytic ozonation runs were performed under 320-800 nm radiation. This wavelength range was chosen to isolate to some extent the catalytic effect. Thus, at those conditions the effect of the photocatalytic route on the MTP mineralization is high while keeping low the contribution of the photolysis of ozone. In each run, the catalyst was kept 30 min in the darkness to reach adsorption equilibrium. Only slight changes in adsorption capacity were observed throughout the reuse of the catalyst, varying the percentage of MTP adsorbed from c.a. 13% to 8% with no trend (not shown). This result points out that adsorbed molecules are also oxidized during the treatment and the adsorption capacity of the catalysts remains almost constant.

Figure 6.9. shows TOC removal percentages obtained after the ten consecutive runs (5 h each) reusing the catalyst. After each run the catalyst was easily separated from the liquid by means of a magnet placed outside at the bottom of the reactor. After removing the liquid, a new fresh MTP solution was added to the reactor to start the following run.

As shown in Figure 6.9. the catalyst exhibited no significant catalytic loss keeping overall TOC removal at about 75-85% decrease surmounting 85% mineralization during the first 6 runs and 75% mineralization for the last 4 runs. It is important to note here that in all runs complete removal of MTP was achieved in less than 2 h.

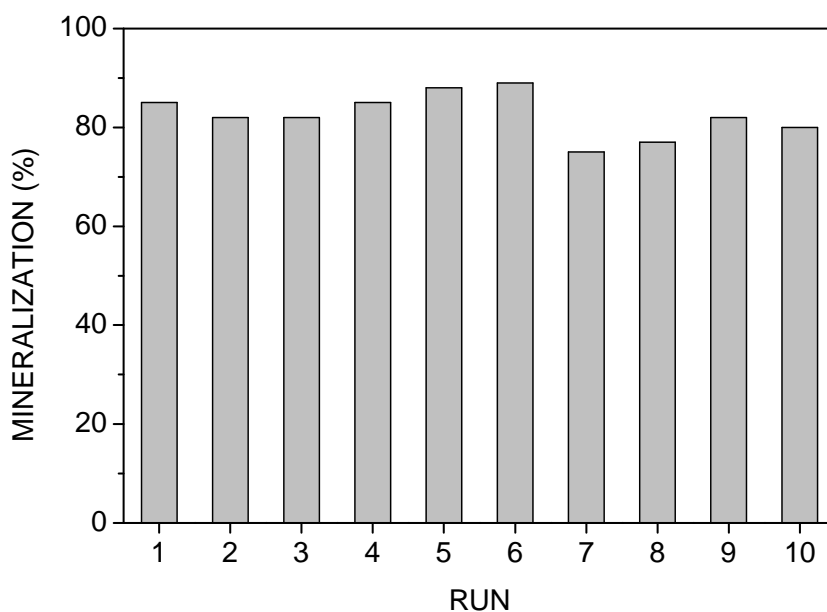


**Figure 6.9.** TOC conversion for consecutive photocatalytic ozonation runs with TiFeC-3 catalyst. Conditions:  $C_{MTP_0} = 50 \text{ mg L}^{-1}$ ,  $C_{CAT} = 375 \text{ mg L}^{-1}$ ,  $Q_g = 20 \text{ L h}^{-1}$ ,  $C_{O_3,g} = 6 \text{ mg L}^{-1}$ , radiation wavelength 320-800 nm

Also, no significant changes were observed throughout the series of runs in the value of the apparent pseudo-first order rate constant calculated for MTP depletion (see Table 6.5.). Table 6.5. also shows the concentration of iron found in solution after each run. As can be observed very low amount of iron was leached from the catalyst being the aqueous concentration always lower than  $0.02 \text{ mg L}^{-1}$ . From the mass balance, the total amount of iron leached out of the catalyst after the ten runs was found to be only a 0.25% of the amount initially present. Regarding titanium, after each run its concentration was lower than  $10 \mu\text{g L}^{-1}$ .

**Table 6.5.** Pseudo-first order apparent rate constant for MTP depletion in consecutive photocatalytic ozonation runs and iron leached out from catalyst TiFeC-3

Run	$k_{app}$ ( $\text{min}^{-1}$ )	$R^2$	$C_{Fe}$ ( $\text{mg L}^{-1}$ )
1	0.040	0.996	0.008
2	0.032	0.997	0.008
3	0.034	0.998	0.006
4	0.037	0.989	0.017
5	0.048	0.990	0.004
6	0.055	0.997	0.014
7	0.036	0.990	0.004

**Table 6.5. (continued)** Pseudo-first order apparent rate constant for MTP depletion in consecutive photocatalytic ozonation runs and iron leached out from catalyst TiFeC-3

Run	$k_{app}$ ( $\text{min}^{-1}$ )	$R^2$	$C_{Fe}$ ( $\text{mg L}^{-1}$ )
8	0.032	0.993	0.002
9	0.041	0.969	0.008
10	0.048	0.983	0.010

Therefore, the catalyst TiFeC-3 seems to be very stable and easily separable to be used in repeated runs or even in continuous flow experiments. However, the reaction medium (ozone, hydroxyl radicals, radiation, etc.) could provoke the modification of some important properties of the catalysts apart from iron or titanium leaching. In this line, the catalyst recovered after being used in the ten consecutive runs (named as TiFeC-3\* in tables and figures) was characterized.

From the XRD patterns (Figure 6.1.) no significant changes were observed when comparing the fresh and used catalysts. Anatase and magnetite/maghemite patterns could be identified in both diffractograms and no substantial changes in the crystallite sizes were observed (Table 6.2.). Also in Table 6.2., textural properties of the fresh and used catalysts are summarized. All the textural parameters underwent a slight decrease after using the catalyst for 50 h, although these lower values seem not to affect the catalytic activity of the material. Also SEM and EDX images (Figure 6.2.) show no apparent modification on the catalyst surface where a non-uniform distribution of iron and titanium is observed. On the other hand, XPS results are summarized in Table 6.3. It can be noticed a slight decrease in the surface carbon content of the used sample respect to the fresh one and an increase in the surface iron content (from 3.4 to 5.1%). This can be due to the reaction between ozone and carbon atoms in the surface of AC, that can release organic products to the liquid reaction medium leading to a catalyst mass loss [39], and leaving more iron exposed on the catalyst surface. Regarding to the surface species on the catalysts, no significant differences were found in the XPS spectra of C 1s, O 1s and Ti 2p. However, iron Fe 2p XPS spectra showed slight differences and it has been plotted in Figure 6.3. for comparison purposes. First of all, it can be observed that the Fe 2p<sub>1/2</sub> and Fe 2p<sub>3/2</sub> peaks are wider in the used catalyst and have been shifted to higher binding energies likely due to the partial oxidation of the surface iron species from Fe<sup>2+</sup> to Fe<sup>3+</sup>, which is also confirmed by the absence of Fe<sup>2+</sup>-satellite peak [20]. This is in a good agreement with the results observed in the magnetization of the sample (Figure 6.4.) where the used catalysts presented a slightly lower saturation magnetization (4.1 vs. 4.4 emu g<sup>-1</sup>) likely due to the partial oxidation of surface magnetite. Therefore, main changes produced in the

catalyst surface after used are related to the partial oxidation of carbon and surface iron species, which reduced its saturation magnetization to a relatively low extent (around 7%). However, the catalyst still presented a fairly high saturation magnetization and could be easily recovered from the reaction medium by an external magnet and also kept high catalytic activity.

## 6.5. Conclusions

---

The TiO<sub>2</sub>-anatase loaded magnetic activated carbon catalysts synthesized in this work showed good photocatalytic activity and separability. Optimization of iron content and heat treatment conditions within the synthesis of the magnetic activated carbon support are crucial to obtain an easily magnetically separable catalyst. TiFeC catalyst led to complete removal of MTP and high levels of mineralization (70-90%) in photocatalytic ozonation experiments with simulated solar light. MTP was mainly removed through direct ozone reaction independently of the catalyst composition. However, MTP mineralization (i.e., conversion up to CO<sub>2</sub>) rate highly depends on the anatase content of the catalyst. Photocatalytic ozonation is a complex process involving a synergy of different reaction pathways (i.e. ozone direct reactions, ozone and hydrogen peroxide electron capture from TiO<sub>2</sub> surface, ozone photolysis with radiation wavelength between 300-320 nm, Fenton and photo-Fenton reactions and catalytic ozonation) leading to the degradation of organic pollutants in water (MTP in the case study).

Stability and reusability of a TiFeC catalyst was demonstrated to be rather good through a series of ten consecutive photocatalytic ozonation runs. After use, the properties of the catalyst did not vary significantly from the fresh sample though partial oxidation of carbon and surface iron species took place. However, the ten times reused catalyst could still be easily separated by an external magnetic field, which makes this type of catalysts an interesting alternative for solar photocatalytic processes.

## 6.6. Supplementary information

---

### 6.6.1. Analytical determination of MTP intermediates

MTP intermediates during photocatalytic oxidation, ozonation and photocatalytic ozonation using TiFeC-3 catalyst were analyzed. Samples were withdrawn at time intervals in which MTP conversion (equation (6.1S.)) was 0, 10, 50 and 99%:



$$X_{\text{MTP}} = \frac{C_{\text{MTP},0} - C_{\text{MTP}}}{C_{\text{MTP},0}} \times 100 \quad (6.1\text{S})$$

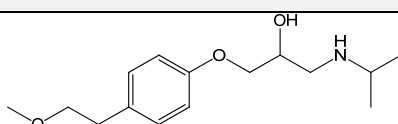
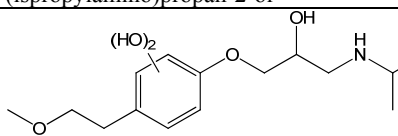
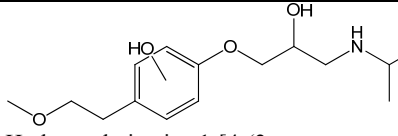
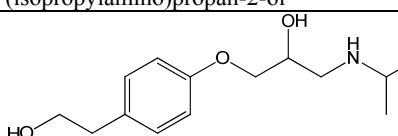
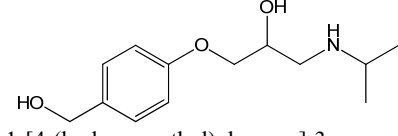
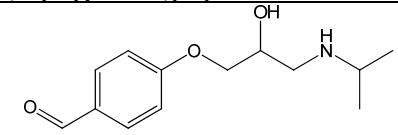
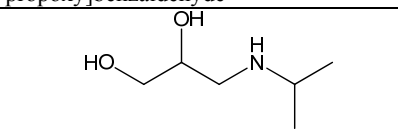
MTP intermediates were analyzed by HPLC-qTOF using an Agilent 6530 accurate mass quadrupole time-of-flight mass spectrometer bearing with electrospray ionization (ESI) source coupled with Agilent 1260 series LC system. A ZORBAX SB-C18 column (3.5  $\mu\text{m}$ , 150 mm long, 4.6 mm diameter) was used as stationary phase. The column was kept at constant temperature of 30°C during each analysis. As mobile phase, 0.2 mLmin<sup>-1</sup> of acetonitrile:acidified water (25 mM formic acid) was used from 10 to 100% of acetonitrile in 40 min with 15 min of equilibration. The injection volume was 10  $\mu\text{L}$ . The qTOF instrument was operated in the 4 GHz high-resolution mode. Ions are generated using an electrospray ion source Dual ESI. Electrospray conditions were the following: capillary, 3500 V; nebulizer, 30 psi; drying gas, 10 L min<sup>-1</sup>; gas temperature, 350°C; skimmer voltage, 65 V; octapole RF, 750 V; fragmentor, 175 V. The mass axis was calibrated using the mixture provided by the manufacturer over the  $m/z$  70–3200 range. A sprayer with a reference solution was used as continuous calibration in positive ion using the following reference masses:  $m/z$  121.0509 and 922.0098. Data were processed using Agilent Mass Hunter Workstation Software (version B.03.01).

### 6.6.2. MTP intermediates identification

Table 6.S1. shows the main intermediate species detected during MTP photocatalytic oxidation, ozonation and photocatalytic ozonation experiments. MTP intermediates detected have been mainly large molecules formed through O<sub>3</sub> and/or •OH attack to MTP as has been previously reported [35,25,36,37,38]. MTP-299 and MTP-283 compounds presented different isomers according to the different peaks observed at different retention times for the same exact mass. This has also been observed in a previous work by Benner and Ternes during MTP ozonation [35]. Thus, the formation of MTP-299 has been proposed to occur through the hydroxylation of MTP due to direct attack of O<sub>3</sub> and then the cleavage of hydroperoxide ion (HO<sub>2</sub><sup>-</sup>) [25,35]. MTP-283 is likely formed due to hydroxylation of MTP by both O<sub>3</sub> and •OH attacks [25,35,36]. Formation of MTP-253 can be due to •OH reaction that takes place at the ether bond of the side chain since O<sub>3</sub> shows no reactivity with ethers [35]. MTP-239 intermediate has been detected during ozonation in absence of tert-butanol, indicating that is likely formed through •OH reactions [35]. The intermediate MTP-237 could be formed by loss of the ether group of MTP, hydrogen abstraction, possibly upon •OH attack on the alkyl group, and oxygen atom addition [36]. Finally, MTP-133 is an

aliphatic chain breakdown product of MTP. It has been proposed that it is formed through  $\bullet\text{OH}$  reaction involving cleavage of carbon-carbon bond [25,35].

**Table 6.S1.** Metoprolol and its main intermediates detected by HPLC-qTOF in photocatalysis, ozonation and photocatalytic ozonation experiments

Label and elemental composition	*Exact mass ( $m/z$ )	Difference (ppm)	Retention time (min)	Proposed structure and name
MTP $\text{C}_{15}\text{H}_{25}\text{NO}_3$	C: 267.1834 M: 267.1817	-6.35	23.88	 1-[4-(2-methoxyethyl)phenoxy]-3-(isopropylamino)propan-2-ol
MTP-299 $\text{C}_{15}\text{H}_{25}\text{NO}_5$	C: 299.1733 M: 299.1715	-5.87	16.72 17.95 18.47 19.70	 Dihydroxy derivative 1-[4-(2-methoxyethyl)phenoxy]-3-(isopropylamino)propan-2-ol
MTP-283 $\text{C}_{15}\text{H}_{25}\text{NO}_4$	C: 283.1784 M: 283.1760	-8.44	11.52 16.90 18.25	 Hydroxy derivative 1-[4-(2-methoxyethyl)phenoxy]-3-(isopropylamino)propan-2-ol
MTP-253 $\text{C}_{14}\text{H}_{23}\text{NO}_3$	C: 253.1678 M: 253.1653	-8.60	18.57	 1-[4-(2-hydroxyethyl)phenoxy]-3-(isopropylamino)propan-2-ol
MTP-239 $\text{C}_{13}\text{H}_{21}\text{NO}_3$	C: 239.1521 M: 239.1505	-5.98	12.95	 1-[4-(hydroxymethyl)phenoxy]-3-(isopropylamino)propan-2-ol
MTP-237 $\text{C}_{13}\text{H}_{19}\text{NO}_3$	C: 237.1365 M: 237.1348	-6.95	18.91	 4-[2-hydroxy-3-(isopropylamino)propoxy]benzaldehyde
MTP-133 $\text{C}_6\text{H}_{15}\text{NO}_2$	C: 133.1103 M: 133.1093	-7.04	6.75	 3-(isopropylamino)propane-1,2-diol

\*C: calculated; M: measured

### 6.6.3. MTP intermediates evolution during different treatments

MTP intermediates detected during photocatalytic oxidation, direct ozonation and photocatalytic ozonation are shown in Figure 6.S1. where areas (i.e., a measure of concentration) have been plotted against the MTP conversion reached.

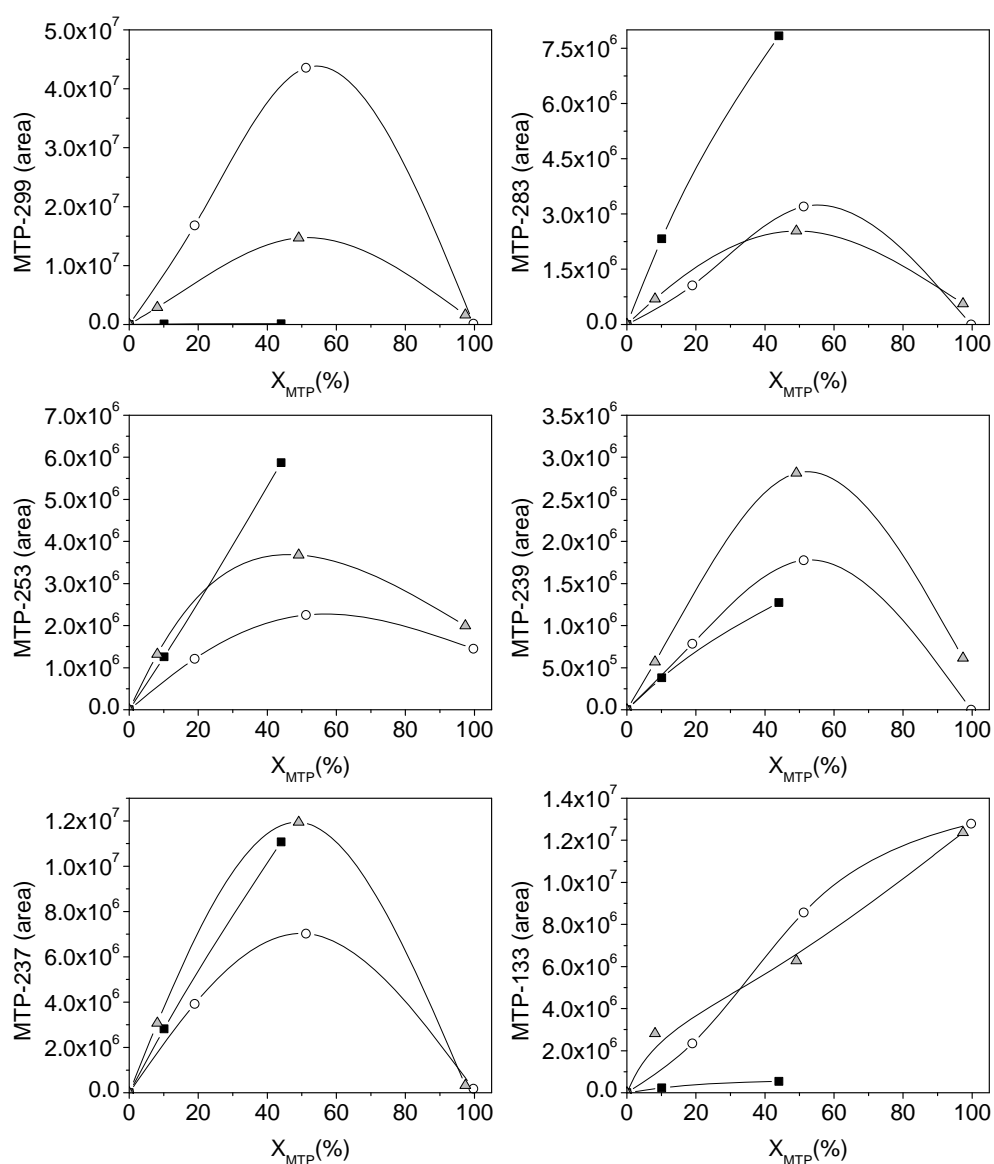


**Figure 6.S1.** Evolution of MTP intermediates detected by HPLC-qTOF vs. MTP conversion. Conditions:  $C_{MTP_0} = 50 \text{ mg L}^{-1}$ ,  $C_{CAT} = 375 \text{ mg L}^{-1}$ ,  $Q_g = 20 \text{ L h}^{-1}$ ,  $C_{O_3,g} = 6$

mg L<sup>-1</sup>. Experiments: photocatalytic oxidation (■), ozonation (○), photocatalytic ozonation (Δ).

It can be noticed that MTP-299 compound has been detected only in ozone processes, which is in accordance with to the comments above. This compound was formed in larger amount during the single ozonation experiment than during the photocatalytic ozonation experiment. In this latter a higher concentration of hydroxyl radicals was formed leading to the formation of intermediates MTP-253, MTP-239 and MTP-237 to a large extent. The concentration of MTP-283 was higher during the photocatalytic oxidation experiment than during ozone experiments. MTP-133 concentration during the photocatalytic oxidation experiment was almost negligible.

## 6.7. Acknowledgements

---

This work has been supported by the Spanish Ministerio de Economía y Competitividad (MINECO) and European Feder Funds through the project CTQ2012-35789-C02-01. Authors acknowledge the SAIUEX service of the University of Extremadura for the characterization analyses. P.M. Álvarez thanks the Ministerio de Educación, Cultura y Deporte of Spain for providing a sabbatical grant (PR2011-0572). A. Rey thanks the University of Extremadura for a postdoctoral research grant. D.H. Quiñones thanks the MINECO for a predoctoral FPI grant.

## 6.8. References

---

- [1] R. Andreozzi, V. Caprio, A. Insolab, R. Marotta, *Advanced oxidation processes (AOP) for water purification and recovery*, Catal. Today 53 (1999) 51–59.
- [2] K. Ikehata, M. Gamal El-Din, S.A. Snyder, *Ozonation and advanced oxidation treatment of emerging organic pollutants in water and wastewater*, Ozone-Sci. Eng. 30 (2008) 21–26.
- [3] S. Malato, P. Fernández-Ibáñez, M.I. Maldonado, J. Blanco, W. Gernjak, *Decontamination and disinfection of water by solar photocatalysis: Recent overview and trends*, Catal. Today 147 (2009) 1–59.
- [4] D.S. Bhatkhande, V.G. Pangarkar, A.A.C.M. Beenackers, *Photocatalytic degradation for environmental applications—a review*, J. Chem. Technol. Biot. 77 (2001) 102–116.

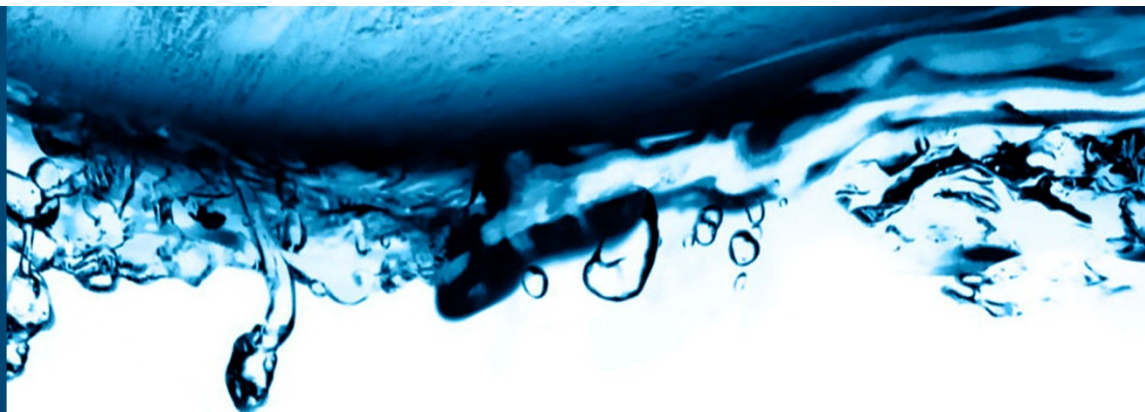
- [5] R. Rajeswari, S. Kanmani, *TiO<sub>2</sub>-based heterogeneous photocatalytic treatment combined with ozonation for carbendazim degradation*, J. Environ. Health Sci. Eng. 6 (2009) 61–66.
- [6] T.E. Agustina, H.M. Ang, V.K. Vareek, *A review of synergistic effect of photocatalysis and ozonation on wastewater treatment*, J. Photochem. Photobiol. C Photochem. Rev. 6 (2005) 264–273.
- [7] E.M. Rodríguez, G. Fernández, P.M. Alvarez, F.J. Beltrán, *TiO<sub>2</sub> and Fe (III) photocatalytic ozonation processes of a mixture of emergent contaminants of water*, Water Res. 46 (2012) 152–166.
- [8] A. Rey, D.H. Quiñones, P.M. Álvarez, F.J. Beltrán, P.K. Plucinski, *Simulated solar-light assisted photocatalytic ozonation of metoprolol over titania-coated magnetic activated carbon*, Appl. Catal. B-Environ. 111-112 (2012) 246–253.
- [9] B. Kasprzyk-Hordern, R.M. Dinsdale, A.J. Guwy, *The removal of pharmaceuticals, personal care products, endocrine disruptors and illicit drugs during wastewater treatment and its impact on the quality of receiving waters*, Water Res. 43 (2009) 363–380.
- [10] M.D. Hernando, M. Mezcuca, A.R. Fernández-Alba, D. Barceló, *Environmental risk assessment of pharmaceutical residues in wastewater effluents, surface waters and sediments*, Talanta 69 (2006) 334–342.
- [11] Y. Ao, J. Xu, D. Fu, C. Yuan, *A simple route for the preparation of anatase titania-coated magnetic porous carbons with enhanced photocatalytic activity*, Carbon 46 (2008) 596–603.
- [12] A.B. Fuertes, P. Tartaj, *A facile route for the preparation of superparamagnetic porous carbons*, Chem. Mater. 18 (2006) 1675–1679.
- [13] H. Bader, J. Hoigné, *Determination of ozone in water by the indigo method*, Water Res. 15 (1981) 449–456.
- [14] W. Masschelein, M. Denis, R. Ledent, *Spectrophotometric determination of residual hydrogen peroxide*, Water & Sewage Works, August (1977) 69–72.
- [15] C.D. Wagner, L.E. Davis, M.V. Zeller, J.A. Taylor, R.H. Raymond, L.H. Gale, *Empirical atomic sensitivity factors for quantitative analysis by electron spectroscopy for chemical analysis*, Surf. Interface Anal. 3 (1981) 211–225.
- [16] P. Fu, Y. Luan, X. Dai, *Preparation of activated carbon fibers supported TiO<sub>2</sub> photocatalyst and evaluation of its photocatalytic reactivity*, J. Mol. Catal. A Chem. 221 (2004) 81–88.

- [17] Y. Zhang, P. Xiao, X. Zhou, D. Liu, B. Batalla, G. Cao, *Carbon monoxide annealed TiO<sub>2</sub> nanotube array electrodes for efficient biosensor applications*, *J. Mater. Chem.* 19 (2009) 948–953.
- [18] J. Mizera, N. Spiridis, R. Socha, R. Grabowski, K. Samson, J. Korecki, B. Grzybowska, J. Gurul, L. Kepinski, M.A. Malecka, *Au/FeO<sub>x</sub> catalysts of different degree of iron oxide reduction*, *Catal. Today* 187 (2012) 20–29.
- [19] W. Temesghen, P.M.A. Sherwood, *Analytical utility of valence band X-ray photoelectron spectroscopy of iron and its oxides, with spectral interpretation by cluster and band structure calculations*, *Anal. Bioanal. Chem.* 373 (2002) 601–608.
- [20] T. Yamashita, P. Hayes, *Analysis of XPS spectra of Fe<sup>2+</sup> and Fe<sup>3+</sup> ions in oxide materials*, *Appl. Surf. Sci.* 254 (2008) 2441–2449.
- [21] R.L. Rebodos, P.J. Vikesland, *Effects of oxidation on the magnetization of nanoparticulate magnetite*, *Langmuir* 26 (2010) 16745–16753.
- [22] F.J. Beltrán, A. Aguinaco, A. Rey, J.F. García-Araya, *Kinetic studies on black light photocatalytic ozonation of diclofenac and sulfamethoxazole in water*, *Ind. Eng. Chem. Res.* 51 (2012) 4533–4544.
- [23] F.J. Benitez, J.L. Acero, F.J. Real, G. Roldán, *Ozonation of pharmaceutical compounds: Rate constants and elimination in various water matrices*, *Chemosphere* 77 (2009) 53–59.
- [24] F.J. Beltrán, *Ozone reaction kinetics for water and wastewater systems*, Lewis Publishers, CRC Press, Boca Raton, Florida USA, 2003.
- [25] K.S. Tay, N.A. Rahman, M.R.B. Abas, *Ozonation of metoprolol in aqueous solution: Ozonation by-products and mechanisms of degradation*, *Environ. Sci. Pollut. R.* 20 (2013) 3115–3121.
- [26] P.C.C. Faria, J.J.M. Órfão, M.F.R. Pereira, *Activated carbon catalytic ozonation of oxamic and oxalic acids*, *Appl. Catal. B-Environ.* 79 (2008) 237–243.
- [27] J.P. Pocostales, P.M. Álvarez, F.J. Beltrán, *Kinetic modeling of powdered activated carbon ozonation of sulfamethoxazole in water*, *Chem. Eng. J.* 164 (2010) 70–76.
- [28] B. Kasprzyk-Hordern, M. Ziolek, J. Nawrocki, *Catalytic ozonation and methods of enhancing molecular ozone reactions in water treatment*, *Appl. Catal. B-Environ.* 46 (2003) 639–669.

- [29] J. Nawrocki, B. Kasprzyk-Hordern, *The efficiency and mechanisms of catalytic ozonation*, Appl. Catal. B-Environ. 99 (2010) 27–42.
- [30] R. Rosal, A. Rodríguez, M.S. Gonzalo, E. García-Calvo, *Catalytic ozonation of naproxen and carbamazepine on titanium dioxide*, Appl. Catal. B-Environ. 84 (2008) 48–57.
- [31] F.J. Beltrán, F.J. Rivas, R. Montero-de-Espinosa, *Iron type catalysts for the ozonation of oxalic acid in water*, Water Res. 15 (2005) 3553–3564.
- [32] H. Taube, *Photochemical reactions of ozone in solution*, T. Faraday Soc. 53 (1957) 656–665.
- [33] L. Sánchez, X. Domènech, J. Casado, J. Peral, *Solar activated ozonation of phenol and malic acid*, Chemosphere 50 (2003) 1085–1093.
- [34] E. Mena, A. Rey, B. Acedo, F.J. Beltrán, S. Malato, *On ozone-photocatalysis synergism in black-light induced reactions: Oxidizing species production in photocatalytic ozonation versus heterogeneous photocatalysis*, Chem. Eng. J. 204–206 (2012) 131–140.
- [35] J. Benner, T. A. Ternes, *Ozonation of metoprolol: Elucidation of oxidation pathways and major oxidation products*, Environ. Sci. Technol. 43 (2009) 5472–5480.
- [36] B. Abramovic, S. Kler, D. Sojic, M. Lausevic, T. Radovic, D. Vione, *Photocatalytic degradation of metoprolol tartrate in suspensions of two TiO<sub>2</sub>-based photocatalysts with different surface area. Identification of intermediates and proposal of degradation pathways*, J. Hazard. Mater. 198 (2011) 123–132.
- [37] W. Song, W.J. Cooper, S.P. Mezyk, J. Greaves, B. Peake, *Free radical destruction of  $\beta$ -blockers in aqueous solution*, Environ. Sci. Technol. 42 (2008) 1256–1261.
- [38] D. Sojic, V. Despotovic, D. Orcic, E. Szabo, E. Arany, S. Armakovic, E. Illes, K. Gajda-Schranz, A. Dombi, T. Alapi, E. Sajben-Nagy, A. Palagyi, Cs. Vagvolgyi, L. Manczinger, L. Bjelica, B. Abramovic, *Degradation of thiamethoxam and metoprolol by UV, O<sub>3</sub> and UV/O<sub>3</sub> hybrid processes: Kinetics, degradation intermediates and toxicity*, J. Hydrol. 472–473 (2012) 314–327.
- [39] F.J. Beltrán, J.P. Pocostales, P.M. Alvarez, J. Jaramillo, *Mechanism and kinetic considerations of TOC removal from the powdered activated carbon ozonation of diclofenac aqueous solutions*, J. Hazard. Mater. 169 (2009) 532–538.







## Chapter VII

### Paper 5:

Boron doped TiO<sub>2</sub> catalysts for photocatalytic ozonation of aqueous mixtures of common herbicides and pesticides: Diuron, o-phenylphenol, MCPA and terbuthylazine

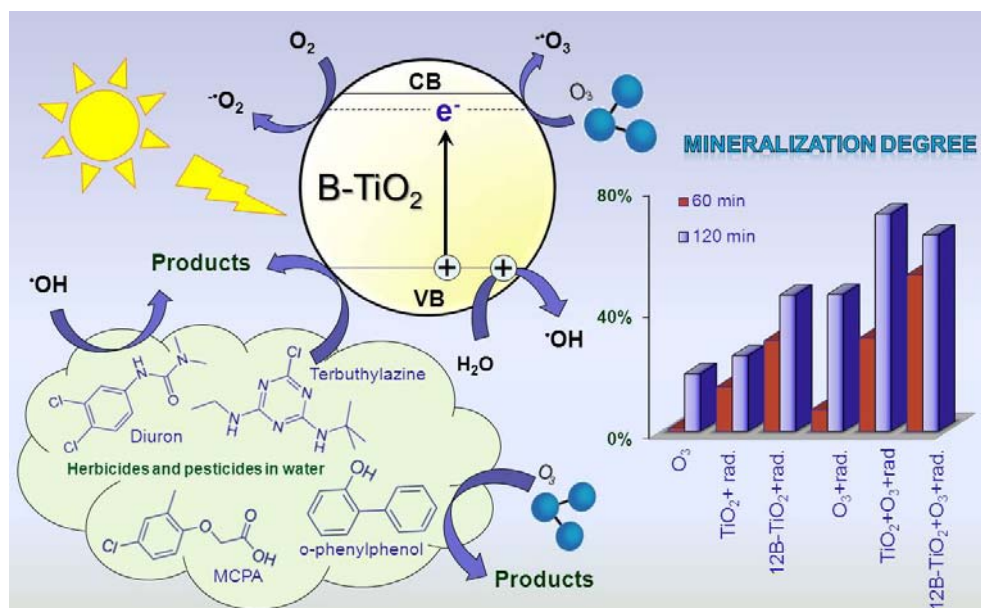
Diego H. Quiñones<sup>1</sup>, Ana Rey<sup>1</sup>, Pedro M. Álvarez<sup>1</sup>, Fernando J. Beltrán<sup>1</sup>, G. Li Puma<sup>2</sup>

<sup>1</sup> Departamento de Ingeniería Química y Química Física, Facultad de Ciencias, Universidad de Extremadura, Av. de Elvas s/n, 06071 Badajoz (Spain)

<sup>2</sup> Environmental Nanocatalysis and Photoreaction Engineering, Department of Chemical Engineering, Loughborough University, LE11 3TU, Loughborough (United Kingdom)

Accepted for publication in: Applied Catalysis B: Environmental, DOI: 10.1016/j.apcatb.2014.10.036.





## 7.1. Abstract

TiO<sub>2</sub> and B-doped TiO<sub>2</sub> catalysts were synthesized using a sol-gel procedure. The photocatalysts were characterized by ICP-EOS, N<sub>2</sub> adsorption-desorption, XRD, XPS, and DR-UV-Vis spectroscopy. Four recalcitrant pesticides (diuron, o-phenylphenol, 2-methyl-4-chlorophenoxyacetic acid (MCPA) and terbuthylazine) were subjected to degradation by ozonation, photolytic ozonation, photocatalysis and photocatalytic ozonation using the prepared catalysts under simulated solar irradiation in a laboratory scale system. The B-doped TiO<sub>2</sub> catalysts, with 0.5-0.8 wt% of interstitial boron, were more active than bare TiO<sub>2</sub> for the removal and mineralization of the target compounds. The combination of ozonation and photocatalysis led to faster mineralization rates than the treatment methods considered individually and allowed the complete removal of the pesticides below the regulatory standards. The B-doped catalyst was stable and maintained 75% mineralization after three consecutive runs.

**Keywords:** Boron doped TiO<sub>2</sub>, boron leaching, pesticides, photocatalytic ozonation, solar light.

## 7.2. Introduction

---

Water pollution and scarcity is a global concern. Agriculture is the industrial activity that has the major impact on aquatic ecosystems, due to the large volumes of water consumed (70% of the world accessible freshwater [1]) and the high content of organic substances (pesticides and fertilizers) which are dispersed in aqueous environments by runoff or leaching. Many pollutants found in water ecosystems are recalcitrant to some degree to biological and physicochemical processes that are conventionally used in wastewater treatment plants. In the last decades, Advanced Oxidation Processes (AOPs) have been pointed out as effective alternatives to deal with this kind of contaminants. These technologies can generate non-selective, highly reactive and short-life oxidizing species, which in turn can completely degrade organic pollutants through oxidation reactions [2].

Photocatalysis is one of the most successfully and extensively studied AOP. It involves the excitation of a semiconductor through the absorption of photons having energy greater than its band gap. This excitation promotes an electron from the valence to the conduction band, which triggers a series of oxidation-reduction reactions involving the excited electron and the generated hole at the valence band [2]. Recently, solar-driven TiO<sub>2</sub> photocatalytic oxidation has attracted considerable attention in water treatment applications. It offers the possibility of using solar energy to activate the semiconductor. However, due to the TiO<sub>2</sub> wide band gap (3.2 eV) its photo-activity is limited to ultraviolet irradiation ( $\lambda < 380$  nm) and thus less than 5% of the solar spectrum can be exploited [3]. In general, doping TiO<sub>2</sub> appears to be an effective way to overcome this limitation, since the photo-activity of the doped semiconductor may be extended to the visible-light region [4,5]. Boron doping constitutes a way to accomplish it, since O atoms in the TiO<sub>2</sub> lattice can be substituted by B atoms mixing the p orbital of B with O 2p orbitals, narrowing the band gap and thus shifting the optical response into the visible range [5]. On the other hand, boron can also be located in interstitial positions of the TiO<sub>2</sub> lattice leading to the partial reduction of Ti(IV) to Ti(III), which could act as an electron trap enhancing the photocatalytic activity of TiO<sub>2</sub> [5,6].

Another way to improve the performance of TiO<sub>2</sub> photocatalytic systems is its simultaneous application with other AOPs, such as ozonation. The combined application of ozone and TiO<sub>2</sub> photocatalysis, known as photocatalytic ozonation, leads to a synergistic effect due to enhanced production of reactive oxygen species (ROS) such as hydroxyl radicals in comparison with the application of either single ozonation or single TiO<sub>2</sub> photocatalysis [7,8].

In this study, the degradation of four herbicides and pesticides: diuron (DIU), o-

phenylphenol (OPP), 2-methyl-4-chlorophenoxyacetic acid (MCPA) and terbuthylazine (TBA), commonly found in water ecosystems, has been studied. Their molecular structures can be found in Table 7.S1. of the supplementary material. The degradation methods used were photocatalysis, ozonation, photolytic ozonation, and photocatalytic ozonation. Different boron doped TiO<sub>2</sub> photocatalysts (B-TiO<sub>2</sub>) were synthesized and used in the photocatalytic treatments.

### 7.3. Experimental section

---

#### 7.3.1. Catalysts preparation

The synthesis of TiO<sub>2</sub> and B-TiO<sub>2</sub> catalysts was carried out following a sol-gel procedure previously reported [9]. Initially, a precursor solution was prepared by diluting the required amount of boric acid (Fisher Scientific) in 10 mL anhydrous ethanol (Panreac, 99.5%), then adding 4.26 mL titanium butoxide (Sigma Aldrich, 97%), adjusting the pH to 3-4 with glacial acetic acid (Merck) and stirring for 30 min. After that, 20 mL ethanol were added to the precursor solution and the stirring was kept for 2 more hours. Ammonia aqueous solution (Fisher Scientific, 35%) was then added dropwise to reach pH 9. Afterward 10 mL ethanol was added and stirring was kept for another 30 min. The suspension was centrifuged and washed with ethanol three times. The resulting solid was dried at 60°C overnight, manually grinded and finally calcined at 500°C for 30 min. Catalysts with 3, 6, 9 and 12 wt.% of B were prepared. The nomenclature and some parameters of the catalysts are shown in Table 1. A fraction of catalysts with 6 and 12 wt% of B were washed with ultrapure water to analyze the effect of B leaching.

#### 7.3.2. Characterization of the catalysts

The characterization of the catalysts was carried out by inductively coupled plasma optical spectroscopy, N<sub>2</sub> adsorption-desorption, X-ray diffraction (XRD), X-ray photoelectron spectroscopy (XPS), and DR-UV-Vis spectroscopy.

Total B content of the catalysts was analyzed by inductively coupled plasma with an ICP-OES Optima 3300DV (Perkin-Elmer) after acidic microwave digestion of the samples.

BET surface area and pore structure of catalysts were determined from their nitrogen adsorption-desorption isotherms obtained at -196°C using an Autosorb 1 apparatus (Quantachrome). Prior to analysis the samples were outgassed at 250°C for 12 h under high vacuum (<10<sup>-4</sup> Pa).

The crystalline structure was analyzed by X-ray diffraction (XRD) using a Bruker D8 Advance XRD diffractometer with a  $\text{CuK}\alpha$  radiation ( $\lambda = 0.1541 \text{ nm}$ ). The data were collected from  $2\theta = 20^\circ$  to  $80^\circ$  at a scan rate of  $0.02 \text{ s}^{-1}$  and 1 s per point.

XPS spectra were obtained with a  $\text{K}\alpha$  Thermo Scientific apparatus with an  $\text{Al K}\alpha$  ( $h\nu=1486.68 \text{ eV}$ ) X-ray source using a voltage of 12 kV under vacuum ( $2 \times 10^{-7}$  mbar). Binding energies were calibrated relative to the C1s peak at 284.6 eV.

Diffuse reflectance UV-Vis spectroscopy (DR-UV-Vis) measurements, useful for the determination of the semiconductor band gap, were performed with an UV-Vis-NIR Cary 5000 spectrophotometer (Varian-Agilent Technologies) equipped with an integrating sphere device.

Transmitted photon flux through a catalyst suspension was analyzed by actinometrical measurements following the method proposed by Loddo et al. in [10], using the solar simulator described below with 250 mL of actinometrical solution and 250 mL of catalyst suspension at  $0.33 \text{ g L}^{-1}$ . Incident radiation flux was determined with ultrapure water replacing the catalyst suspension and was found to be  $8.96 \times 10^{-4} \text{ Einstein min}^{-1}$ .

### 7.3.3. Photocatalytic activity measurements

Photocatalytic experiments were carried out in a laboratory-scale system consisting of a 250 mL Pyrex made 3-neck round-bottom flask (8.8 cm outer diameter) provided with a gas inlet, a gas outlet and a liquid sampling port. The reactor was placed in the chamber of a commercial solar simulator (Suntest CPS, Atlas) equipped with a 1500 W air-cooled Xe lamp with emission restricted to wavelengths over 300 nm (quartz and glass cut-off filters). The emission spectrum of the solar simulator can be seen in Figure 7.S1. of the supplementary material. The irradiation intensity was kept at  $550 \text{ W m}^{-2}$  and the temperature of the system was maintained between 25 and  $40^\circ\text{C}$  throughout the experiments. If required, a laboratory ozone generator (Anseros Ozomat Com AD-02) was used to produce a gaseous ozone-oxygen stream that was fed to the reactor.

In a typical photocatalytic ozonation experiment, the reactor was first loaded with 250 mL of an aqueous solution containing  $5 \text{ mg L}^{-1}$  initial concentration of each pesticide (in a mixture). Then, the catalyst was added at a concentration of  $0.33 \text{ g L}^{-1}$  and the suspension was stirred in the darkness for 30 min (dark adsorption stage). Then, the lamp was switched on and, simultaneously, a mixture of ozone-oxygen ( $5 \text{ mg L}^{-1}$  ozone concentration) was fed to the reactor at a flow rate of 10 L

$\text{h}^{-1}$ . The irradiation time for each experiment was 2 h. Samples were withdrawn from the reactor at intervals and filtered through a  $0.2 \mu\text{m}$  PET membrane to remove the photocatalyst particles.

Photolysis experiments (i.e. absence of catalyst and ozone), adsorption (i.e., absence of radiation and ozone), ozonation alone (i.e., absence of radiation and catalyst), and photolytic ozonation (i.e., absence of catalyst) were also carried out for comparative purposes.

Pesticides concentrations were analyzed by HPLC (Hewlett Packard) provided with a Kromasil C18 column ( $5 \mu\text{m}$ , 150 mm long, 4 mm diameter, Teknokroma). As mobile phase a mixture of acetonitrile (solvent A) and 0.1% (v/v) phosphoric acid solution (solvent B) was used at  $1 \text{ mL}\cdot\text{min}^{-1}$ . Initially the mobile phase composition was varied from 40 to 25% solvent A in 12.5 min, then varied to 40% in 7.5 min and finally maintained at that composition for more 10 min. The retention times for DIU, MCPA, TBA and OPP were 10, 15.2, 23.2 and 25.8 min, respectively. The detection system was set at 220 nm.

Total organic carbon content (TOC) was measured using a Shimadzu TOC-V<sub>SCH</sub> analyzer. Dissolved ozone was measured photometrically by following the indigo method at 600 nm [11]. Ozone in the gas phase was continuously monitored by means of an Anseros Ozomat GM-6000Pro analyzer. Hydrogen peroxide concentration was determined photometrically by the cobalt/bicarbonate method at 260 nm [12]. Boron leached from the catalysts was determined photometrically after complexation with azomethine-H at 410 nm [13]. Photometric measurements were carried out in a UV-Visible spectrophotometer (Evolution 201, Thermospectronic).

## 7.4. Results and discussion

---

### 7.4.1. Catalysts characterization

Table 7.1. summarizes some characteristics of the B-doped  $\text{TiO}_2$  catalysts. Firstly, it can be noticed that the amounts of B incorporated to the catalysts are much lower than the theoretical values. Similar results have been observed in previous studies where around only 5-10% of the theoretical B was introduced in the final catalyst following sol-gel synthesis techniques [14,15].

The structure of the catalysts was analyzed by means of XRD and diffraction patterns are shown in Figure 7.1. Anatase was identified as the only  $\text{TiO}_2$

crystalline phase in all the catalysts together with the appearance of the sassolite boron structure ( $\text{H}_3\text{BO}_3$ ) with the main diffraction peak at  $2\theta=28^\circ$  for the catalysts with B content equal or greater than the theoretical 6 wt%. In addition, from the XRD patterns it can also be noticed that anatase diffraction peaks intensity decreased with the increasing B content. The crystallite size of anatase in the catalysts was calculated through Scherrer's equation. The values, which are shown in Table 7.1., reveal that the crystal size decreases with the increasing B content. This effect has been previously reported for similar catalysts and it has been attributed to the restrained  $\text{TiO}_2$  crystal growing due to the existence of large amount of boron [16–18].

**Table 7.1.** Nomenclature and some properties of the B- $\text{TiO}_2$  catalysts

Catalyst	B (wt%)	$d_A$ (nm)	$S_{\text{BET}}$ ( $\text{m}^2 \text{g}^{-1}$ )	$V_P$ ( $\text{cm}^3 \text{g}^{-1}$ )	$(\text{B}/\text{Ti})_{\text{ICP}}$ (at/at)	$(\text{B}/\text{Ti})_{\text{XPS}}$ (at/at)	$E_g$ (eV)
$\text{TiO}_2$	n.d.	16.8	68.3	0.102	0	0	3.07
3B- $\text{TiO}_2$	0.91	9.9	121.3	0.209	0.068	0.469	3.12
6B- $\text{TiO}_2$	1.06	9.2	120.1	0.147	0.079	0.531	3.03
9B- $\text{TiO}_2$	1.81	7.6	122.4	0.163	0.137	0.541	3.05
12B- $\text{TiO}_2$	3.55	7.5	125.5	0.180	0.273	0.693	3.01
6B- $\text{TiO}_2$ -w	0.42	9.8	n.m.	n.m.	0.031	0.018	n.m.
12B- $\text{TiO}_2$ -w	0.49	7.9	n.m.	n.m.	0.036	0.029	n.m.

n.d.: not detected, n.m.: not measured

Textural parameters (BET surface area and total pore volume) were calculated from the adsorption-desorption isotherms presented in Fig 7.S2. of the supplementary information and are summarized in Table 7.1. In general, the sol-gel synthesis procedure together with the relatively short time of calcination led to catalysts with fairly high surface areas. In addition, it can be observed that both, BET surface area and total pore volume, increased with the increasing B content, effect that can be attributed to the lower crystal size of the anatase phase in the B- $\text{TiO}_2$  catalysts [16].



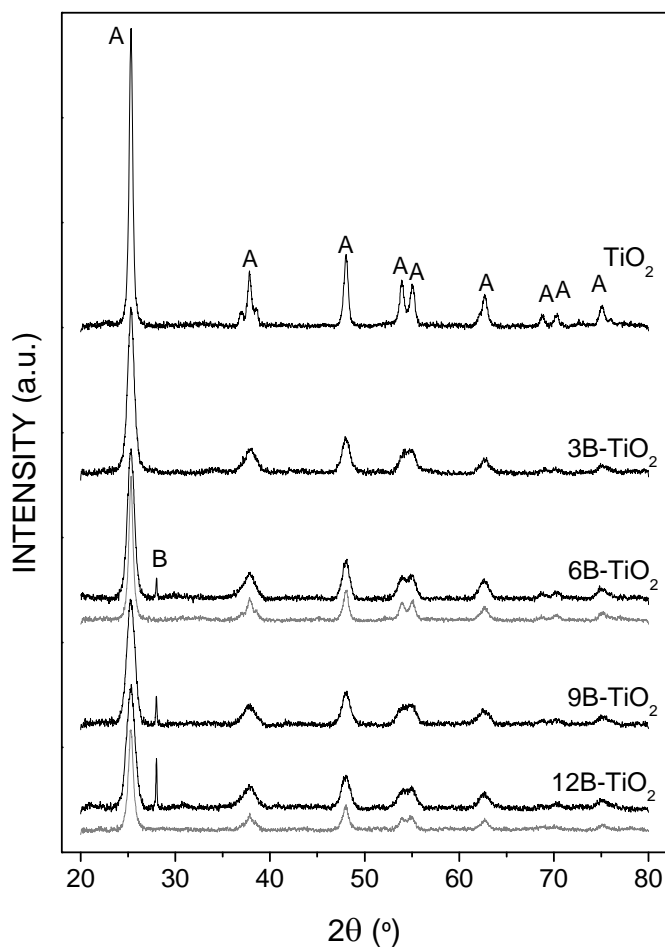


**Figure 7.1.** XRD patterns of the photocatalysts (Grey: washed samples, A: anatase, B: boron  $B_2O_3/H_3BO_3$ )

Surface composition of the  $TiO_2$  and  $B-TiO_2$  catalysts was analyzed by XPS. Figure 7.2A. shows, as an example, the high-resolution XPS spectra of the B 1s spectral region corresponding to 12B- $TiO_2$  catalyst. The binding energy for B 1s core level in  $H_3BO_3$  or  $B_2O_3$  is centered at 193.0 eV (B-O bond), whereas B located in the  $TiO_2$  lattice corresponding to B occupying O sites as B-Ti bond in  $TiB_2$  or O-Ti-B, and interstitial B as Ti-O-B presents lower binding energies at 187.5, 189.6 and 191.7 eV, respectively [16,18,19]. The symmetric peak found for all the B- $TiO_2$  catalysts was at 192.6 eV, thus indicating that B is mainly as  $H_3BO_3$  or  $B_2O_3$  in the catalysts surface, according to XRD results. However, the shift observed from 193.0 eV may be also indicative of the contribution of interstitial B. The presence of substitutional B (O-Ti-B or  $TiB_2$ ) can be disregarded according to the absence of signal at binding energies lower than 190 eV. Ti 2p spectral region for

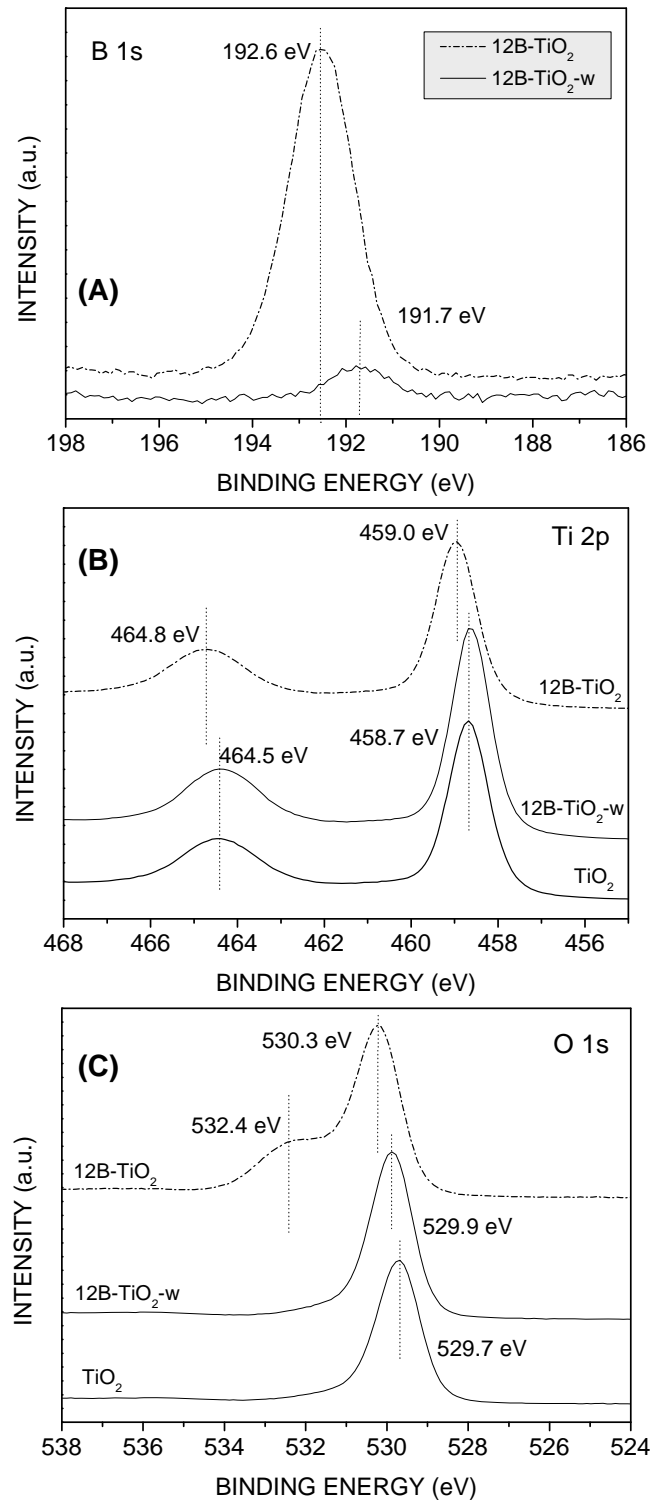


**Figure 7.2.** High resolution XPS spectra of B 1s, O 1s and Ti 2p spectral regions of the catalysts  $\text{TiO}_2$ ,  $12\text{B-TiO}_2$  and  $12\text{B-TiO}_2\text{-w}$

12B-TiO<sub>2</sub> and TiO<sub>2</sub> catalysts is depicted in Figure 7.2B. The binding energy of the Ti 2p core levels at 464.5 and 458.7 eV, and the separation of the peaks around 5.8 eV, confirm the valence state of Ti(IV) in TiO<sub>2</sub> [20,21]. However, for 12B-TiO<sub>2</sub> catalysts the peaks have been shifted towards higher binding energy values that can be explained on the basis of the higher electronegativity of boron, thus confirming the formation of Ti-O-B structures (interstitial B) [16]. Finally, Figure 7.2C. shows the high-resolution XPS spectra of O 1s spectral region for TiO<sub>2</sub> and 12B-TiO<sub>2</sub> catalysts. The main peak located around 530 eV corresponds to Ti-O bonds with a widening at higher binding energy that has been assigned to hydroxyl groups in the TiO<sub>2</sub> surface. On the other hand, a second contribution to the O 1s spectra is observed in the boron doped catalyst at 532.4 eV corresponding to B-O bonds in H<sub>3</sub>BO<sub>3</sub> or B<sub>2</sub>O<sub>3</sub> [18]. Boron to titanium atomic surface ratio was calculated for all the catalysts from peak areas and Wagner atomic sensitivity factors [22]. These results are summarized in Table 7.1. together with B/Ti bulk ratio calculated from ICP results. It can be noticed that the surface ratios are larger than bulk ratios, suggesting that most of B is located on the surface of TiO<sub>2</sub> during the sol-gel synthesis. This has also been previously reported in La-B co-doped TiO<sub>2</sub> catalysts [14,23].

Table 7.1. also reports the band gap energy of the catalysts determined according to Tauc's expression from the UV-Vis diffuse reflectance spectra (Figure 7.S3. and Figure 7.S4. of the supplementary material). The E<sub>g</sub> value for bare TiO<sub>2</sub> was 3.07 eV, whereas for B-doped catalysts fluctuated from 3.01 to 3.12 eV with no distinguishable trend with the increasing B content. This is in a good agreement with previous results from Zaleska et al. [18] who reported similar values of E<sub>g</sub> for B-doped TiO<sub>2</sub> catalysts with B content from 0.5 to 10 wt.%. This is likely the result of low or no mixing of 2p boron bands with 2p oxygen bands since no substitutional B is achieved [5].

The catalysts were tested in photocatalysis and photocatalytic ozonation of the selected pesticides DIU, MCPA, TBA and OPP (not shown). However, during the experiments, dissolved boron was detected in the reaction medium, suggesting leaching to some extent. To analyze the leaching phenomenon, the catalysts were submitted to water washing at the same conditions of the reaction medium (catalyst concentration and pH). These results for 12B-TiO<sub>2</sub> photocatalyst are depicted in Figure 7.3. together with the evolution of dissolved boron during the photocatalytic ozonation treatment. It can be noticed that unstable boron was leached from the catalyst surface to the aqueous solution just at the beginning of the test and then remained constant up to 2 h. The differences found between pesticides solution or water washing are lower than 1 mg L<sup>-1</sup> of B and can be due to experimental deviations.

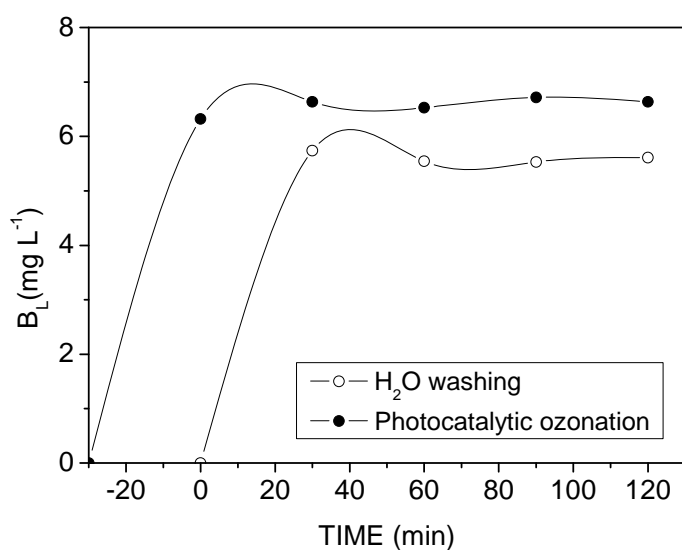


**Figure 7.3.** B leaching of the 12B-TiO<sub>2</sub> catalyst during washing procedure and photocatalytic ozonation reaction (0.33 g L<sup>-1</sup>)

Total boron leached from all the catalysts during the washing procedure is summarized in Table 7.2. Boron concentration in solution reached values as high as 5.5 mg L<sup>-1</sup> in the case of the highest loading B-doped catalyst, being the loss of the total boron from 46 to 70%. To our knowledge, boron leaching phenomenon has not been previously considered in B-doped TiO<sub>2</sub> catalysts application to wastewater treatment but it is mandatory since the limit of B ions in drinking water is 1 mg L<sup>-1</sup> according to the European Union standards [24].

**Table 7.2.** B leaching from the B-TiO<sub>2</sub> catalysts during washing procedure (0.33 g L<sup>-1</sup>)

Catalyst	B (mg L <sup>-1</sup> )	B (%)
TiO <sub>2</sub>	n.d.	n.d.
3B-TiO <sub>2</sub>	1.83	60.6
6B-TiO <sub>2</sub>	1.91	54.3
9B-TiO <sub>2</sub>	4.20	69.9
12B-TiO <sub>2</sub>	5.50	46.6

n.d.: not detected

On the basis of these results, two of the catalysts were washed with ultrapure water until no dissolved boron was detected (6B-TiO<sub>2</sub>-w and 12B-TiO<sub>2</sub>-w catalysts). Some characterization results of the washed samples are summarized in Table 7.1.. It can be observed a decrease of B bulk content until 0.42-0.49%. The similar percentage of boron after washing both catalysts suggests that only this amount can be introduced in the TiO<sub>2</sub> lattice regardless of the initial amount of boron used. XRD patterns of the washed catalysts do not display the diffraction peak of boron species H<sub>3</sub>BO<sub>3</sub> or B<sub>2</sub>O<sub>3</sub> but, as expected, the washing procedure did not substantially modify the crystal size of the anatase phase. In this line, it is reasonable to assume that no significant changes in the textural properties due to washing procedure develop. On the other hand, the washed catalysts were analyzed by XPS and the results of 12B-TiO<sub>2</sub>-w are also plotted in Figure 7.2. for comparative purposes. First of all, the intensity of the B 1s core level signal decreased significantly as a result of the loss of boron. However, the peak position located at 191.7 eV confirms the existence of boron in interstitial positions in the TiO<sub>2</sub> lattice (Ti-O-B bonds). The Ti 2p and O 1s spectra of 12B-TiO<sub>2</sub>-w catalyst were similar to those of bare TiO<sub>2</sub>. These results seem to point out that only a small portion of the initial boron was introduced as interstitial boron in the TiO<sub>2</sub> lattice during the sol-gel method used, and also that this B is strongly bonded and stable in aqueous suspension whereas the surface boron forming H<sub>3</sub>BO<sub>3</sub> or B<sub>2</sub>O<sub>3</sub> entities is easily dissolved. Two extra catalysts were prepared increasing the calcination time from 30 min to 1 h and 3 h, but this operating variable did not improve the B stability leading to similar results (not shown). In addition, besides the band gap, other optical properties of the catalysts such absorption and scattering could be modified through B incorporation. The transmitted photon flux through a catalyst suspension could be an indirect measurement of these properties. In that case, the percentage of transmitted photon flux was 58.1% for TiO<sub>2</sub>, 47.7% for 6B-TiO<sub>2</sub>-w and 76.7% for 12B-TiO<sub>2</sub>-w. According to this, 6B-TiO<sub>2</sub>-w is expected to make a better use of radiation although no trend with other properties was observed and additional analyses would be necessary to reach stronger conclusions.

#### 7.4.2. Photocatalytic activity

B-doped washed catalysts were tested in the photocatalytic oxidation and photocatalytic ozonation of the selected pesticides and compared with bare TiO<sub>2</sub> using simulated solar light as radiation source. The evolution of DIU, MCPA, TBA and OPP during photocatalytic oxidation treatment is depicted in Figure 7.4. The catalysts were stirred with the solution of the pesticides in the dark for 30 min to reach the adsorption equilibrium. Low adsorption capacity was observed for DIU, MCPA and OPP whereas around 20% of TBA adsorption was achieved. In general, the adsorption capacity increased in the B-doped catalysts likely due to their more

developed surface area and porosity. Direct photolysis of the pesticides did not produce significant degradation of DIU, MCPA and TBA, though a slight decrease of OPP concentration up to 10% was observed. These results are consistent with the UV-Vis absorbance spectra of the target compounds shown in Figure 7.S5. For photocatalytic oxidation with bare and B-doped TiO<sub>2</sub> photocatalysts, in general, the presence of the catalyst improves the depletion rate of all the pesticides, which show different reactivity in the mixture. The order of the reactivity was found to be MCPA>OPP>DIU>TBA. The rate constants of the reaction between these compounds and the hydroxyl radical are  $k_{\text{OH-MCPA}} = 4.5 \times 10^9$ ,  $k_{\text{OH-OPP}} = 9.8 \times 10^9$ ,  $k_{\text{OH-DIU}} = 7.1 \times 10^9$ ,  $k_{\text{OH-TBA}} = 2.8 \times 10^9 \text{ L mol}^{-1} \text{ s}^{-1}$  [25,26]. It is commonly assumed that in photocatalytic oxidation, the main degradation of organics takes place through hydroxyl radicals, especially when direct photolysis and/or adsorption have negligible contributions. The highest degradation rate of MCPA was not in agreement with the order of reactivity derived from the rate constant values. It could be possible that the hydroxyl radical reaction was not the only predominant degradation route for MCPA. In fact, some organic peroxyradicals formed as intermediates during MCPA photocatalytic oxidation are responsible of an autocatalytic behavior, as previously reported [27].

The incorporation of B to the catalysts lattice conferred an important effect in its catalytic activity. Thus, the degradation rate of all the pesticides was clearly enhanced in the presence of 6B-TiO<sub>2</sub>-w and 12B-TiO<sub>2</sub>-w catalysts. Similar behavior was observed for DIU and OPP, as 70-80% degradation was achieved with 12B-TiO<sub>2</sub>-w catalyst vs. 20-30% obtained with bare TiO<sub>2</sub>. For MCPA, around 45 min were necessary to reach almost complete removal whereas around 10% of MCPA still remained in solution with TiO<sub>2</sub> after 120 min of treatment. TBA depletion also improved with B-doped catalysts, reaching around 50% degradation compared to 35% with TiO<sub>2</sub>. However, TBA showed a refractory character towards its photocatalytic oxidation, since its concentration decreased faster during the first 15 min and then the degradation rate slowed down. These results point out the benefits of incorporating boron to the TiO<sub>2</sub> lattice. The role of B in interstitial positions of TiO<sub>2</sub> has not been unequivocally defined. It seems that B tends to lose its three valence electrons, which are donated to the 3d states of lattice Ti ions, thus giving rise to Ti(III) species. These latter have been postulated to reduce the recombination of photo-excited electrons and holes [5,28]. A boron content of about 0.5 wt% seems to be enough to enhance the photocatalytic activity of TiO<sub>2</sub>. The differences found in the activity of both doped catalysts could be related to the higher content of surface B detected by XPS in the 12B-TiO<sub>2</sub>-w catalyst. On the other hand, the differences found in the textural properties and crystallinity of bare TiO<sub>2</sub> and B-TiO<sub>2</sub> catalysts might also play an important role in the behavior of the catalysts. However, it has been reported the improvement of photocatalytic

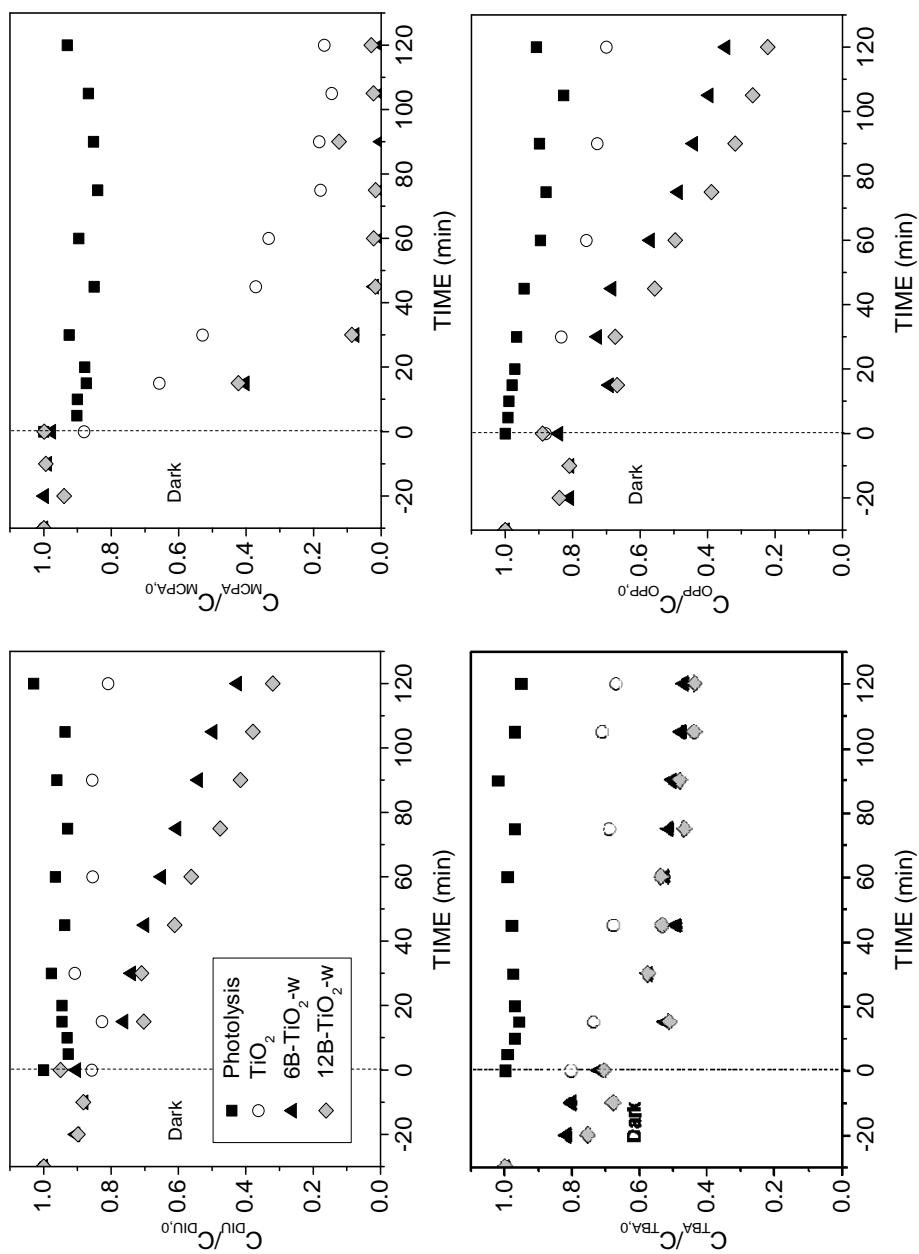


**Figure 7.4.** Evolution of dimensionless herbicides and pesticides concentration during photocatalysis with  $TiO_2$  and B- $TiO_2$  catalysts. Conditions:  $pH_0 = 6.5$ ,  $T = 25-40^\circ C$ ,  $C_{PES,0} = 5 \text{ mg L}^{-1}$  (in the mixture),  $C_{CAT} = 0.33 \text{ g L}^{-1}$ ,  $Q_e = 10 \text{ L h}^{-1}$  ( $O_2$ ).

performance with the increased crystallinity of the anatase particles since recombination process is prevented to some extent, though larger crystal size leads to lower specific surface areas [29]. Therefore, the improvement observed in the catalytic activity could be related to the presence of boron in TiO<sub>2</sub> interstitial positions more than to the changes produced in TiO<sub>2</sub> crystal size and textural properties. Also, the modification on the radiation absorption and scattering properties cannot be disregarded although transmitted photon flux measurements were not conclusive at this respect.

The evolution of the pesticides concentration during photocatalytic ozonation is shown in Figure 7.5. Also, for comparative purposes, ozonation alone and the combination of ozone and radiation (photolytic ozonation) were applied. It can be observed that, regardless of the presence of catalysts and/or radiation, all the ozone treatments led to higher degradation rate of the pesticides than the photocatalytic oxidation process. The average time needed to reach 99% of pesticides removal with ozone treatments was around 60 min for DIU and TBA, and 30 min for MCPA and OPP. These are, in general, in agreement with the values of the rate constants of the ozone-pesticide reaction ( $k_{O_3-MCPA} = 323$ ,  $k_{O_3-OPP} = 379$ ,  $k_{O_3-DIU} = 3.7$ ,  $k_{O_3-TBA} = 20 \text{ L mol}^{-1} \text{ s}^{-1}$  [25,30,31]). Nevertheless, indirect reactions due to ozone decomposition into hydroxyl radicals could take place at the reaction pH [32,33], also according with the high rate constant values between hydroxyl radical-pesticides commented above.

Main differences among the ozone treatments were found in terms of TOC removal. Previously, as seen in Figure 7.6., in all cases, after the dark stage, low TOC removal due to adsorption on the catalysts was observed in comparison of the reaction stage. However, doped catalysts presented higher adsorption capacity compared to bare TiO<sub>2</sub>, probably due to their higher surface areas. On the other hand, the TOC removal observed in the direct photolysis run was negligible, as expected. These results were improved by photocatalytic oxidation reaching 25% TOC removal with bare TiO<sub>2</sub> after 2 h. This mineralization level increased up to 37% and 45% using 6B-TiO<sub>2</sub>-w and 12B-TiO<sub>2</sub>-w catalysts, respectively. The higher efficiency of the doped catalysts compared to that of bare TiO<sub>2</sub> was also observed when applying the combined photocatalytic ozonation treatment. Although only 20% of the contaminant mixture was mineralized by single ozonation, the presence of radiation during photolytic ozonation increased up to 45% the mineralization degree. In the presence of radiation, a fraction of the ozone molecules that have not directly reacted with contaminants are photolyzed under wavelengths near to 300 nm to produce reactive oxygen species (ROS), which enhance the mineralization rate [34]. These results were highly improved with the photocatalytic ozonation treatment, reaching 65–70% TOC removal. Ozone, as an



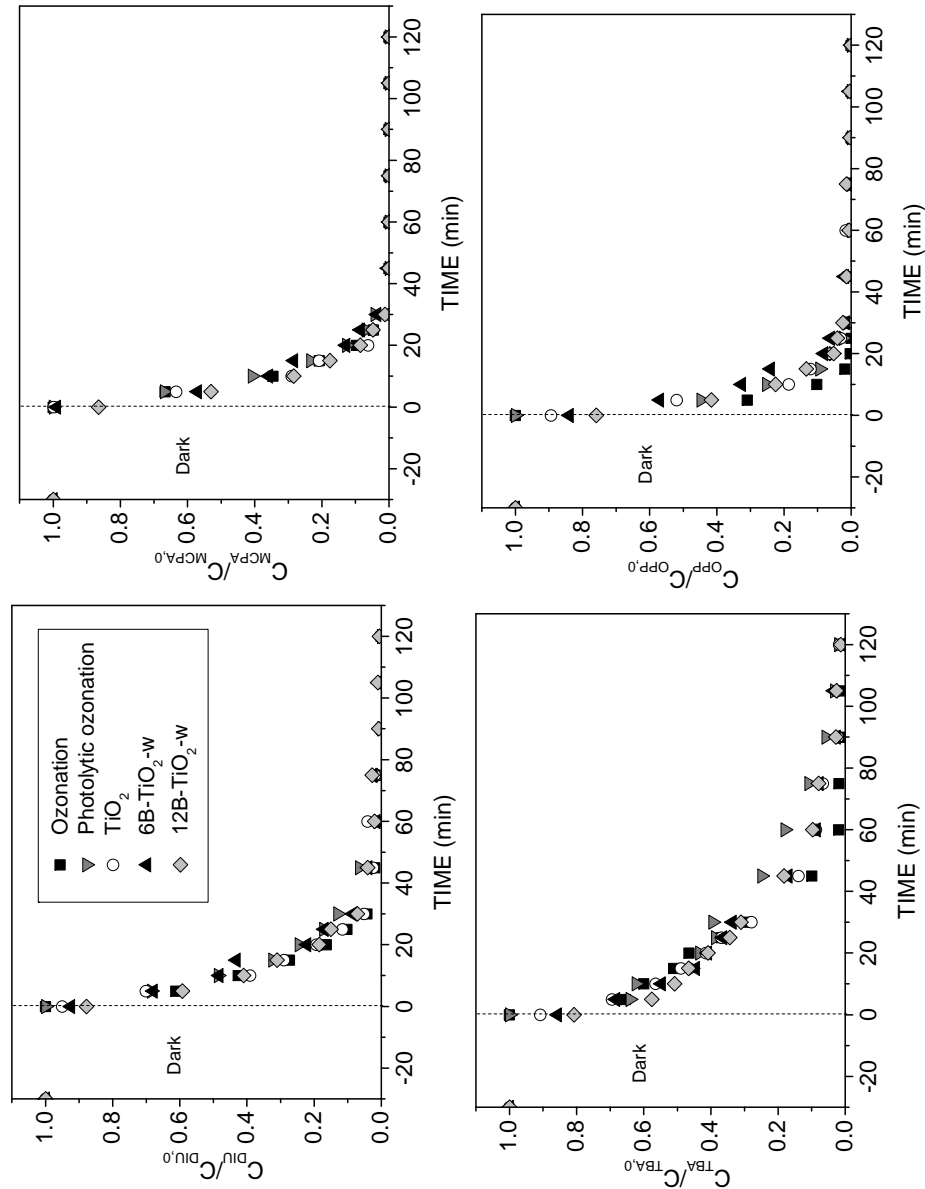


**Figure 7.5.** Evolution of dimensionless pesticides concentration during ozone treatments with TiO<sub>2</sub> and B-TiO<sub>2</sub> catalysts. Conditions: pH<sub>0</sub> = 6.5, T = 25-40°C, C<sub>PES,0</sub> = 5 mg L<sup>-1</sup> (in the mixture), C<sub>CAT</sub> = 0.33 g L<sup>-1</sup>, Q<sub>t</sub> = 10 L h<sup>-1</sup> (O<sub>3</sub>/O<sub>2</sub>), C<sub>O3,t</sub> = 5 mg L<sup>-1</sup>

electrophilic molecule, can trap electrons from the conduction band of the catalyst yielding ozonide ion radicals that decompose into ROS [7,8]. B-doped catalysts were more active than bare  $\text{TiO}_2$  and led to faster mineralization rate according to TOC removal reached at 60 min reaction time, though the final mineralization degree was similar (around  $1 \text{ mg L}^{-1}$  TOC is the difference between bare and doped- $\text{TiO}_2$  catalysts at the end of the treatment).

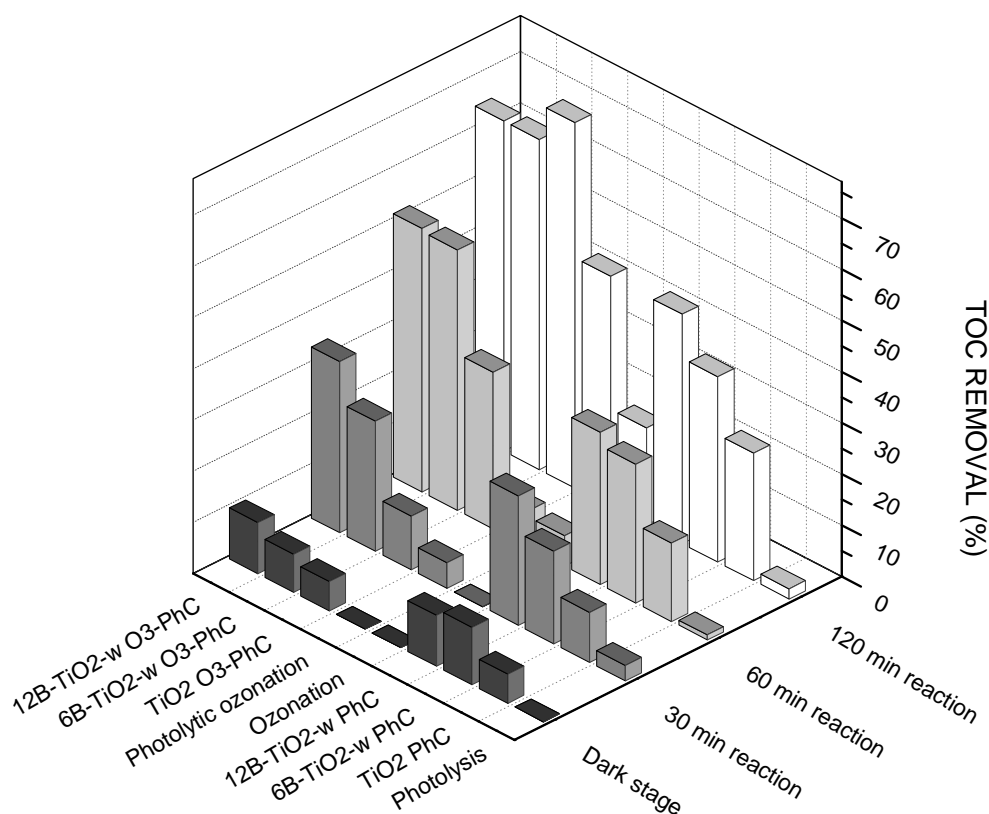


**Figure 7.6.** TOC removal during all the treatments applied with  $\text{TiO}_2$  and B- $\text{TiO}_2$  catalysts. Conditions:  $\text{pH}_0 = 6.5$ ,  $T = 25\text{--}40^\circ\text{C}$ ,  $C_{\text{PES},0} = 5 \text{ mg L}^{-1}$  (in the mixture),  $C_{\text{CAT}} = 0.33 \text{ g L}^{-1}$ ,  $Q_g = 10 \text{ L h}^{-1}$  ( $\text{O}_3/\text{O}_2$ ),  $C_{\text{O}_3\text{g}} = 5 \text{ mg L}^{-1}$ .

It is known that hydrogen peroxide can be generated during photocatalytic treatments and also through direct ozone reactions [35–37]. The role of  $\text{H}_2\text{O}_2$  and  $\text{O}_3$  involved in photocatalytic reactions has been analyzed through the results depicted in Figure 7.7. When comparing the dissolved ozone profiles (Figure 7.7A.) for single ozonation and photolytic ozonation it is observed that ozone accumulated in the solution from the beginning and its concentration remained

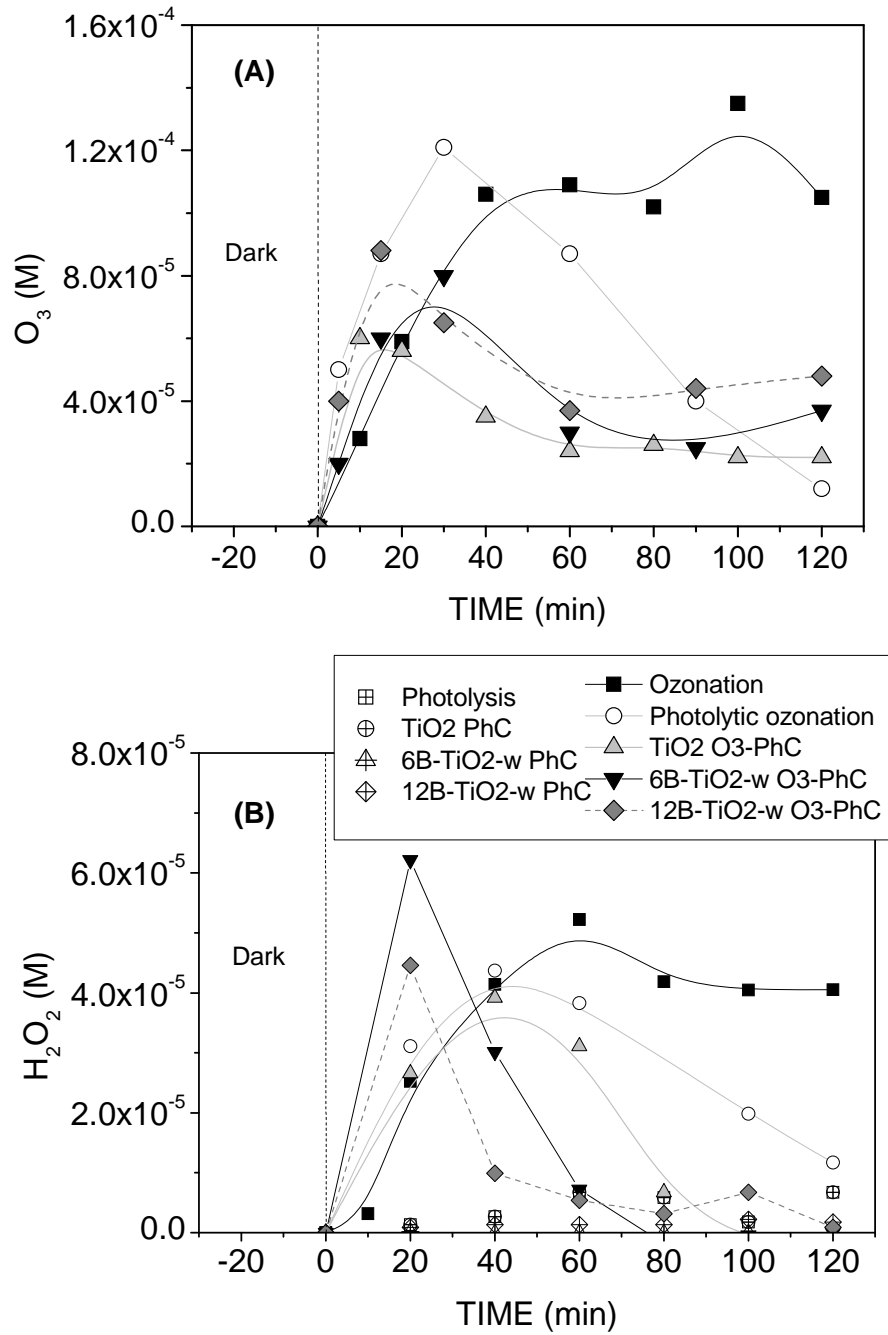


**Figure 7.7.** Evolution of dissolved O<sub>2</sub> and H<sub>2</sub>O<sub>2</sub> concentrations during all the treatments applied. Conditions: pH<sub>0</sub> = 6.5, T = 25-40°C, C<sub>PES,0</sub> = 5 mg L<sup>-1</sup> (in the mixture), C<sub>CAT</sub> = 0.33 g L<sup>-1</sup>, Q<sub>g</sub> = 10 L h<sup>-1</sup> (O<sub>3</sub>/O<sub>2</sub>), C<sub>O<sub>3g</sub></sub> = 5 mg L<sup>-1</sup>

almost constant along the experiment in contrast to photolytic ozonation which presented a maximum in the ozone concentration, which then decreased dramatically. This suggests that ozone is photolyzed with the radiation used to give rise to ROS, which enhanced the mineralization rate. The low accumulation of ozone in solution during the photocatalytic ozonation experiment can be explained taking into account the electrophilic character of ozone, which can act as an electron acceptor and trap the electrons photo-generated on the photocatalysts surface. On the other hand, the hydrogen peroxide concentration evolution is also shown in Figure 7.7B. Photolysis and photocatalytic oxidation gave place to very low  $\text{H}_2\text{O}_2$  concentrations. However, in all the ozone treatments the concentration of hydrogen peroxide was significantly higher. Thus, the formation of  $\text{H}_2\text{O}_2$  through direct ozone reactions of the four pesticides was experimentally confirmed. During single ozonation,  $\text{H}_2\text{O}_2$  concentration increased up to 40 min and then remained almost constant until the end of the experiment. A higher  $\text{H}_2\text{O}_2$  decomposition rate was observed during photolytic ozonation, resulting in lower concentration at the end of the treatment. The  $\text{H}_2\text{O}_2$  could undergo photolytic decomposition under wavelengths near 300 nm, thus improving the degradation and mineralization of the contaminants [38]. On the other hand, during photocatalytic ozonation with bare  $\text{TiO}_2$  a higher decomposition rate of  $\text{H}_2\text{O}_2$  was also observed, the concentration being negligible after 100 min of treatment. With B-doped  $\text{TiO}_2$  catalysts, the formation of hydrogen peroxide took place at higher rate reaching a maximum concentration at about 20 min and then the consumption was also faster and the concentration negligible at the end of the treatment. These results point out that  $\text{H}_2\text{O}_2$  is likely being consumed through photocatalytic reactions acting as electron acceptor in the  $\text{TiO}_2$  surface. This process is more efficient with B-doped  $\text{TiO}_2$  catalysts compared to bare  $\text{TiO}_2$  also indicating their higher photocatalytic activity.

#### 7.4.3. Catalyst stability

The stability and reusability of the 12B- $\text{TiO}_2$ -w catalyst was tested in three consecutive runs of photocatalytic ozonation process. The catalyst was easily separated by sedimentation after each run and used without any treatment in the next experiment. After removing the supernatant solution, a new fresh solution of the four pesticides was added to start the following run. In all the experiments the catalyst from the previous run was kept 30 min in the darkness with the new fresh solution to reach adsorption equilibrium.

Taking into account that main differences found between the ozone treatments were found in mineralization, Figure 7.8. shows TOC removal percentages during the dark adsorption stage and after 1 and 2 hours of photocatalytic ozonation.

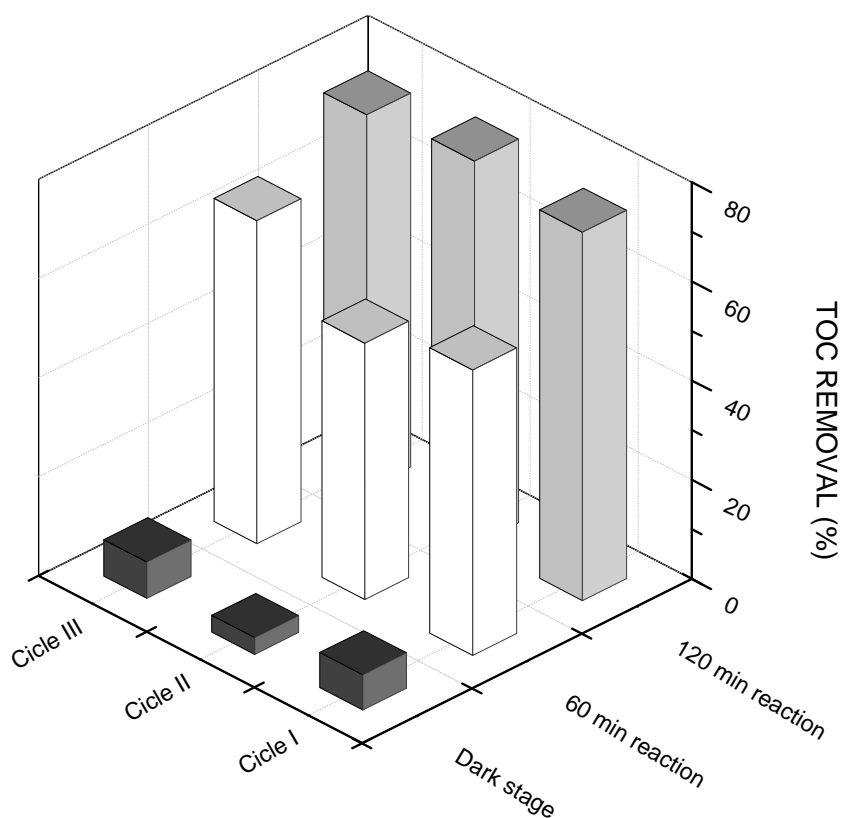


**Figure 7.8.** TOC removal during consecutive photocatalytic ozonation runs. Conditions:  $\text{pH}_0 = 6.5$ ,  $T = 25\text{-}40^\circ\text{C}$ ,  $C_{\text{PES},0} = 5 \text{ mg L}^{-1}$  (in the mixture),  $C_{\text{CAT}} = 0.33 \text{ g L}^{-1}$ ,  $Q_g = 10 \text{ L h}^{-1}$  ( $\text{O}_3/\text{O}_2$ ),  $C_{\text{O}_3\text{g}} = 5 \text{ mg L}^{-1}$

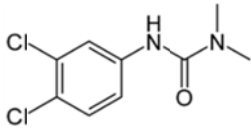
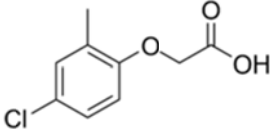
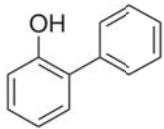
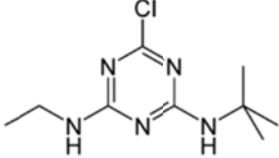
During the dark stage, only slight changes were observed in adsorption capacity of the reused catalyst varying the percentage of TOC adsorbed between 3-7% with no trend which indicates that the small amount of initial pesticides adsorbed onto the catalyst surface is oxidized during the photocatalytic treatment. On the other hand, the mineralization reached at 2 h reaction time was maintained at about 75% during the consecutive runs. Furthermore, the mineralization rate seems to slightly increase when compared TOC removal at 1 h reaction time being mineralization increased from 55 to 65% during the reutilization of the catalyst. In addition no boron leached was detected after the consecutive use of the catalyst. Therefore, although additional experiments would be needed to test the long term performance of the catalyst, this results point out the stability and reusability of these B-doped  $\text{TiO}_2$  catalysts once the non-structural remaining boron was washed.

## 7.5. Conclusions

The sol-gel method used to dope the TiO<sub>2</sub> catalysts led to the incorporation of a lower amount of boron than the theoretical value. A part of the amount of boron on the catalysts was in the form of B<sub>2</sub>O<sub>3</sub>/H<sub>3</sub>BO<sub>3</sub> species, which was unstable in aqueous solution and released boron to the reaction medium. An extra washing of the catalysts with water led to the removal of unstable boron and no further leaching. The rest of the boron on the catalysts was incorporated in interstitial positions of TiO<sub>2</sub> and did not modify the band gap energy with respect to bare TiO<sub>2</sub>. The presence of boron on the catalysts also caused the reduction of the crystal size of the anatase particles of TiO<sub>2</sub> and an increase of the pore volume and specific surface area respect to the bare TiO<sub>2</sub>. The washed B-doped TiO<sub>2</sub> were more active than bare TiO<sub>2</sub> for the removal and mineralization of the target compounds due to the effect of boron in interstitial positions of TiO<sub>2</sub> avoiding the recombination process to some extent. The efficiency of the studied systems regarding mineralization rate followed the order: single ozonation < photocatalysis with TiO<sub>2</sub> < photocatalysis with B-TiO<sub>2</sub> < photolytic ozonation < photocatalytic ozonation with TiO<sub>2</sub> < photocatalytic ozonation with B-TiO<sub>2</sub>. Photocatalytic ozonation with B-TiO<sub>2</sub> catalysts was the most efficient process in terms of mineralization, leading to the complete removal of the pesticides in less than 90 min with 75% mineralization after 120 min. The catalytic activity was maintained after 3 consecutive runs with no leaching boron detected.

## 7.6. Supplementary information

**Table 7.S1.** Molecular structure of the selected pesticides

Diuron (DIU)	2-methyl-4-chlorophenoxyacetic acid (MCPA)
	
orto-phenylphenol (OPP)	terbutylazine (TBA)
	

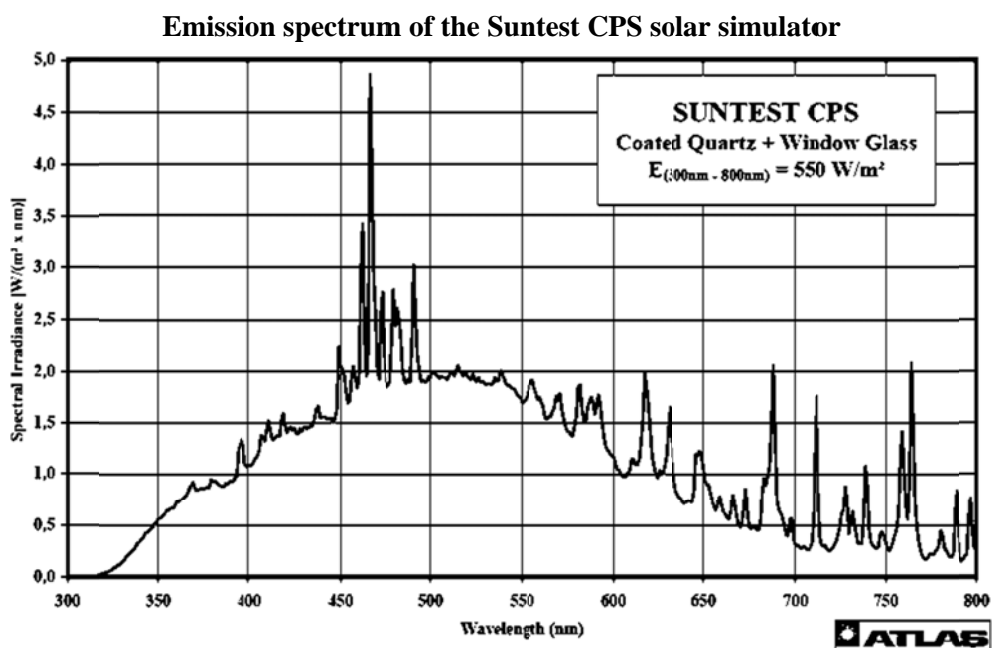


Figure 7.S1. Emission spectrum of the solar simulator

**Adsorption-desorption isotherm of the B-TiO<sub>2</sub> and CNT composite catalysts**

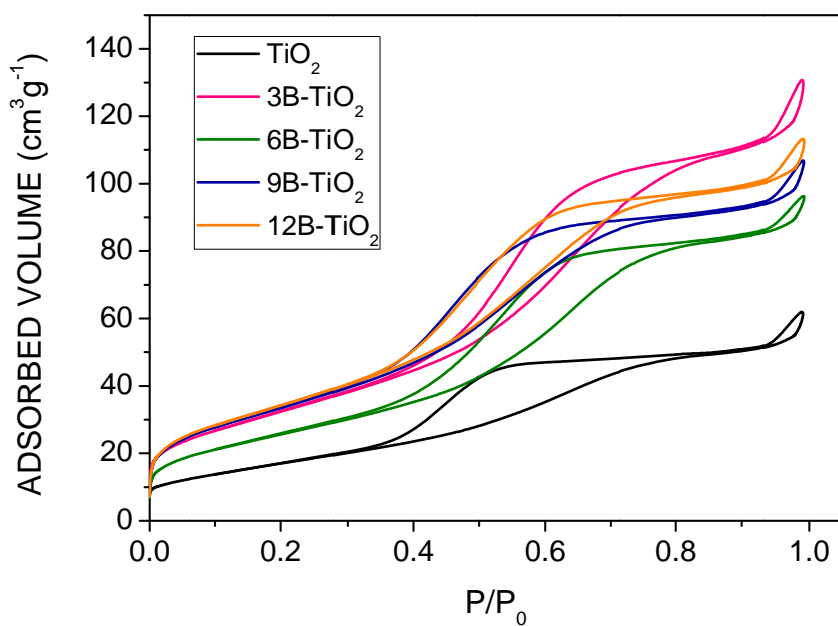
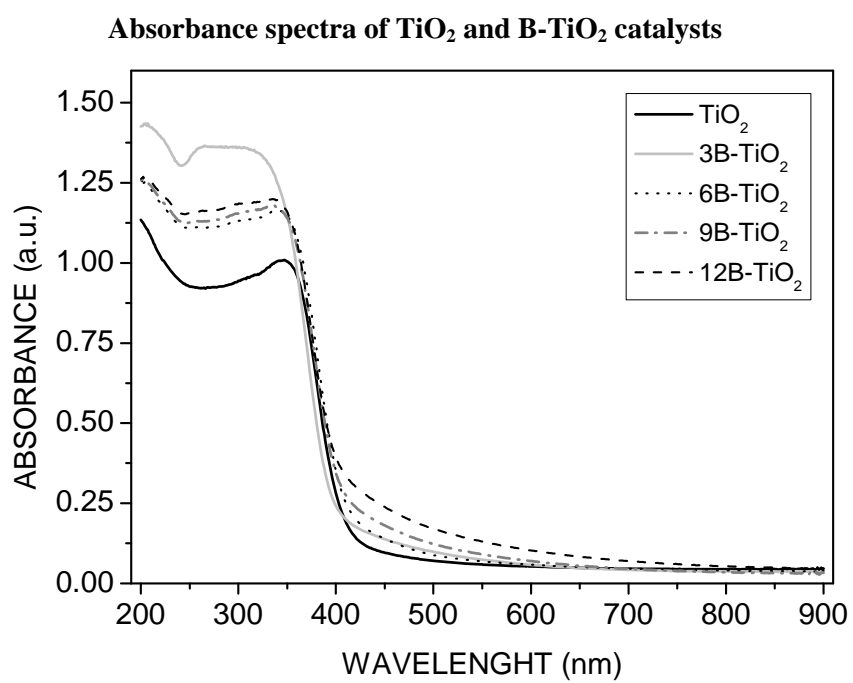
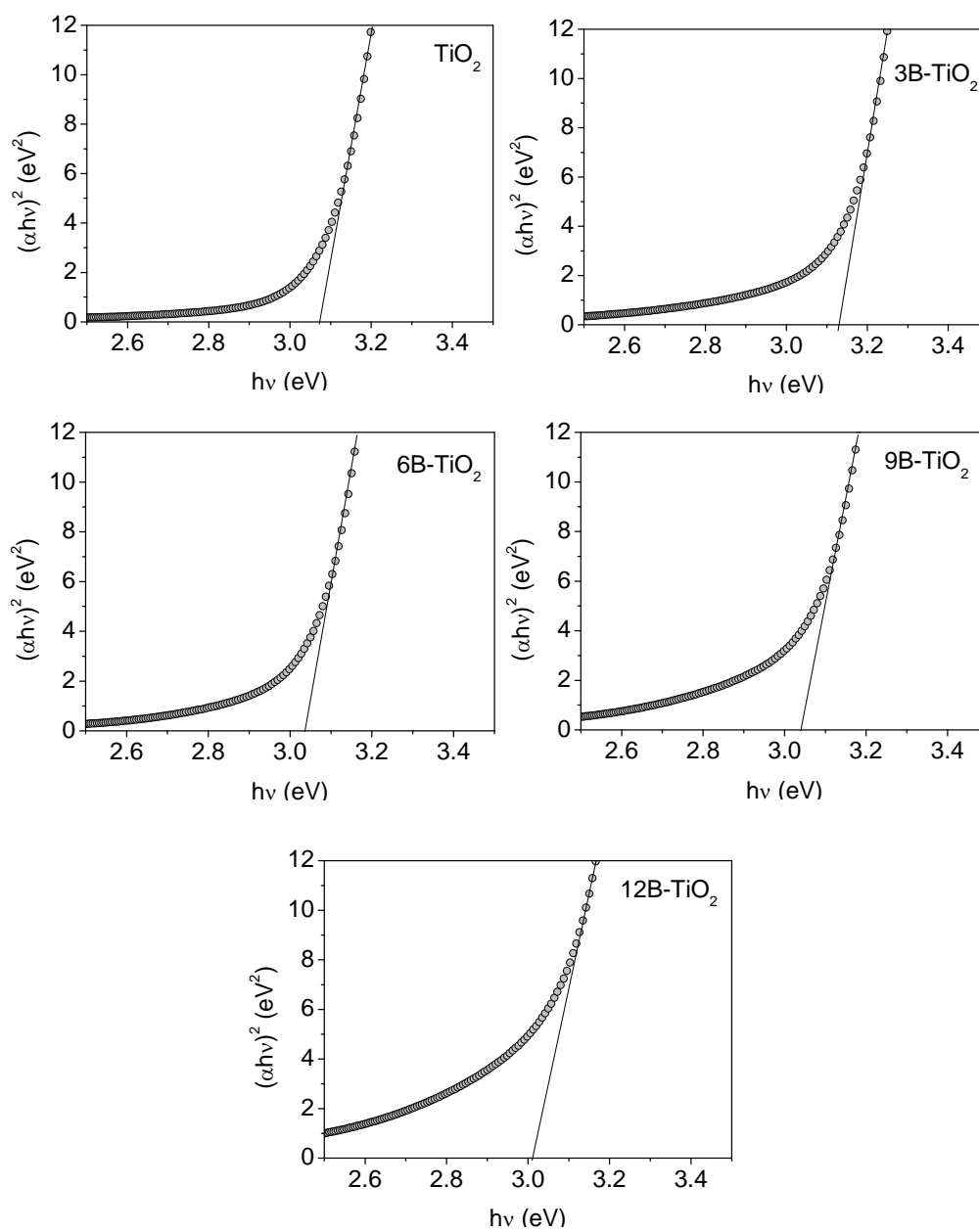


Figure 7.S2. N<sub>2</sub> adsorption-desorption isotherms

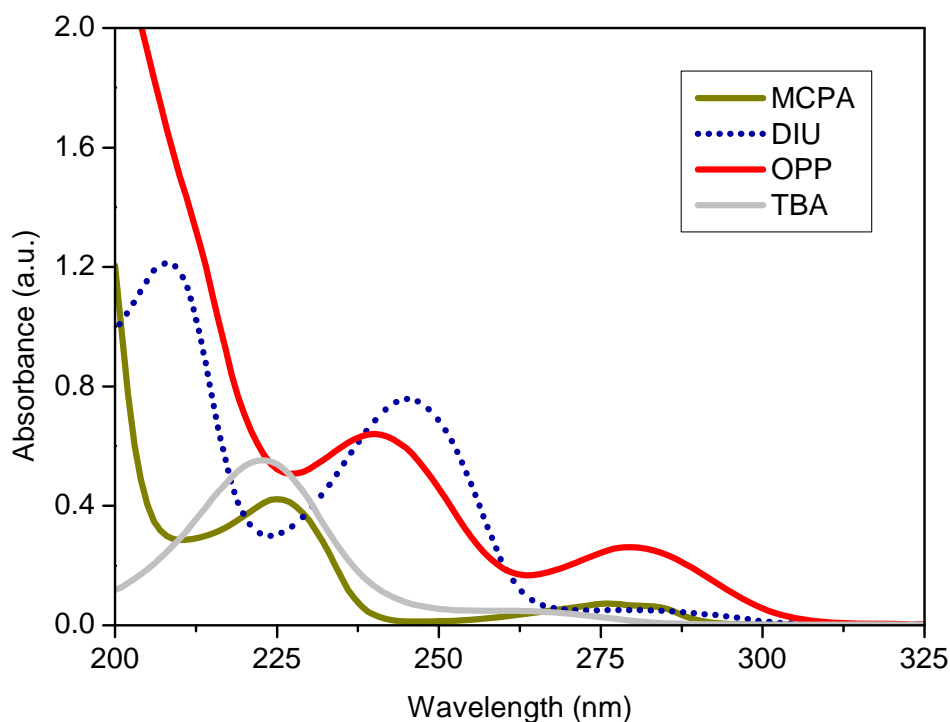


**Figure 7.S3.** DR-UV-Vis spectra of the catalysts



Band-gap determination of  $\text{TiO}_2$  and B- $\text{TiO}_2$  catalysts

**Figure 7.S4.** Band-gap determination from DR-UV-Vis analysis of the B-doped catalysts

**UV-Vis Absorbance spectra of DIU, MCPA, OPP and TBA**

**Figure 7.S5.** Absorbance UV-Visible spectra of the target compounds in ultrapure water from 200-325 nm

**7.7. Acknowledgements**

This work has been supported by the Spanish Ministerio de Economía y Competitividad (MINECO) and European Feder Funds through the project CTQ2012-35789-C02-01. Authors acknowledge the SAIUEX service of the University of Extremadura for the characterization analyses. D. H. Quiñones thanks the MINECO the concession of a predoctoral FPI grant and an aid for a research stay at the Loughborough University.

## 7.8. References

---

- [1] A. Calzadilla, K. Rehdanz, R. Tol, *The economic impact of more sustainable water use in agriculture: A computable general equilibrium analysis*, J. Hydrol. 384 (2010) 292-305.
- [2] A. Fujishima, T. N. Rao, D. A. Tryk, *Titanium dioxide photocatalysis*, J. Photochem. Photobiol. C Photochem. Rev. 1 (2000) 1-21.
- [3] X. Gao, P. Chen, J. Liu, *Enhanced visible-light absorption of nitrogen-doped titania induced by shock wave*, Mater. Lett. 65 (2011) 685-687.
- [4] P. Dharmarajan, A. Sabastiyan, M. Yosuva Suvaikin, S. Titus, C. Muthukumar, *Photocatalytic degradation of reactive dyes in effluents employing copper doped titanium dioxide nanocrystals and direct sunlight*, Chemical Science Transactions, 2 (2013) 1450-1458.
- [5] M.V. Dozzi, E. Selli, *Doping TiO<sub>2</sub> with p-block elements: Effects on photocatalytic activity*, J. Photochem. Photobiol. C Photochem. Rev. 14 (2013) 13-28.
- [6] N.S. Begum, H.M.F. Ahmed, O.M. Hussain, *Characterization and photocatalytic activity of boron-doped TiO<sub>2</sub> thinfilms prepared by liquid phase deposition technique*, Bull. Mater. Sci. 31 (2008) 741-745.
- [7] E.M. Rodríguez, G. Márquez, E.A. León, P.M. Álvarez, A.M. Amat, F.J. Beltrán, *Mechanism considerations for photocatalytic oxidation, ozonation and photocatalytic ozonation of some pharmaceutical compounds in water*, J. Environ. Manag. 127 (2013) 114-124.
- [8] T.E. Agustina, H.M. Ang, V.K. Vareek, *A review of synergistic effect of photocatalysis and ozonation on wastewater treatment*, J. Photochem. Photobiol. C Photochem. Rev. 6 (2005) 264-273.
- [9] Z. Li, B. Gao, G. Z. Chen, R. Mokaya, S. Sotiropoulos, G. Li Puma, *Carbon nanotube/titanium dioxide (CNT/TiO<sub>2</sub>) core-shell nanocomposites with tailored shell thickness, CNT content and photocatalytic/photoelectrocatalytic properties*, Appl. Catal. B-Environ. 110 (2011) 50-57.
- [10] V. Loddo, M. Addamo, V. Augugliaro, L. Palmisano, M. Schiavello, E. Garrone, *A method for determining optical properties and quantum yields of photocatalytic suspensions*, AIChE J. 52 (2006) 2565-2574.
- [11] H. Bader, J. Hoigné, *Determination of ozone in water by the indigo method*, Water Res. 15 (1981) 449-456.

- [12] W. Masschelein, M. Denis, R. Ledent, *Spectrophotometric determination of residual hydrogen peroxide*, Water Management. Water Sewage Works, August (1977) 69-72.
- [13] F.J. López, E. Giménez, F. Hernández, *Analytical study on the determination of boron in environmental water samples*, Fresenius J. Anal. Chem. 346 (1993) 984-987.
- [14] J.W. Liu, R. Han, H.T. Wang, Y. Zhao, W.J. Lu, H.Y. Wu, T.F. Yu, Y.X. Zhang, *Degradation of PCP-Na with La-B co-doped TiO<sub>2</sub> series synthesized by the sol-gel hydrothermal method under visible and solar light irradiation*, J. Mol. Catal. A Chem. 344 (2011) 145-152.
- [15] S. Bagwasi, B. Tian, J. Zhang, M. Nasir, *Synthesis, characterization and application of bismuth and boron co-doped TiO<sub>2</sub>: A visible light active photocatalyst*, Chem. Eng. J. 217 (2013) 108-118.
- [16] W. Zhang, T. Hu, B. Yang, P. Sun, H. He, *The effect of boron content on properties of B-TiO<sub>2</sub> photocatalyst prepared by sol-gel method*, J. Adv. Oxid. Technol. 16 (2013) 261-267.
- [17] D. Chen, D. Yang, Q. Wang, Z. Jiang, *Effects of boron doping on photocatalytic activity and microstructure of titanium dioxide nanoparticles*, Ind. Eng. Chem. Res. 45 (2006) 4110-4116.
- [18] A. Zaleska, J.W. Sobczak, E. Grabowska, J. Hupka, *Preparation and photocatalytic activity of boron-modified TiO<sub>2</sub> under UV and visible light*, Appl. Catal. B-Environ. 78 (2008) 92-100.
- [19] E. Finazzi, C. Di Valentin, G. Pacchioni, *Boron-doped anatase TiO<sub>2</sub>: Pure and hybrid DFT calculations*, J. Phys. Chem. C 113 (2009) 220-228.
- [20] M.W. Xiao, L. Wang, X.J. Huang, Y.D. Wu, Z. Dang, *Synthesis and characterization of WO<sub>3</sub>/titanate nanotubes nanocomposite with enhanced photocatalytic properties*, J. Alloys Comp. 470 (2009) 486-491.
- [21] Y. Li, L. Chen, Y. Guo, X. Sun, Y. Wei, *Preparation and characterization of WO<sub>3</sub>/TiO<sub>2</sub> hollow microsphere composites with catalytic activity in dark*, Chem. Eng. J. 181-182 (2012) 734-739.
- [22] C.D. Wagner, L.E. Davis, M.V. Zeller, J.A. Taylor, R.H. Raymond, L.H. Gale, *Empirical atomic sensitivity factors for quantitative analysis by electron spectroscopy for chemical analysis*, Surf. Interf. Anal. 3 (1981) 211-225.
- [23] X. Lan, L. Wang, B. Zhang, B. Tian, J. Zhang, *Preparation of lanthanum and boron co-doped TiO<sub>2</sub> by modified sol-gel method and study their photocatalytic activity*, Catal. Today 224 (2014) 163-170.

- [24] Council of the European Union, *Council Directive 98/83/EC of 3 November 1998. On the quality of water intended for human consumption* (1998).
- [25] M. Olak-Kucharczyk, J.S. Miller, S. Ledakowicz, *Ozonation kinetics of o-phenylphenol in aqueous solutions*, *Ozone-Sci. Eng.* 34 (2012) 300-305.
- [26] B.A. Wols, C.H.M. Hofman-Caris, *Review of photochemical reaction constants of organic micropollutants required for UV advanced oxidation processes in water*, *Water Res.* 46 (2012) 2815-2827.
- [27] J. Rivas, R.R. Solis, O. Gimeno, J. Sagasti, *Photocatalytic elimination of aqueous 2-methyl-4-chlorophenoxyacetic acid in the presence of commercial and nitrogen-doped TiO<sub>2</sub>*, *Int. J. Environ. Sci. Technol.* December 2013, DOI 10.1007/s13762-013-0452-4.
- [28] V. Gombac, L. De Rogatis, A. Gasparotto, G. Vicario, T. Montini, D. Barreca, G. Calducci, P. Fornasiero, E. Tondello, M. Graziani, *TiO<sub>2</sub> nanopowders doped with boron and nitrogen for photocatalytic applications*, *Chem. Phys.* 339 (2007) 111-123.
- [29] M.A. Henderson, *A surface science perspective on TiO<sub>2</sub> photocatalysis*, *Surf. Sci. Reports* 66 (2011) 185-297.
- [30] J.Y. Hu, T. Morita, Y. Magara, T. Aizawa, *Evaluation of reactivity of pesticides with ozone in water using the energies of frontier molecular orbitals*, *Water Res.* 34 (2000) 2215-2222.
- [31] F. J. Benítez, F. J. Real, J. L. Acero, C. García, *Kinetics of the transformation of phenyl-urea herbicides during ozonation of natural waters: Rate constants and model predictions*, *Water Res.* 41 (2007) 4073 – 4084.
- [32] U. von Gunten, *Ozonation of drinking water: Part I. Oxidation kinetics and product formation*, *Water Res.* 37 (2003) 1443-1467.
- [33] F. J. Beltran, *Ozone reaction kinetics for water and wastewater systems*, Boca Raton, CRC Press, Florida USA, 2004.
- [34] L. Sánchez, X. Domenech, J. Casado, J. Peral, *Solar activated ozonation of phenol and malic acid*, *Chemosphere* 50 (2003) 1085-1093.
- [35] M. Mvula, C. von Sonntag, *Ozonolysis of phenols in aqueous solution*, *Org. Biomol. Chem.* 1 (2003) 1749-1756.
- [36] A. Leitzke, C. von Sonntag, *Ozonolysis of unsaturated acids in aqueous solution: acrylic, methacrylic, maleic, fumaric and muconic acids*, *Ozone-Sci. Eng.* 31 (2009) 301-308.

- [37] S. Rakowski, D. Cherneva, *Kinetics and mechanism of the reaction of ozone with aliphatic alcohols*, Int. J. Chem. Kinetics 22 (1990) 321-329.
- [38] J.H. Baxendale, J.A. Wilson, *The photolysis of hydrogen peroxide at high light intensities*, Trans. Faraday Soc. 53 (1957) 344-356.

# Conclusions



## Chapter VIII

The main conclusions drawn from the present research are summarized in this chapter.

### Contents

**8.1.** General conclusions

**8.2.** Conclusiones generales





## 8.1. General conclusions

---

The work in this Thesis aims to make a contribution to the study of new strategies to deal with the treatment of emerging contaminants in water and wastewater. Particularly, it is an approach to solar photocatalytic ozonation processes as a viable alternative to efficiently degrade emerging contaminants. To this end, a series of objectives were established in order to achieve specific goals, as detailed in Chapter I. In connection with each objective a number of general conclusions can be withdrawn after discussing the results obtained.

**Objective 1:** Application of AOPs at pilot scale in a CPC reactor using solar radiation for the degradation of a mixture of emerging compounds (acetaminophen, antipyrine, bisphenol A, caffeine, metoprolol and testosterone) in ultrapure water and municipal wastewater:

Conclusions:

- 1.1. Under the operational conditions used in this work ( $C_{\text{Fe(III)}} = 2.79 \text{ mg L}^{-1}$ ,  $\text{H}_2\text{O}_2/\text{Fe(III)} = 6.09$  (mass ratio),  $C_{\text{TiO}_2} = 200 \text{ mg L}^{-1}$ ), it was observed that photo-Fenton system at pH 3 allows degradation rates higher than the  $\text{TiO}_2/\text{hv}$  system at pH 7.
- 1.2. Single ozonation (i.e. ozone in absence of light and catalyst) could be highlighted as a good treatment choice to eliminate organic pollutants since this treatment method was found to be able to degrade fast and completely the target compounds. However, single ozonation led to low mineralization degree (i.e., TOC removal). This behaviour suggests that, though the parent compounds react fast with ozone, there is an accumulation of degradation products that are recalcitrant to the ozone attack. Then, the use of more energetic processes is suggested to enhance EC mineralization.
- 1.3. The simultaneous application of ozone and solar radiation (i.e., photolytic ozonation) enhances considerably the efficiency of the systems considered individually, especially in terms of mineralization. This enhancement is

attributed to a higher production of hydroxyl radicals through the decomposition of ozone by solar radiation.

- 1.4. Under the experimental conditions applied in this work (Mixture of six ECs at  $10^{-5}$  mol L<sup>-1</sup>, each,  $C_{\text{Fe(III)}} = 2.79$  mg L<sup>-1</sup>,  $\text{H}_2\text{O}_2/\text{Fe(III)} = 6.09$  (mass ratio),  $C_{\text{TiO}_2} = 200$  mg L<sup>-1</sup>,  $Q_g = 0.67$  L min<sup>-1</sup>,  $C_{\text{O}_3, \text{g}} = 13$  mg L<sup>-1</sup>, average incident UVA solar radiation 41.2 W m<sup>-2</sup>), solar photocatalytic ozonation processes (Fe(III)/O<sub>3</sub>/hv/pH 3, Fe(III)/H<sub>2</sub>O<sub>2</sub>/O<sub>3</sub>/hv/pH 3 and TiO<sub>2</sub>/O<sub>3</sub>/hv) were found effective enough to remove the selected ECs and mineralize them to some extent. In addition, the consumptions of ozone in these solar photocatalytic processes were found to be much lower than those in single ozonation processes.
- 1.5. TOC removal by solar photocatalytic ozonation processes was found to follow a pseudo first order kinetics. This allows the determination of apparent reaction constants that can be used to estimate the importance of reaction pathways leading to TOC degradation. In this way, it can be concluded that oxidation by hydroxyl radicals played a major role in solar photocatalytic processes.
- 1.6. The degradation of ECs in a secondary effluent from a domestic WWTP by ozonation, solar photocatalytic oxidation and solar photocatalytic ozonation is less efficient than in ultrapure water, especially in terms of TOC removal. This is due to the presence of typically occurring species in effluents which are more refractory to oxidation than ECs but compete for oxidizing species such as ozone and hydroxyl radicals.
- 1.7. Toxicity bioassays showed that the selected ECs are toxic to *Daphnia Magna* (0.2 mg L<sup>-1</sup> each in mixture, in secondary MWWTP effluent led to 25% inhibition). Moreover, the application of solar photocatalytic oxidation and solar photocatalytic ozonation to treat the ECs in a secondary effluent from a domestic WWTP led initially to the formation of toxic intermediates, which were further removed leading to non-toxic effluents.
- 1.8. In terms of operating costs (reagent and electricity consumption) it was found that the systems using ozone, except the TiO<sub>2</sub>/O<sub>3</sub>/hv/pH 7, are the most economic choices when the goal is the complete removal of the ECs. Also when the goal is to remove TOC to some extent, the solar photocatalytic ozonation systems using Fe(III) or Fe(III)/H<sub>2</sub>O<sub>2</sub> have the lowest operating costs.

**Objective 2:** Improvement of heterogeneous photocatalytic processes based on TiO<sub>2</sub> by the application of photocatalysts with improved adsorption and separation properties.

Conclusions:

- 2.1. The commercial sample of activated carbon (Darco) used during the preparation of the magnetic catalysts, resulted to be a suitable support. Because of its textural properties and chemical surface, it is possible to prepare stable composites consisting on titania and magnetite/maghemite particles supported on the activated carbon.
- 2.2. Under the experimental conditions applied in this work for the preparation of the catalyst (consisting in magnetization of activated carbon by incipient wetness impregnation with iron nitrate solution followed by a reducing heat treatment at 350-550°C for 2-4 h in N<sub>2</sub>; and synthesis of TiO<sub>2</sub> particles by a sol-gel method using titanium butoxide as precursor and hydrolysis at pH 2 and 75°C for 24 h), it is not possible to load the activated carbon support with more than 65wt% TiO<sub>2</sub>. The crystallite phase of TiO<sub>2</sub> on the catalyst is anatase and, as a consequence, the catalyst presents good photoactivity leading, under the conditions applied in this work ( $C_{\text{cat}} = 365 \text{ mg L}^{-1}$ ,  $C_{\text{MTP},0} = 50 \text{ mg L}^{-1}$ ,  $m_{\text{O}_3,\text{g}} = 120 \text{ mg h}^{-1}$ , incident radiation =  $550 \text{ W m}^{-2}$  and 5 h treatment), up to 85% metoprolol mineralization in 10 successive photocatalytic ozonation experiments with simulated solar light.
- 2.3. The magnetic photocatalysts synthesized show good stability throughout solar photocatalytic ozonation runs and also excellent separability by the action of an external magnetic field. This latter due to the magnetic properties of the magnetite/maghemite particles supported on the activated carbon.
- 2.4. It was also found that the photolysis of ozone under 300-320 nm radiation starts an important pathway leading to the degradation of organic compounds in water. This may represent a significant contribution to the overall degradation of organic compounds in solar photocatalytic ozonation systems.

**Objective 3:** Preparation of TiO<sub>2</sub> catalysts doped with boron to improve catalyst performance in solar photocatalytic processes.

**Conclusions:**

- 3.1. The sol-gel method used in the preparation of doped TiO<sub>2</sub> catalysts (Acidic hydrolysis at room temperature of titanium butoxide in the presence of boric acid, gel formation at pH 9 and calcination at 500°C) leads to the incorporation of 0.5-0.8 wt% of boron in interstitial positions, which was only a fraction of the theoretical amount of boron. The amount of boron not incorporated in such positions is in the form of B<sub>2</sub>O<sub>3</sub>/H<sub>3</sub>BO<sub>3</sub> species, being unstable and therefore may leach out to the aqueous medium. This unstable fraction of boron can be removed from the catalyst by washing in ultrapure water. After that, the catalysts are stable (no more boron is leached out) and with enhanced activity compared to bare TiO<sub>2</sub>.
- 3.2. The preparation procedure does not modify significantly the band gap energy with respect to that of bare TiO<sub>2</sub>. However it decreases the crystal size of anatase particles, and increases the pore volume and specific surface area of the catalyst.
- 3.3. It was observed that the efficiency of the various treatment systems tested to mineralize a mixture of pesticides (diuron, o-phenylphenol, 2-methyl-4-chlorophenoxyacetic acid (MCPA) and terbuthylazine) at the experimental conditions applied in this work ( $C_{EC,0} = 5 \text{ mg L}^{-1}$  each,  $C_{cat} = 333 \text{ mg L}^{-1}$ ,  $m_{O_3,g} = 50 \text{ mg h}^{-1}$ , incident radiation =  $550 \text{ W m}^{-2}$  and 2 h treatment) follows the order: single ozonation < photocatalysis with TiO<sub>2</sub> < photocatalysis with B-TiO<sub>2</sub> < photolytic ozonation < photocatalytic ozonation with TiO<sub>2</sub> < photocatalytic ozonation with B-TiO<sub>2</sub>.
- 3.4. The B-doped TiO<sub>2</sub> catalysts are stable and easily recoverable by settling and filtration. In addition, no leaching of boron was detected throughout the repetitive use of the catalyst.

## 8.2. Conclusiones generales

---

Esta Tesis Doctoral se ha desarrollado con el objetivo principal de contribuir en el estudio de nuevas estrategias para el tratamiento de contaminantes emergentes en aguas, realizando un enfoque especial hacia los procesos de ozonación solar fotocatalítica como alternativa viable y eficiente para la degradación completa de dichos contaminantes. Así, se establecieron una serie de objetivos específicos durante la investigación, tal como se detalla en el Capítulo I. A continuación se presentan las principales conclusiones obtenidas durante el desarrollo de cada objetivo.

**Objetivo 1:** Aplicación de PAOs a escala piloto en un reactor CPC empleando radiación solar para la degradación de una mezcla de compuestos emergentes (acetaminofeno, antipirina, bisfenol A, cafeína, metoprolol y testosterona) presentes en agua ultrapura y residual (efluente secundario de EDAR):

Conclusiones:

- 1.1. En las condiciones de operación empleadas en este trabajo ( $C_{\text{Fe(III)}} = 2.79 \text{ mg L}^{-1}$ ,  $\text{H}_2\text{O}_2/\text{Fe(III)} = 6.09$  (relación másica),  $C_{\text{TiO}_2} = 200 \text{ mg L}^{-1}$ ), el sistema foto-Fenton a pH 3 ha permitido alcanzar mayores velocidades de degradación de los contaminantes seleccionados que el sistema  $\text{TiO}_2/h\nu$  a pH 7.
- 1.2. La ozonación sencilla (es decir, la aplicación de ozono en ausencia de radiación y catalizadores) es una buena alternativa para el tratamiento de contaminantes orgánicos; sin embargo, mediante este sistema suelen conseguirse bajos grados de mineralización. Aunque se ha observado que los contaminantes iniciales desaparecen rápidamente, el tratamiento da lugar a la acumulación de subproductos de degradación que son recalcitrantes al ataque del ozono. Por tanto, es conveniente el uso de procesos más energéticos (como la ozonación fotolítica o fotocatalítica) para favorecer la mineralización de estos compuestos.

- 1.3. La aplicación de forma simultánea de ozono y radiación solar (es decir, ozonación fotolítica solar) mejora considerablemente la eficiencia de los sistemas individuales (ozonación y fotólisis), especialmente en términos de mineralización. Este efecto positivo se atribuye a que en presencia de radiación hay una mayor producción de radicales hidroxilo debido a descomposición del ozono con radiación solar.
- 1.4. En las condiciones de operación empleadas en este trabajo (6 ECs en mezcla, a una concentración de  $10^{-5}$  mol L<sup>-1</sup> (cada uno),  $C_{\text{Fe(III)}} = 2,79$  mg L<sup>-1</sup>,  $\text{H}_2\text{O}_2/\text{Fe(III)} = 6,09$  (relación másica),  $C_{\text{TiO}_2} = 200$  mg L<sup>-1</sup>,  $Q_g = 0,67$  L min<sup>-1</sup>,  $C_{\text{O}_3,\text{g}} = 13$  mg L<sup>-1</sup>, radiación UVA solar incidente promedio =  $41,2$  W m<sup>-2</sup>), los procesos de ozonación fotocatalítica solar (Fe(III)/O<sub>3</sub>/hv/pH 3, Fe(III)/H<sub>2</sub>O<sub>2</sub>/O<sub>3</sub>/hv/pH 3 y TiO<sub>2</sub>/O<sub>3</sub>/hv) demostraron ser efectivos para eliminar los ECs estudiados y conseguir altos grados de mineralización. Además, la demanda de ozono en estos procesos es mucho menor que en reacciones de ozonación sencilla.
- 1.5. El perfil de conversión del carbón orgánico total (COT) en procesos de ozonación fotocatalítica solar puede ajustarse a una cinética de pseudo primer orden. De esta manera es posible determinar unas constantes de mineralización aparentes, con las que puede hacerse una estimación de la importancia relativa de los mecanismos de reacción que conllevan a la mineralización. De esta forma, se concluyó que la oxidación mediante radicales hidroxilo es una contribución importante en la conversión del COT.
- 1.6. La eficacia en el tratamiento mediante ozonación, oxidación fotocatalítica solar y ozonación fotocatalítica solar de los ECs estudiados en efluentes secundarios de aguas residuales municipales, sufre una disminución comparado con los ensayos en agua ultrapura, especialmente en la mineralización. Esto se debe a la presencia de especies recalcitrantes que compiten con los ECs por las especies oxidantes durante el proceso como el ozono y el radical hidroxilo.
- 1.7. Mediante el uso de *Daphnia Magna* como indicador de toxicidad, se observó que los ECs seleccionados son tóxicos en las concentraciones empleadas (0.2 mg L<sup>-1</sup> en efluente secundario; 25% de inhibición). Durante la aplicación de procesos de fotocatalisis solar y ozonación fotocatalítica solar se produce un aumento de la toxicidad de las muestras debido a la acumulación de intermedios tóxicos y que disminuye cuando se alcanzan mayores grados de mineralización.

1.8. En cuanto a la evaluación de costes de operación (teniendo en cuenta el consumo de reactivos y electricidad durante los procesos aplicados) se encontró que los procesos en los que se usa ozono, excepto en el caso de  $\text{TiO}_2/\text{O}_3/\text{hv}/\text{pH } 7$ , representan la mejor opción de tratamiento siempre que el objetivo sea la eliminación de los contaminantes iniciales. En el caso de requerir un grado de mineralización determinado, los sistemas de ozonación fotocatalítica empleando  $\text{Fe(III)}$  o  $\text{Fe(III)}/\text{H}_2\text{O}_2$  a  $\text{pH } 3$  representan las menores opciones en cuanto a costes de operación.

**Objetivo 2:** Mejora de los procesos de fotocatalisis heterogénea basados en  $\text{TiO}_2$  mediante la síntesis y aplicación de fotocatalizadores con propiedades de adsorción y separación mejoradas.

Conclusiones:

2.1. El carbón activo comercial empleado (Darco) es un soporte adecuado para la preparación de fotocatalizadores magnéticos. Debido a sus propiedades texturales y su química superficial ha sido posible la preparación de catalizadores estables que consisten en partículas de  $\text{TiO}_2$  y magnetita/maghemita soportadas sobre el carbón.

2.2. Mediante el método empleado para la preparación de los catalizadores magnéticos (que consiste en magnetizar el carbón activo por impregnación incipiente con una disolución de nitrato férrico y posterior tratamiento térmico reductor a  $350\text{-}550^\circ\text{C}$  durante 2-4 h en  $\text{N}_2$ , y síntesis de las partículas de  $\text{TiO}_2$  mediante hidrólisis de butóxido de titanio a  $\text{pH } 2$  y reflujo a  $75^\circ\text{C}$  durante 24 h) sólo ha sido posible soportar hasta un 65% en peso de  $\text{TiO}_2$ . La fase cristalina de las partículas de  $\text{TiO}_2$  soportadas corresponde a anatasa y en consecuencia, los catalizadores presentan buena fotoactividad en las condiciones experimentales empleadas ( $C_{\text{cat}} = 365 \text{ mg L}^{-1}$ ,  $C_{\text{MTP},0} = 50 \text{ mg L}^{-1}$ ,  $m_{\text{O}_3,\text{g}} = 120 \text{ mg h}^{-1}$ , intensidad de radiación incidente en simulador solar =  $550 \text{ W m}^{-2}$  y 5 h de reacción). En estas condiciones se obtuvo un 85% de mineralización de metoprolol durante 10 tratamientos sucesivos de ozonación fotocatalítica.

2.3. Los catalizadores magnéticos sintetizados son estables en procesos de ozonación solar fotocatalítica y además fácilmente separables mediante el uso de un campo magnético externo, gracias a las partículas de magnetita/maghemita soportadas en el carbón activo.

- 2.4. La fotólisis de ozono bajo radiación con longitudes de onda entre 300-320 nm representa una contribución importante en el mecanismo de degradación de los contaminantes orgánicos en agua.

**Objetivo 3:** Preparación de catalizadores de  $\text{TiO}_2$  dopados con boro con propiedades mejoradas.

Conclusiones:

- 3.1. A través del método sol-gel empleado en la preparación de los catalizadores de  $\text{TiO}_2$  dopados con boro (que consiste en una hidrólisis ácida a temperatura ambiente de butóxido de titanio en presencia de ácido bórico, formación del gel a pH 9 y calcinación a  $500^\circ\text{C}$ ) se consigue únicamente la incorporación de un 0,5-0,8 % en peso de boro intersticial, independientemente de la cantidad de boro utilizado durante la preparación. El boro que no logra incorporarse, se encuentra como  $\text{B}_2\text{O}_3/\text{H}_3\text{BO}_3$ , que es inestable y por tanto se lixivia al medio de reacción. Esta fracción de boro se elimina mediante lavados en agua.
- 3.2. El procedimiento de preparación no conlleva modificaciones en la anchura del salto de banda de los catalizadores dopados respecto al  $\text{TiO}_2$  puro. Sin embargo, se observa una disminución del tamaño de cristal de anatasa y un incremento en el volumen de poro y área específica de los catalizadores.
- 3.3. Los catalizadores preparados se emplearon en procesos fotocatalíticos a escala de laboratorio en un simulador solar para mineralizar una mezcla de pesticidas seleccionados como compuestos modelo (diurón, o-fenilfenol, MCPA y terbutilazina). En las condiciones experimentales utilizadas durante los ensayos ( $C_{\text{EC},0} = 5 \text{ mg L}^{-1}$ ,  $C_{\text{cat}} = 333 \text{ mg L}^{-1}$ ,  $m_{\text{O}_3,\text{g}} = 50 \text{ mg h}^{-1}$ , intensidad de radiación incidente =  $550 \text{ W m}^{-2}$  y 2 h de reacción), la eficiencia de los sistemas sigue el orden: ozonación sencilla < oxidación fotocatalítica con  $\text{TiO}_2$  < oxidación fotocatalítica con B- $\text{TiO}_2$  < ozonación fotolítica < ozonación fotocatalítica con  $\text{TiO}_2$  < ozonación fotocatalítica con B- $\text{TiO}_2$ .
- 3.4. Los catalizadores de  $\text{TiO}_2$  dopados con boro son estables y fácilmente separables por sedimentación y filtración. No se produce lixiviación de boro durante ensayos de recuperación y reutilización de los catalizadores en procesos sucesivos de ozonación fotocatalítica solar.



# Annex



## Annex

This Annex presents a list of papers resulting from the research carried out during this Thesis, indicating their status at the time of the presentation of the dissertation. Additionally, the resulting peer reviewed conference papers, which have been presented at different scientific conferences, are also listed.

### Contents

**A.1.** Journal publications

**A.2.** Peer reviewed conference papers



## **A.1. Journal publications**

---

Ana Rey, Diego H. Quiñones, Pedro M. Álvarez, Fernando J. Beltrán, Pawel K. Plucinski, Simulated solar-light assisted photocatalytic ozonation of metoprolol over titania-coated magnetic activated carbon. *Applied Catalysis B: Environmental* 111-112 (2012) 246–253.

Diego H. Quiñones, Ana Rey, Pedro M. Álvarez, Fernando J. Beltrán, Pawel K. Plucinski, Enhanced activity and reusability of TiO<sub>2</sub> loaded magnetic activated carbon for solar photocatalytic ozonation. *Applied Catalysis B: Environmental* 144 (2014) 96–106.

Diego H. Quiñones, Pedro M. Álvarez, Ana Rey, Sandra Contreras, Fernando J. Beltrán, Application of solar photocatalytic ozonation for the degradation of emerging contaminants in water in a pilot plant. *Chemical Engineering Journal* 260 (2015) 399–410.

Diego H. Quiñones, Ana Rey, Pedro M. Álvarez, Fernando J. Beltrán, G. Li Puma, Boron doped TiO<sub>2</sub> catalysts for photocatalytic ozonation of aqueous mixtures of common herbicides and pesticides: Diuron, o-phenylphenol, MCPA and terbuthylazine. Accepted for publication in *Applied Catalysis B: Environmental*, DOI: 10.1016/j.apcatb.2014.10.036.

Diego H. Quiñones, Pedro M. Álvarez, Fernando J. Beltrán, Ana Rey, Removal of emerging contaminants from municipal WWTP secondary effluents by solar photocatalytic ozonation. A pilot-scale study. Submitted for publication in: *Separation and Purification Technology*.

## **A.2. Peer reviewed conference papers**

---

Diego H. Quiñones, Pedro M. Álvarez, Fernando J. Beltrán, M. Azahara Espejo, Degradation of six emerging contaminants in water by Fe(III) and Fe(III)-oxalate solar photocatalytic ozonation, 12th Mediterranean Congress of Chemical Engineering – Expoquimia. Barcelona, Spain (Nov. 2011).

Diego H. Quiñones, Ana Rey, Pedro M. Álvarez, Fernando J. Beltrán, Azahara. Espejo, Catalizadores magnéticos de dióxido de titanio soportado sobre carbón activo para la depuración de contaminantes emergentes mediante ozonación

fotocatalítica solar, Mesa Española de Tratamiento de Aguas, META. Almería, Spain (Oct. 2012)

Diego H. Quiñones, Ana Rey, Pedro M. Álvarez, Fernando J. Beltrán, On the reaction mechanism of metoprolol removal through photocatalytic ozonation with TiFeAC catalyst under simulated solar radiation, 3rd European Symposium on Photocatalysis. Portoroz, Slovenia (Sept. 2013)

Diego H. Quiñones, Ana Rey, Sandra Contreras, Fernando J. Beltrán, Pedro M. Álvarez, Aplicación simultánea de ozonación y oxidación fotocatalítica mediante foto-Fenton para la depuración de contaminantes emergentes en planta piloto, Mesa Española de Tratamiento de Aguas, META. Alicante, Spain (Jun. 2014)

Ana Rey, Diego H. Quiñones, Pedro M. Álvarez, Fernando J. Beltrán, Gianluca Li Puma, Synthesis of a B-doped TiO<sub>2</sub> photocatalyst for the removal of selected pesticides in laboratory waters by solar photocatalytic ozonation, 8th European Meeting on Solar Chemistry and Photocatalysis: Environmental Applications – SPEA8. Thessaloniki, Greece (Jun. 2014)

Diego H. Quiñones, Ana Rey, Pedro M. Álvarez, Estefanía Mena, Fernando J. Beltrán, Gianluca Li Puma, Boron doped TiO<sub>2</sub> photocatalysts for solar photocatalytic treatments of selected pesticides, 13th Mediterranean Congress of Chemical Engineering – Expoquimia. Barcelona, Spain (Sept. 2014).



## Simulated solar-light assisted photocatalytic ozonation of metoprolol over titania-coated magnetic activated carbon

Ana Rey<sup>a,\*</sup>, Diego H. Quiñones<sup>a</sup>, Pedro M. Álvarez<sup>a</sup>, Fernando J. Beltrán<sup>a</sup>, Pawel K. Plucinski<sup>b</sup>

<sup>a</sup> Departamento de Ingeniería Química y Química Física, Universidad de Extremadura, Avenida de Elvas S/N, 06006 Badajoz, Spain  
<sup>b</sup> Department of Chemical Engineering, University of Bath, BA2 7AY Bath, United Kingdom

### ARTICLE INFO

#### Article history:

Received 21 July 2011  
 Received in revised form  
 26 September 2011  
 Accepted 4 October 2011  
 Available online 8 October 2011

#### Keywords:

Solar photocatalysis  
 Ozone  
 Magnetic catalyst  
 Pharmaceuticals  
 Water treatment

### ABSTRACT

A magnetically separable photocatalyst consisting of magnetic porous activated carbon with attached anatase TiO<sub>2</sub> particles has been prepared and tested for the degradation of metoprolol (MTP) in aqueous solution. The synthesized photocatalyst (TiFeC) was characterized by nitrogen adsorption, XRD, FTIR, SEM, EDX and SQUID magnetometer. The obtained catalyst with a TiO<sub>2</sub> composition of 61 wt.% (mostly anatase) had moderate surface area (BET surface of 331 m<sup>2</sup> g<sup>-1</sup>) and volume of micropores and exhibited magnetic properties with saturation magnetization of 1.6 emu g<sup>-1</sup> and neither remanent magnetization nor coercivity. The photocatalytic activity of TiFeC samples was tested by degrading MTP by simulated solar photocatalytic ozonation. The results were compared to those obtained with a commercial titania (Degussa P25) and by photolytic ozonation (i.e., absence of catalyst). Complete MTP removal and more than 60% TOC conversion were achieved after 3 h of photocatalytic ozonation of an aqueous solution containing as much as 50 mg L<sup>-1</sup> MTP initial concentration. The reusability and stability of the catalyst were tested through a series of five photocatalytic ozonation experiments. Minor amounts of iron and titanium were leached out from the catalyst and the catalytic activity decreased to a very low extent with the reuse of the catalyst.

© 2011 Elsevier B.V. All rights reserved.

### 1. Introduction

Solar photocatalytic detoxification of water and wastewater is an emerging area of research and commercial development as it may be considered as one of the most cost effective treatment technologies in regions of high incoming solar radiation [1,2]. Solar photocatalytic detoxification is a relatively new clean technology to remove toxic and persistent pollutants in water and wastewater by focusing sunlight onto a reactor through which the contaminated water is flowing in the presence of a catalyst. Among candidates for solar photocatalysis, TiO<sub>2</sub> in the form of anatase is the most suitable material for industrial use at present because it is a non-toxic material with high chemical stability, low cost and high oxidation power. It is a semiconductor with a band gap of about 3.2 eV allowing absorption of UV light with wavelengths below 387.5 nm (about 5% of solar spectrum) to generate electron-hole pairs (e<sup>-</sup>/h<sup>+</sup>) on the catalyst surface. Electron-hole pairs, in turn, trigger a series of reactions generating free-radicals (mainly hydroxyl radicals, HO<sup>\*</sup>), which are very efficient non-selective oxidizers of water pollutants, both chemical compounds and microorganisms

(disinfection). Solar TiO<sub>2</sub> photocatalysis is receiving great attention for water and wastewater remediation and it has been extensively investigated for the removal of organic recalcitrant pollutants as for example, pharmaceuticals [3–6], dyes [7] or pesticides [8] as well as to inactivate pathogenic microorganisms such as *Escherichia coli* [9].

Given the concern over the risk posed by the presence of pharmaceutical compounds in water bodies, and hence the possible impacts on public health and aquatic ecosystems a great deal of research is being carried out on technologies for the removal of these compounds [10–12]. In general, pharmaceutical compounds are hardly biodegradable so they are not eliminated by conventional treatment at wastewater treatment plants (WWTPs) and, as a consequence, they are frequently reported to be present in WWTP effluents at ng L<sup>-1</sup> and even µg L<sup>-1</sup> concentration levels [13]. Although solar TiO<sub>2</sub> photocatalysis has been found effective for the removal of different pharmaceutical compounds from aqueous solution, to achieve complete mineralization long reaction times are needed because of the formation of a number of intermediates which, frequently, are hard to degrade [2].

In this work, with the aim of enhancing process performance regarding mineralization rate of complex organic molecules such those of pharmaceutical compounds, solar photocatalytic ozonation has been applied. Photocatalytic ozonation, which is the

\* Corresponding author. Tel.: +34 924289385; fax: +34 924289385.  
 E-mail address: anarey@unex.es (A. Rey).



Contents lists available at ScienceDirect

Applied Catalysis B: Environmental

journal homepage: [www.elsevier.com/locate/apcatb](http://www.elsevier.com/locate/apcatb)

## Enhanced activity and reusability of TiO<sub>2</sub> loaded magnetic activated carbon for solar photocatalytic ozonation



Diego H. Quiñones<sup>a</sup>, Ana Rey<sup>a,\*</sup>, Pedro M. Álvarez<sup>a</sup>,  
Fernando J. Beltrán<sup>a</sup>, Pawel K. Plucinski<sup>b</sup>

<sup>a</sup> Dpto. Ingeniería Química y Química Física, Universidad de Extremadura, Avda. Elvas s/n, 06006 Badajoz, Spain  
<sup>b</sup> Department of Chemical Engineering, University of Bath, BA2 7AY Bath, United Kingdom

### ARTICLE INFO

**Article history:**  
Received 18 March 2013  
Received in revised form 26 June 2013  
Accepted 1 July 2013  
Available online 12 July 2013

**Keywords:**  
Photocatalytic ozonation  
TiO<sub>2</sub> magnetic photocatalyst  
Metoprolol  
Water treatment  
Reusability

### ABSTRACT

Magnetically separable photocatalysts with high activity under solar illumination were successfully synthesized from a commercial meso-to-microporous activated carbon. First magnetite and then titania (anatase) were deposited onto the activated carbon support by impregnation and sol-gel methods, respectively. Various catalyst samples were prepared with different iron and titania contents. The synthesized photocatalysts were characterized by nitrogen adsorption, XRD, SEM, EDX, XPS and SQUID magnetometer. Photocatalytic performance of some selected samples was examined under various irradiation conditions in the wavelength ranges of 300–800 nm, 320–800 nm and 390–800 nm. Metoprolol tartrate (MTP) in aqueous solution (50 mg L<sup>-1</sup>) was chosen as target compound for catalytic activity tests. The most efficient catalyst had TiO<sub>2</sub> and Fe mass compositions of 64 wt% and 9 wt%, respectively. It showed high activity in photocatalytic ozonation with complete removal of MTP in less than 2 h reaction time and 85% mineralization after 5 h. This catalyst was also easily separable due to its developed magnetic properties. Catalyst reusability and stability was proved to be rather good after completing a series of 10 consecutive photocatalytic ozonation runs.

© 2013 Elsevier B.V. All rights reserved.

### 1. Introduction

Given the global concern generated by the increasingly occurrence of emerging contaminants (ECs) in wastewater and aquatic environments, the research and development of novel water treatment technologies that can remove these compounds in a cost-efficient way is challenging.

Advanced oxidation processes (AOPs) involve the formation of highly reactive species, such as hydroxyl radical (\*OH,  $E^{\circ} = 2.8$  V), which is capable of oxidizing most of the organic compounds in water [1]. Thus, various AOPs have demonstrated their ability to degrade many ECs transforming them into harmless products [2]. Among these AOPs, solar photocatalytic oxidation using TiO<sub>2</sub> as catalyst is one of the most promising cost-effective alternatives since it is a method capable of completely degrade organic ECs up to CO<sub>2</sub> and H<sub>2</sub>O and also perform oxidative transformation of some inorganic compounds and deactivation of pathogenic microorganisms [3,4]. Recently, it has been shown that the combination of TiO<sub>2</sub> and ozone under sunlight illumination (i.e. solar photocatalytic ozonation) can greatly enhance the ECs degradation rates achieved by the

single processes (i.e. ozonation and solar photocatalytic oxidation). The reason for such behavior is likely due to the adsorption of ozone onto the TiO<sub>2</sub> surface where it traps electrons promoted to the conduction band of the semiconductor, thus avoiding, to some extent, ineffective electron-hole recombination and generating ozonide radicals (\*O<sub>3</sub><sup>-</sup>), which can be further transformed into hydroxyl radicals [5–7].

A key factor in the development of solar photocatalytic ozonation processes for the removal of ECs from water is the use of a suitable photocatalyst. In a previous work, a TiO<sub>2</sub> (anatase)-magnetic carbon composite (TiFeC) was synthesized and used for the degradation of metoprolol tartrate (MTP) [8]. MTP is a  $\beta$ -blocker pharmaceutical compound frequently found in effluents from sewage treatment plants [9,10]. After the treatment, the catalyst particles could be separated from the solution by an external magnet due to their superparamagnetic behavior, though their saturation magnetization was rather low (1.6 emu g<sup>-1</sup>) compared to bulk magnetite (92 emu g<sup>-1</sup>). Photocatalytic activity was fairly good though somewhat lower than that found for the commercially available catalyst AEROXIDE® TiO<sub>2</sub> P25. As part of our ongoing work on photocatalytic ozonation, this paper is focused on the optimization of TiFeC catalysts to improve their photocatalytic activity, separability and reusability by means of the synthesis of catalysts with different magnetite and titanium dioxide loadings. Also, this

\* Corresponding author. Tel.: +34 924289383; fax: +34 924289385.  
E-mail address: [anarey@unex.es](mailto:anarey@unex.es) (A. Rey).



Contents lists available at ScienceDirect

Chemical Engineering Journal

journal homepage: [www.elsevier.com/locate/cej](http://www.elsevier.com/locate/cej)Chemical  
Engineering  
Journal

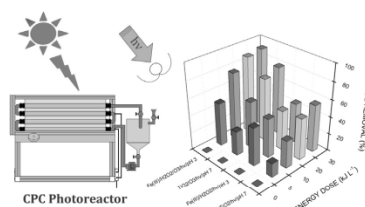
## Application of solar photocatalytic ozonation for the degradation of emerging contaminants in water in a pilot plant

Diego H. Quiñones<sup>a</sup>, Pedro M. Álvarez<sup>a</sup>, Ana Rey<sup>a</sup>, Sandra Contreras<sup>b</sup>, Fernando J. Beltrán<sup>a,\*</sup><sup>a</sup>Departamento de Ingeniería Química y Química Física, Facultad de Ciencias, Universidad de Extremadura, Av. de Elvas s/n, 06071 Badajoz, Spain<sup>b</sup>Departament d'Enginyeria Química, Universitat Rovira i Virgili, Campus Sescelades, Av. Països Catalans 26, 43007 Tarragona, Spain

### HIGHLIGHTS

- Emerging pollutants were successfully degraded by solar AOPs in a CPC photo reactor.
- Ozonation and photolytic ozonation can completely remove the emerging compounds.
- Combination of photocatalysis and ozone enhances considerably the system efficiency.
- TOC conversion kinetics can be fitted to pseudo-first order reaction models.

### GRAPHICAL ABSTRACT



### ARTICLE INFO

#### Article history:

Received 28 March 2014  
 Received in revised form 2 August 2014  
 Accepted 18 August 2014  
 Available online 27 August 2014

#### Keywords:

Photocatalytic ozonation  
 Emerging compound  
 Compound parabolic collector  
 Synergy  
 Ozonation kinetic regime

### ABSTRACT

Aqueous mixtures of six commonly detected emerging contaminants (acetaminophen, antipyrine, bisphenol A, caffeine, metoprolol and testosterone), selected as model compounds, were treated by different solar-driven photochemical processes including photolysis, photocatalytic oxidation with Fe(III) or TiO<sub>2</sub>, photo-Fenton and single, photolytic and photocatalytic ozonations. Experiments were carried out in a compound parabolic collector photoreactor. It was found that photolysis and photocatalytic oxidation using Fe(III) are not effective for the complete removal of the selected contaminants, while TiO<sub>2</sub> photocatalysis, photo-Fenton, single, photolytic and photocatalytic ozonations can rapidly remove them and decrease total organic carbon to some extent. The combination of photocatalytic oxidation and ozonation considerably enhances the system efficiency by reducing the ozone demand and energy requirements to completely remove the contaminants. Results also demonstrate that, at the operational conditions applied in this work, the contaminant removal and mineralization by ozone processes takes place in the slow kinetic regime, therefore the application of the ozone combined processes studied instead of single ozonation is recommended. Kinetic considerations on the application of solar photocatalytic processes for mineralization have been also assessed.

© 2014 Elsevier B.V. All rights reserved.

### 1. Introduction

Nowadays a great number of pharmaceuticals and personal care products, commonly known as emerging contaminants (ECs), are being detected in aqueous systems such as rivers, lakes, streams,

aquifers and wastewater treatment plant influents and effluents. These compounds are considered potentially hazardous as some are ubiquitous, persistent to conventional wastewater treatments and biologically active, many of them with recognized endocrine disruption functions [1,2].

Advanced Oxidation Processes (AOPs) constitute an alternative for the degradation of ECs. AOPs are physicochemical processes based on the generation of hydroxyl radicals ( $\cdot\text{OH}$ ) under mild

\* Corresponding author. Tel.: +34 924289300; fax: +34 924289385.  
 E-mail address: [fbeltran@unex.es](mailto:fbeltran@unex.es) (F.J. Beltrán).

## Accepted Manuscript

Title: Boron doped TiO<sub>2</sub> catalysts for photocatalytic ozonation of aqueous mixtures of common pesticides: Diuron, o-phenylphenol, MCPA and terbuthylazine

Author: D.H. Quiñones A. Rey P.M. Álvarez F.J. Beltrán G. Li Puma



PII: S0926-3373(14)00649-3  
DOI: <http://dx.doi.org/doi:10.1016/j.apcatb.2014.10.036>  
Reference: APCATB 13658

To appear in: *Applied Catalysis B: Environmental*

Received date: 11-7-2014  
Revised date: 10-10-2014  
Accepted date: 12-10-2014

Please cite this article as: D.H. Quiñones, A. Rey, P.M. Álvarez, F.J. Beltrán, G.L. Puma, Boron doped TiO<sub>2</sub> catalysts for photocatalytic ozonation of aqueous mixtures of common pesticides: Diuron, o-phenylphenol, MCPA and terbuthylazine, *Applied Catalysis B, Environmental* (2014), <http://dx.doi.org/10.1016/j.apcatb.2014.10.036>

This is a PDF file of an unedited manuscript that has been accepted for publication. As a service to our customers we are providing this early version of the manuscript. The manuscript will undergo copyediting, typesetting, and review of the resulting proof before it is published in its final form. Please note that during the production process errors may be discovered which could affect the content, and all legal disclaimers that apply to the journal pertain.





## Degradation of six emerging contaminants in water by Fe(III) and Fe(III)-oxalate solar photocatalytic ozonation

D. H. Quiñones\*, P. M. Álvarez, F. J. Beltrán, A. Esjejo.

Universidad de Extremadura, Departamento de Ingeniería Química y Química Física, Avenida de Elvas s/n, 06071 Badajoz, Spain.  
Phone: +34 924289300, Fax: +34 924289385, \*dquinone@alumnos.unex.es

### Introduction

Recently, an increasing number of emerging contaminants is being detected in water bodies. These pollutants represent serious risk for aquatic life and the environment [1].

Advanced Oxidation Processes (AOPs), such as photocatalysis, which involve the transformation of the chemical structure of the pollutants by the generation of highly oxidant species such as the hydroxyl radical, can be highlighted as effective methods for removing these emerging compounds [1].

In this research, the degradation of an aqueous mixture of six emerging compounds by solar photocatalysis in the presence of Fe(III) and Fe(III)-oxalate, ozonation and solar photocatalytic ozonation has been studied.

### Experimental

Degradation experiments were carried out in a pilot-scale cylindrical-parabolic solar collector (CPC), with 5 L capacity (1.8 L irradiated), 0.25 m<sup>2</sup> of reflection surface and provided with gas inlets and outlets.



Figure 1. Experimental set-up.

The CPC was placed in Badajoz, Spain (38°52'43" N, 6°58'15" W). The average incident UVA radiation throughout the experiments was measured to be 35 Wm<sup>-2</sup>.

Emerging contaminants acetaminophen (AC), antipyrin (AN), bisphenol A (BI), caffeine (CA), metoprolol (ME) and testosterone (TE) were selected as target compounds. Their chemical structures are shown in Fig. 2.

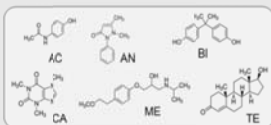


Figure 2. Chemical structures of the target compounds.

Solutions of these contaminants (1x10<sup>-5</sup> M each) were prepared in unbuffered ultrapure water at pH 3 and subjected to treatment. The initial concentrations for Fe(III), H<sub>2</sub>O<sub>2</sub> and oxalate were 5x10<sup>-5</sup>, 5x10<sup>-4</sup> and 4x10<sup>-4</sup> M, respectively. In photocatalytic ozonation experiments, the inlet gas was an ozone-air mixture containing 10 mg L<sup>-1</sup> ozone at 40 L h<sup>-1</sup>. Evaluated systems are shown in Table 1.

Exp.	Radiation	Fe	O <sub>3</sub>	H <sub>2</sub> O <sub>2</sub>	Oxalate
R1	x				
R2	x	x			
R3			x		
R4	x	x	x		
R5	x	x	x		x
R6	x	x	x		
R7	x	x	x	x	
R8	x	x	x	x	x
R9	x	x	x	x	x

Table 1. Systems evaluated in this research.

### Results and Discussion

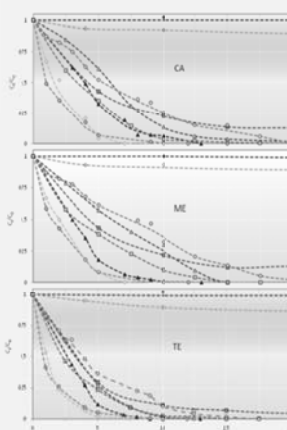


Figure 3. Profiles of concentration for CA, ME and TE.

• R1 ◊ R2 ▲ R3 ■ R4 □ R5 ◊ R6 ◊ R7 ◊ R8 ◊ R9

Fig. 3 shows the dimensionless remaining concentration for CA, ME and TE during the course of experiments.

The sole use of direct solar radiation did not degrade the compounds completely. This is because borosilicate glass tubes of the reactor do not transmit radiation of wavelength under 300 nm and the selected compounds do not absorb radiation of wavelength higher than 300 nm.

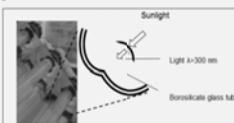


Figure 4. Scheme of a reactor's glass borosilicate tube.

In other hand, there is a partial decomposition of ozone into hydroxyl radicals by photolysis at wavelengths near 300 nm [2]. Then, the oxidation systems using ozone plus sunlight were effective in the removal of the target compounds as can be seen in Fig. 3.

The acidic hydrolysis of aqueous Fe(III) gives Fe(OH)<sup>2+</sup> species, which absorb solar radiation to yield Fe(II) and hydroxyl radicals, which in turn are responsible for the degradation of the target compounds. The presence of oxalate led to the formation of photoactive Fe-oxalate complexes and eventually hydrogen peroxide, thus triggering photo-Fenton reactions [3].

Mineralization percentages of the organic matter at 30, 60 and 120 min of reaction and total radiation accumulated after 5 h of irradiation for each experiment are indicated in Fig. 5.

Due to the selective reactivity of the ozone molecule, single ozonation under acidic conditions did not produce high mineralization [4]. However, photolytic ozonation led to a mineralization over 60%.

Photocatalysis with Fe(III) (in the absence of other reagents) also led to negligible mineralization while in the presence of ozone, oxalate and hydrogen peroxide showed high mineralization efficiency.

In summary, the efficiency of the studied systems regarding the mineralization of organic pollutants follows the order:

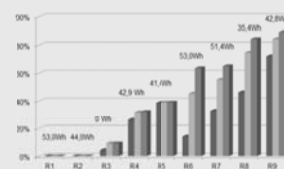
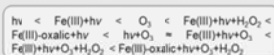


Figure 5. Mineralization achieved at different reaction times and total accumulated energy for each system. ■ 30 min, ■ 60 min, □ ≥120 min

The most efficient system was the combination Fe(III)-oxalic+hv+O<sub>3</sub>+H<sub>2</sub>O<sub>2</sub>. At pH 6.5 this system (R9) led to 15, 34, 70 and 85% of mineralization degree in 30, 60, 120 and 180 min, respectively.

### Conclusions

• The results of this work demonstrated that all the oxidation systems except R1, R2 and R5 are effective for the complete removal of the target compounds studied in this work (see Table 1).

• The presence of oxalate and/or hydrogen peroxide greatly enhanced the process efficiency because of the formation of photoactive complexes and/or photo-Fenton reactions.

• The most efficient oxidation system was the photocatalytic ozonation in the presence of Fe(III), oxalate and hydrogen peroxide at pH 3. This system led to the fastest mineralization rate achieving high TOC removal levels.

### References

- [1] M.S. Diaz et al. Trends Ana. Chem., 28 (2009) 1263-1275
- [2] H. Taube, Trans. Faraday Soc. 53 (1957) 656-665.
- [3] C. Y. Kwan, W. Chu. Water Res. 37 (2003) 4405-4412
- [4] H. Kusic et al. Chem. Eng. J., 123 (2006) 127-137

### Acknowledgements

This work has been financed by the Spanish Ministerio de Ciencia e Innovación (MICINN) and the European Feder Funds through the project CFG2009-13459-C05-05. D.H. Quiñones also thanks the MICINN for a FPI grant.



**CATALIZADORES MAGNÉTICOS DE DIÓXIDO DE TITANIO SOPORTADO SOBRE CARBÓN ACTIVO PARA LA DEPURACIÓN DE CONTAMINANTES EMERGENTES MEDIANTE OZONACIÓN FOTOCATALÍTICA SOLAR**

D. Quiñones\*, A. Rey, P. Álvarez F. Beltrán y A. Espejo  
 Dpto. Ingeniería Química y Química Física. Universidad de Extremadura, Av. Elvas, s/h, 06071 Badajoz (España).  
 Teléfono: +34 924289300, Fax: +34 924289385, \*E-mail: dquinone@alumnos.unex.es



**Introducción**

La presencia de contaminantes orgánicos emergentes en el agua es un tema de preocupación mundial. La combinación de fotocatalisis y ozonación, denominada ozonación fotocatalítica ha demostrado ser una alternativa muy eficiente para la depuración de estos contaminantes. Esta técnica requiere el uso de un material semiconductor que al absorber radiación se excita promoviendo un salto energético de los electrones de la banda de valencia hasta la banda de conducción, generando pares electrón-hueco y desencadenando una serie de reacciones de oxidación-reducción a través de las cuales se degrada la materia orgánica presente en el medio. La presencia de ozono (O<sub>3</sub>) aporta nuevos mecanismos de degradación al reaccionar directamente con estos compuestos o a través de la generación de radicales hidroxilo adicionales (OH<sup>•</sup>). Estos últimos se pueden generar por la disociación fotolítica de O<sub>3</sub>, o por la captura de los electrones promovidos a la banda de conducción del semiconductor formando el radical ozonido (O<sub>3</sub><sup>-•</sup>) que finalmente da lugar a más radicales OH<sup>•</sup> [1]. Además, la generación de H<sub>2</sub>O<sub>2</sub> en las reacciones directas del O<sub>3</sub> con determinados compuestos orgánicos puede suponer una fuente adicional de formación de radicales OH<sup>•</sup> [2]. En este trabajo se sintetizaron y caracterizaron varios catalizadores magnéticos basados en TiO<sub>2</sub> sobre carbón activo que pueden ser empleados en procesos de ozonación solar fotocatalítica. Los catalizadores se evaluaron a escala de laboratorio en un simulador solar usando como compuesto modelo metoprolol tartrato (MTP), un β-bloqueante utilizado en el tratamiento de enfermedades cardiovasculares.

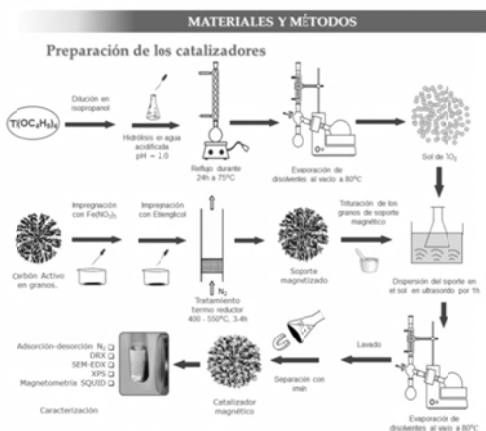


Figura 1. Proceso de síntesis de los catalizadores

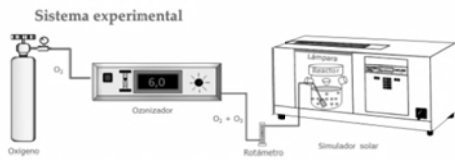


Figura 2. Esquema del sistema experimental empleado y condiciones de reacción

**RESULTADOS**

Tabla 1. Propiedades texturales y composición de los catalizadores y el carbón de partida.

	Fe (%)	TiO <sub>2</sub> (%)	C (%)	S <sub>BET</sub> (m <sup>2</sup> g <sup>-1</sup> )	S <sub>EXT</sub> (m <sup>2</sup> g <sup>-1</sup> )	V <sub>micro</sub> (cm <sup>3</sup> g <sup>-1</sup> )	M <sub>s</sub> (emu g <sup>-1</sup> )
Carbón activo	0	84,9	640	51	0,299	0	
CAT1	5,0	53,5	34,3	331	65	0,163	1,6
CAT2	7,6	65,4	21,2	271	72	0,221	9,1
CAT3	8,9	64,0	20,0	263	52	0,216	15,6

- ❑ No se consigue retener todo el TiO<sub>2</sub> esparcido y parte se pierde durante el lavado al final de la preparación de los catalizadores.
- ❑ Según análisis de XRD las nanopartículas de TiO<sub>2</sub> soportadas se encuentran en forma de anatasa.
- ❑ El catalizador CAT3 ha sido sintetizado con las condiciones más severas del tratamiento térmico reductor (T<sup>•</sup> y t), tiene mayor contenido de Fe y saturación de magnetización debido a una mayor conversión del metal en hierro magnético (magnetita, maghemita) según análisis de XRD.

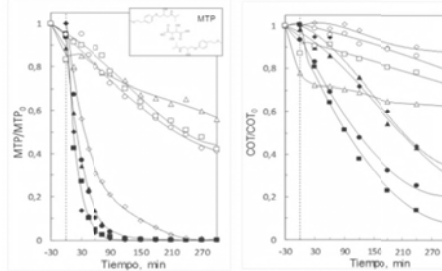


Figura 3. Fotocatalisis con CAT1(Δ), CAT2(◊) y CAT3(◻); ozonación simple (○), ozonación fotocatalítica (◐), y ozonación fotocatalítica con CAT1(▲), CAT2(●) y CAT3 (■).

- ❑ CAT1 presenta mayor capacidad de adsorción pero más baja fotoactividad.
- ❑ La combinación de ozonación y fotocatalisis genera un efecto sinérgico que conlleva a rendimientos mayores a los obtenidos a través de la fotocatalisis simple, la ozonación y la ozonación fotocatalítica.
- ❑ CAT3 tiene contenido de Fe y puede presentar reacciones secundarias tipo Fenton, por tanto tiene un mayor rendimiento en ozonación fotocatalítica.
- ❑ Tras 50 horas de reacción, el CAT3 aún conserva su capacidad fotocatalítica (100% de eliminación del MTP y mineralización del 79,6%).

**CONCLUSIONES**

- ❑ Se han sintetizado catalizadores fotoactivos que permiten la eliminación completa de metoprolol tartrato y una mineralización entre el 69,1 y 90,9% en procesos de ozonación fotocatalítica. Los catalizadores presentan áreas superficiales moderadas y volumen de poros que permiten la adsorción de compuestos orgánicos en cierta medida.
- ❑ El catalizador que mejor rendimiento demostró en la ozonación fotocatalítica es el CAT3 con una composición fina de Fe y 64,0% de TiO<sub>2</sub>.
- ❑ Los catalizadores pueden ser fácilmente recuperados del medio de reacción mediante el uso de un campo magnético externo, lo que los convierte en una alternativa eficiente y de bajos costos de operación para este tipo de procesos fotocatalíticos.


**Agradecimientos**

Este trabajo ha sido financiado por el Plan Nacional de I+D+i del MINECO y el FEDER mediante el proyecto CT2009-13459-C05-05/PPQ. D. Quiñones agradece la concesión de una beca FP del MINECO. A. Rey agradece a la UEX la concesión de un contrato posdoctoral. A. Espejo agradece la concesión de una beca FPI al Gobierno de Extremadura como a la Consejería de Empleo, Empresa e Innovación y al Fondo Social Europeo.

**Referencias**


1. Agustina T, Ang H, Vareek V. J. Photochem. Photobiol. C., 6 (2005) 264-273
2. Mena E., Rey A., Acedo B., Beltrán F.J., Malato S. Chem. Eng. J. 204-205 (2012) 131-140





**On the reaction mechanism of metoprolol removal through photocatalytic ozonation with TIFeAC catalyst under simulated solar radiation**

D.H. Quiñones, A. Rey, P.M. Álvarez, F.J. Beltrán  
 Dpto. Ingeniería Química y Química Física, Universidad de Extremadura, Avda. Elvas s/n 06006 Badajoz (Spain)  
 e-mail: fbeltran@unex.es  
 www.unex.es/investigacion/grupos/trataguas



---

### INTRODUCTION

Emerging contaminants detected in aqueous environments, wastewater treatment plant effluents and even in drinking water treatment plants are a big environmental concern nowadays. Most of them present xenobiotic, endocrine disrupting, persistent and other non-desirable properties, which make necessary their removal prior to water discharge. Photocatalytic ozonation based on the combination of photocatalytic oxidation with ozone has demonstrated to be very efficient to remove this kind of pollutants [1]. Although the photocatalyst commonly used has been TiO<sub>2</sub> powder due to its properties (activity, stability, cost, etc.), one of its main drawbacks is the separation of the catalysts in suspension after the reaction [2]. In this line, supported TiO<sub>2</sub> onto magnetic activated carbon (AC) has demonstrated to be active, stable and easily separable in the photocatalytic ozonation of metoprolol (MTP), a β-blocker pharmaceutical compound [3].

This work has been focused on the elucidation of solar photocatalytic ozonation of MTP mechanism using an own-made TIFeAC catalyst based on anatase-TiO<sub>2</sub> supported onto magnetic AC. The contribution of different reaction pathways and the main intermediates formed in the overall MTP degradation process have been considered.

### EXPERIMENTAL

**CATALYST SYNTHESIS**

Ti(OBu)<sub>4</sub> [1-PtOH-Ti(OBu)<sub>3</sub>]+H<sub>2</sub>O (pH=2) Stirred under reflux, 75°C, 24h. Org. solvent vacuum evaporation → TiO<sub>2</sub> aqueous suspension → US dispersion, 1h. Drying under vacuum, 80°C. Washing magnetic separation. Drying, 100°C, 24h → Magnetic TIFeAC

Granular AC → Fe(NO<sub>3</sub>)<sub>3</sub>·9H<sub>2</sub>O impregnation. Ethylene glycol impregnation. Heat treatment, N<sub>2</sub>, 550°C, 4h → Magnetic AC → Scheme 1. Synthesis steps → Magnetic TIFeAC

**CHARACTERIZATION**

Chemical analysis, N<sub>2</sub>-adsorption-desorption, XRD, SQUID magnetometry, XPS.

**CATALYTIC ACTIVITY TESTS**

Experimental conditions: Semicontinuous reactor, T=35 °C, pH=6, V=750 mL, v=20 L h<sup>-1</sup>, C<sub>MTP</sub>=0.37 g L<sup>-1</sup>, C<sub>O<sub>3</sub></sub>=6 mg L<sup>-1</sup>, C<sub>UVIS</sub>=50 mg L<sup>-1</sup>, λ=320-800 nm, 550 W m<sup>-2</sup>.

**Processes:** Adsorption → CAT, Ozonation → O<sub>3</sub>, Photocatalytic oxidation → CAT/L/O<sub>2</sub>, Catalytic ozonation → CAT/O<sub>3</sub>, Photolytic ozonation → L/O<sub>3</sub>, Photocatalytic ozonation → CAT/L/O<sub>3</sub>.

**Analysis parameters:** MTP → HPLC-PDA, TOC → TOC-analyzer, O<sub>3</sub>, O<sub>3</sub>, H<sub>2</sub>O<sub>2</sub> → Spect. UV-Vis, INTERMEDIATES → HPLC-QTOF.

---

### CHARACTERIZATION

Sample	Fe (%)	TiO <sub>2</sub> (%)	C (%)	S <sub>BET</sub> (m <sup>2</sup> g <sup>-1</sup> )	S <sub>EXT</sub> (m <sup>2</sup> g <sup>-1</sup> )	V <sub>MICRO</sub> (cm <sup>3</sup> g <sup>-1</sup> )	M <sub>s</sub> (mmol g <sup>-1</sup> )	F <sub>Fe2p</sub> (%at)
AC	—	—	84.9	640	51	0.299	0	—
TIFeAC	8.9	64.0	20.0	263	118	0.147	4.4	3.4

- ✓ TiO<sub>2</sub> content lower than expected due to washing procedure.
- ✓ TiO<sub>2</sub> as anatase particles by XRD.
- ✓ Significant magnetization, catalyst easily recoverable by means of a magnet.
- ✓ Fe exposed at the catalyst surface by XPS.

### CATALYTIC ACTIVITY

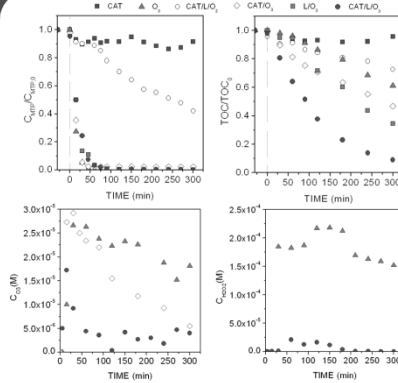


Fig. 1. Experimental results with TIFeAC catalysts and all the treatments applied

**Hydroxyl radical formation:**

- ✓ O<sub>3</sub> + CAT<sub>Fe</sub> → [·] → ·OH
- ✓ H<sub>2</sub>O<sub>2</sub> + CAT<sub>Fe</sub> → [·] → ·OH
- ✓ O<sub>3</sub> + CAT<sub>TiO<sub>2</sub></sub> + hν<sub>300-390nm</sub> → [·] → ·OH
- ✓ O<sub>3</sub> + CAT<sub>TiO<sub>2</sub></sub> + hν<sub>300-390nm</sub> → [·] → ·OH
- ✓ H<sub>2</sub>O<sub>2</sub> + CAT<sub>TiO<sub>2</sub></sub> + hν<sub>300-390nm</sub> → [·] → ·OH
- ✓ H<sub>2</sub>O<sub>2</sub> + CAT<sub>Fe</sub> + hν<sub>300-390nm</sub> → [·] → ·OH
- ✓ O<sub>3</sub> + hν<sub>300-320nm</sub> → [·] → ·OH
- ✓ H<sub>2</sub>O<sub>2</sub> + hν<sub>280-310nm</sub> → [·] → ·OH
- ✓ O<sub>3</sub> + HO<sub>2</sub> → [·] → ·OH

- ✓ Catalytic ozonation over AC and Fe sites
- ✓ Dark Fenton
- ✓ Photocatalytic oxidation, O<sub>2</sub> electron acceptor
- ✓ Photocatalytic oxidation, O<sub>3</sub> electron acceptor
- ✓ Photocatalytic oxidation, H<sub>2</sub>O<sub>2</sub> electron acceptor
- ✓ Photo-Fenton
- ✓ O<sub>3</sub> Photolytic decomposition
- ✓ O<sub>3</sub>-H<sub>2</sub>O<sub>2</sub> reactions

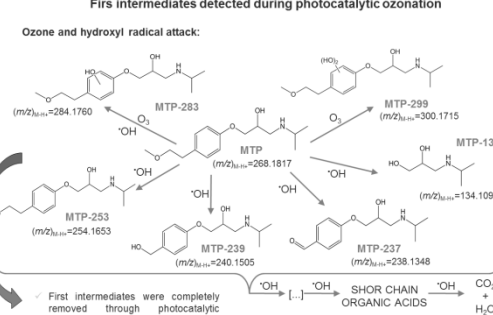
---

### CONCLUSIONS

- ✓ TIFeAC catalyst was very efficient in photocatalytic ozonation process which gave place to a complete MTP and its first intermediates removal reaching 90% mineralization.
- ✓ TIFeAC catalyst was easily recoverable.
- ✓ MTP is mainly depleted through direct O<sub>3</sub> reaction in the ozone processes
- ✓ Hydrogen peroxide is formed during MTP ozonation.
- ✓ Mineralization of MTP is mainly due to hydroxyl radicals attack which are formed through a complex reaction mechanism involving O<sub>3</sub> and H<sub>2</sub>O<sub>2</sub> electron capture from TiO<sub>2</sub> surface, O<sub>3</sub> photolysis, dark and photo-Fenton reactions, catalytic ozone decomposition over AC and Fe active sites and O<sub>3</sub>-H<sub>2</sub>O<sub>2</sub> reactions. The importance of the different pathways will be the subject of a future work.

### Firs intermediates detected during photocatalytic ozonation

Ozone and hydroxyl radical attack:



✓ First intermediates were completely removed through photocatalytic ozonation (90% mineralization)

---

**References**

[1] J. A. Reyes et al., J. Environ. Monit., 100 (2012) 10.  
 [2] S. Masato et al., Catal. Today, 147 (2009) 1.  
 [3] D.H. Quiñones et al., Appl. Catal. B Environ., 144 (2014) 96.

**Acknowledgements**

This work has been supported by the MINECO of Spain and Europe: 01PPOD. P.M. Álvarez thanks the MECO for providing a sabbatical grant (PR2011-0572). A. Rey thanks the UEX for a post-doctoral research grant. D.H. Quiñones thanks the MINECO for a predoctoral FPI grant.

meta.2014 Alicante

XI Reunión de la Mesa Española de Tratamiento de Aguas

**PT42** Aplicación simultánea de ozonación y oxidación fotocatalítica mediante foto-Fenton para la depuración de contaminantes emergentes en planta piloto

D.H. Quiñones<sup>1(\*)</sup>, A. Rey<sup>1</sup>, S. Contreras<sup>2</sup>, F.J. Beltrán<sup>1</sup>, P.M. Álvarez<sup>1</sup>.

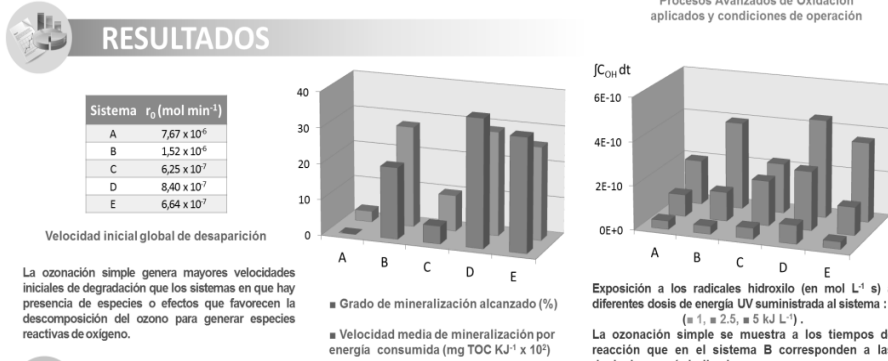
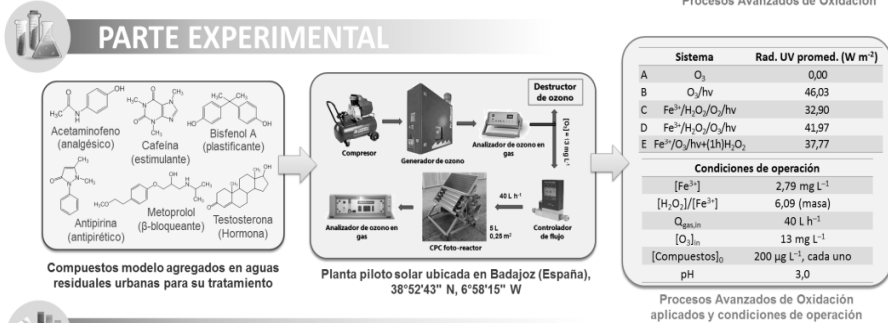
<sup>1</sup>- Depto. de Ingeniería Química y Química Física, Universidad de Extremadura, Avenida de Elvas s/n, 06071 Badajoz (España).

<sup>2</sup>- Departament d'Enginyeria Química, Universitat Rovira i Virgili, Av. Paisos Catalans 26, 43007 Tarragona (España).

\*dquinones@unex.es



UNIVERSIDAD DE EXTREMADURA - GRUPO DE TRATAMIENTO DE AGUAS



### CONCLUSIONES

- La reacción directa de oxidación con el ozono molecular es el mecanismo principal de degradación de los compuestos modelo. Sin embargo, la degradación de los intermedios de reacción que se generan durante el proceso se da fundamentalmente por vía de radicales libres.
- La aplicación en forma simultánea de ozono y foto-Fenton genera un efecto sinérgico que aumenta la velocidad de producción de radicales hidroxilo y el aprovechamiento de la radiación solar. De esta forma se consigue un mayor grado de mineralización

### AGRADECIMIENTOS

Este trabajo ha sido financiado por los fondos FEDER y el Plan Nacional de I+D+i del Ministerio de Economía y Competitividad (MINECO) de España, mediante los proyectos CTQ2009-13459-C05-05 y CTQ2012-35789-C02-01. D.H. Quiñones agradece al MINECO la concesión de una beca FPI.

## SYNTHESIS OF A B-DOPED TiO<sub>2</sub> PHOTOCATALYST FOR THE REMOVAL OF SELECTED PESTICIDES IN LABORATORY WATERS BY SOLAR PHOTOCATALYTIC OZONATION

A. Rey<sup>1\*</sup>, D.H. Quiñones<sup>1</sup>, P.M. Alvarez<sup>1</sup>, F.J. Beltrán<sup>1</sup>, G. Li Puma<sup>2</sup>  
 (1) University of Extremadura, Avenida de Elvas S/N, 06071 Badajoz, Spain.  
 (2) Loughborough University, Loughborough LE11 3TU, UK.  
 \*E-mail: anarey@unex.es

### Introduction

Agriculture is the industrial activity that has the major impact on aquatic ecosystems, due to the large volumes of water consumed (70% of the world accessible freshwater) and the high content of organic substances (pesticides and fertilizers) which are dispersed in aqueous environments by runoff or leaching.

Advanced Oxidation Processes, such as TiO<sub>2</sub> photocatalysis and ozonation, are being pointed out as effective alternatives to deal with this kind of contaminants. However TiO<sub>2</sub> photoactivity is limited to ultraviolet irradiation and single ozonation usually leads to low mineralization. To overcome these limitations, TiO<sub>2</sub> can be doped to extend its activity to the visible-light region. And also it can be used with ozone, which can trap electrons from the conduction band to yield oxygen reactive species (ROS).

In this work, nanosized photocatalyst samples of TiO<sub>2</sub> and B-doped TiO<sub>2</sub> were synthesized using a sol-gel method. The photocatalysts were characterized by powder XRD, N<sub>2</sub> isotherms, SEM, DR-UV-Vis, ICP and XPS. Four recalcitrant pesticides (diuron, o-phenylphenol, MCPA and terbutylazine) were subjected to degradation by ozonation, photocatalytic ozonation, photocatalysis and photocatalytic ozonation using the prepared catalysts under simulated solar irradiation in a laboratory scale system.

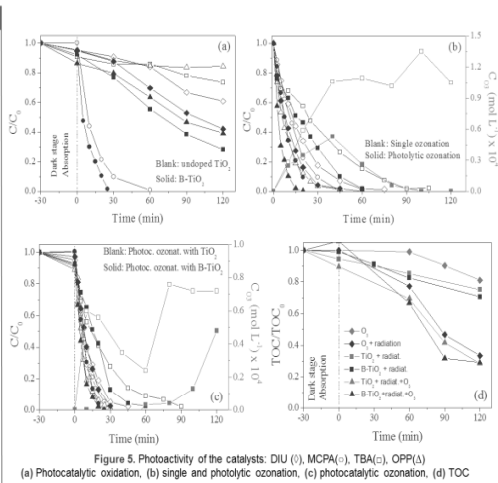
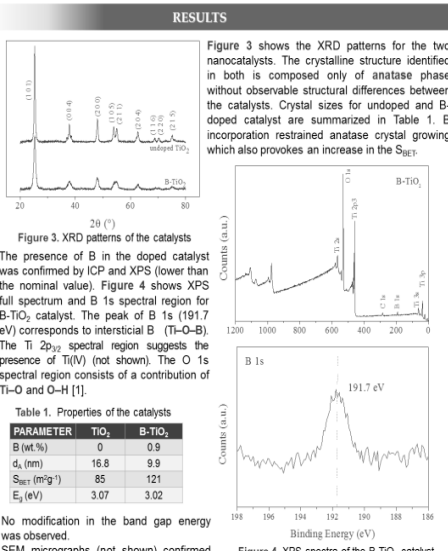
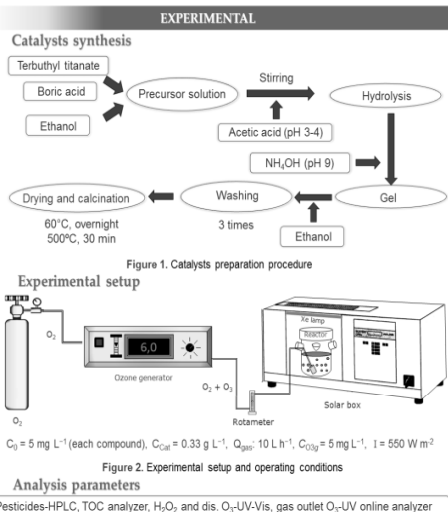
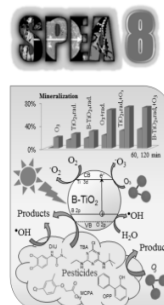


Figure 5 shows the profiles of removal of the target pesticides during the application of various AOPs. As shown in Figure 5a, after 30 min of stirring in the dark, a low adsorption of compounds on the catalysts was reached. B-doped catalyst showed higher activity than bare TiO<sub>2</sub> for photocatalytic ozonation. MCPA presents the highest depletion rate by photocatalytic oxidation. According to Figure 5b photocatalytic ozonation is more efficient than single ozonation for the removal of the pesticides. This is due to the ozone photolysis which also leads to lower O<sub>3</sub> accumulation. From Figure 5c can be seen that B-doped TiO<sub>2</sub> is still more efficient than bare TiO<sub>2</sub> in photocatalytic ozonation. Figure 5d shows TOC removal profiles for all the systems studied. Single ozonation led to a low TOC removal. However the use of radiation and catalysts promoted ozone decomposition into ROS and therefore, higher mineralization is achieved. B-doped catalyst was observed to be more active than TiO<sub>2</sub> and led to the higher mineralization rate.

### CONCLUSIONS

Bare and B-doped TiO<sub>2</sub> catalysts were synthesized by a sol gel method and were found to be effective in the degradation of diuron, o-phenylphenol, MCPA and terbutylazine by photocatalytic oxidation and photocatalytic ozonation. The efficiency of the studied systems regarding the mineralization rates followed the order: single ozonation < photocatalysis with TiO<sub>2</sub> < photocatalysis with B-TiO<sub>2</sub> < photocatalytic ozonation < photocatalytic ozonation with TiO<sub>2</sub> < photocatalytic ozonation with B-TiO<sub>2</sub>.

### Acknowledgements

This work has been financed by MINECO (Spain) and ERDF through project CTQ2012-35789-C02-01. D. Quiñones thanks the MINECO for the concession of a FPI grant. D. Quiñones is also grateful to Loughborough University and MINECO for making possible a research stay.

### References

1. D. Chen, D. Yang, Q. Wang, Z. Jiang. *Industrial & Engineering Chemistry Research*, 45 (2006) 4110-4116



**BORON DOPED TiO<sub>2</sub> PHOTOCATALYSTS FOR SOLAR PHOTOCATALYTIC TREATMENTS OF SELECTED PESTICIDES**

D.H. Quiñones<sup>1</sup>, A. Rey<sup>1</sup>, P.M. Álvarez<sup>1</sup>, E. Mena<sup>1\*</sup>, F.J. Beltrán<sup>1</sup>, G. Li Puma<sup>2</sup>.

<sup>1</sup> Departamento de Ingeniería Química y Química Física. Universidad de Extremadura, Avda. Elvas, s/n. 06006 Badajoz, Spain.

<sup>2</sup> Department of Chemical Engineering, Loughborough University, LE11 3TU, Loughborough, United Kingdom.

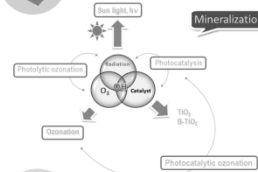
\*emenarub@alumnos.unex.es



EXPOQUIMIA  
13th Mediterranean Congress of Chemical Engineering

UNIVERSIDAD DE EXTREMADURA - GRUPO DE TRATAMIENTO DE AGUAS

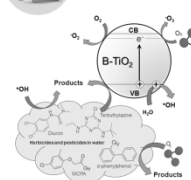
**INTRODUCTION**



**Agricultural industry** is considered as one of the productive sectors with the most negative effects on **aquatic environments**, since it generates water residues with high content of **agrochemicals** as pesticides and fertilizers. Most of them have been found to be **persistent** against conventional physicochemical treatments applied in wastewater treatment plants.

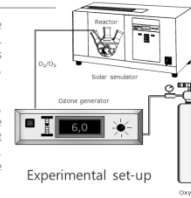
**Photocatalytic ozonation** (i.e. the combination of an irradiated semiconductor with ozone) has demonstrated to efficiently remove a great variety of organic pollutants. In this work, the degradation of four pesticides: **Diuron (DIU)**, **o-phenylphenol (OPP)**, **2-methyl-4-chlorophenoxyacetic acid (MCPA)** and **terbutylazine (TBA)** is studied. The degradation methods used were **photocatalytic oxidation**, **ozonation**, **photolytic ozonation**, and **photocatalytic ozonation** with different **B-TiO<sub>2</sub>** catalysts studying the effect of B loading on the catalytic activity.

**EXPERIMENTAL**



TiO<sub>2</sub> and several B-TiO<sub>2</sub> catalysts with nominal boron content between 0-12 wt.% were prepared by a **sol-gel** procedure using **boric acid** and **tert-butyl titanate** as precursors. The suspended solids obtained were centrifuged, washed, and the resulting precipitates were calcined at 500°C. Characterization of the catalysts was carried out by **XRD, SEM, ICP, N<sub>2</sub> adsorption-desorption isotherms, XPS** and **DR-UV-Vis spectroscopy**.

Photoactivity was evaluated using a **solar simulator** equipped with a Xe lamp ( $\lambda > 300$  nm, 550 W m<sup>-2</sup>) feeding 10 L h<sup>-1</sup> of an O<sub>2</sub>/O<sub>3</sub> mixture (5 mg L<sup>-1</sup> ozone) in a pH free ultrapure water matrix containing 5 mg L<sup>-1</sup> of each target compound. Experiments were carried out with a 30 min period of adsorption in the dark followed by a 2 h period of irradiation. Pesticides, dissolved O<sub>3</sub>, H<sub>2</sub>O<sub>2</sub> and total organic carbon (TOC) concentrations were analysed to follow the reaction evolution.



Experimental set-up

**RESULTS AND DISCUSSION**

B content in the doped catalyst was measured by ICP and XPS, and it was found to be lower than the nominal value (see Table 1).

Part of B in the catalysts was as B<sub>2</sub>O<sub>3</sub>/H<sub>3</sub>BO<sub>3</sub> unstable in aqueous solution. Thus, an extra washing step with water was added to the synthesis procedure to remove unstable B and avoid further leaching. The rest of B in the catalysts was incorporated in interstitial positions of TiO<sub>2</sub> and was confirmed by DR-UV-Vis spectroscopy that it did not modify the band gap energy with respect to bare TiO<sub>2</sub> (see Table 1).

Table 1. B-TiO<sub>2</sub> catalysts properties

CATALYST	B (wt.%)	d <sub>A</sub> (nm)	S <sub>BET</sub> (m <sup>2</sup> g <sup>-1</sup> )	E <sub>g</sub> (eV)
TiO <sub>2</sub>	n.d.	16.8	68.3	3.07
3B-TiO <sub>2</sub>	0.91	9.9	121.3	3.12
6B-TiO <sub>2</sub>	1.06	9.2	120.1	3.03
9B-TiO <sub>2</sub>	1.81	7.6	122.4	3.05
12B-TiO <sub>2</sub>	3.55	7.5	125.5	3.01
6B-TiO <sub>2</sub> (washed)	0.42	9.8	n.m.	n.m.
12B-TiO <sub>2</sub> (washed)	0.49	7.9	n.m.	n.m.

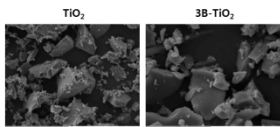


Figure 1. SEM Micrographs

Figure 1 shows, as an example, the SEM micrographs for bare TiO<sub>2</sub> and 3B-TiO<sub>2</sub> catalysts. These micrographs confirmed irregular forms and a wide particle size distribution for the catalysts.

As shown in Figure 2, the crystalline structure identified

in all catalysts is composed only of anatase phase without observable structural differences between the catalysts.

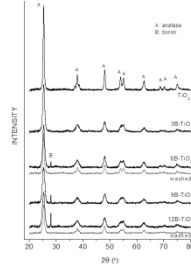


Figure 2. XRD diffractograms for the prepared catalysts

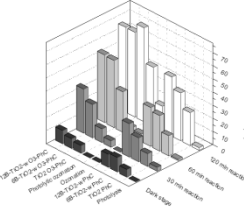


Figure 3. Mineralization profiles

Authors thank MINECO and ERDF Funds for the support through the Project CTQ2012-33789-C02-01. D.H. Quiñones thanks the MINECO for a predoctoral FPI grant and an aid to do a research stay. E. Mena thanks the Consejería de Empleo, Empresa e Innovación (Gobierno de Extremadura) and European Social Fund for a predoctoral FPI grant (Ref. PD12059).

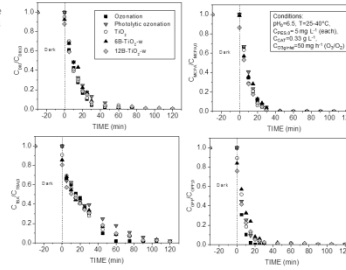


Figure 4. Compounds degradation profiles

As shown in Figure 3, a low TOC adsorption was achieved in all cases after the dark stage. However doped catalysts, which have higher surface areas (see Table 1), presented higher adsorption capacity compared to bare TiO<sub>2</sub>. Direct photolysis led to a negligible mineralization. Photocatalytic oxidation systems led to 25, 37 and 45% mineralization when using bare TiO<sub>2</sub>, 6B-TiO<sub>2</sub> and 12B-TiO<sub>2</sub> (both washed), respectively. These results were highly improved during photocatalytic ozonation treatment, reaching 55-70% TOC removal. It is noteworthy that B-doped catalysts led to faster mineralization rates than bare TiO<sub>2</sub> although the final mineralization was similar.

Regarding compounds degradation (see Figure 4), all the ozone treatments lead to higher degradation rate of the pesticides than photocatalytic oxidation processes.

The stability and reusability of the 12B-TiO<sub>2</sub> (washed) catalyst was tested in three consecutive runs of photocatalytic ozonation process in which the catalyst was recycled by filtration (not shown). It was observed that after 3 consecutive runs with no boron leaching the catalytic activity was maintained reaching about 75% mineralization.

**ACKNOWLEDGEMENTS**

As shown in Figure 2, the crystalline structure identified

